

TECHNICAL REPORT

**Remediation and Treatment Technology
Development and Support for DOE Oak Ridge
Office: EFPC Model Update, Calibration and
Uncertainty Analysis**

Date submitted:

July 31, 2014

Principal Investigators:

Leonel E. Lagos, Ph.D., PMP®

Florida International University Collaborators:

Georgio Tachiev, PhD, PE (Project Manager)

Angelique Lawrence, MS, GISP

David Roelant, Ph.D.

Siamak Malek-Mohammadi, PhD

Amy Cook, MS

Mandar Zope, MS

Lilian Marrero, MS and DOE Fellow

Heidi Henderson, PE, MS and DOE Fellow

Elsa Cabrejo, MS and DOE Fellow

Nantaporn Noosai, PhD

Viviana Villamizar, MS

Michelle Embon, BS Candidate and DOE Fellow

Submitted to:

U.S. Department of Energy

Office of Environmental Management

Under Grant # DE-EM0000598



Applied Research Center

FLORIDA INTERNATIONAL UNIVERSITY

DISCLAIMER

This report was prepared as an account of work sponsored by an agency of the United States government. Neither the United States government nor any agency thereof, nor any of their employees, nor any of its contractors, subcontractors, nor their employees makes any warranty, express or implied, or assumes any legal liability or responsibility for the accuracy, completeness, or usefulness of any information, apparatus, product, or process disclosed, or represents that its use would not infringe upon privately owned rights. Reference herein to any specific commercial product, process, or service by trade name, trademark, manufacturer, or otherwise does not necessarily constitute or imply its endorsement, recommendation, or favoring by the United States government or any other agency thereof. The views and opinions of authors expressed herein do not necessarily state or reflect those of the United States government or any agency thereof.

EXECUTIVE SUMMARY

This research is part of continued efforts to correlate the hydrology of East Fork Poplar Creek (EFPC) and Bear Creek (BC) with the long-term distribution of mercury within the overland, subsurface, and river sub-domains. The main objective of this study was to add a sedimentation module (ECO Lab) capable of simulating the reactive transport mercury exchange mechanisms within sediments and porewater throughout the watershed. That application used historical precipitation, groundwater levels, river discharges, and mercury concentrations data that were retrieved from government databases and input to the model. The model was run to reduce overall computational time and to predict: flow discharges, total mercury concentration, flow duration and mercury load curves at key monitoring stations under various hydrological and environmental conditions and scenarios. The computational results provided much detail on the relationship between discharges and mercury loads at various stations throughout EFPC, which is important to best understand and support the management of mercury contamination and remediation efforts within EFPC. Furthermore, An XPSWWM surface water model was developed to provide a better understanding of the surface water flow rates and water stages during rainfall events for the selected 4500 ORNL area. The specific system of interest, the stormwater collection system up to Outfall 211, is approximately 4.5 acres and encompasses several ORNL buildings. The system is bounded by mostly impervious area (due to roof top runoff through storm drains and pavement to the north, south, east, and west) with minor pervious areas sparsely connected within. Ms. Henderson, the author of the XPSWWM surface water study, conducted an internship during the summer of 2012 and collected information about the physical parameters of the stormwater drainage system. A stormwater hydraulic-hydrologic computer model was developed using XPSWWM software. The objective of the model is to provide detailed information about flow rate and stage timeseries during various stormwater events. ORNL provided monitored timeseries flow rates at OF-211. Dates that rainfall occurred during the monitoring period were noted and simulated through the network for calibration of the model. The model produced results that agreed with the monitored data resulting in credible validation of the model. In addition, a sensitivity analysis was prepared where actual rainfall data was simulated through the network varying Manning's roughness coefficient, infiltration parameters, and percent imperviousness in order to assess the impacts of the variables on the

model results. Design storms were simulated and examined. In addition, a hypothetical conservative contaminant was introduced into the system at various locations. The flow rates, concentrations, and loads were fit to a probability distribution which describes the character of the data. The resulting flow rates from the model may be utilized in conjunction with contaminant data to assess where remediation may be necessary within the area of interest.

TABLE OF CONTENTS

INTRODUCTION 1

DEVELOPMENT OF AN INTEGRATED SURFACE AND SUBSURFACE FLOW MODEL
15

 Model Theoretical Basis15

 Coupling of MIKE SHE and MIKE 11 HD 16

 Model Domain19

 Topography20

 Climate Data21

 Precipitation 22

 Evapotranspiration 23

 Land Use24

 Saturated Zone28

 Unsaturated Flow30

 Rivers and Lakes.....32

 River Network and Cross Sections 32

 Boundary Conditions 35

 Overland Flow36

 Grid Size43

 Sensitivity Analysis and Uncertainty of the Hydrologic Model43

 Hydrologic Simulations44

 Groundwater Flow 44

 Surface Water Flow 45

Flow in Rivers 46

DEVELOPMENT OF A MERCURY FATE AND TRANSPORT MODEL 58

Transport Parameters58

Model Calibration and Verification62

Assumptions and Limitations66

Parameters Affecting Suspended Solids Transport in ECO Lab69

Parameters Affecting Mercury’s Fate and Transport in ECO Lab75

Modeling the Impact of Extreme Flood Events on Mercury Fate and Transport 83

Mercury TMDL of East Fork Poplar Creek 84

A SURFACE WATER MODEL FOR THE ORNL 4500 AREA 115

Study Area115

Research Objective121

Site Analysis122

Model Development.....124

Basic Theory 125

Model Input..... 130

Hydrology Analysis142

Steady Uniform Flow Calibrations 143

Unsteady Non-Uniform Flow Calibration 145

Sensitivity Analysis 151

Probability of Exceedance Analysis 152

Probability Distribution (PD) Fitting 153

Design Storm Simulations 154

Transport Analysis155

 Transport Analysis Simulation 1 158

 Transport Analysis Simulation 2 159

 Transport Analysis Simulation 3 160

 Transport Analysis Simulation 4 160

Hydrology Analysis Results161

 Steady Uniform Flow Calibration Results 161

 Unsteady Non-Uniform Flow Calibration Results 164

 Sensitivity Analysis Results..... 173

 Design Storm Simulation Results 182

Transport Analysis Results189

 Transport Analysis Simulation 1 Results..... 190

 Transport Analysis Simulation 2 Results..... 196

 Transport Analysis Simulation 3 Results..... 202

 Transport Analysis Simulation 4 Results..... 207

 Transport Analysis - Probability of Exceedance Results..... 213

 Probability Distribution Fitting Results215

CONCLUSIONS..... 219

REFERENCES 225

APPENDIX A RIVER NETWORK AND MIKE-SHE COUPLING 233

LIST OF TABLES

Table 1. NLCD 2001 Land Cover..... 10

Table 2. NLCD 2001 Land Use Classification and Manning’s Number 11

Table 3. Land Use, Area and Fraction of EFPC 12

Table 4. Basin Characteristics..... 19

Table 5. Vegetation Data 27

Table 6. Van Genuchten’s Soil Hydraulic Parameters 32

Table 7. Boundary Conditions 35

Table 8. Manning’s Number for Each Land Use Type..... 40

Table 9. Model Calibration Parameters 41

Table 10. Basin Characteristics..... 42

Table 11. Peak Flow Basin Characteristics..... 42

Table 12. Low Flow Basin Characteristics 42

Table 13. Streamflow Statistics 42

Table 14. Model Components and Parameters Used for Uncertainty Analysis 43

Table 15. Streamflow Statistics for EFPC 2119 (Flow Duration, General Flow and Base Flow) for Measurements at USGS Station 03538230 47

Table 16. Streamflow Statistics (Flow Duration, General Flow and Base Flow) for Measurements at USGS Station 03538230 49

Table 17. Physical Characteristics of the Stream..... 51

Table 18. Peakflow Statistics 54

Table 19. Flood Volume Statistics..... 54

Table 20. Low Flow Statistics 55

Table 21. Flow Duration Statistics..... 56

Table 22. Annual Flow Statistics 56

Table 23. Monthly Flow Statistics 56

Table 24. General Flow Statistics 57

Table 25. Baseflow Statistics 57

Table 26. Climate Characteristics 57

Table 27. Transport Parameters Used in the Model 59

Table 28. Summary of ECO Lab Input 65

Table 29. ECO Lab State Variables 68

Table 30. Settling Velocity 71

Table 31. Shields Dimensionless Parameters [141]..... 72

Table 32. Mass of Sediment at Station 17 [130]..... 73

Table 33. Log K_d (L/kg) Values for Inorganic Mercury 76

Table 34. Model Components & Parameters Used for Uncertainty Analysis (from Table 27).... 78

Table 35. Precipitation Frequency Estimates (inches)..... 83

Table 36. Precipitation Frequency Estimates (mm)..... 84

Table 37. Probabilistic Distribution of Observed Flow at UEFPC Station 17 91

Table 38. TSS, Load of TSS, Load of Hg, 90th and 50th Percentile, Under Different Flow Conditions (Data from OREIS Database, Years 1996-2008) 93

Table 39. Effect of Changes in k_{oc} on Mercury Concentrations in Water and Sediment 104

Table 40. XPSWMM Node Data Entry 131

Table 41. XPSWMM Link Data Entry 135

Table 42. Rainfall Data for Calibration Trial 1..... 147

Table 43. Rainfall Data for Calibration Trial 2..... 148

Table 44. Rainfall Data for Calibration Trial 3..... 149

Table 45. Rainfall Data for Calibration Trial 4..... 150

Table 46. NOAA Precipitation 155

Table 47. Transport Simulations Hypothetical Timeseries..... 157

Table 48. Transport Simulation Scenarios..... 158

Table 49. Rational Method Runoff Coefficients..... 162

Table 50. Manning's n for Concrete Pipe 175

Table 51. Design Storm Stage and Flow Rate Results 185

Table 52. Continuity Results..... 190

Table 53. Scenario 1 ‘Goodness of Fit’ Results 216

Table 54. Scenario 2 ‘Goodness of Fit’ Results 216

Table 55. Scenario 3 ‘Goodness of Fit’ Results 217

Table 56. Scenario 4 ‘Goodness of Fit’ Results 217

Table 57. River Network and MIKE-SHE Coupling Branches 233

LIST OF FIGURES

Figure 1. Lower Clinch River Watershed in Tennessee. 3

Figure 2. Location of the Oak Ridge Reservation. 4

Figure 3. Digital Elevation Map of East Fork Poplar Creek Watershed. 5

Figure 4. Appalachian Valley and Ridge Province..... 7

Figure 5. Streams within East Fork Poplar Creek Watershed. 9

Figure 6. EFPC land use. 11

Figure 7. Discretization of land cover data used for the hydrological model..... 12

Figure 8. Percent imperviousness. 14

Figure 9. A typical MIKE SHE river link cross-section..... 18

Figure 10. Model Domain..... 20

Figure 11. Site Topography. 21

Figure 12. Precipitation at ORR..... 22

Figure 13. Land Use maps (A)..... 25

Figure 14. Land Use maps (B)..... 26

Figure 15. Leaf Area Index and Root Depth Grid Codes. 27

Figure 16. Geologic layers..... 28

Figure 17. River network and domain with cross section locations, boundaries and intersections.
..... 33

Figure 18. Typical cross section profile from East Fork Poplar Creek. 34

Figure 19. Procedure for determining Manning’s number (Part I)..... 38

Figure 20. Procedure for determining Manning’s number (Part II)..... 39

Figure 21. Example of a calculation of the groundwater table, including vectors showing groundwater movement in the XY direction. 44

Figure 22. Location of USGS Station 03538320 and DOE station EFK 24.4 used for data comparison..... 45

Figure 23. USGS stations used for calibration of discharges in LEFPC streams, the legend shows the USGS station number..... 45

Figure 24. Computed and observed values at USGS Station 03238230..... 46

Figure 25. Duration curve computed for EFPC 2119 (near EFK 24.4, and USGS Station 03538230), CT - Cumulative Time, MCT – Maximum Continuous Period. 47

Figure 26. Location of USGS Station 03538235 and Station 17 (EFK 23.4)..... 48

Figure 27. Computed and measured discharges at EFPC 3209, EFK 23.4, and USGS Station 03538235..... 50

Figure 28. Duration curve computed for EFPC 3209 (near EFK 23.4, and USGS Station 03538235), CT - Cumulative Time, MCT – Maximum Continuous Period. 50

Figure 29 Computed and measured discharges at EFPC 20267 and USGS station 03538250 (0.4 miles downstream of EFK 6.3), 51

Figure 30. Location of USGS Stations 03538250. 52

Figure 31. Duration curve computed for EFPC 20267 (near EFK 6.3, and USGS Station 03538250), CT - Cumulative Time, MCT – Maximum Continuous Period. 52

Figure 32. Cumulative distribution function of computed and observed discharge at EFPC 20267 (near EFK 6.3, and USGS Station 03538250). 53

Figure 33. Boxplot of Computed and observed discharge at at EFPC 20267 (near EFK 6.3, and USGS Station 03538250)..... 53

Figure 34. Model domain of East Fork Poplar Creek [52]. 64

Figure 35. Measured concentrations of total mercury (mg/l) and discharges (cfs) at station 17 (EFK 23.4) on East Fork Poplar Creek. 79

Figure 36. Simulation of mercury transport in EFPC (shown are Stations EFK 2.1, EFK 6.3, EFK 10.0, EFK 13.8, EFK 18.2, EFK 23.4, EFK 24.4). 79

Figure 37. Simulated distribution of mercury transport a) mass per unit area and b) sorbed concentration in the saturated zone. 80

Figure 38. Mercury concentration used in the model. 81

Figure 39. Observed and computed mercury concentration at Station 17. 82

Figure 40. Observed and computed mercury leaving EFPC watershed. 82

Figure 41. Simulated rainfall events. 84

Figure 42. Average Concentration and average yearly load at Station 17 (EFK 23.4). 88

Figure 43. Flowchart of TMDL studies. 89

Figure 44. Flow duration curve UEFPC Station 17 (data from OREIS database years 1996-2008). 91

Figure 45. Load duration curve for suspended solids ranked by discharge at UEFPC Station 17 (data from OREIS database, years 1996-2009). 92

Figure 46. Total suspended solids by discharge at UEFPC Station 17 (data from OREIS database, years 1996-2009). 93

Figure 47. Load duration curve for mercury ranked by discharge at UEFPC Station 17 (data from OREIS database, years 1996-2008). 94

Figure 48. Total Suspended Solids at the UEFPC Station 17. Data from OREIS database year 2000. 95

Figure 49. Effect of critical current velocity on the load of TSS. 96

Figure 50. Effect on TSS load from decreasing critical velocity. 97

Figure 51. Effect of resuspension rate on the load of TSS. 98

Figure 52. Effect on TSS load from increasing the resuspension rate. 98

Figure 53. Effect of settling velocity on the load of TSS. 99

Figure 54. Effect on TSS load from decreasing settling velocity from 8 to 6 m/d. 100

Figure 55. Effect of particle production rate on the load of TSS. 100

Figure 56. Effect on TSS load from increasing PPR from 7 to 10 g/m²/d. 101

Figure 57. TSS load simulated and observed (2000 – 2008), UEFPC-Station 17..... 101

Figure 58. Effect on mercury concentration in water from changing k_w 104

Figure 59. Effect on load of mercury as desorption rate in water changes..... 105

Figure 60. Effect on load of mercury as TSS load changes..... 106

Figure 61. A summary of the processes which are currently included for modeling total mercury and methylmercury. 107

Figure 62. Relation between total mercury and methylmercury at ORR from experimental data. 109

Figure 63. Nearly proportional distribution between dissolved mercury (SHM) and methylmercury species (MeM) is shown (based on the ECO Lab kinetic model) 111

Figure 64. River network in the model indicating point nodes, boundary conditions and cross-sections. 112

Figure 65. Monthly-based variations of average mercury concentration at selected stations along EFPC..... 114

Figure 66. Area of Interest and Building Identification..... 115

Figure 67. Area of Interest Boundary. 116

Figure 68. Stormwater Collection System. 117

Figure 69. Sub-catchment Delineation of System. 118

Figure 70. Outfall 211..... 119

Figure 71. WOC East of Outfall 211..... 120

Figure 72. Dechlorinator in WOC. 120

Figure 73. XPSWMM Digital Terrain Model..... 121

Figure 74. Location of MH B-4500S_E. 122

Figure 75. Location of Inlet I-2..... 123

Figure 76. Location of Inlet I-4..... 123

Figure 77. Location of I-8 and I-9. 124

Figure 78. XPSWMM Model Main Storm Line..... 125

Figure 79. XPSWMM Node Data Dialog..... 131

Figure 80. XPSWMM Conduit Shapes..... 134

Figure 81. XPSWMM Conduit Profile..... 135

Figure 82. Runoff Node Dialog..... 137

Figure 83. Runoff Node Sub-catchment Dialog..... 138

Figure 84. Infiltration Parameters..... 140

Figure 85. Green Ampt Parameters..... 141

Figure 86. Horton Infiltration Dry Clay Parameter..... 142

Figure 87. Horton Equation Dry Clay Parameter..... 142

Figure 88. Rainfall Hyetograph for Steady Uniform Flow..... 143

Figure 89. Stormwater Collection System for Steady Uniform Flow..... 144

Figure 90. Rainfall Hyetograph for Calibration Trial 1..... 147

Figure 91. Rainfall Hyetograph for Calibration Trial 2..... 148

Figure 92. Rainfall Hyetograph for Calibration Trial 3..... 149

Figure 93. Rainfall Hyetograph for Calibration Trial 4..... 150

Figure 94. Year 2010 Rainfall Data..... 151

Figure 95. Storm System..... 152

Figure 96. SCS Type II Unit Hyetograph..... 154

Figure 97. XPSWMM User Inflow..... 156

Figure 98. Transport Scenario 1 Entrance of Pollutant Location..... 159

Figure 99. Transport Analysis Scenario 2 Pollutant Entrance Locations..... 159

Figure 100. Transport Analysis Scenario 3 Entrance of Pollutant..... 160

Figure 101. Transport Analysis Scenario 4 Pollutant Entrance Locations. 161

Figure 102. XPSWMM Profile for Links P-2 thru P-26..... 161

Figure 103. Conduit P-20 Results for Steady Uniform Flow. 163

Figure 104. Conduit P-26 Results for Steady Uniform Flow. 164

Figure 105. ORNL Data with Base Flow..... 165

Figure 106. ORNL Data and XPSWMM Results Hydrograph..... 166

Figure 107. ORNL Data and XPSWMM Results Cumulative Flow Rates. 167

Figure 108. ORNL Data with Base Flow..... 167

Figure 109. ORNL Data and XPSWMM Results Hydrograph..... 168

Figure 110. ORNL Data and XPSWMM Results Cumulative Flow Rates. 169

Figure 111. ORNL Data with Base Flow..... 169

Figure 112. ORNL Data and XPSWMM Results Hydrograph..... 170

Figure 113. ORNL Data and XPSWMM Results Cumulative Flow Rates. 171

Figure 114. ORNL Data with Base Flow..... 171

Figure 115. ORNL Data and XPSWMM Results Hydrograph..... 172

Figure 116. ORNL Data and XPSWMM Results Cumulative Flow Rates. 173

Figure 117. MH211-3 Hydrograph and PE Curves for Manning's Roughness Coefficient Sensitivity Analysis. 174

Figure 118. OF-211 Hydrograph and PE Curves for Manning's Roughness Coefficient Sensitivity Analysis. 174

Figure 119. P-15 Hydrograph and PE Curves for Infiltration Sensitivity Analysis. 176

Figure 120. P-26 Hydrograph and PE Curves for Infiltration Sensitivity Analysis. 176

Figure 121. OF-211 Hydrograph and PE Curves for Infiltration Sensitivity Analysis. 177

Figure 122. P-10 and P-11 PE Curves for Percent Imperviousness Sensitivity Analysis. 178

Figure 123. P-27 PE Curves for Percent Imperviousness Sensitivity Analysis..... 178

Figure 124. P-26 Hydrograph and PE Curves for Percent Imperviousness Sensitivity Analysis.
..... 179

Figure 125. OF-211 Hydrograph and PE Curves for Percent Imperviousness Sensitivity Analysis.
..... 179

Figure 126. XPSWMM North-South Storm Line Results for Base Conditions. 180

Figure 127. XPSWMM East-West Storm Line Results for Base Conditions..... 181

Figure 128. XPSWMM Results for Base Conditions. 182

Figure 129. XPSWMM Design Storm Hydrographs..... 183

Figure 130. P-10 PE Curves for Design Storm Events..... 183

Figure 131. P-27 PE Curves for Design Storm Events..... 184

Figure 132. MH211-3 PE Curves for Design Storm Events..... 184

Figure 133. XPSWMM 5-Year 24-Hour Storm Event. 186

Figure 134. XPSWMM 10-Year 24-Hour Storm Event. 186

Figure 135. XPSWMM 25-Year 24-Hour Storm Event. 187

Figure 136. XPSWMM 25-Year 24-Hour Storm Event Areas of Flooding 188

Figure 137. XPSWMM 100-Year 24-Hour Storm Event. 188

Figure 138. XPSWMM 100-Year 24-Hour Storm Event Areas of Flooding 189

Figure 139. XPSWMM P-10 Hydrograph..... 191

Figure 140. XPSWMM P-10 Pollutograph..... 192

Figure 141. XPSWMM P-11 Hydrograph..... 192

Figure 142. XPSWMM P-11 Pollutograph..... 193

Figure 143. XPSWMM P-15 Hydrograph..... 193

Figure 144. XPSWMM P-15 Pollutograph..... 194

Figure 145. XPSWMM P-26 Hydrograph..... 194

Figure 146. XPSWMM P-26 Pollutograph..... 195

Figure 147. XPSWMM P-27 Hydrograph..... 195

Figure 148. XPSWMM P-27 Pollutograph..... 196

Figure 149. XPSWMM P-10 Hydrograph..... 197

Figure 150. XPSWMM P-10 Pollutograph..... 197

Figure 151. XPSWMM P-11 Hydrograph..... 198

Figure 152. XPSWMM P-11 Pollutograph..... 198

Figure 153. XPSWMM P-15 Hydrograph..... 199

Figure 154. XPSWMM P-15 Hydrograph..... 199

Figure 155. XPSWMM P-26 Hydrograph..... 200

Figure 156. XPSWMM P-26 Pollutograph..... 200

Figure 157. XPSWMM P-27 Hydrograph..... 201

Figure 158. XPSWMM P-27 Pollutograph..... 201

Figure 159. XPSWMM P-10 Hydrograph..... 202

Figure 160. XPSWMM P-10 Pollutograph..... 203

Figure 161. XPSWMM P-11 Hydrograph..... 203

Figure 162. XPSWMM P-11 Pollutograph..... 204

Figure 163. XPSWMM P-15 Hydrograph..... 204

Figure 164. XPSWMM P-15 Pollutograph..... 205

Figure 165. XPSWMM P-26 Hydrograph..... 205

Figure 166. XPSWMM P-26 Pollutograph..... 206

Figure 167. XPSWMM P-27 Hydrograph..... 206

Figure 168. XPSWMM P-27 Pollutograph..... 207

Figure 169. XPSWMM P-10 Hydrograph..... 208

Figure 170. XPSWMM P-10 Pollutograph..... 208

Figure 171. XPSWMM P-11 Hydrograph..... 209

Figure 172. XPSWMM P-11 Pollutograph..... 209

Figure 173. XPSWMM P-15 Hydrograph..... 210

Figure 174. XPSWMM P-15 Pollutograph..... 210

Figure 175. XPSWMM P-26 Hydrograph..... 211

Figure 176. XPSWMM P-26 Pollutograph..... 211

Figure 177. XPSWMM P-27 Hydrograph..... 212

Figure 178. XPSWMM P-27 Pollutograph..... 212

Figure 179. P-10 Hydrographs Indicating Simulations 1-4 and their PE Curves..... 213

Figure 180. P-11 Hydrographs Indicating Simulations 1-4 and their PE Curves..... 213

Figure 181. P-15 Hydrographs Indicating Simulations 1-4 and their PE Curves..... 214

Figure 182. P-26 Hydrographs Indicating Simulations 1-4 and their PE Curves..... 214

Figure 183. P-27 Hydrographs Indicating Simulations 1-4 and their PE Curves..... 215

LIST OF ACRONYMS

ARC	Applied Research Center
BC	Bear Creek
CI	Confidence Interval
DHI	Danish Hydraulic Institute
DOE	Department of Energy
EFPC	East Fork Poplar Creek
EPA	Environmental Protection Agency
OREIS	Oak Ridge Environmental Information System
ORNL	Oak Ridge National Laboratory
ORR	Oak Ridge Reservation
PPT	Parts Per Trillion
ROD	Record of Decision
RMSE	Root Mean Square Error
TMDL	Total Maximum Daily Load
TSS	Total Suspended Solids
UEFPC	Upper East Fork Poplar Creek
USGS	United States Geologic Survey
Y-12	Y-12 National Security Complex

LIST OF VARIABLES

A_{ft}	Cross sectional area
AD_c	ECO Lab advection-dispersion coefficient
$adss$	Adsorption
c	ECO Lab concentration
C	Soil water capacity
$dess$	Desorption
$difv$	Diffusion transfer coefficient in water
dz	Computational grid layer thickness
$dzds$	Thickness of diffusion layer in sediment
$dzwf$	Average thickness of water film through which metals diffuse
D_x, D_y, D_z	Dispersion coefficients in the x,y, and z-direction
$f_{biot.difw}$	Factor for diffusion due to bioturbation
h	Flow depth or hydraulic head
k_a	Adsorption rate [d^{-1}]
K_d	Mercury partitioning coefficient between particulate matter and water
K_{ds}	Mercury partitioning coefficient between sediment and pore water
K_s	Saturated hydraulic conductivity
k_s	Desorption rate in sediment [d^{-1}]
k_w	Desorption rate [d^{-1}]
M	Manning's M, the reciprocal of Manning's n (1/n)
P_c	ECO Lab processes
$pors$	Porosity of sediment
PPR	Particle production rate [g/m^2d]
q	Volumetric flow or discharge
$resv$	Resuspension
RR	Resuspension rate [g/m^2d]
S	Specific storage coefficient
S_c	ECO Lab sources and sinks
sev	Sedimentation

S_{fx}, S_{fy}	Friction slopes in x and y-direction
S_{HM}	Dissolved mercury concentration in water
S_{HMS}	Dissolved mercury concentration in sediment pore water
t	Time
TSS	Total suspended solids concentration
u, v, w	Flow velocities in the x, y, and z-direction
uh, vh	Discharge per unit length in x and y-direction
v_s	Settling velocity [m/d]
v_c	Critical current velocity for initiation of the movement [m/s]
X_{HM}	Adsorbed mercury concentration in suspended matter
X_{HMS}	Adsorbed mercury concentration in sediment
X_{SED}	Mass of sediment
Z	Ground surface elevation

INTRODUCTION

The United States remains adversely affected by the nuclear arms race of the Second World War. Today, uranium manufacturing plants like Y-12 in Tennessee are part of a long-term clean-up strategy in the US. In the 1950's and 60's Y-12 used millions of pounds of mercury to separate isotopes of lithium associated with nuclear weapons production at the site. Mercury deposits in sewers and surface waters continue to contaminate the watershed in which Y-12 resides. Contamination is found in groundwater, soils, surface water, and infrastructure. Mercury loading on East Fork Poplar Creek is carried downstream to Poplar Creek, the Clinch River, and Watts Bar Reservoir; affecting over 50 river miles in length and 2,336 lake acres in surface area. In 2008 the State of Tennessee listed portions of East Fork Poplar Creek as not supporting designated use classifications (including fish and aquatic life, irrigation, livestock watering and wildlife, and recreation) due to mercury.

It is possible to approximately determine the path of mercury through the affected watershed using advanced watershed modeling software. MIKE SHE is an integrated surface water and groundwater software that can simulate the entire land phase of the hydrologic cycle, map the vulnerability of the aquifer, and delineate the flood-plain for the watershed.

The Y-12 National Security Complex is situated in the northeast section of East Fork Poplar Creek watershed; a 12-digit HUC watershed of about 77 sq km (19,000 acres). The model offers the ability to input relevant hydrologic parameters to create a watershed model which is capable of simulating flow in the subsurface (saturated and unsaturated zones) and surface sub-domains (overland and river) and contaminant transport and exchange between various sub-domains using an advection-dispersion module. Topography, river networks, flow velocities, precipitation, soils, aquifers, vegetation, and land use are some of the parameters included in the development of the watershed model.

A 3-D model was developed for visualization of the estimated localized mercury distribution under the Y-12 study site, as well as an integrated surface and groundwater model to simulate the

broader range mercury distribution throughout the East Fork Poplar Creek watershed. Historical records derived from the preliminary data search were used as input for model development.

A series of 3-dimensional numerical simulations modeled the mercury fate and transport in the soil and groundwater in East Fork Poplar Creek watershed for different hypothetical scenarios to provide useful information that can support future cleanup activities across ORR. Simulations include:

- Seasonal fluctuation of precipitation
- Extreme flood events

A primary emphasis was on: effects of seasonal rainfall; surface and groundwater flow rates; and contaminant adsorption/desorption and retardation mechanisms and rates.

The model can be also used to simulate biogeochemical processes and the sources and cycling of nutrients, sulfur, and organics in the ecosystem which can be analyzed to examine the complex involvement of nutrients, organics, and inorganic species (including sulfur) in methylmercury production and bioaccumulation. A major focus will be on ecosystem responses to variations in contaminant loading (changes in external and internal loading in time and space), and how imminent ecosystem restoration may affect existing contaminant pools.

The overall objective of this project was to develop an integrated soil and groundwater model to predict the fate and transport of mercury in the soil, sediment, groundwater and surface water at Oak Ridge Reservation under varying environmental conditions. The focal objectives are to provide critical data on the spatial distribution of mercury species to develop a three-dimensional model of the site and to allow accurate simulations of the current seasonal transport of mercury in the area.

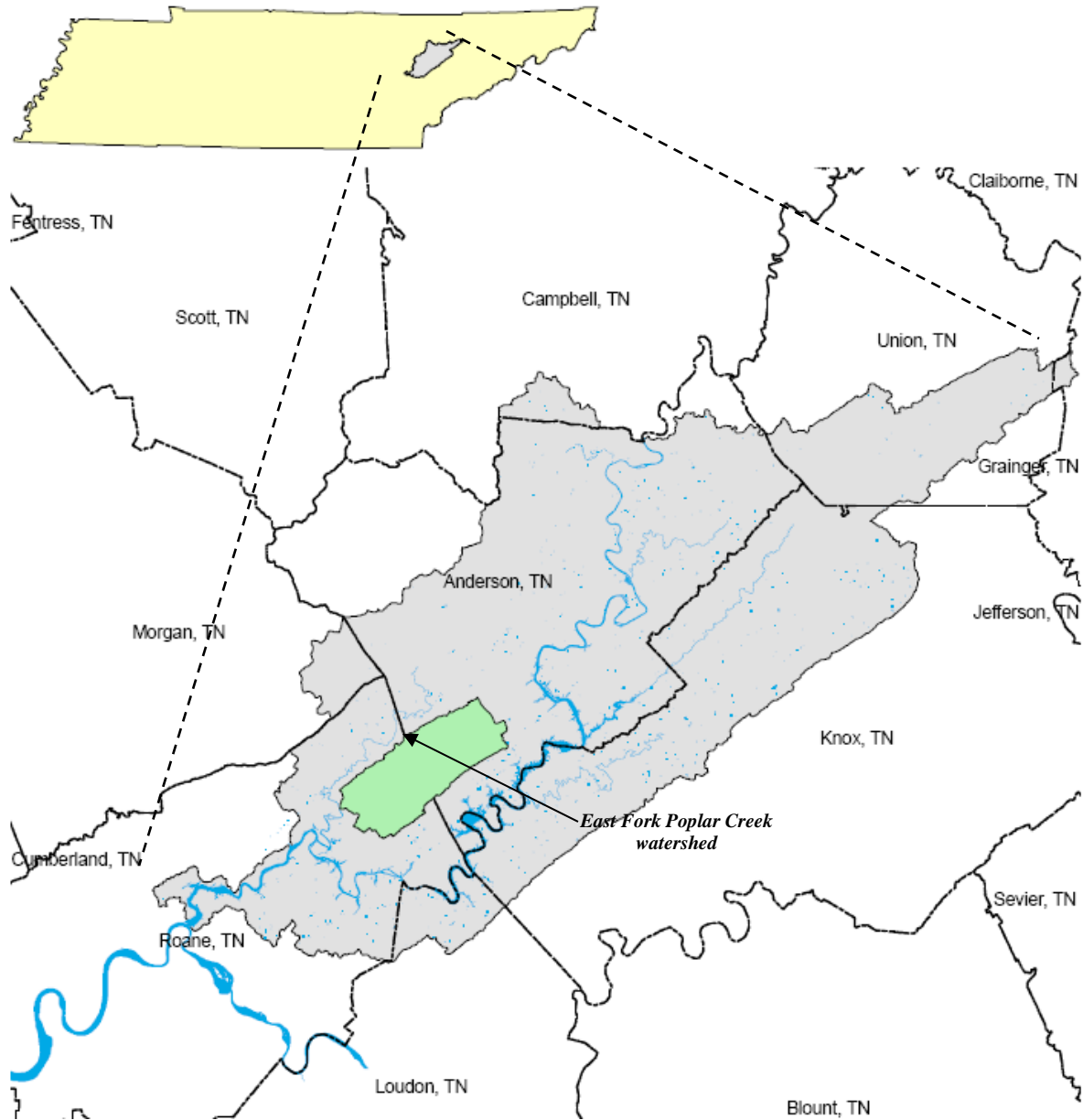


Figure 1. Lower Clinch River Watershed in Tennessee.

The process of development of the integrated hydrological model was based on input of a number of hydrological, transport and mercury speciation parameters. Modeling aids in the determination of potential mercury soil and groundwater contamination risks and appropriate remedial alternatives during future cleanup operations at ORR.

East Fork Poplar Creek watershed is enclosed by the City of Oak Ridge in Tennessee. Oak Ridge is divided by Anderson County to the north and east and Roane County to the south and west. The entire city is about 233 sq km, or 122 sq km in Anderson County and 112 sq km in Roane County.

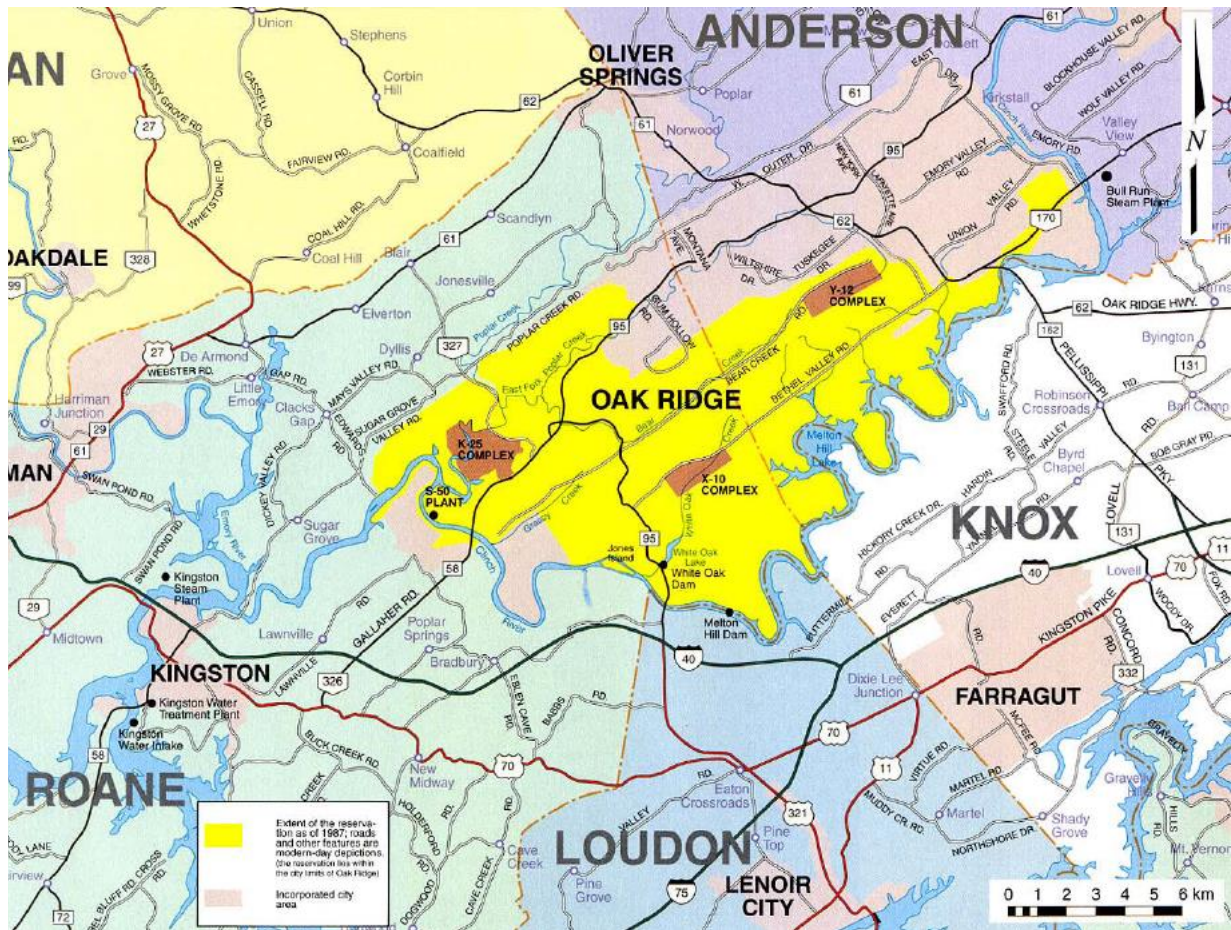


Figure 2. Location of the Oak Ridge Reservation.

East Fork Poplar Creek watershed is a sub-watershed within the Poplar Creek watershed. Poplar Creek watershed is one of four sub-watersheds of the Lower Clinch River watershed in eastern Tennessee. Figure 1 shows the location of East Fork Poplar Creek watershed within the Lower Clinch River watershed.

For the East Fork Poplar Creek watershed, the population as of 1990 was 15,483 people. This number is obtained from the Tennessee Block Centroid Populations produced by ESRI in 2000.

Oak Ridge Reservation (ORR) is located in Roane and Anderson Counties in the City of Oak Ridge, Tennessee as shown in yellow in Figure 2.

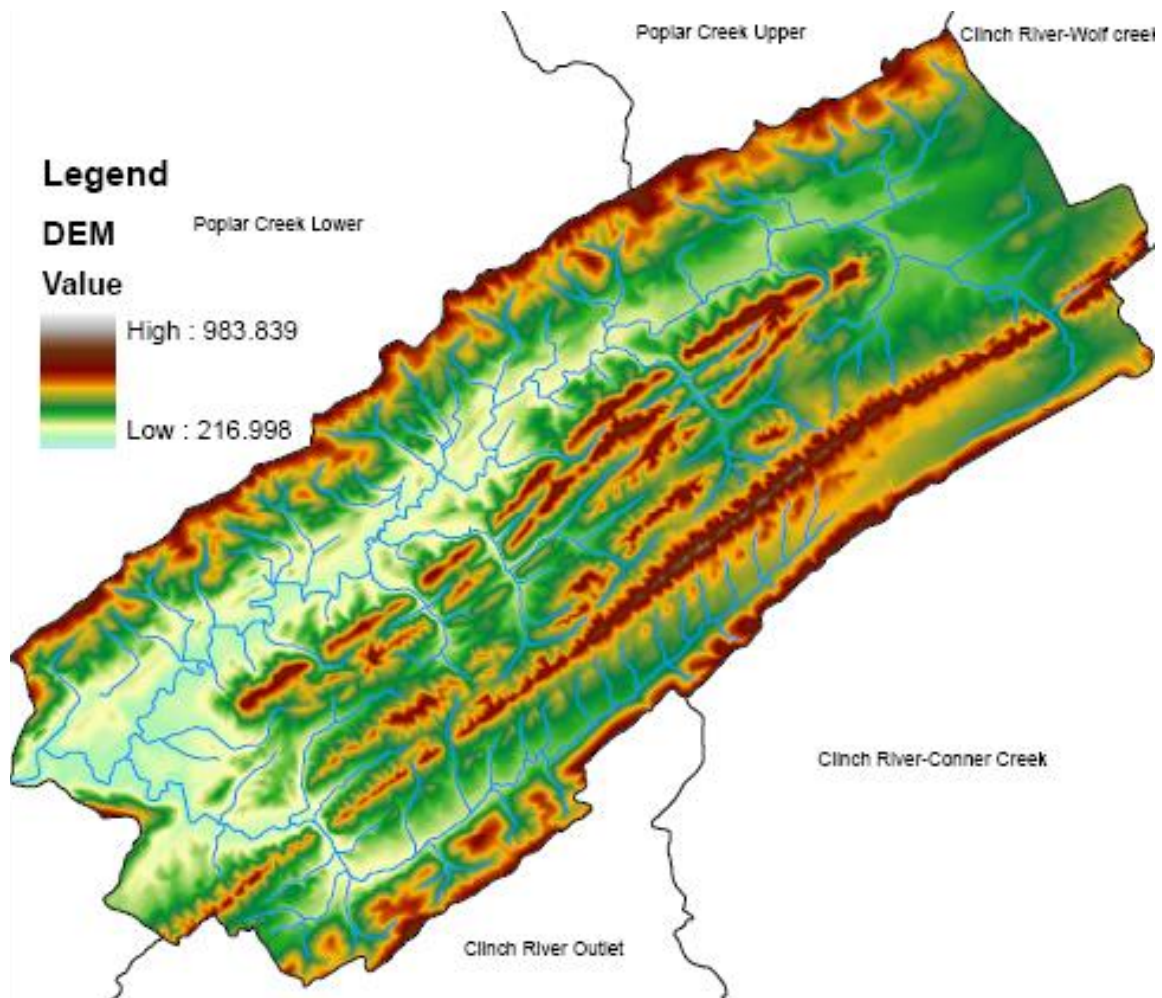


Figure 3. Digital Elevation Map of East Fork Poplar Creek Watershed.

Tennessee Block Centroid Populations provides population for each U.S. Census block centroid within Tennessee. The points represent the centroids for the smallest entity for which the Census Bureau collects and tabulates decennial census information within Tennessee; bounded on all sides by visible features such as streets, streams, and railroad tracks, and by invisible boundaries such as city, town, and county limits.

East Fork Poplar Creek watershed is home to the Y-12 National Security Complex. Built in 1943, the complex served as the first offensive of the Manhattan Project with the primary

mission of separating uranium-235 from natural uranium via electromagnetic separation. The Y-12 Complex is part of Oak Ridge Reservation (ORR) and is within the city of Oak Ridge.

Within the watershed, Y-12 is located between the upper reaches of East Fork Poplar Creek and the upper reaches of Bear Creek. It lies in the valley (Bear Creek Valley) between the northern Pine Ridge and the southern Chestnut Ridge. Figure 3 shows the location and size of EFPC as well as the terrain. While Y-12 is a part of ORR, East Fork Poplar Creek watershed also encompasses large areas that are not part of ORR but that might drain into ORR.

From the Digital Elevation Model of East Fork Poplar Creek Watershed, the corduroy-like features of the Appalachian Valley and Ridge Province are visible. The Appalachian Valley and Ridge Province, as shown in Figure 4, consists of alternating beds of hard and soft Paleozoic sedimentary rocks, which have been folded as a result of several continental collisions that formed the Appalachian chain and the Pangaea supercontinent some 300 to 400 million years ago. Black Oak Ridge to the northwest and Chestnut Ridge to the southeast form the two major boundaries of East Fork Poplar Creek, as illustrated in Figure 3. Small rivers, such as East Fork Poplar Creek and Bear Creek, have taken their shape and direction from the valleys of the region where the soft sedimentary rock is easily eroded.

The watershed lies within the Ridge and Valley Level III ecoregion and contains two Level IV ecoregions:

- The Southern Limestone /Dolomite Valleys and Low Rolling Hills – predominately limestone or cherty dolomite in low rolling ridges and valleys
- The Southern Dissected Ridges and Knobs – crenulated, broken, or hummocky ridges; shale is common, mixed with other geologic materials

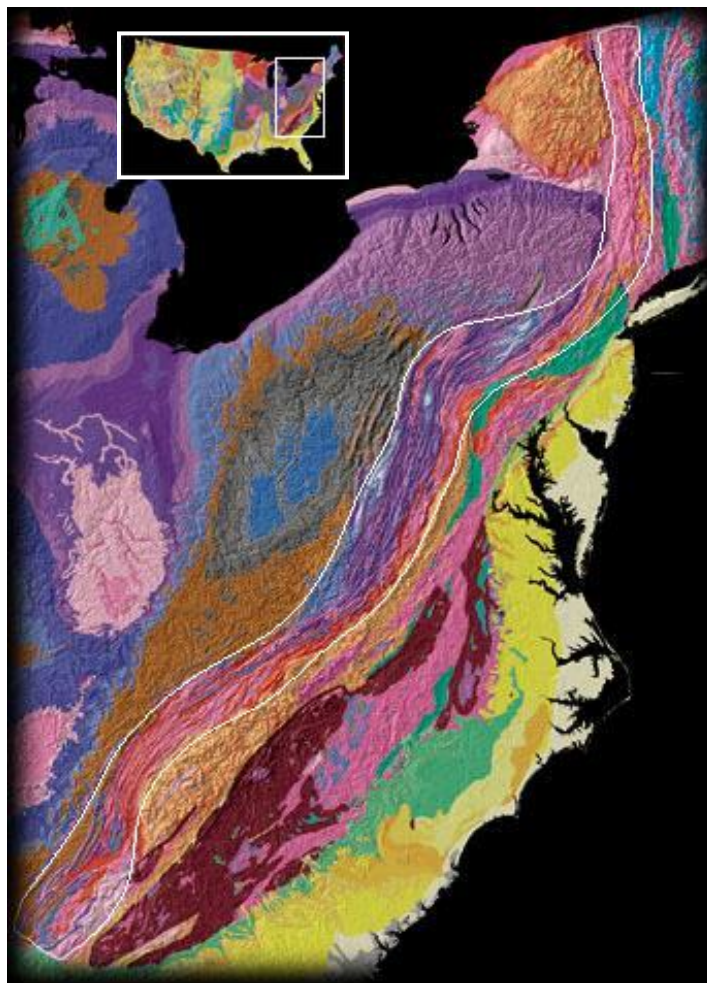


Figure 4. Appalachian Valley and Ridge Province.

East Fork Poplar Creek Watershed contains two small rivers (>12,500 km long) and several tributaries which are illustrated in Figure 5.

East Fork Poplar Creek runs primarily in a NE to SW direction and is about 24,610 meters long. The creek bottom begins at a depth of about 287 m above sea level and ends at about 226 m near the river's hydrologic boundary, for a general slope of about 0.23% or 0.13°. Stream valley widths, along East Fork Poplar Creek, range from about 60 to 300 meters. East Fork Poplar Creek receives discharge from four major streams (Bear Creek, Gum Hollow Branch, Mill Branch, and Pin Hook Branch) and about 30 unnamed tributaries. In total, East Fork Poplar Creek receives discharge from about 107 kilometers of streams.

- *Bear Creek* is the second largest stream in the watershed at about 12,700 meters long. This stream runs mostly parallel to East Fork Poplar Creek. The creek bottom begins at a depth of about 309 m above sea level and ends at about 227 m where the river discharges to East Fork Poplar Creek, for a general slope of about 0.62% or 0.354°. Stream valley widths, along Bear Creek, range from about 50 to 300 meters. Bear Creek receives discharge from about 28 unnamed tributaries for a total of about 24 kilometers of streams.
- *Gum Hollow Branch* is the third largest stream in the watershed at about 4,130 meters long. This stream receives discharge from about 8 unnamed tributaries. In total, Gum Hollow Branch receives discharge from about 6.7 kilometers of streams before discharging to East Fork Poplar Creek.
- *Mill Branch* is about 3,270 meters long and receives discharge from about 5 unnamed tributaries. In total, Mill Branch receives discharge from about 7.2 kilometers of streams before discharging to East Fork Poplar Creek.
- *Pin Hook Branch* is about 2,040 meters long and receives discharge from about 4 unnamed tributaries. In total, Pin Hook Branch receives discharge from about 1.8 kilometers of streams before discharging to East Fork Poplar Creek.

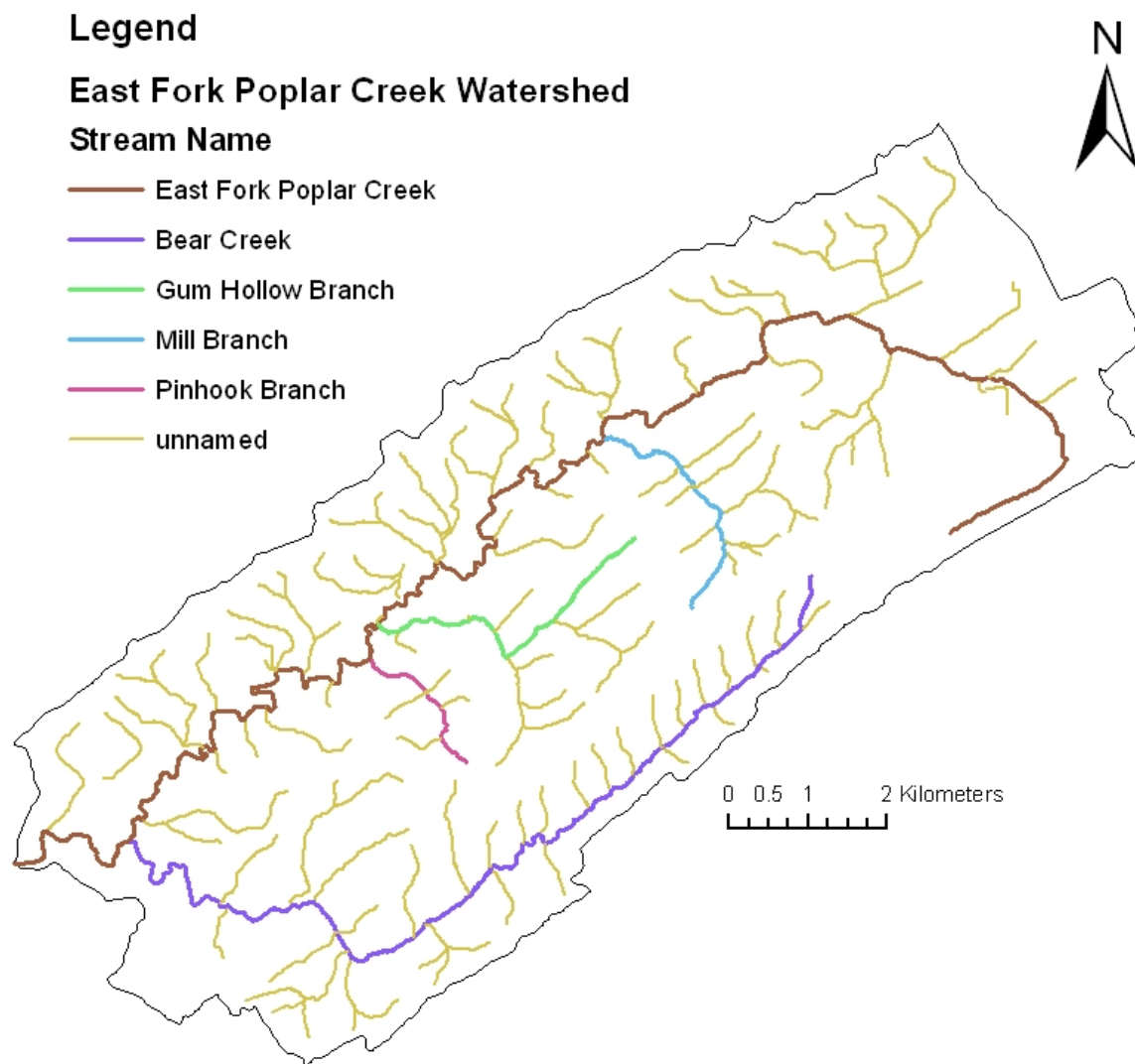


Figure 5. Streams within East Fork Poplar Creek Watershed.

Figure 5 shows the named streams in EFPC watershed. All unnamed streams are named with 2-digit numbers with a prefix of “Branch”, starting the count at 1.

East Fork Poplar Creek watershed is host to a variety of land uses within its 19,000 acre expanse. The city of Oak Ridge, TN is located in the northeast section of the watershed and is home to over 30,000 people. Adjacent to Oak Ridge, the Y-12 National Security Complex operates within 811 acres of the East Fork Poplar Creek watershed and employs over 6,000 workers. The Y-12 Complex alone occupies about 4.3% of the total watershed area. An aerial sweep of the

watershed reveals new residential areas along East Fork Poplar Creek and southwest of the City of Oak Ridge.

The 2001 National Land Cover Dataset provides 21 classifications of land uses for the US. The Dataset is gathered over large areas using LANDSAT imagery and high-altitude, infrared photography. Due to the level of accuracy of this data (Level I and II), it will only be used to provide general characteristics about the watershed.

Table 1. NLCD 2001 Land Cover

Land Use	Percent of Total Area
Forest Land	55.3%
Agricultural Land	33.3%
Treeless area	5.2%
Urban or Built-Up	0.076%

According to Table 1, the watershed is over 55% forest land, with about 87% of the forested areas considered deciduous forests (typical hardwoods such as oaks, maples, hickories, etc.). About one third of East Fork Poplar Creek watershed is used for agricultural purposes. The agricultural area is fairly evenly divided between cropland and pasture (e.g., wheat fields and grazing pastures), orchards and groves (fruit and nut crops), and confined feeding operations (livestock pens).

The Tennessee Wildlife Resources Agency produced a more detailed and specified land use map in 1997 called Tennessee Land Use/Land Cover. This map is a generalized version of the detailed vegetation map that was prepared in compliance with the National Gap Analysis Program effort. The land cover types were derived from classification techniques performed on Landsat TM imagery. The forest classes from the land use/land cover file were extracted from the satellite imagery and reclassified. Forest communities were interpreted from aerial videography acquired in April 1995 and correlated to the satellite imagery.

Table 2. NLCD 2001 Land Use Classification and Manning’s Number

Classification (NLCD2001)	NLCD 2001 Code	Anderson Level 1 Code	Area(m ²)	%/Area	Manning’s M number
Open Water	11	1	11410200	4%	50
Developed, Open Space	21	2	28142100	10%	50
Developed, Low Intensity	22	2	23315400	8%	20
Developed, Medium Intensity	23	2	11262600	4%	10
Developed, High Intensity	24	2	5488200	2%	7
Barren Land, Rock, Sand, Clay	31	3	1053900	0%	11
Deciduous Forest	41	4	124686000	45%	10
Evergreen Forest	42	4	15189300	5%	9
Mixed Forest	43	4	9044100	3%	10
Shrub, Scrub	52	5	300600	0%	20
Grassland, Herbaceous	71	5	4901400	2%	29
Pasture, Hay	81	6	34282800	12%	30
Cultivated Crops	82	6	799200	0%	27
Woody Wetlands	90	7	9374400	3%	10
Emergent Herbaceous Wetlands	95	7	5400	0%	22

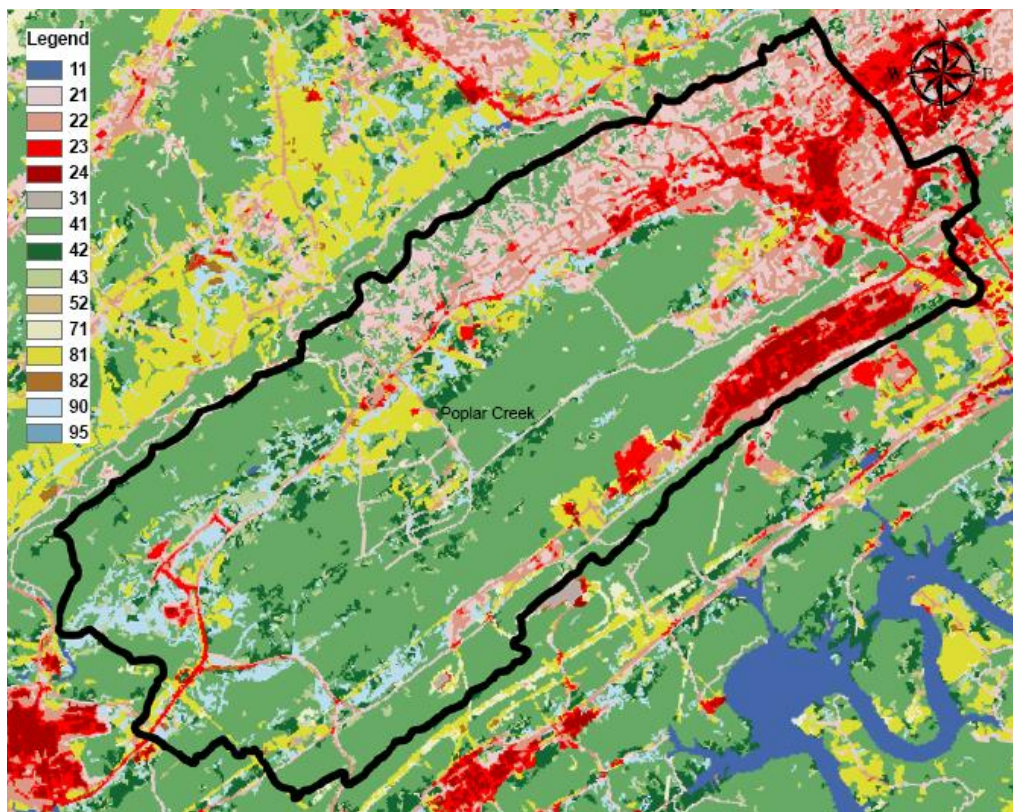


Figure 6. EFPC land use.

The vegetation of the EFPC watershed area was described in 8 types:

Table 3. Land Use, Area and Fraction of EFPC

Row Labels	Code	AREA[m ²]	Percent
Open Water	1	322733	0.03%
Forested Wetland	2	107534	0.01%
Pasture/Grassland	4	227479956	18.13%
Row Crop	5	11293652	0.90%
Upland Deciduous Forest	7	695902742	55.46%
Upland Mixed Forest	8	50445337	4.02%
Upland Coniferous Forest	9	108314635	8.63%
Urban/Developed	10	160899077	12.82%

Legend

tnlandcov_Clip_Project

VALUE, CLASS_NAME, CLASS_NAME

- 1, Open Water, Open Water
- 2, Forested Wetland, Forested Wetland
- 4, Pasture/Grassland, Pasture/Grassland
- 5, Row Crop, Row Crop
- 7, Upland Deciduous Forest, Upland Deciduous Forest
- 8, Upland Mixed Forest, Upland Mixed Forest
- 9, Upland Coniferous Forest, Upland Coniferous Forest
- 10, Urban/Developed, Urban/Developed

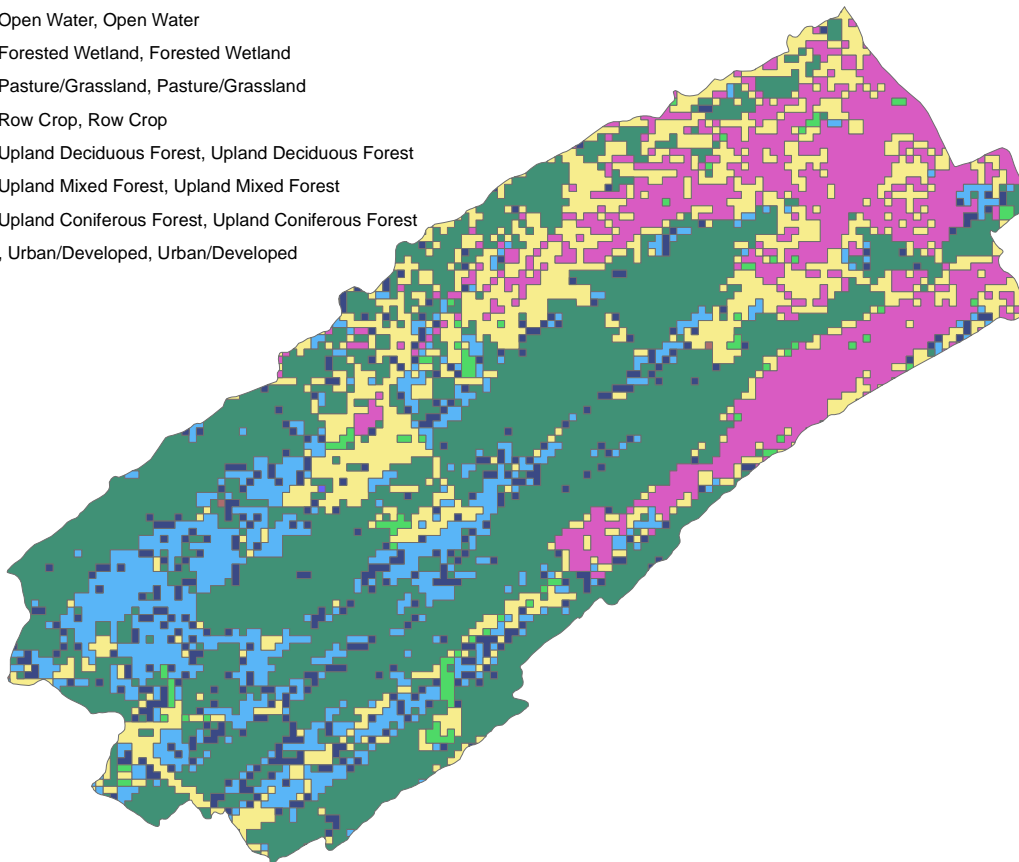


Figure 7. Discretization of land cover data used for the hydrological model.

Figure 7 illustrates the Tennessee Land Use/Land Cover data that will be used for the model development. The land use classifications were assigned to the grid using Landsat imagery combined with aerial videography, creating a more accurate map.

The data also located about 5.2% treeless areas (classified as tundra) which, upon further review of aerial photography, consisted of golf courses, memorial parks, and other recreational areas where the trees were cleared. About 3.7% of the area covered in perennial ice or snow, which is an obvious error in the data and, upon further review of the aerial photography, consisted of various buildings and roadways (anything that was highly reflective).

Although only 0.076% of the land cover was considered urban or built-up, errors in land use classification could probably bring the number up to about 9%. To further illustrate the urbanity of the watershed, a 2001 NLCD Impervious Surface raster was analyzed. About 9.3% of the total watershed area has an imperviousness of 50% or greater. This could be anything from residential areas to cities and highway. About 4.4% of the total area has an imperviousness of 75% or greater. This includes most of the Y-12 National Security Complex and the commercial areas in the City of Oak Ridge.

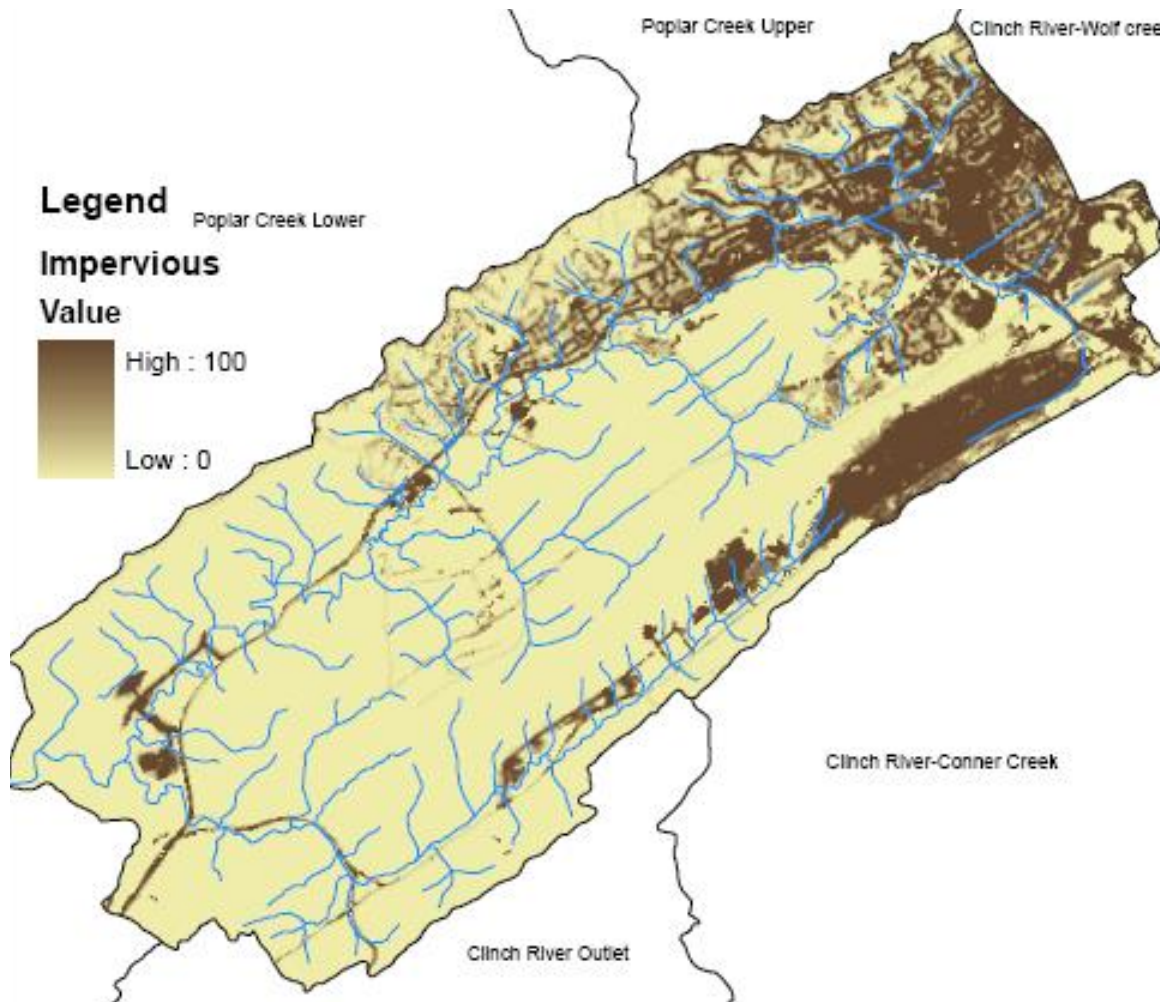


Figure 8. Percent imperviousness.

Figure 8 maps the developed areas of EFPC watershed, including roads and buildings, by illustrating the percent of impervious cover. Over 82.3% of the total area of East Fork Poplar Creek watershed has an imperviousness of 25% or less. This indicates that, overall, the watershed is mostly undeveloped or agricultural land. This conclusion is compatible with the land use data, which establishes that about 88.6% of the watershed is forested or agricultural.

DEVELOPMENT OF AN INTEGRATED SURFACE AND SUBSURFACE FLOW MODEL

Model Theoretical Basis

The modeling system consists of coupled MIKE SHE (a 3-dimensional saturated and unsaturated groundwater flow, 2-dimensional overland flow model) and MIKE 11 (1-dimensional river flow model). MIKE SHE is a deterministic, physically based & full distributed hydrological modeling system, Abbott and Refsgaard [2]. It consists of the Water Movement and Water Quality modules. The hydrological processes are described mostly by physical laws (laws of conservation of mass, momentum and energy). The 1-D and 2-D diffusive wave Saint Venant equations describe channel and overland flow, respectively. The Kristensen and Jensen methods are used for evapotranspiration, the 1-D Richards's equation for unsaturated zone flow, and a 3-D Boussinesq equation for saturated zone flow. These partial differential equations are solved by finite difference methods, while other methods (interception, evapotranspiration and snowmelt) in the model are empirical equations obtained from independent experimental research [13]. MIKE 11 is a one-dimensional modeling tool for the detailed analysis, design, management and operation of both simple and complex river and channel systems. The MIKE 11 Hydrodynamic (HD) module solves the vertically integrated equations for the conservation of continuity and momentum, i.e. the Saint Venant equations [13]. The HD module is the nucleus of the MIKE 11 modeling system and forms the basis for most modules including Flood Forecasting, Advection-Dispersion, Water Quality and Non-cohesive sediment transport modules. The basic steps for modeling the surface and subsurface hydrology include:

- i. Modeling of the saturated flow using MIKE SHE.
- ii. Incorporation of evapotranspiration and unsaturated flow into MIKE SHE.
- iii. Modeling the river flow using MIKE 11.
- iv. Adding the advection and dispersion component into MIKE SHE and MIKE 11.
- v. Coupling MIKE SHE and MIKE 11 to create an integrated hydrological model.
- vi. Uncertainty analysis of hydrologic and advection-dispersion parameters, model calibration and verification.

- vii. Simulation of accidental mercury releases in the environment caused by demolition activities.

Coupling of MIKE SHE and MIKE 11 HD

MIKE SHE and MIKE 11 were coupled by defining branches (reaches) where MIKE 11 HD interacts with MIKE SHE. The hydrologic components of MIKE SHE are directly coupled to DHI's river hydraulic program MIKE 11. The MIKE SHE-MIKE 11 coupling enables:

- One-dimensional simulation of river flows and water levels using the fully dynamic Saint Venant equations.
- Simulation of a wide range of hydraulic control structures, such as weirs, gates and culverts.
- Area-inundation modelling, using a simple flood-mapping procedure that is based on simulated river water levels and a digital terrain model.
- Dynamic overland flooding flow to and from the MIKE 11 river network.
- Full, dynamic coupling of surface and sub-surface flow processes in MIKE 11 and MIKE SHE.

The list of streams and the coupling with MIKE SHE is shown in the Appendices Table 57 on page 233.

To simulate flooding on the flood plain the option for Direct Overbank Spilling to and from MIKE 11 was used. In this case the MIKE 11 cross-sections are normally restricted to the main channel. The flood plain is defined as part of the MIKE SHE topography. Since, the bank elevation is used to define when a cell floods, a special emphasis was placed on ensuring that the cross-sections are consistent with the topography, especially in the areas where flooding was simulated. The table in the simulation log file was used to locate any inconsistencies and the elevation data of the cross section was revised. The availability of fine grid and detailed DEM has reduced the inconsistencies and the amount of interpolation and averaging when creating the model topography.

Subsequently the MIKE SHE and MIKE 11 models were modified to work together properly by removing the specified groundwater table in MIKE 11 and adjusting the SZ drainage elevations using for testing purposes.

To simulate the exchange between river and groundwater an assumption was made that the river is in full contact with the aquifer material lack of low permeable lining of the river bed which is typical for mountain areas. In this case, the only head loss between the river and the grid node is that created by the flow from the grid node to the river itself. This is typical of gaining streams, or streams that are fast moving.

Figure 9 shows a typical MIKE SHE river cross section compared to an equivalent MIKE 11 HD cross section. In this case, the conductance, C , between the grid node and the river link is given by:

$$C = \frac{K \cdot da \cdot dx}{ds} \quad (1)$$

where K is the horizontal hydraulic conductivity in the grid cell, da is the vertical surface available for exchange flow, dx is the grid size used in the saturated zone component, and ds is the average flow length. The average flow length, ds , is the distance from the grid node to the middle of the river bank in the triangular, river-link cross-section. ds is limited to between 1/2 and 1/4 of a cell width, since the maximum river-link width is one cell width (half cell width per side).

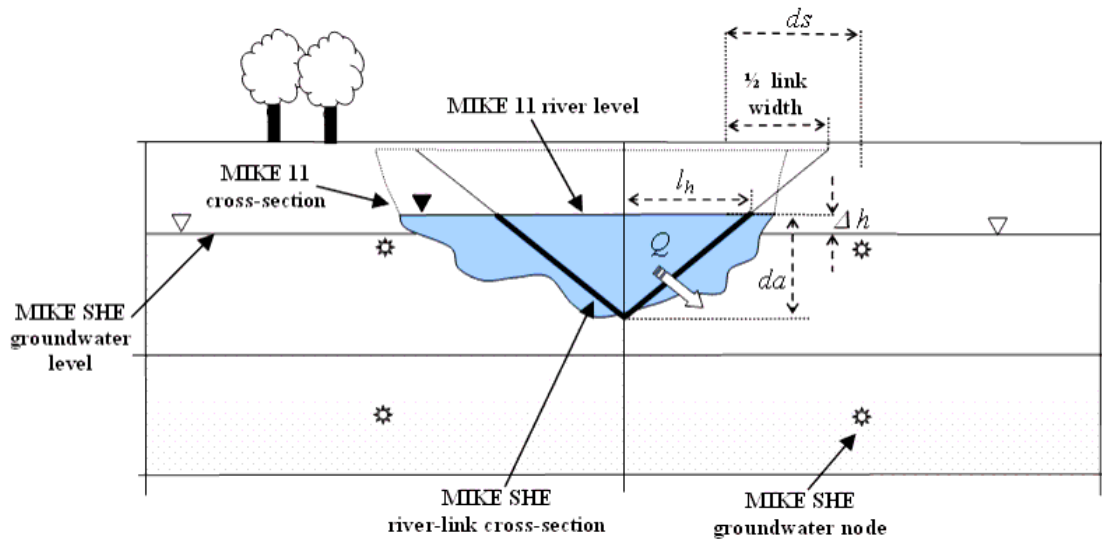


Figure 9. A typical MIKE SHE river link cross-section.

The program allows three methods for calculating da :

- If the water table is higher than the river water level, da is the saturated aquifer thickness above the bottom of the river bed. Note, however, that da is not limited by the bank elevation of the river cross-section, which means that if the water table in the cell is above the bank of the river, da accounts for overland seepage above the bank of the river.
- If the water table is below the river level, then da is the depth of water in the river.
- If the river cross-section crosses multiple model layers, then da (and therefore C) is limited by the available saturated thickness in each layer. The exchange with each layer is calculated independently, based on the da calculated for each layer. This makes the total exchange independent of the number of layers the river intersects.

This formulation for da assumes that the river-aquifer exchange is primarily via the river banks, which is consistent with the limitation that there is no unsaturated flow calculated beneath the river.

The MIKE 11(HD) hydraulic model uses the precise cross-sections, as defined in the MIKE 11 .xns11 (cross-section) file, for calculating the river water levels and the river volumes. However, the exchange of water between MIKE 11 and MIKE SHE is calculated based the river-link cross-

section. The river-link uses is a simplified, triangular cross-section interpolated (distance weighted) from the two nearest MIKE 11 cross-sections. The top width is equal to the distance between the cross-section's left and right bank markers. The elevation of the bottom of the triangle equals the lowest depth of the MIKE 11 cross-section (the elevation of Marker 2 in the cross-section). The left and right bank elevations in MIKE 11 (cross-section markers 1 and 3 in MIKE 11) are used to define the left and right bank elevations of the river link.

Model Domain

The domain of the project is defined as the entire East Fork Poplar Creek watershed as delineated by the USGS. It is formally recognized by its assigned 12-digit Hydrologic Unit Code (HUC) 060102070302. EFPC watershed has a large drainage area of about 29.7 square miles (mi²). This domain was chosen to illustrate large-scale fluctuations in the mercury cycling and transport.

Table 4. Basin Characteristics

Parameter	Value
Total drainage area, in square miles	28.8
Area that contributes flow to a point on a stream, in square miles	28.8
Percent of area within Hydrologic Area 1	100
Percent of area within Hydrologic Area 2	0
Percent of area within Hydrologic Area 3	0
Percent of area within Hydrologic Area 4	0
Tennessee climate factor, 2-year interval	2.249
Streamflow-recession index, in days per log cycle of decrease in discharge	67
Stream slope 10 and 85 method in feet per mile	11.3
Percent area underlain by soil permeability of at least 2 in/hr	39
Soil Permeability - in/hr	2.43

The basin delineation was obtained from reference [52].

The domain was created by utilizing a GIS shapefile of the East Fork Poplar Creek watershed (derived from the USGS National Hydrography Dataset). In Figure 10, grid cells inside the model domain are assigned a value of 1 and grid cells on the model boundary are assign a value

of 2 as required. This distinction between interior grid cells and boundary cells is to facilitate the definition of boundary conditions. For example, drainage flow can be routed to external boundaries but not to internal boundaries.

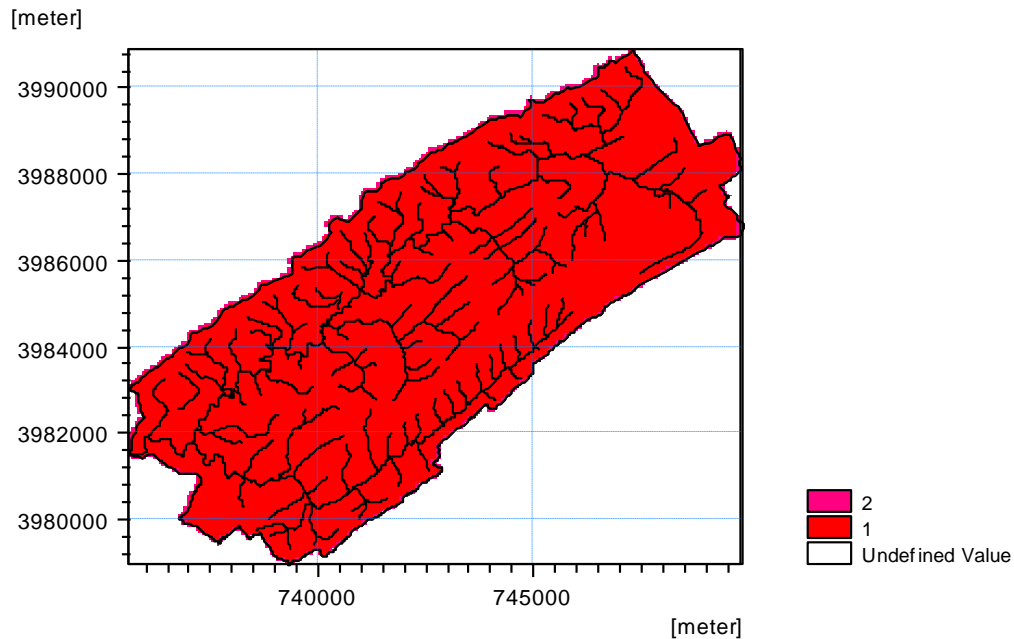


Figure 10. Model Domain.

Topography

The model input for topography was generated by adding a 5 m Contour GIS shapefile derived from the USGS GIS database to the MIKE SHE model. The model interpolates this via inverse distance weighted (IDW) gapfilling into a gridded surface. This was then exported as a .dfs2 file, which is a native MIKE SHE file format. The .dfs2 file was then used to replace the Contour shapefile in the model.

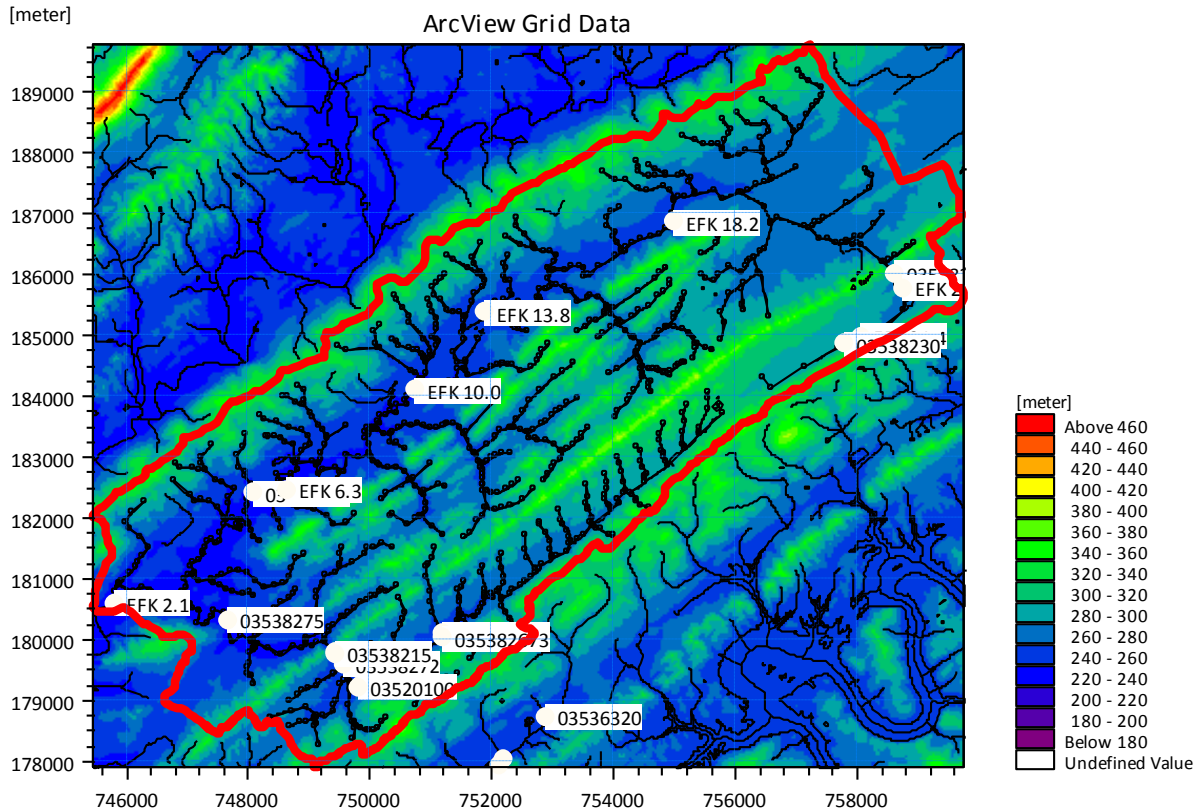


Figure 11. Site Topography.

Topography of the site shows the parallel ridge and valley features which run diagonally in the graph. Another visible feature is the increasing steepness of the East Fork Poplar Creek river valley banks from the upper to the lower reaches of the river; this feature relates to increasing stream flows due to diverging streams and basin flow. The City of Oak Ridge lies on relatively even surface at around 270 to 280 meters above mean sea level.

Climate Data

The climate data was acquired from the NOAA climatological dataset compiled for the state of Tennessee. Precipitation data is represented as water equivalent totals and includes liquid and melted frozen precipitation. For the purposes of this project it is unnecessary to include separate snow melt data, as it is summarized in the precipitation data.

Precipitation

For use in MIKE SHE, the Precipitation Rate can be specified as a rate (e.g., mm/hr) or as an amount (e.g., mm). If an amount is used, MIKE SHE automatically converts this to a rate during the simulation. If a rate is used, then the EUM Data Units must be Precipitation and the time series must be Mean Step Accumulated. If an amount is used, the EUM Data Units must be Rainfall and the time series must be Step Accumulated. (See MIKE SHE Manual Volume 2, page 58).

For the model, the precipitation rate time series used a Step Accumulated Rainfall for the Rainfall data in millimeters for the duration of one day. Data has been gathered for approximately 50 years (01/01/1950-12/31/2008); however, MIKE SHE will only use the data within the specified Simulation Period.

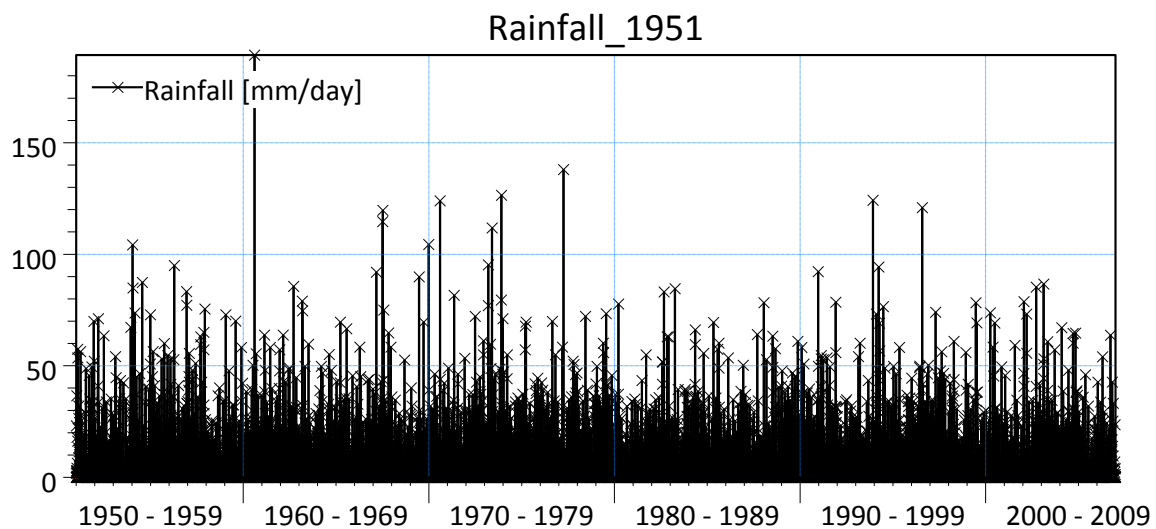


Figure 12. Precipitation at ORR.

Figure 12 illustrates the variations of the Rainfall timeseries for the period between 1/1/1950 and 12/31/2008.

The precipitation is one of the critical variables in the integrated hydrological model, which determines the surface water flows in the watershed and the dynamics of the groundwater table. The selected time period shows a typical variability of rainfall events within a month and

includes the highest daily rainfall event (85 mm/day). This approach ensures the performance of the model for critical events.

Figure 12 shows the average recurrence interval and the duration of precipitation events which were obtained from NOAA [226] and used to determine the effect of extreme events on the hydrology of the site.

For each of the simulation runs, a preliminary simulation was executed starting three months earlier than the specified time period and the result were saved and used for hot start. The purpose of this preliminary simulation was to ensure that the system is fully developed.

Evapotranspiration

The calculation of evapotranspiration uses meteorological and vegetative data to predict the total evapotranspiration and net rainfall due to:

- Interception of rainfall by the canopy,
- Drainage from the canopy to the soil surface,
- Evaporation from the canopy surface,
- Evaporation from the soil surface, and
- Uptake of water by plant roots and its transpiration, based on soil moisture in the unsaturated root zone.

MIKE SHE models ET using two distinct methods. The primary ET model is utilizes formulas derived from the work of Kristensen and Jensen (1975). In this model, the actual evapotranspiration and the actual soil moisture status in the root zone is calculated from the potential evaporation rate, along with maximum root depth and leaf area index for the plants.

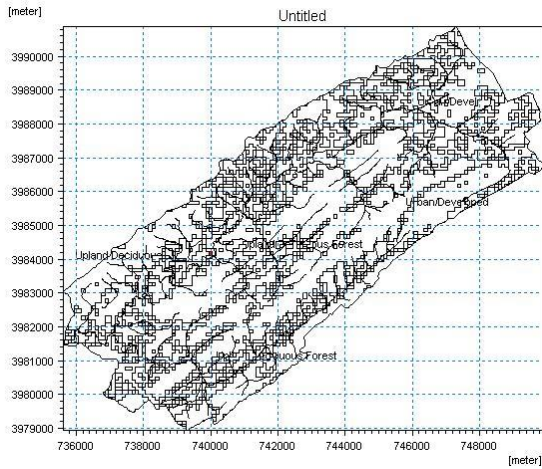
The 2-Layer Water Balance Method is an alternative to the more complex unsaturated flow process coupled to the Kristensen and Jensen module for describing evapotranspiration. The 2-

Layer Water Balance Method is based on a formulation presented in Yan and Smith (1994), the main purpose of which is to calculate actual evapotranspiration and the amount of water that recharges the saturated zone. The module is particularly useful for areas with a shallow ground water table, such as swamps or wetlands areas, where the actual evapotranspiration rate is close to the reference rate. The 2-Layer Water Balance Method includes the processes of interception, ponding, and evapotranspiration, while considering the entire unsaturated zone to consist of two 'layers' representing average conditions in the unsaturated zone. The vegetation is described in terms of leaf area index (LAI) and root depth.

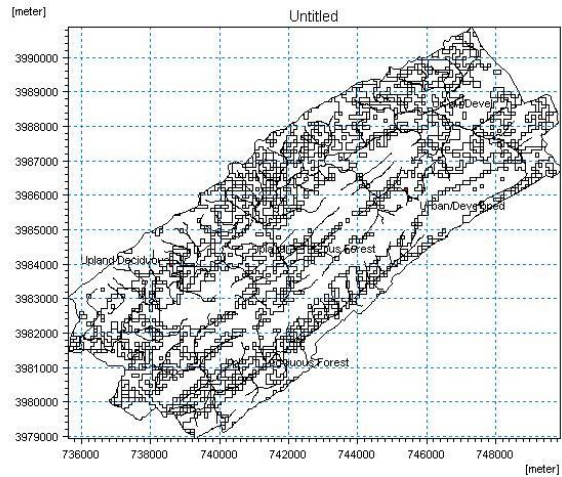
At this point in the model setup, only a reference ET is needed for the Climate section. The reference evapotranspiration is the rate of ET from a reference surface with an unlimited amount of water. This value is independent of everything but climate and can be calculated from weather data. Tennessee has an annual evapotranspiration of about 28.7 inches, therefore a constant Reference ET value of 0.0033 inches/hr was used. The reference ET will then be adjusted according to the vegetation data (leaf area index and root depth) found in the following section (see Table 5).

Land Use

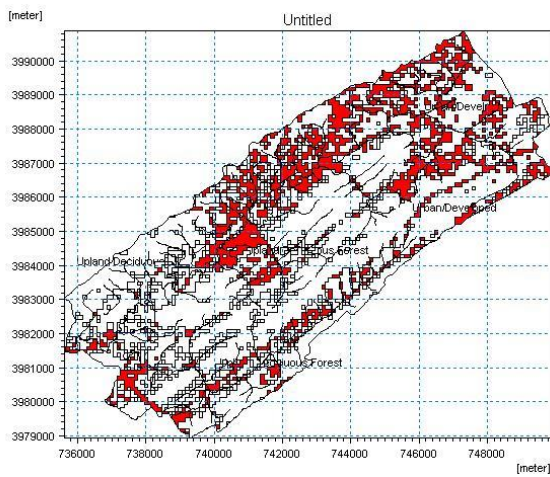
Land cover data was downloaded from the Tennessee Spatial Data Server in the form of a GIS shapefile, which was imported into the model. The following figures display snapshots of the polygons (highlighted in red in each figure) representing various vegetation types.



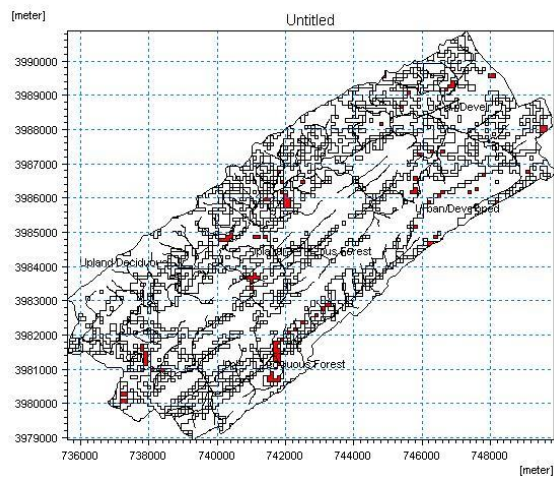
Forested Wetland



Open Water

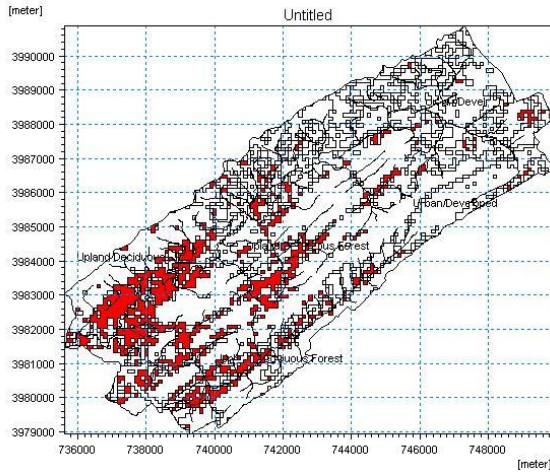


Pasture/Grassland

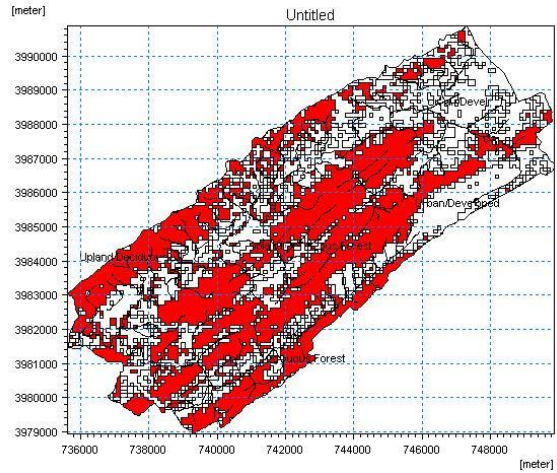


Row Crop

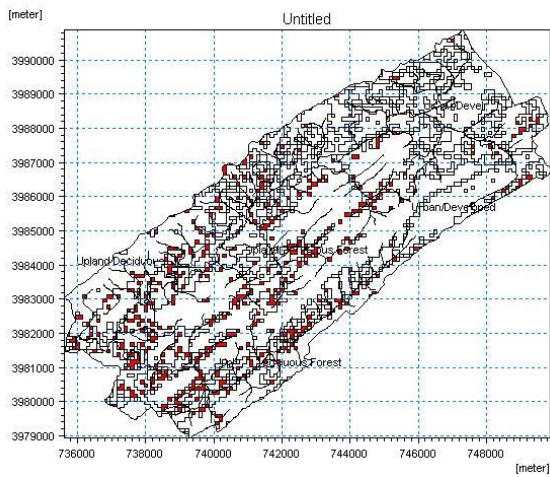
Figure 13. Land Use maps (A).



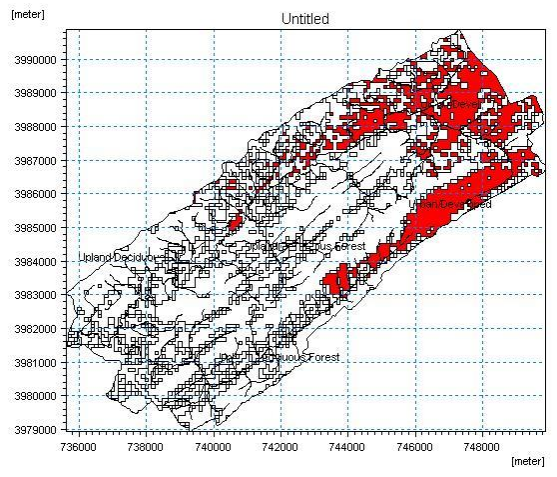
Upland Coniferous Forest



Upland Deciduous Forest



Upland Mixed Forest



Urban/Developed

Figure 14. Land Use maps (B).

The land use was imported as vegetation maps and assigned Leaf Area Index (LAI) constant values and Root Depth (RD) constant values defined the MIKE SHE Vegetation Database. Table 5 shows the LAI and RD values assigned for each feature.

Table 5. Vegetation Data

Grid Code	Class Name	LAI	RD (inch)
1	Upland Deciduous Forest	4.9	173.228
2	Pasture/Grassland	2.6	43.037
3	Urban/Developed	0	0
4	Upland Mixed Forest	3.8	157.48
5	Upland Coniferous Forest	8.75	70.866
6	Row Crop	2.2	55.118
7	Open Water	0	0
8	Forested Wetland	8.4	59.055

These parameters are used to spatially adjust the reference evapotranspiration described in the Climate section (see page 23). In MIKE SHE, the ET process proceeds as follows: a portion of rainfall is intercepted by the canopy and evaporates, the remainder reaches the soil and adds to runoff or percolates into the upper soil layer, part of the infiltrating water is either transpired by plant roots or evaporated, and the remaining water recharges the groundwater. The various sections where plants intercept the path of water are spatially distributed by the LAI and RD parameters of the vegetation maps.

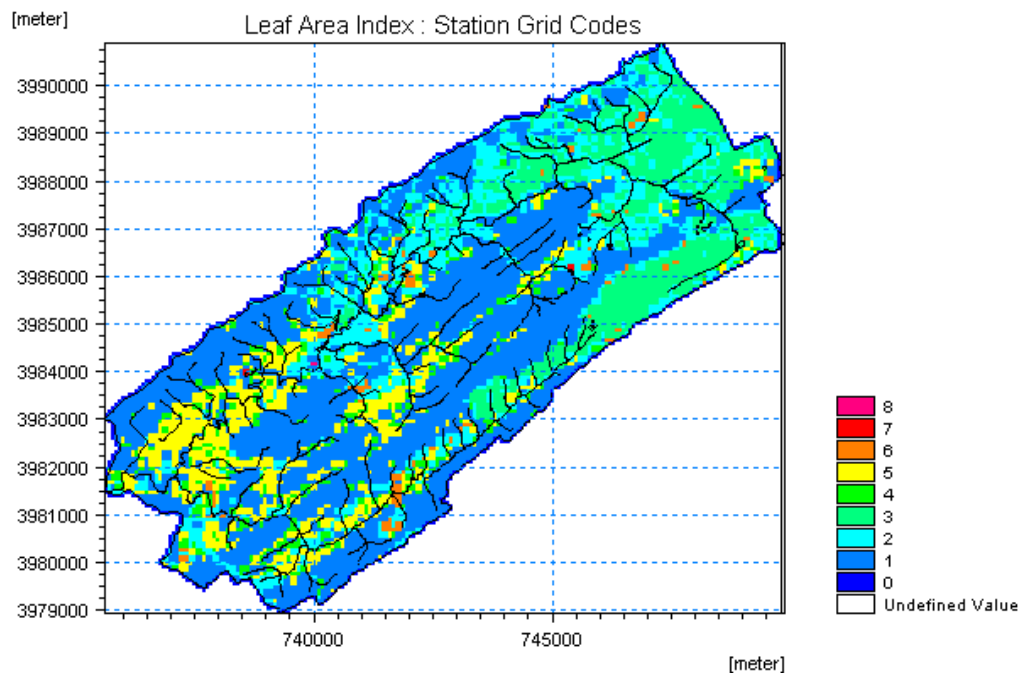


Figure 15. Leaf Area Index and Root Depth Grid Codes.

Figure 15 illustrates the assigned grid codes for the Leaf Area Index and the Root Depth.

Saturated Zone

Development of site-specific hydrological models requires knowledge of the Oak Ridge Reservation (ORR) geology to adequately correlate the composition of soil parent material with soil hydrological properties. Soil geologic properties also provide basic information about factors controlling groundwater flow. Figure 16 shows the geological layers which have been identified according to the classification found in the Geologic Map of Tennessee, published by the Tennessee Division of Geology [54].

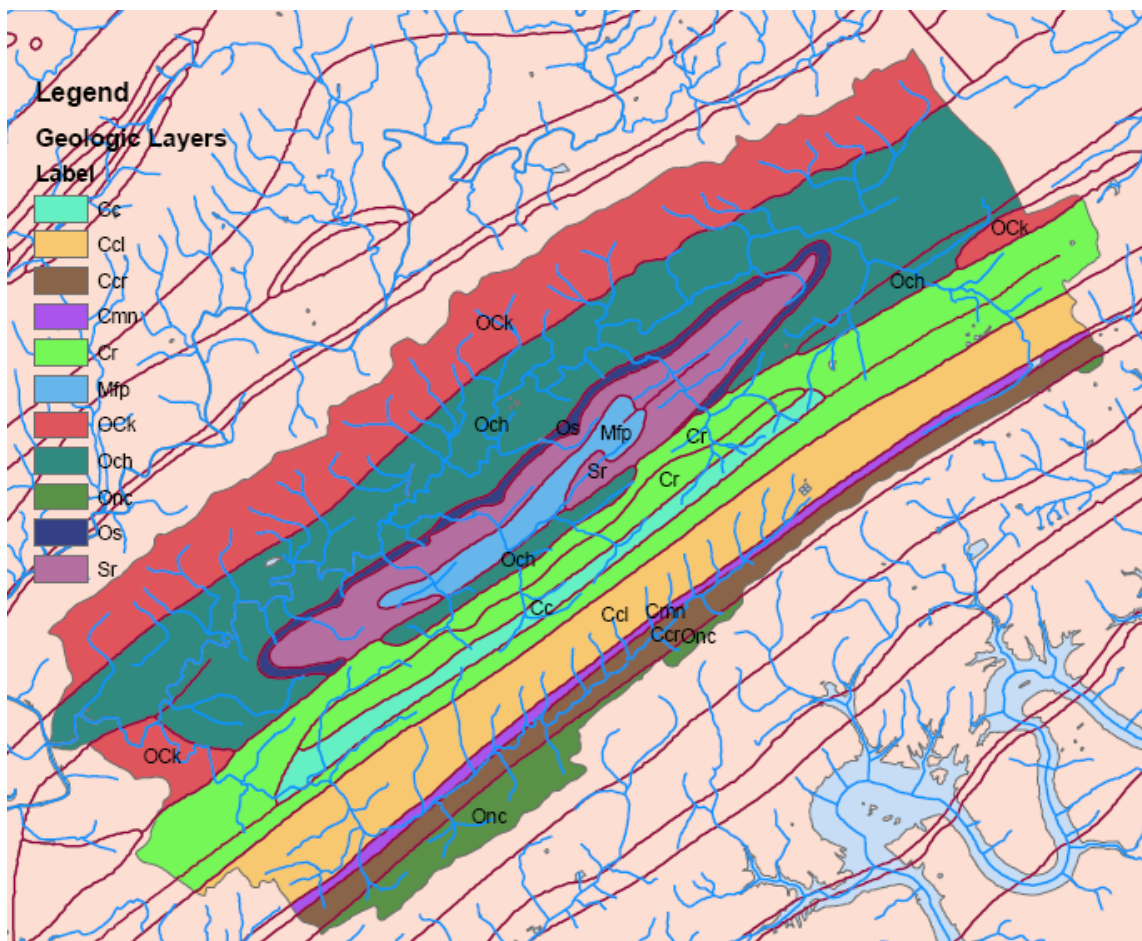


Figure 16. Geologic layers.

A variety of geological formations lies beneath ORR. The Rome and Chickamauga Group Formations underlie the ORNL complex, which is situated within two watersheds – Bethel Valley and Melton Valley. The defining characteristics of the Valley and Ridge Province are the southwest trending series of ridges and valleys caused by crustal folding and faulting due to compressive tectonic forces as well as the differential weathering of the various formations underlying the area.

The ORNL complex lies above the geologic formation known as the Chickamauga Group, which is an aquitard with flow limiting strata and relatively low hydraulic conductivity, (ATSDR 2006). A shallow subsurface stormflow zone (1-2 m thick) which approximately translates to the root zone (ASER 2005) is underlain by an unsaturated zone of variable thickness (1-15 m) which separates the stormflow zone and the water table. Approximately 95% of all groundwater flow in the ORR Aquitards occurs in the shallow saturated zone (i.e., the upper 15-30m) and ends up either as diffuse discharge to surface waters or discharge via springs and seeps, (ATSDR 2006). The vertical discretization includes 2 layers, the lowest level of the upper layer 30 meters below the surface and the lowest level of the lower layer is 100 meters below the ground surface elevation. Horizontal and Vertical Hydraulic Conductivity are functions of the soil texture and are related to the ease with which water can flow through the soil. MIKE SHE assumes that the horizontal conductivity is isotropic in the x and y directions. For initial approximation of the flow, the horizontal hydraulic conductivity was assumed 10 times higher than the vertical hydraulic conductivity. A horizontal hydraulic conductivity of 1.0×10^{-4} m/s and a vertical hydraulic conductivity of 1.0×10^{-5} m/s were used.

In unconfined aquifer, Specific Yield is defined as the volume of water released per unit surface area of aquifer per unit decline in head. It is a dimensionless characteristic that is used only in transient simulations in cells that contain the water table. (See MIKE SHE manual Volume 2 page 114). Specific Storage is similar, but is defined as the volume of water released per volume of aquifer per unit decline in head and has units of L^{-1} . A Specific Yield of 0.2 and a Specific Storage of 3.048×10^{-5} (Engineering Study Work Plan, Appendix D, Table D.1) were used.

MIKE SHE requires a reference system for linking the drainage to a recipient node or cell. The recipient can be a MIKE 11 river node, another SZ grid cell, or a model boundary. Drainage routed downhill based on adjacent drain levels was the option used for all simulations. Whenever drain flow is produced during a simulation, the computed drain flow is routed to the recipient point using a linear reservoir routing technique. The reference system is created automatically by the pre-processor using the slope of the drains calculated from the drainage levels in each cell. Thus, the pre-processor calculates the drainage source-recipient reference system by:

- a) looking at each cell in turn and then
- b) look for the neighboring cell with the lowest drain level,
- c) If this cell is an outer boundary cell or contains a river link, the search stops.

If the cell does not contain a boundary or river link, then the next search is repeated until either a local minimum is found or a boundary cell or river link is located. The result of the above search for each cell is used to build the source recipient reference system. If local depressions in the drainage levels exist, the SZ nodes in these depressions may become the recipients for a number of drain flow producing nodes. This often results in the creation of a small lake at such local depressions. If overland flow is simulated, then the drainage water will become part of the local overland flow system. The drainage level was assumed -1.0 m relative to the ground, the drainage time constant was assumed $1.0 \times 10^{-6} \text{ sec}^{-1}$, after performing calibration studies and uncertainty analysis.

Unsaturated Flow

Texture types of the soils within the ORNL study area were identified by investigating ORR soil map units on the basis of geologic formation, geomorphology, and soil parent material. Soil map units were delineated within the watershed according to the ORR soil coding legend and classifications described by Lietzke and Lee (Hatcher et al, 1992). All soil map units were reviewed, from which 73 soil map unit codes which intersected creeks and rivers within the ORNL study area were extracted. The dominant soil units identified were 00361-01241 (Rome formation), 40541-43041 (Knox-Copper Ridge/Chepultepec/Longview/Kingsport/Mascot

group), 50031-60843 (Chickamauga Group formation), and 96051-99521 (Alluvium). Each of the intersecting soil map unit codes was reviewed for its distinctive morphology, parent materials, and soil texture.

Each soil textural type has certain hydrological properties which are essential for the solute transport theory. The soil literature contains numerous assessments of soil water characteristics and hydraulic conductivity values, which are often not easy to determine experimentally. The van Genuchten model (1976) is a simplified widely used approach for prediction of soil water content as a function of pressure head. This model is represented by the following algorithm:

$$\theta = \theta_r + \frac{(\theta_s - \theta_r)}{[1 + (\alpha h)^N]^M} \quad (2)$$

where: θ -water content; θ_r -residual water content; θ_s -total saturated water content; α -empirical constant, cm^{-1} ; N-empirical constant; M-empirical constant; and h -capillary head in cm. The correlation between N and M is as follows:

$$M = 1 - 1/N \quad (3)$$

Hydraulic conductivity is expressed by:

$$\frac{K(\theta)}{K_s} = \left\{ \frac{\theta - \theta_r}{\theta_s - \theta_r} \right\}^{1/2} \left\{ 1 - \left[1 - \left(\frac{\theta - \theta_r}{\theta_s - \theta_r} \right)^{1/M} \right]^M \right\}^2 \quad (4)$$

where $K(\theta)$ is the hydraulic conductivity for a given water content (cm h^{-1}) and K_s is the saturated hydraulic conductivity (cm h^{-1}). Parameters for equation (1) were obtained from the Carsel and Parrish database (1988). All acquired values of saturated hydraulic conductivities (K_s) and van Genuchten water retention parameters (θ_r , α , N) for each of the soil texture types identified in the WOC are presented in Table 6.

The identified soil groups were further categorized into the five textural types such as loam, silt loam, clay loam, silty clay loam, and clay (Hatcher et al., 1992) presented in Table 6:

Table 6. Van Genuchten’s Soil Hydraulic Parameters

Texture	Loam	Silt Loam	Clay Loam	Silty Clay Loam	Clay	No data
Residual Water Content, θ_r	0.078	0.067	0.095	0.089	0.068	
Saturated Water Content, θ_s	0.43	0.45	0.41	0.43	0.38	
Water Retention Parameter, a, cm^{-1}	0.036	0.02	0.019	0.01	0.008	
Water Retention Model Parameter, N	1.56	1.41	1.31	1.23	1.09	
Hydraulic Conductivity, $K_s, \text{cm hr}^{-1}$	1.04	0.45	0.26	0.07	0.2	
Area near WOC, m^2	276,990.60	909,295.70	377,261.90	203,359.70	602,149.50	165,583.30
% Total Soil Area near WOC	10.9	35.9	14.9	8	23.8	6.5

MIKE SHE was applied to a two-layer surficial aquifer profile, an unsaturated layer which incorporates an approximated 1m root zone and a 5m underlying soil matrix, and the upper shallow saturated zone with a groundwater depth of 17m.

Rivers and Lakes

This study focuses on East Fork Poplar Creek Watershed and its primary streams, East Fork Poplar Creek and Bear Creek.

The morphological characteristics of a river channel and floodplain are important parameters needed to create an accurate hydraulic simulation. These characteristics include channel width and depth, as well as floodplain cross-section area. Geometric data was developed by utilizing a high resolution DEM with an approximate resolution of two meters. The first step was to identify cross sections locations that would accurately depict the morphological characteristics of the channels in the East Fork Poplar Creek (EFPC) watershed.

River Network and Cross Sections

The major streams in East Fork Poplar Creek were identified using a shape file from USGS. Streams identified in the shapefile include up to 115 tributaries, however, the flow from these streams can be estimated in the topography and are not required for model calibration.

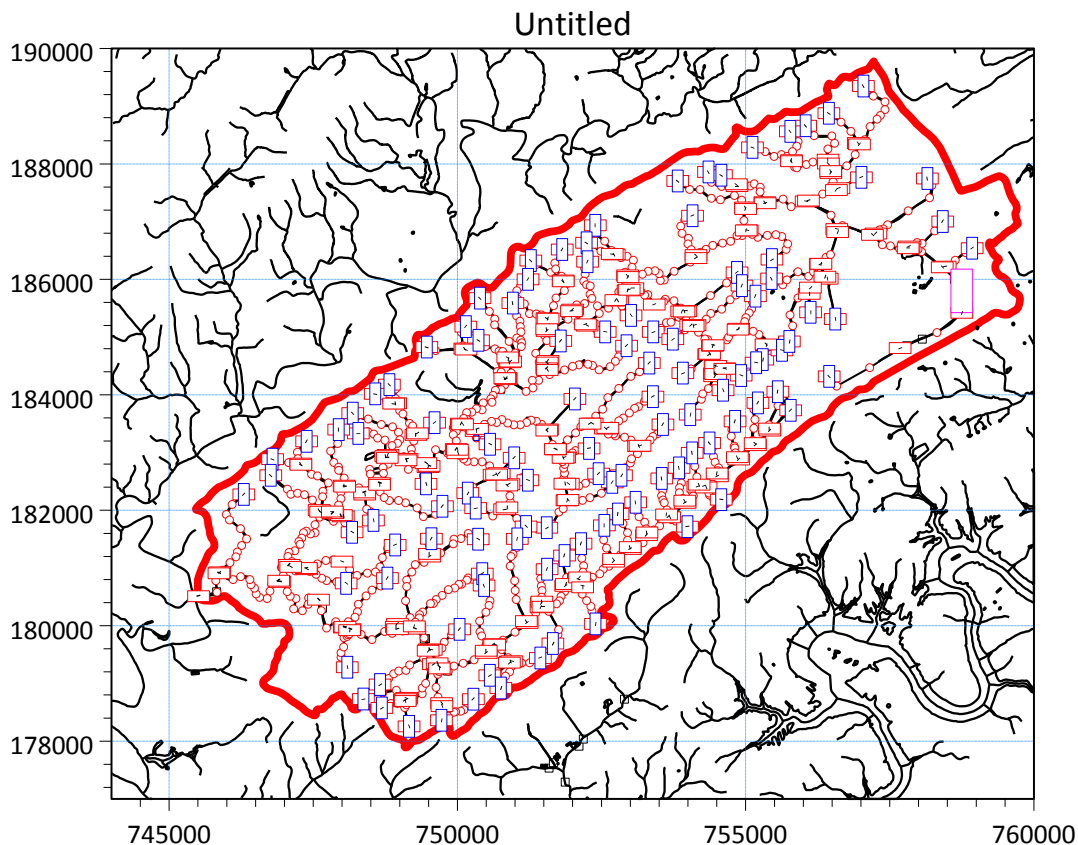


Figure 17. River network and domain with cross section locations, boundaries and intersections.

A sufficient number of cross sections were gathered for each stream to accurately reproduce the river profile after inspecting the profile of each tributary and determining the locations of slope changes. A point shapefile was created to identify the locations of cross sections. This provided an accurate description of the river system with respect to slopes and river profiles.

Using the 3-D analyst extension in ArcGIS, profile graphs were created by interpolating lines along the established cross section locations. These lines depicted a horizontal profile of the channel when intersected by the DEM. Cross section lines were drawn perpendicular to the direction of flow by visualizing the topographic features. A key step involved drawing all the lines from left bank to right bank when facing upstream. Cross sections were wide enough to cover the entire floodplain. Cross sections of approximately 100 meters wide were gathered.

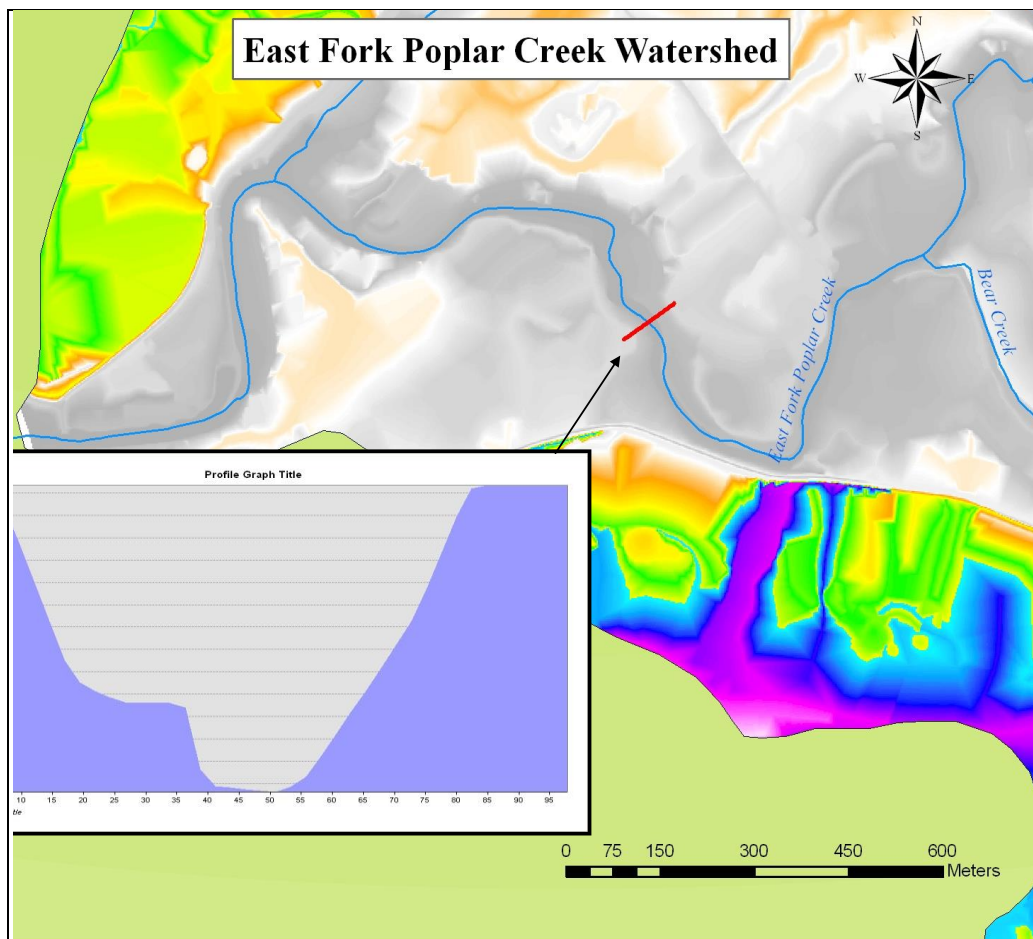


Figure 18. Typical cross section profile from East Fork Poplar Creek.

An example demonstrating the procedure is shown on Figure 18. The cross sectional profile in this figure is a typical representation of the procedure used to determine all cross sections. Although the discharge on these tributaries is minimal, years of scouring have formed clearly defined channels in the area. Once a cross section profile was established, ArcGIS through the 3-D Analyst tool bar allowed exporting the data as elevation points. A separate spreadsheet was created for each cross section containing anywhere between 35 to 50 points. By adding the cross sections locations GIS shapefile to the MIKE11 network editor, cross sections were established precisely at the point where they were drawn on GIS. The data for the cross section coordinates were further transferred in the river cross sectional editor of MIKE 11. A reasonably high number of river cross-sections were included to ensure that the river elevations are reasonably

consistent with the surface topographic features. More than 800 cross sections were created from the DEM and entered into the MIKE 11 model.

Boundary Conditions

An Open Boundary was specified assuming free upstream and downstream ends of the model domain. The boundary conditions used in the river model are shown in Table 7. When the Open option is selected in a Boundary Description cell, a branch name and chainage are also needed in order to identify the location of the boundary.

Table 7. Boundary Conditions

River Name	Boundary Description	Boundary Type	Chainage
East Fork Poplar Creek	Open	Q-h	22293.37
East Fork Poplar Creek	Open	Inflow	0
Bear Creek	Open	Inflow	0

An open boundary condition has the following valid Boundary Types:

- Inflow was specified when a time-varying or constant flow hydrograph condition (for the HD model) is required with or without a solute component (for the AD model).
- Q-h was specified when the relationship between the discharge and the water level (HD model) is known and used with or without a solute component (used in the AD model).

After establishing a MIKE 11 HD hydraulic model as a stand-alone model a series of performance tests were executed and a rough calibration using prescribed inflow and stage boundaries was conducted. After testing the MIKE 11 HD hydraulic model as a stand-alone model a MIKE SHE model was established that includes the overland flow component, the saturated zone and unsaturated zone components. SZ drainage boundaries were used to prevent excessive surface flows in low lying areas and the river flood plain.

Overland Flow

When the net rainfall rate exceeds the infiltration capacity of the soil, water is ponded on the ground surface. This water is available as surface runoff, to be routed downhill towards the river system. The exact route and quantity is determined by the topography and flow resistance, as well as the losses due to evaporation and infiltration along the flow path. If it is unnecessary to simulate overland flow, a Manning's M of 0 will disable overland flow.

The overland flow can be calculated using either a semi-distributed method or a finite difference method using the diffusive wave approximation. The finite difference method should be used when calculating detailed overland flow, while the semi-distributed, simplified method should be used for regional applications where detailed overland flow is not required.

The outer boundary condition for the overland flow solver is a specified head, based on the initial water depth in the outer nodes of the model domain. Thus, if the water depth inside the model domain is greater than the initial depth on the boundary, water will flow out of the model. If the water depth is less than the initial depth on the boundary, the boundary will act as a source of water. The domain of the model is a delineated watershed, which should indicate that all of the water that falls within the domain flows to the rivers and out toward Poplar Creek. For this reason all of the overland flow within the domain is treated as a source of water and the Initial Water Depth is set to zero to ensure flow in this direction and not out of the domain. Detention Storage is used to limit the amount of water that can flow over the ground surface. For the model, detention storage is set to zero.

When the net rainfall rate exceeds the infiltration capacity of the soil, water is ponded on the ground surface. This water is available as surface runoff, to be routed downhill towards the river system. The exact route and quantity is determined by the topography and flow resistance, as well as the losses due to evaporation and infiltration along the flow path. The water flow on the ground surface is calculated by MIKE SHE's Overland Flow Module, using the diffusive wave approximation of the Saint Venant equations, or using a semi-distributed approach based on the Manning's equation. USGS has described a procedure for estimating the roughness factor

(Manning's number) for densely vegetated flood plains [67]. The n value is determined from the values of the factors that affect the roughness of channels and flood plains. In densely vegetated flood plains, the major roughness is caused by trees, vines, and brush. The n value for this type of flood plain can be determined by measuring the vegetation density of the flood plain.

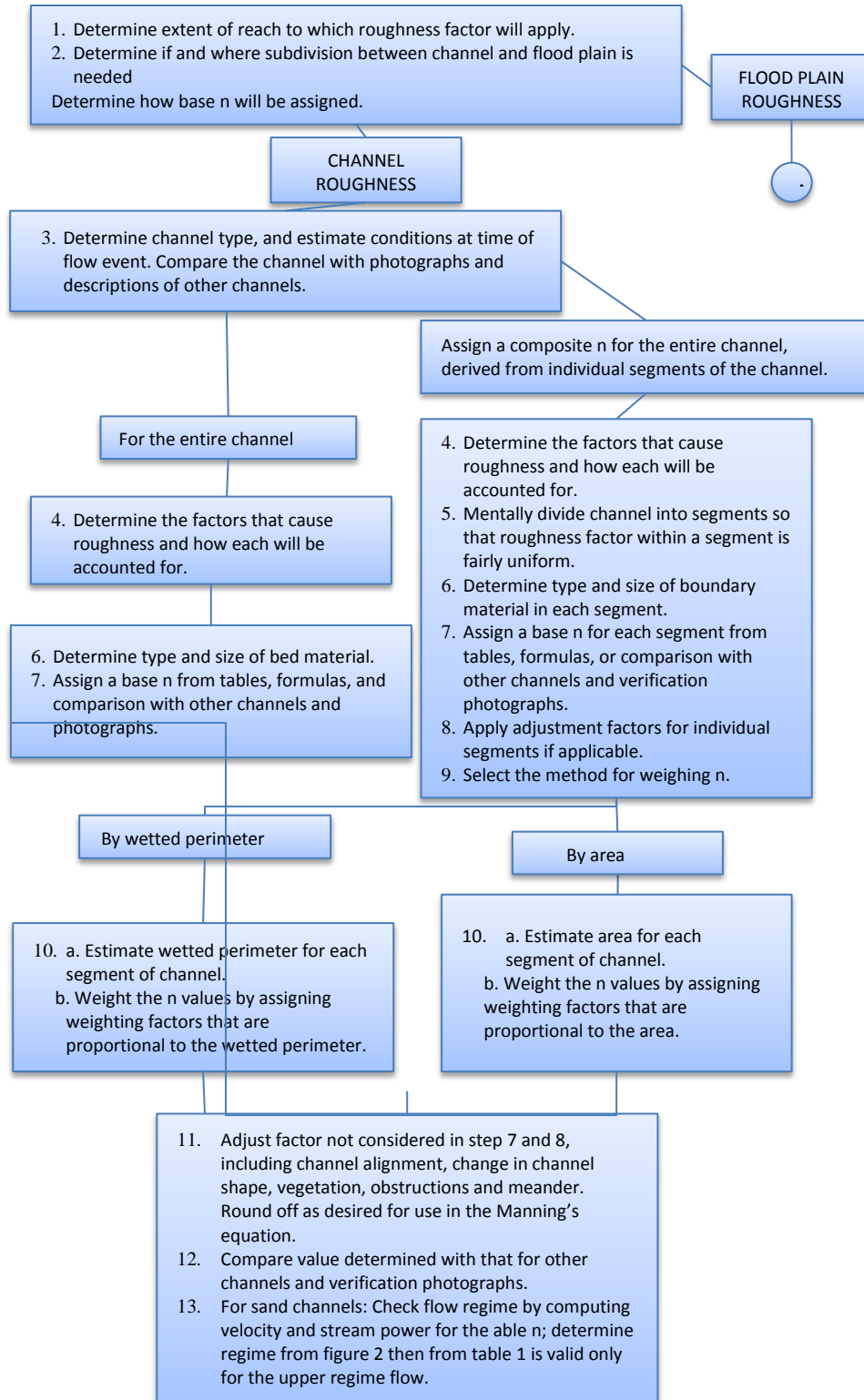


Figure 19. Procedure for determining Manning’s number (Part I).

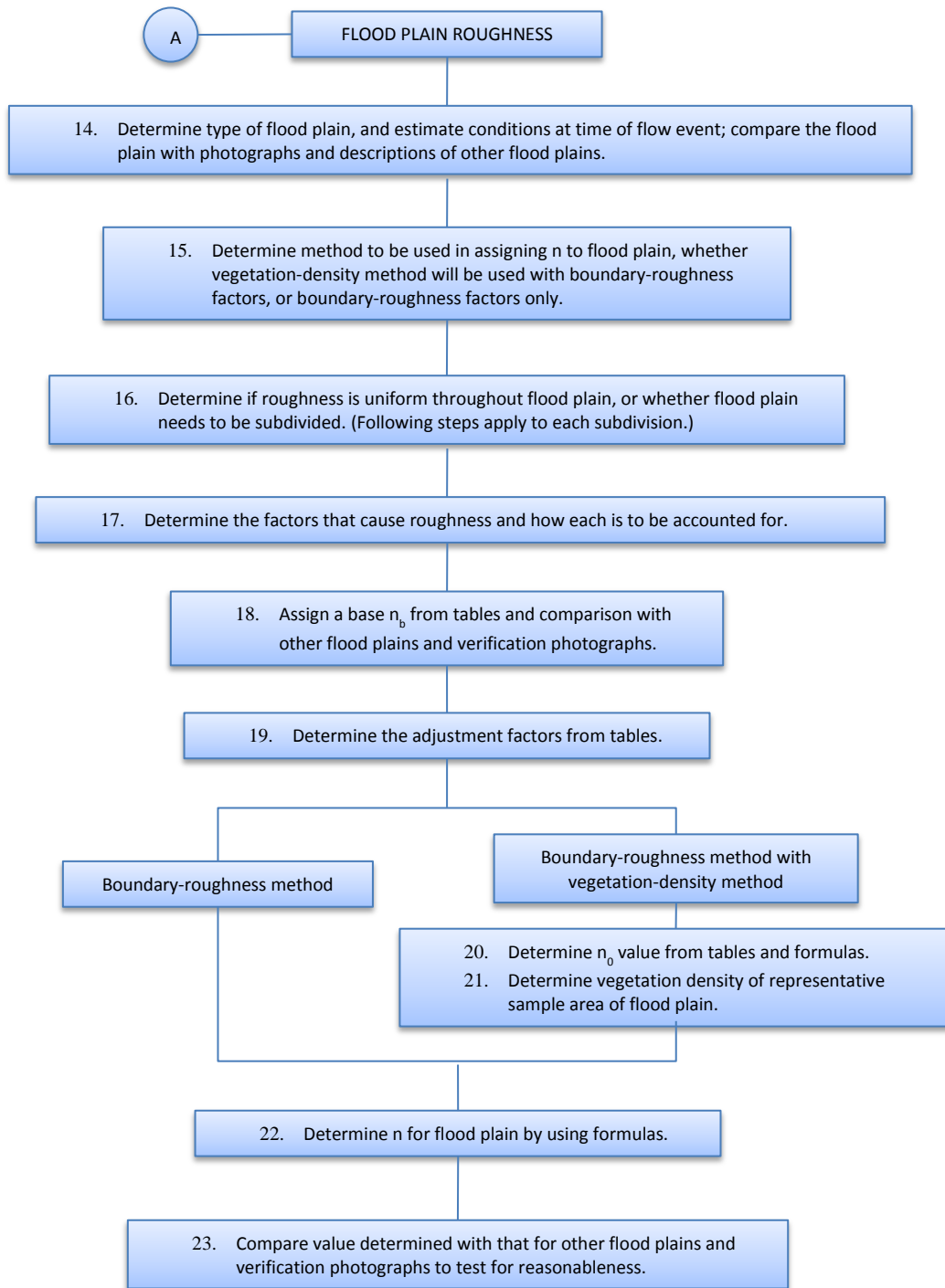


Figure 20. Procedure for determining Manning’s number (Part II).

MIKE SHE assumes Manning’s number equal to: $1/n$ (i.e., inverse of Manning n) for a planar surface of infinite width with uniform rainfall. Precipitation falls on the plane, accumulates on the surface in response to the surface roughness, and flows down the slope in the positive x -direction. In the figure, L is the length of the slope, y is the local depth of water on the surface at any point along the surface and α is the slope.

$$q = M \cdot y^{5/3} \sqrt{\alpha} \tag{5}$$

Manning n units = $\text{s/m}^{1/3}$ in software, Manning M units = $\text{m}^{1/3}/\text{s}$

Table 8. Manning’s Number for Each Land Use Type

Grid Code	Class Name	Manning n
1	Open Water	100
2	Forested Wetland	3
4	Pasture/Grassland	10
5	Row Crop	15
7	Upland Deciduous Forest	3
8	Upland Mixed Forest	3
9	Upland Coniferous Forest	3
10	Urban/Developed	10

Assumed value for Manning n (Chow, 1959 and U.S. EPA, 2004) ranges between 0.01-0.05 (i.e., range between concrete and vegetated area, heavily vegetated areas can have n as high as 0.20), therefore the value $n = 0.20$ used, and Manning $M = 1/n = 1/0.20 = 5$

Initially, a calibration of the model was carried out to evaluate and refine parameter values by comparing simulated and observed values in an attempt to generate a model that is closely representative of reality within a certain level of accuracy. This process was intended to improve the predictive capability and reliability of the model.

The main steps used for model calibration include:

1. Identification of calibration parameters.

2. Sensitivity Analysis – to identify parameters to which model predictions are most sensitive.
3. Numerical optimization – to determine a set of optimal or best-fit parameters which can be used to evaluate the model’s predictive capability for certain hydrological or meteorological processes.

Table 9. Model Calibration Parameters

Model component	Calibration Parameters
River discharges	Watershed hydrology (Manning’s number, drainage constant, drainage level, hydraulic conductivities)
Saturated zone	Hydraulic Conductivity
Unsaturated zone	Saturated hydraulic conductivity
Drainage system	Drainage Constant
Drainage system	Drainage Level
Evapotranspiration	Crop coefficient
Unsaturated zone	Saturated hydraulic conductivity

Variation of the selected calibration parameters in the range of 2 to 50% will require several simulations to be carried out. The results obtained from these simulations will provide the deviations observed between the simulated and the observed values and will therefore aid in determination of the optimal parameter values to be used for calibrating the model.

The East Fork Poplar Creek watershed is assumed to consist of an upper layer with high hydraulic conductivity (1e-04 m/s) also known as a “stormflow zone,” the vadose zone and the shallow aquifer.

The stormflow zone which is the pathway for transporting and retention of contaminants from the subsurface sources to the local streams occurs through a 1-2m thick zone which approximately corresponds to the root zone of the vegetation. Most of the groundwater flow and the transport of the contaminants occur through a few widely spaced (10-50m) permeable regions. The horizontal conductivities of these storm flow zones and the groundwater zones are subject to calibration. Two soil profiles which are used in the model are the silty clay loam and clay loam to a depth of 5 meters. The hydraulic conductivities and the soil moisture content of these soil types are also subject to calibration.

Table 10. Basin Characteristics

Parameter	Value
Total drainage area, in square miles	28.8
Area that contributes flow to a point on a stream, in square miles	28.8
Percent of area within Hydrologic Area 1	100
Percent of area within Hydrologic Area 2	0
Percent of area within Hydrologic Area 3	0
Percent of area within Hydrologic Area 4	0
Tennessee climate factor, 2-year interval	2.249
Streamflow-recession index, in days per log cycle of decrease in discharge	67
Stream slope 10 and 85 method in feet per mile	11.3
Percent area underlain by soil permeability of at least 2 in./hr	39
Soil Permeability – in./hr	2.43

Table 11. Peak Flow Basin Characteristics

Parameter	Value	Min	Max
Contributing Drainage Area (square miles)	28.8	0.2	9000
Stream Slope 10 and 85 Method (feet per mi)	11.3	3.29	950
Tennessee Climate Factor 2 Year (dimensionless)	2.249	2.06	2.32

Table 12. Low Flow Basin Characteristics

Parameter	Value	Min	Max
Drainage Area (square miles)	28.8	2.68	2557
Recession Index (days per log cycle)	67	32	175

Table 13. Streamflow Statistics

Peak-Flow Statistics	Flow (ft³/s)	Prediction Error (percent)	Equivalent years of record	Minimum 90-Percent Prediction Interval	Maximum 90-Percent Prediction Interval
PK2	1350	39	1.7	724	2510
PK5	2080	38	2.6	1120	3870
PK10	2620	40	3.4	1390	4950
PK25	3350	43	4.3	1710	6560
PK50	3910	45	4.9	1920	7940
PK100	4530	48	5.3	2140	9580
PK500	6050	55	5.8	2590	14200

Grid Size

The objective of these series of simulations was to determine if variable grid cell size values of the model domain would have an effect on the computed discharge, surface and groundwater levels and depth of overland flow. The final simulations were obtained from a 50 m cell size with dimensions of 290 horizontal by 240 vertical cells

Sensitivity Analysis and Uncertainty of the Hydrologic Model

The objective is to determine the sensitivity of model output to input parameters:

1. Discharges of computed versus measured values in know points (NWT), we have only one point where we have timeseries. Another USGS discharge location could be added for comparison purposes.
2. Groundwater level fluctuations will be compared with well data
3. The resolution of overland flow will be compared in order to determine the flooding has sufficient accuracy.

The model components and the parameters used to analyze the uncertainties of the model are listed in Table 14 below.

Table 14. Model Components and Parameters Used for Uncertainty Analysis

Model component	Calibration Parameters	Variation %
Saturated zone	Hydraulic Conductivity, vertical and horizontal	±50%
Vegetation	Leaf Area Index	±50%
	Root Depth	±50%
Overland Flow	Manning's Coefficient	±50%
Evapotranspiration	Crop coefficient	±50%

Hydrologic Simulations

The model uses the hydrological parameters (flow in overland, rivers and subsurface) to determine the transport. The model has been calibrated and validated using historical hydrological data. More details for the results obtained from the simulations and comparison with the discharges from each station are shown in the sections below.

Groundwater Flow

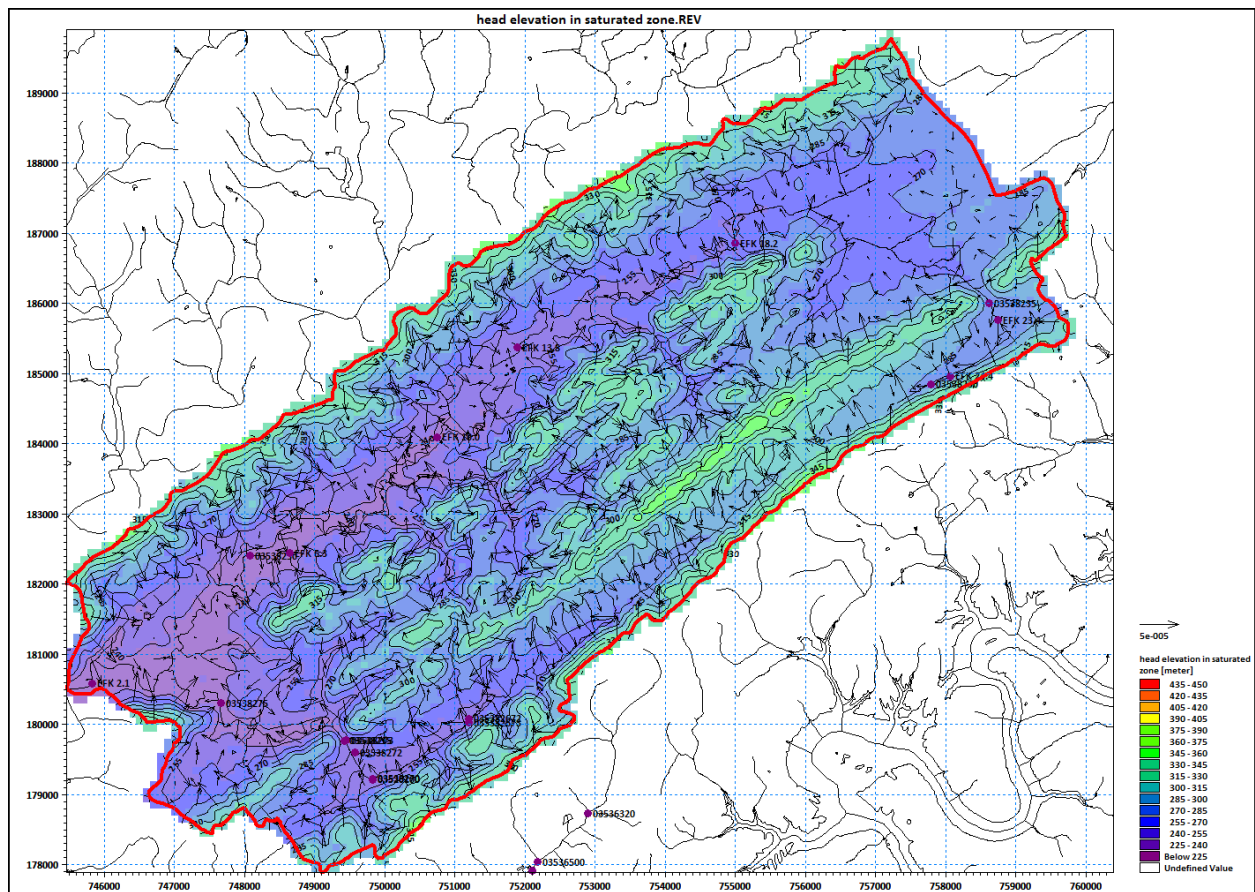


Figure 21. Example of a calculation of the groundwater table, including vectors showing groundwater movement in the XY direction.

Surface Water Flow

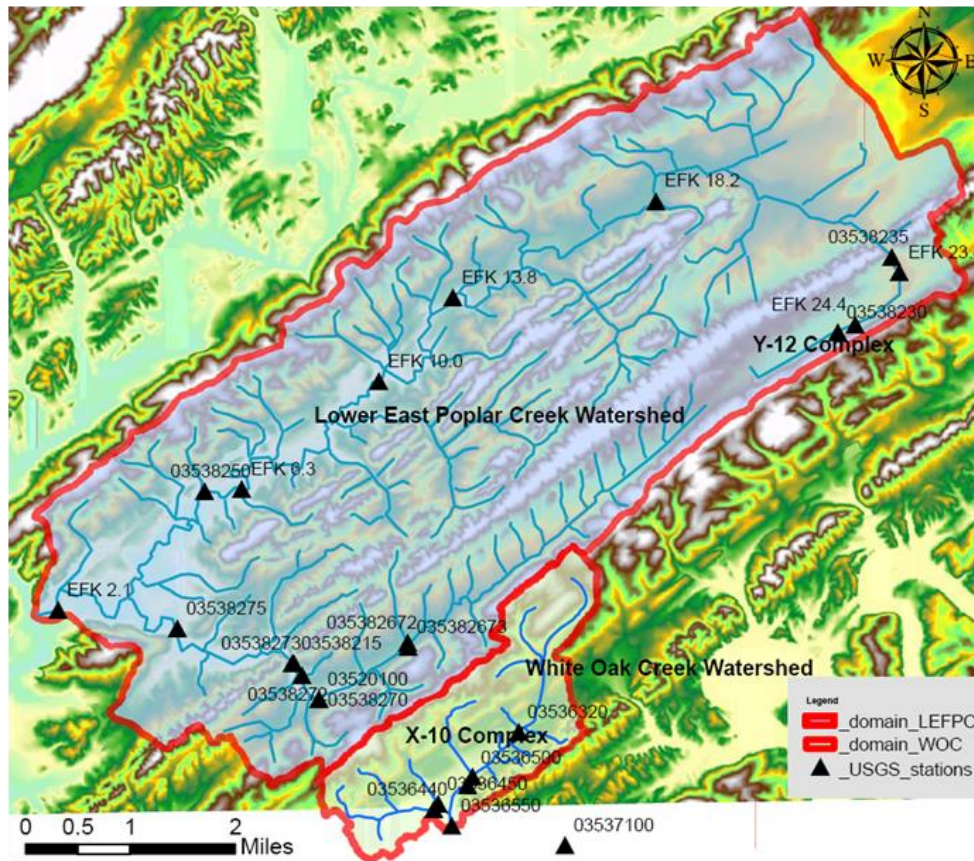


Figure 22. Location of USGS Station 03538320 and DOE station EFK 24.4 used for data comparison.

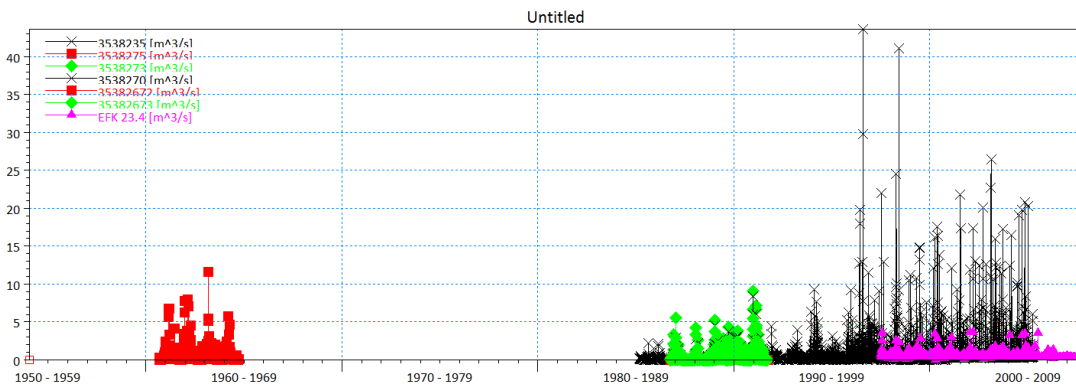


Figure 23. USGS stations used for calibration of discharges in LEFPC streams, the legend shows the USGS station number.

Flow in Rivers

Discharges at USGS 03538230. Available data was obtained from Tennessee StreamStat¹ for Latitude (NAD83): 35.9189 (35 55 08) and Longitude (NAD83): -84.3168 (-84 19 00).

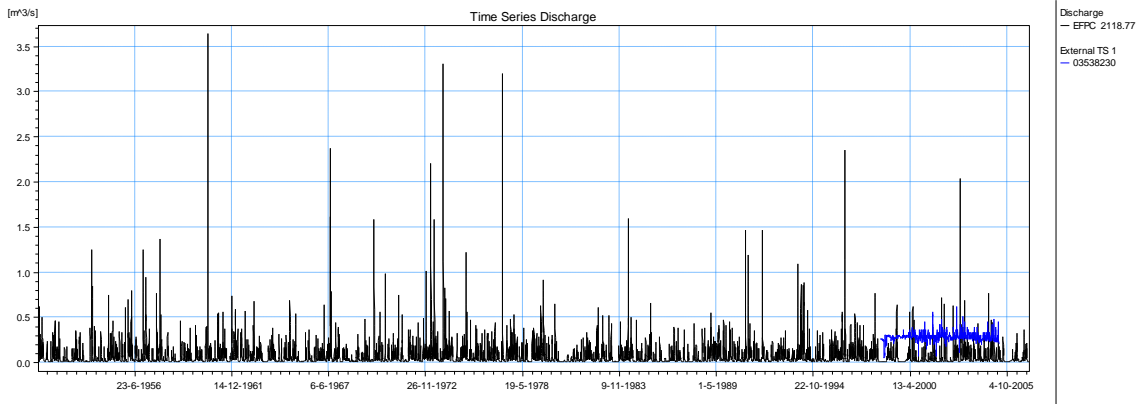


Figure 24. Computed and observed values at USGS Station 03238230.

The blue line shows the observed discharges, which has a baseline of approximately 0.30 m³/s. The model did not account for this baseline, which is most likely a result from additional discharges in the river.

¹ <http://streamstats.usgs.gov/tstreamstats/index.asp>

Table 15. Streamflow Statistics for EFPC 2119 (Flow Duration, General Flow and Base Flow) for Measurements at USGS Station 03538230

Statistic Name	Value	Units	Citation Number
Flow-Duration Statistics			
1_Percent_Duration	14	cfs	[77]
10_Percent_Duration	11	cfs	[77]
20_Percent_Duration	11	cfs	[77]
25_Percent_Duration	11	cfs	[77]
30_Percent_Duration	10	cfs	[77]
40_Percent_Duration	10	cfs	[77]
5_Percent_Duration	12	cfs	[77]
50_Percent_Duration	10	cfs	[77]
60_Percent_Duration	9.9	cfs	[77]
70_Percent_Duration	9.6	cfs	[77]
75_Percent_Duration	9.5	cfs	[77]
80_Percent_Duration	9.3	cfs	[77]
90_Percent_Duration	8.8	cfs	[77]
95_Percent_Duration	8	cfs	[77]
99_Percent_Duration	2.511	cfs	[77]
General Flow Statistics			
Average_daily_streamflow	9.982	cfs	[77]
Maximum_daily_flow	22	cfs	[77]
Minimum_daily_flow	1.9	cfs	[77]
Std_Dev_of_daily_flows	1.651	cfs	[77]

The duration curve for EFPC 2119 is shown below.

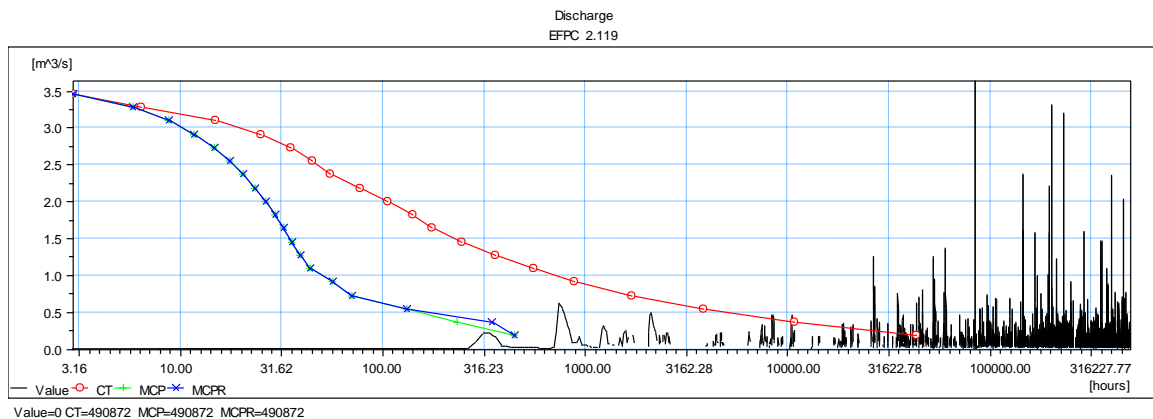


Figure 25. Duration curve computed for EFPC 2119 (near EFK 24.4, and USGS Station 03538230), CT - Cumulative Time, MCT – Maximum Continuous Period.

Discharges at USGS 03538235 (downstream of EFK 23.4 known as Station 17). Computed data were compared with measurements from USGS Station 03539235 and Station 17 (EFK 23.4) which is positioned approximately 0.2 miles downstream.

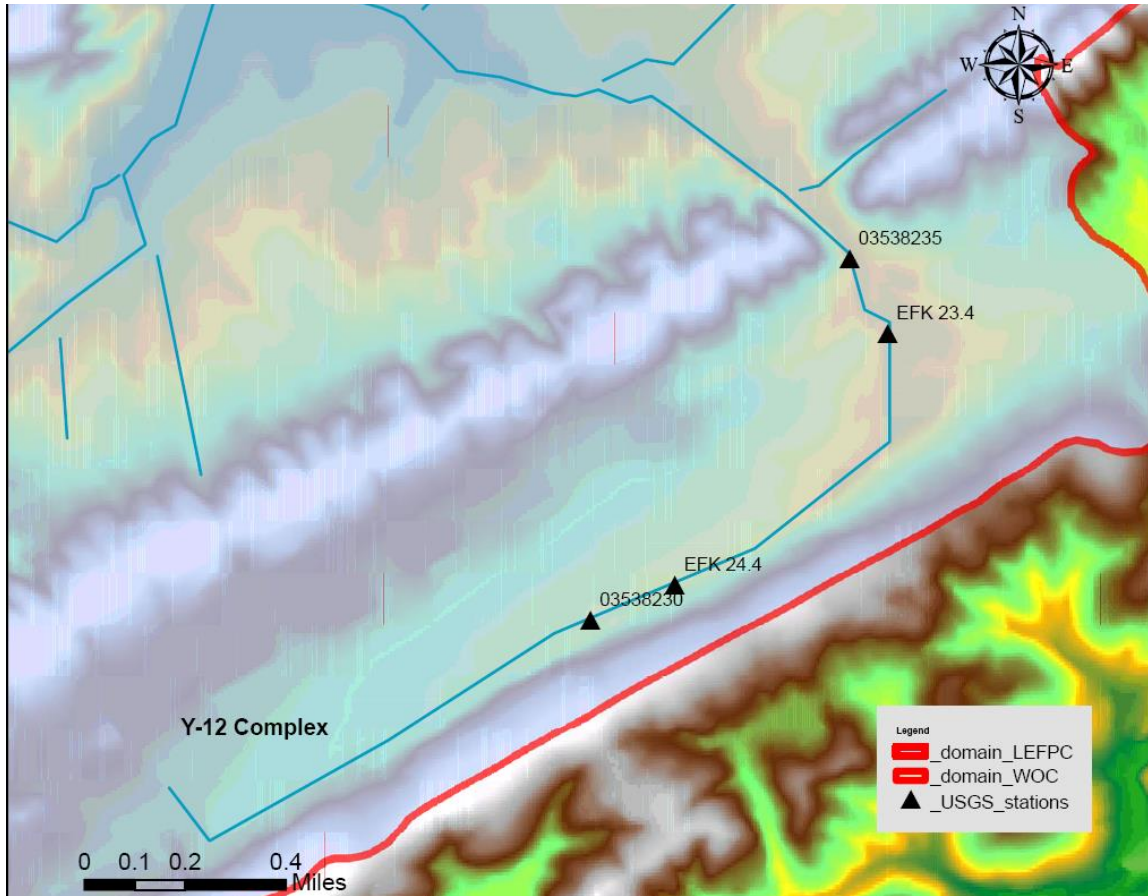


Figure 26. Location of USGS Station 03538235 and Station 17 (EFK 23.4).

The stream flow characteristics are listed in Table 16.

Table 16. Streamflow Statistics (Flow Duration, General Flow and Base Flow) for Measurements at USGS Station 03538230

Statistic Name	Value	Units	Citation Number
<i>Flow-Duration Statistics</i>			
1_Percent_Duration	57.76	cfs	[77]
10_Percent_Duration	16	cfs	[77]
20_Percent_Duration	13	cfs	[77]
25_Percent_Duration	13	cfs	[77]
30_Percent_Duration	12	cfs	[77]
40_Percent_Duration	12	cfs	[77]
5_Percent_Duration	25	cfs	[77]
50_Percent_Duration	11	cfs	[77]
60_Percent_Duration	11	cfs	[77]
70_Percent_Duration	9.1	cfs	[77]
75_Percent_Duration	6.6	cfs	[77]
80_Percent_Duration	5.8	cfs	[77]
90_Percent_Duration	5	cfs	[77]
95_Percent_Duration	4.3	cfs	[77]
99_Percent_Duration	3.7	cfs	[77]
<i>General Flow Statistics</i>			
Average_daily_streamflow	12.016	cfs	[77]
Maximum_daily_flow	205	cfs	[77]
Minimum_daily_flow	3.3	cfs	[77]
Std_Dev_of_daily_flows	10.539	cfs	[77]
<i>Base Flow Statistics</i>			
Average_BFI_value	0.717	dimensionless	[78]
Number_of_years_to_compute_BFI	10	years	[78]
Std_dev_of_annual_BFI_values	0.086	dimensionless	[78]

The computed and measured (or observed) values are shown in Figure 27.

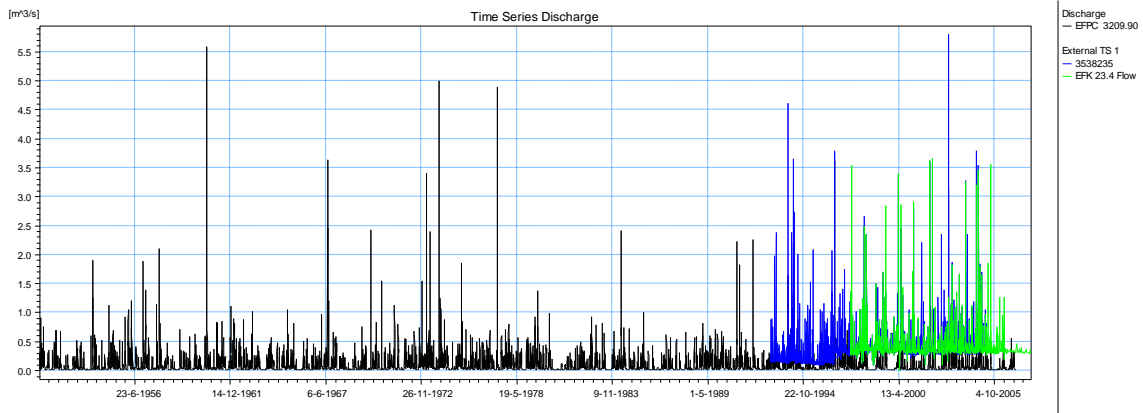


Figure 27. Computed and measured discharges at EFPC 3209, EFK 23.4, and USGS Station 03538235.

The flow duration curves for this station are shown on Figure 28.

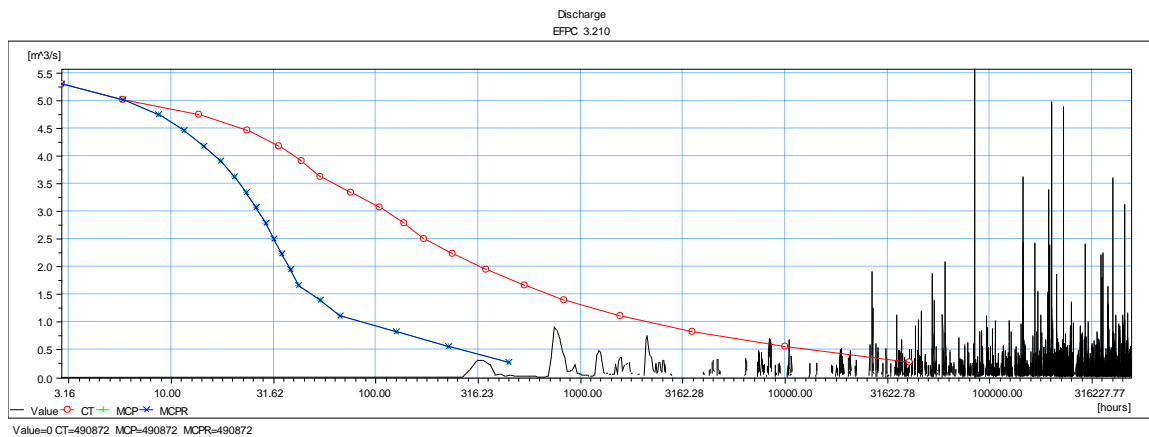


Figure 28. Duration curve computed for EFPC 3209 (near EFK 23.4, and USGS Station 03538235), CT - Cumulative Time, MCT – Maximum Continuous Period.

Discharges at USGS stations 03538250. The discharges at USGS Station 03538250 (the location of these stations is shown on Figure 30) have been compared with computed values.

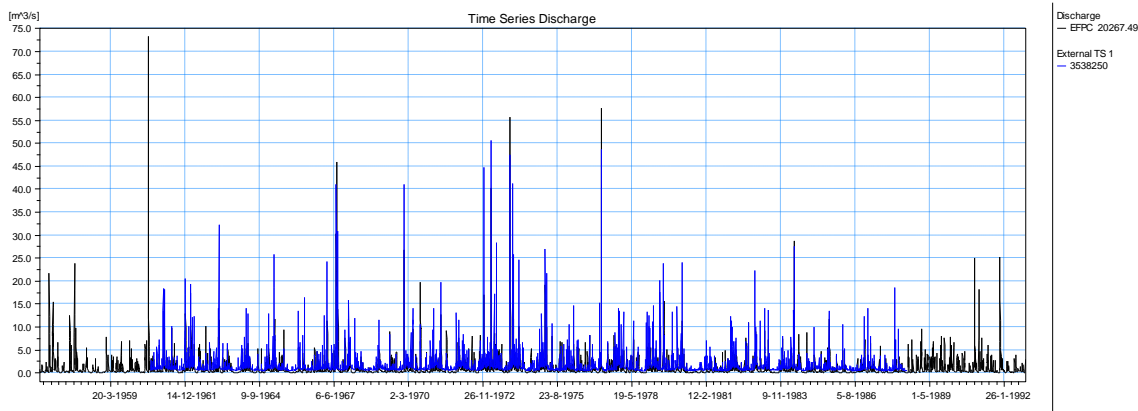


Figure 29 Computed and measured discharges at EFPC 20267 and USGS station 03538250 (0.4 miles downstream of EFK 6.3),

The data shows excellent correlation between computed and observed values. Table 17 lists the physical characteristics of the stream.

Table 17. Physical Characteristics of the Stream

Characteristic Name	Value	Units	Citation Number
Contributing_Drainage_Area	19.5	square miles	31
Drainage_Area	19.5	square miles	31
Main_Channel_Length	12.65	miles	31
Mean_Basin_Elevation	910	feet	31
Shape_Factor	0.121857864	dimensionless	43
Percent_Forest	24.2	percent	31
Percent_Storage	0	percent	31
Soil_Infiltration	3.89	inches	31
Stream_Slope_10_and_85_Method	12.87	feet per mi	31
Tennessee_Climate_Factor_2_Year	2.248	dimensionless	43
Tennessee_Physiographic_Factor	0.737544002	dimensionless	43

The locations of the stations considered in the analysis are shown on the map below.

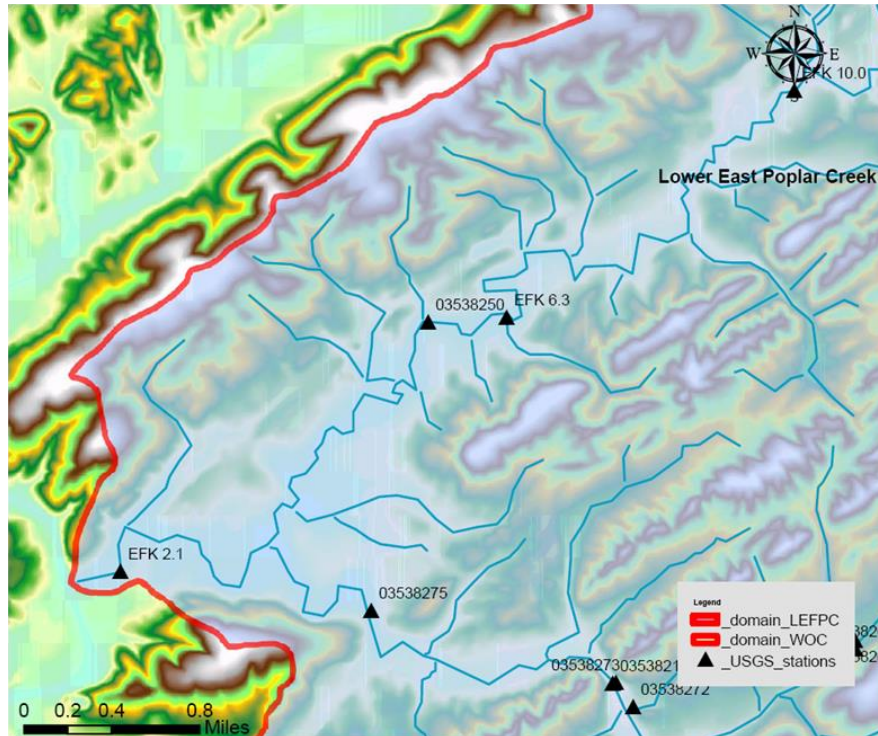


Figure 30. Location of USGS Stations 03538250.

The flow duration curve is shown in the next figure:

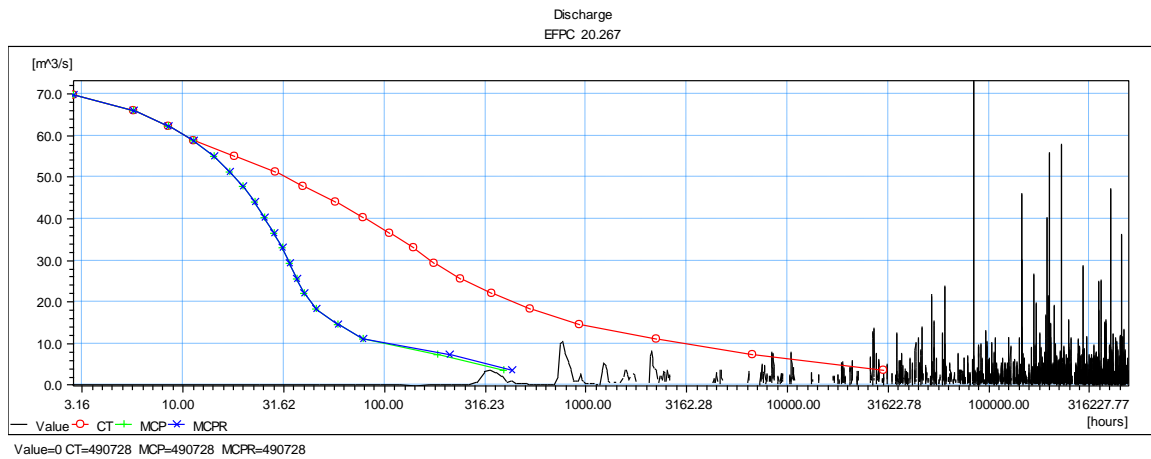


Figure 31. Duration curve computed for EFPC 20267 (near EFK 6.3, and USGS Station 03538250), CT - Cumulative Time, MCT – Maximum Continuous Period.

A plot of the cumulative distribution functions of EFPC 20267 and USGS station 03538250 (near EFK 6,3) is shown on Figure 32.

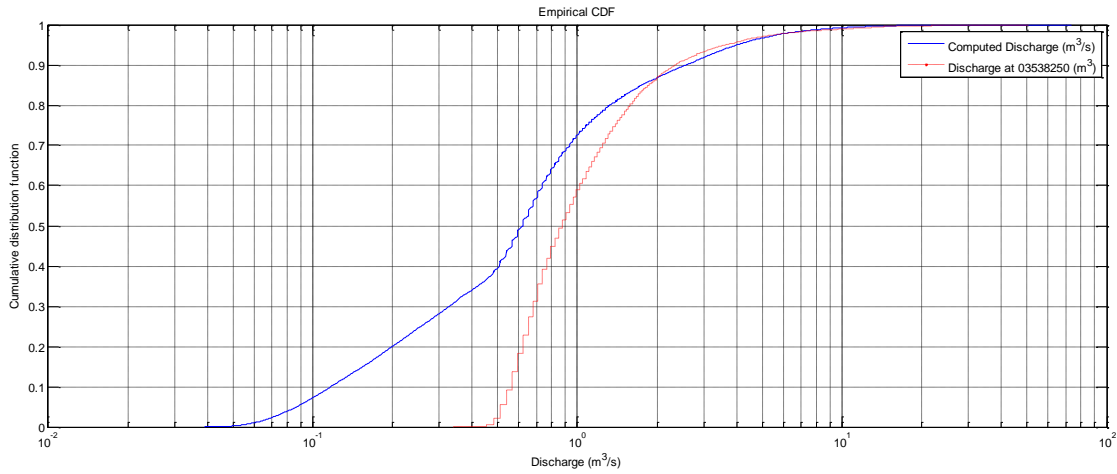


Figure 32. Cumulative distribution function of computed and observed discharge at EFPC 20267 (near EFK 6.3, and USGS Station 03538250).

A boxplot (Figure 33) shows that there is a discrepancy between the average values of computed (respectively 0.6 m³/s vs. 0.9 m³/s, a difference of approximately 0.3 m³/s, which is likely a result of adding water upstream for dilution).

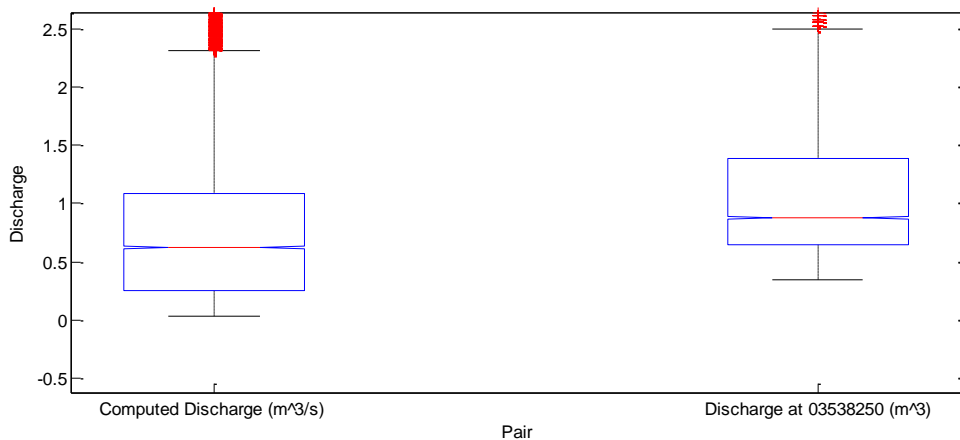


Figure 33. Boxplot of Computed and observed discharge at at EFPC 20267 (near EFK 6.3, and USGS Station 03538250).

Table 18. Peakflow Statistics

Parameter	Value	Units	Citation Number
10_Year_Peak_Flood	2630	cfs	43
100_Year_Peak_Flood	4880	cfs	43
2_Year_Peak_Flood	1370	cfs	43
200_Year_Peak_Flood	5930	cfs	31
25_Year_Peak_Flood	3430	cfs	43
5_Year_Peak_Flood	2070	cfs	43
50_Year_Peak_Flood	4120	cfs	43
500_Year_Peak_Flood	6990	cfs	43
Log_Mean_of_Annual_Peaks	3.137	Log base 10	43
Log_Skew_of_Annual_Peaks	-0.059	Log base 10	43
Log_STD_of_Annual_Peaks	0.231	Log base 10	43
Mean_Annual_Flood	949	cfs	31
Systematic_peak_years	28	cfs	43
Weighted_1_5_Year_Peak_Flood	1360	cfs	43
Weighted_10_Year_Peak_Flood	2590	cfs	43
Weighted_100_Year_Peak_Flood	4780	cfs	43
Weighted_25_Year_Peak_Flood	3360	cfs	43
Weighted_5_Year_Peak_Flood	2050	cfs	43
Weighted_50_Year_Peak_Flood	4020	cfs	43
Weighted_500_Year_Peak_Flood	6780	cfs	43
WRC_Mean	3.151	Log base 10	43
WRC_Skew	0.433	Log base 10	43
WRC_STD	0.204	Log base 10	43

Table 19. Flood Volume Statistics

Parameter	Value	Units	Citation Number
1_Day_10_Year_Maximum	1565.5	cfs	31
1_Day_2_Year_Maximum	797.7	cfs	31
1_Day_20_Year_Maximum	1928.2	cfs	31
1_Day_25_Year_Maximum	2051.8	cfs	31
1_Day_5_Year_Maximum	1229	cfs	31
1_Day_50_Year_Maximum	2460.7	cfs	31
15_Day_10_Year_Maximum	280.4	cfs	31
15_Day_100_Year_Maximum	361.8	cfs	31
15_Day_2_Year_Maximum	190.6	cfs	31
15_Day_20_Year_Maximum	308.2	cfs	31
15_Day_25_Year_Maximum	316.4	cfs	31
15_Day_50_Year_Maximum	340.2	cfs	31
3_Day_10_Year_Maximum	879.2	cfs	31

3_Day_100_Year_Maximum	1534.4	cfs	31
3_Day_2_Year_Maximum	460.8	cfs	31
3_Day_20_Year_Maximum	1063.8	cfs	31
3_Day_25_Year_Maximum	1125.2	cfs	31
3_Day_5_Year_Maximum	701.1	cfs	31
3_Day_50_Year_Maximum	1323.4	cfs	31
30_Day_10_Year_Maximum	197.4	cfs	31
30_Day_2_Year_Maximum	137.6	cfs	31
30_Day_25_Year_Maximum	224.5	cfs	31
30_Day_50_Year_Maximum	243.8	cfs	31
7_Day_10_Year_Maximum	492.4	cfs	31
7_Day_100_Year_Maximum	741	cfs	31
7_Day_2_Year_Maximum	289.1	cfs	31
7_Day_20_Year_Maximum	569	cfs	31
7_Day_25_Year_Maximum	593.2	cfs	31
7_Day_5_Year_Maximum	411.7	cfs	31
7_Day_50_Year_Maximum	667.5	cfs	31

Table 20. Low Flow Statistics

Parameter	Value	Units	Citation Number
1_Day_10_Year_Low_Flow	14.987	cfs	31
1_Day_2_Year_Low_Flow	17.985	cfs	31
1_Day_20_Year_Low_Flow	14.143	cfs	31
14_Day_10_Year_Low_Flow	17.408	cfs	31
14_Day_2_Year_Low_Flow	20.136	cfs	31
14_Day_20_Year_Low_Flow	16.678	cfs	31
3_Day_10_Year_Low_Flow	16.066	cfs	31
3_Day_2_Year_Low_Flow	18.539	cfs	31
3_Day_20_Year_Low_Flow	15.405	cfs	31
30_Day_10_Year_Low_Flow	18.578	cfs	31
30_Day_2_Year_Low_Flow	21.349	cfs	31
30_Day_20_Year_Low_Flow	17.829	cfs	31
7_Day_10_Year_Low_Flow	16.733	cfs	31
7_Day_2_Year_Low_Flow	19.345	cfs	31
7_Day_20_Year_Low_Flow	15.985	cfs	31
7_Day_5_Year_Low_Flow	17.638	cfs	31
90_Day_10_Year_Low_Flow	20.358	cfs	31
90_Day_2_Year_Low_Flow	25.086	cfs	31
90_Day_20_Year_Low_Flow	19.167	cfs	31
Low_flow_years	18	years	31

Table 21. Flow Duration Statistics

Parameter	Value	Units	Citation Number
1_Percent_Duration	370.8	cfs	41
10_Percent_Duration	83	cfs	41
20_Percent_Duration	56	cfs	41
25_Percent_Duration	49	cfs	41
30_Percent_Duration	44	cfs	41
40_Percent_Duration	36	cfs	41
5_Percent_Duration	129	cfs	41
50_Percent_Duration	31	cfs	41
60_Percent_Duration	27	cfs	41
70_Percent_Duration	24	cfs	41
75_Percent_Duration	23	cfs	41
80_Percent_Duration	22	cfs	41
90_Percent_Duration	20	cfs	41
95_Percent_Duration	18	cfs	41
99_Percent_Duration	17	cfs	41

Table 22. Annual Flow Statistics

Parameter	Value	Units	Citation Number
Daily_flow_years	19	years	31
Mean_Annual_Flow	53.2	cfs	31
Stand_Dev_of_Mean_Annual_Flow	11.4	cfs	31

Table 23. Monthly Flow Statistics

Parameter	Value	Units	Citation Number
April_Mean_Flow	62.1	cfs	31
April_STD	28.1	cfs	31
August_Mean_Flow	31.7	cfs	31
August_STD	8.05	cfs	31
December_Mean_Flow	68.4	cfs	31
December_STD	34.6	cfs	31
February_Mean_Flow	70.9	cfs	31
February_STD	26.9	cfs	31
January_Mean_Flow	75.2	cfs	31
January_STD	30.3	cfs	31
July_Mean_Flow	44.7	cfs	31
July_STD	45.3	cfs	31
June_Mean_Flow	40.3	cfs	31

June_STD	13.5	cfs	31
March_Mean_Flow	91.1	cfs	31
March_STD	39.7	cfs	31
May_Mean_Flow	49	cfs	31
May_STD	28.5	cfs	31
November_Mean_Flow	45.8	cfs	31
November_STD	33.9	cfs	31
October_Mean_Flow	30.9	cfs	31
October_STD	11.4	cfs	31
September_Mean_Flow	28.8	cfs	31
September_STD	8.71	cfs	31

Table 24. General Flow Statistics

Parameter	Value	Units	Citation Number
Average_daily_streamflow	49.803	cfs	41
Maximum_daily_flow	1790	cfs	41
Minimum_daily_flow	12	cfs	41
Std_Dev_of_daily_flows	77.92	cfs	41

Table 25. Baseflow Statistics

Parameter	Value	Units	Citation Number
Average_BFI_value	0.558	dimensionless	42
Number_of_years_to_compute_BFI	27	years	42
Std_dev_of_annual_BFI_values	0.073	dimensionless	42

Table 26. Climate Characteristics

Parameter	Value	Units	Citation Number
<i>Precipitation Statistics</i>			
24_Hour_2_Year_Precipitation	3.5	inches	31
Mean_Annual_Precipitation	52	inches	31
<i>Temperature Statistics</i>			
Mean_Min_January_Temperature	29	degrees F	31

DEVELOPMENT OF A MERCURY FATE AND TRANSPORT MODEL

The advection-dispersion (AD) model uses the flow fields computed by the hydrological model. The MIKE SHE AD module is comprised of four independent components, each describing the transport processes in one of the parts of the hydrological cycle, including overland transport, transport in rivers (MIKE 11), transport in the vadose zone, and transport in the saturated zone. A number of processes relevant for simulating reactive solute transport are included in MIKE SHE including: water and solute transport in macro pores, sorption of solutes described by either equilibrium sorption isotherms (Linear, Freundlich or Langmuir) or kinetic sorption isotherms (which include effects of hysteresis in the sorption process), attenuation of solutes described by an exponential decay, and plant uptake of solutes. This model did not consider plant uptake and kinetic sorption. More description of the model is provided in the next sections. The model allows simulation with constant flow field (selected by the user), recycled flow field (the period is selected by the user) or complete flow field. In addition a double porosity model can be developed for simulation of transport in fractured rock.

Transport Parameters

The sorption type that MIKE SHE accepts can be equilibrium or equilibrium-kinetic. In the first case, the sorption is assumed to be instantaneous. In the second case, the sorption is rate dependent. This model assumed instantaneous sorption type (equilibrium). The equilibrium isotherm can be either a linear, or a non-linear isotherm (Freundlich or Langmuir). The model used a linear sorption isotherm which can be described as a linear relationship between the amount of solute sorbed onto the soil material and the aqueous concentration of the solute, where K_d is the distribution coefficient, which was determined from experimental work using ORR soils and it was equivalent to $0.50 \text{ m}^3/\text{g}$ (with uncertainty of $\pm 0.05 \text{ m}^3/\text{g}$).

Table 27. Transport Parameters Used in the Model

Input Data	EUM autotype in dfs file	Typical values and base unit for constant values	Value
effective porosity	Porosity Coefficient	fraction between 0 and 1	0.4-0.1
matrix porosity	Porosity Coefficient	fraction between 0 and 1	0.1-0.04
diffusivity (SZ, UZ)	Dispersion Velocity Factor	[m]	0.005
source location	Grid Codes	[integer codes]	Provided in a .dfs2 file
diffusion coefficient (OC, River)	Dispersion coefficient	[m ² /s]	6e-008

Effective porosity. Fluxes of water are automatically read from a flow result file according to the storage frequency in the specified simulation period. Together with these fluxes the effective porosity in the groundwater determines the advective velocity of the species. The effective porosity is in the range between 0 and 1 i.e. for porous media usually 0.15 to 0.3 depending of the grain size distribution (the more uniform the higher effective porosity) and for fractured media usually 0.01 to 0.05. The effective porosity can be given either as a uniform value over the entire domain, or through a spatially distributed file (if necessary the porosity can be specified for each cell using a dfs2 file). This model used a uniform distribution of 0.4 and a single layer.

Matrix porosity. Solutes in a fractured media will be transported by diffusion in and out of the soil matrix of the media causing fast breakthroughs and long tailings. This process can be included in MIKE SHE AD by activating the dual porosity transport component (this requires providing information about the matrix porosity and mass transfer coefficient of the medium). Matrix porosity is given as a value between 0 and 1, which can be specified by either a uniform value for the entire area or distributed values using dfs2 files. Matrix porosities are generally very difficult to measure and application of this component may require calibration against breakthrough curves to give realistic estimates of the parameters. Furthermore, input should be the “effective” matrix porosity i.e. the matrix porosity that is “actively” involved in the solute diffusion. This can be significantly lower than the matrix porosity measured by core analysis.

This model used a value of 0.04 which is typical for a limestone aquifer (for a clay sample this factor can vary up to 0.30 or slightly below the effective porosity).

Dual porosity transport. This feature can be used to describe solute transport in both the fractures and in the aquifer matrix. The exchange of mass between the fractures and the matrix is described by a diffusion process and the mass transfer coefficient controls rate of solute exchange between the two phases. As this coefficient is increased, solute diffusion takes place at a faster rate which causes lower peaks but a slower attenuation of the peak in a concentration break through curve. It is an empirical constant and cannot be compared directly with the diffusion coefficient for the species. Since the mass transfer coefficient is an empirical constant and varies both with the characteristics of the species and of the media it is difficult to determine its range. For initial simulations, the model used the diffusion parameters equal to $6e-008 \text{ sec}^{-1}$, which were in the range of the diffusion parameters, obtained from experimental work, (this parameter can be as low as $1e-012 \text{ sec}^{-1}$). The model allows for spatial variations using dfs2 files.

Dispersion in SZ. The dispersion model allows two different options (isotropy and anisotropy with axial symmetry around the z-axis). Assuming isotropic conditions, only the longitudinal dispersivity, $\alpha_L=0.005 \text{ m}$, and the transversal dispersivity, $\alpha_T=0.005 \text{ m}$ were used. Under anisotropic conditions five dispersivities parameters are required, which depend on the degree of heterogeneity in the geology (and factors affecting the velocity field). Larger dispersivities are characteristic for greater heterogeneities of the geology. Furthermore, the magnitudes of the dispersivity factors depend on the scale of modelling and on the applied grid size. The larger scale the larger dispersivities and the larger grid size the smaller dispersivities are in general used because of numerical dispersion. According to [13] the longitudinal dispersivity is recommended to be in the range of 1% or less of the travel distance, the transversal, horizontal dispersivity should be at least 2% of longitudinal and the transversal, vertical dispersivity should 1% of the transversal. Dispersivities are specified in the unit meters and the values can be given as a constant value or as a map using dfs2 files.

Sources in SZ. Sources can externally be introduced into the groundwater transport component in two different ways i.e., as a point or line (over depth) source in specific grids or as a spatially

distributed source in a certain depth interval. In both cases the source can either be time varying flux of mass (mass/time [point or line] or mass/area/time [area source]) or fixed concentrations (mass/volume) which may vary in time. A point or line source is introduced by specifying the upper and lower layer and the X and Y coordinates of the horizontal location of the point (“grid”) in the model coordinate system. A spatially distributed source is introduced by specifying the upper and lower layers and the spatial distribution as a dfs2 file with code '1' in the source area and '0' elsewhere.

Dispersivity for UZ. For UZ, which is 1D, the dispersivity is specified as a single dispersivity value. Each of the input elements consists of a depth input indicating the depth in meters below ground surface to which the dispersion input is valid and the actual value to use which can be either a constant value or a dfs2 file. The same comments as given for dispersion in groundwater apply for solute transport in unsaturated media. According to [13] in unsaturated porous media recommended values for dispersivity are 0.1 meter for travel distances less than 2 meters. The longitudinal dispersivity can be distributed over depth by specifying depth intervals (as described above).

UZ sources. Normally, solutes are introduced in the unsaturated zone by the precipitation, and MIKE SHE determines the infiltration rate and thereby the mass flux in the upper node. However, mass of solutes can externally be introduced into the unsaturated zone transport component in two other ways namely as a point or line source over a certain depth in a specific soil column (grid) or as spatially distributed source in a certain depth interval. In both cases the source is given as time varying flux of mass (mass/time or mass/area/time). A point or line source is introduced by specifying the upper and lower layer and the X and Y coordinates of the horizontal location of the point (“grid”) in the model coordinate system. A spatially distributed source is introduced by specifying the upper and lower depth and the spatial distribution as a dfs2 file with code '1' in the source area and '0' elsewhere. Input that varies with depth can be given in UZ over depth intervals i.e. the user specifies the depths (depth1, depth2, depthN as numbers) and the parameter distributions in the entire model area for that depth interval as a dfs2 data file or a constant value. The parameters will then be uniform in each grid from soil surface to depth1 from depth1 to depth2 etc. until the bottom of the unsaturated zone is reached. While

this method has the advantage of easily describing the vertical discretisation, it does not take into account the discretisation which can vary from one UZ column to the next. Source strengths are specified in the Species Dependent input part.

Dispersion in overland flow. For the 2D overland transport component two dispersion coefficients (m^2/s) are specified, which are different from the dispersivity (m) used for SZ and UZ.

Overland sources. A point source is introduced by specifying the X and Y coordinates of the location of the point (“grid”) in the model coordinate system. A spatially distributed source is introduced by specifying the spatial distribution as a dfs2 file with code '1' in the source area and '0' elsewhere. Source strengths are specified in the Species Dependent input part.

Source from precipitation. By specifying a concentration in the precipitation, the model can take into account the mercury content from atmospheric deposition. This option is also available if only the subsurface zone is used for the simulation. The source will then be treated as an infiltration source instead. The precipitation is specified in MIKE SHE WM as a combination of the spatial distribution and the temporal variation. A “precipitation source” is specified in a similar way as the extend of each source is determined by its spatial distribution (a dfs2 file with the value '1' in grids included in the source and '0' elsewhere) and its concentration is specified in a time series data file (in the Species Dependent input part). Enter the location number (1, 2, etc.), the source type (the only valid type is 1 corresponding to a time varying concentration) and the spatial distribution as a dfs2 file.

Model Calibration and Verification

Calibration of the model was carried out to evaluate and refine parameter values by comparing simulated and observed values in an attempt to generate a model that is closely representative of reality within a certain level of accuracy. This process is intended to improve the predictive reliability of the model. This is an ongoing process and data values will be constantly updated throughout the duration of the project.

The main steps used for model calibration include:

1. Identification of calibration parameters.
2. Sensitivity Analysis – to identify parameters to which model predictions are most sensitive.
3. Numerical optimization – to determine a set of optimal or best-fit parameters which can be used to evaluate the model’s predictive capability for certain hydrological or meteorological processes.

Variation of the selected calibration parameters in the range of 2 to 50% will require several simulations to be carried out. The results obtained from these simulations will provide the deviations observed between the simulated and the observed values and will therefore aid in determination of the optimal parameter values to be used for calibrating the model.

The following sections present comparison of model results with selected stations on the watershed.

To evaluate the model performance we use three error measures: the Local Quadratic Error (LQE), the Mean Quadratic Error and the Relative Error (RE). The Local Quadratic Error is defined as follows:

$$LQE = \frac{(Q_{data} - Q_{model})^2}{Q_{data}^2} \quad (6)$$

Where LQE is the local quadratic Relative Error, Q_{data} is the measured discharge, and Q_{model} is the model prediction. The Mean Quadratic Error is defined as:

$$MQE = \frac{\sum_i (Q_{data_i} - Q_{model_i})^2}{\sum_i Q_{data_i}^2} \quad (7)$$

where the sum goes over the number of data values in the flow duration curve.

The Relative Error is calculated using:

$$RE = \frac{Q_{data} - Q_{model}}{Q_{data}} \tag{8}$$

Available data was obtained from Tennessee StreamStat for Latitude (NAD83): 35.9189 (35 55 08) and Longitude (NAD83): -84.3168 (-84 19 00). The location of the USGS stations is shown in Figure 34:

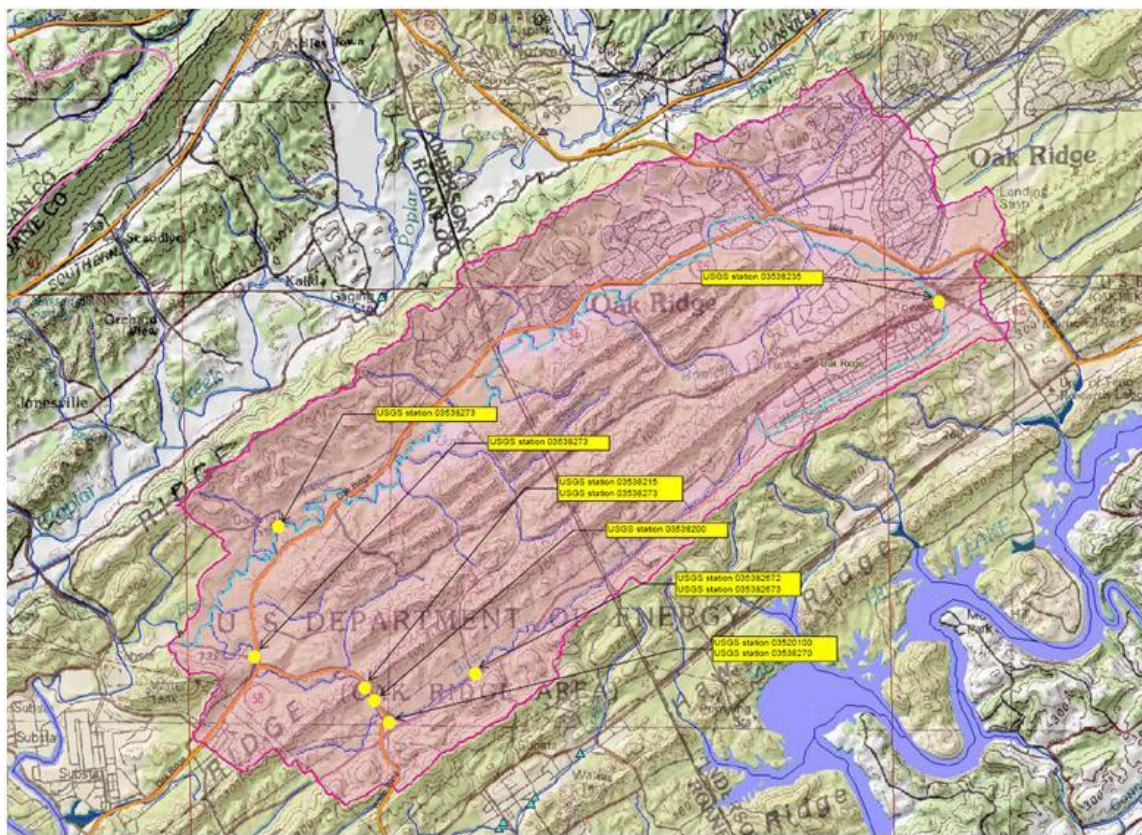


Figure 34. Model domain of East Fork Poplar Creek [52].

The activated ECO Lab module within the advection component of rivers and lakes currently contains 6 state variables, 11 auxiliary variables, 16 constants, 15 processes, 3 forcing variables, and 11 derived outputs. The description of the ecosystem state variables is formulated via a series of ordinary coupled differential equations describing the rate of change of each state variable within the ecosystem: mercury, adsorbed mercury, dissolved mercury in sediment,

adsorbed mercury in sediment, suspended solids, and mass of sediment constitute the state variables. Model constants account for the organic-carbon partitioning coefficient, desorption rate in both water and sediment, the fraction of organic carbon in suspended solids and sediment, thickness of the water film, the ratio between the thickness of diffusion layer in sediment, factor for diffusion as a byproduct of bioturbation, molecular weight of heavy metal, density and porosity of dry sediment, settling velocity of suspended solids, re-suspension rate, particle production rate, and critical current velocity for sediment re-suspension. The forcing used to represent external variables affecting the ecosystem under analysis includes the current speed, total water depth, and thickness of the computational layer. These components are summarized in the table below.

Table 28. Summary of ECO Lab Input

State Variables	Value	Constants	Value
Mercury	0.01 mg/l	Organic-carbon partitioning coefficient	50000 l/kg
Adsorbed mercury	0.1 mg/l	Desorption rate in water	1 day ⁻¹
Dissolved mercury in sediment pore water	0.1 g/m ²	Desorption rate in sediment	0.1 day ⁻¹
Adsorbed mercury in sediment	10 g/m ²	Fraction of organic carbon in SS	0.1
Suspended solids	50 mg/l	Fraction of organic carbon in sediment	0.2
Mass of sediment	10000 g/m ²	Thickness of water film	0.1 mm
Forcing		Mole weight of heavy metal	92 g/mole
Thickness computational grid layer	2 m	Density of dry sediment	250 kg/m ³ bulk
Total water depth	8 m	Porosity of sediment	0.8 m ³ H ₂ O / m ³ Bulk
Current speed	0.2 m/s	Settling velocity of SS	0.1 m/day

In previous years, the sediment transport module was calibrated by Cabrejo and Malek-Mohammadi for the Y-12 Model using an extensive collection of historical records of mercury and total suspended solids (TSS) at Station 17. During the calibration process they considered four parameters that directly affect the concentration of TSS in the water column. These parameters consisted of critical current velocity, settling velocity, resuspension rate, and particle production rate. Since sensitivity and uncertainty analysis on each of the parameters mentioned above has been extensively performed for the micro-scale model (Y-12); the best values selected from those studies were directly applied to the EFPC Watershed model without extensively investing resources and time in sensitivity and model calibration.

Assumptions and Limitations

The EFPC watershed model is subject to a series of assumptions originating primarily from the internal computational generalizations made by the software developers and those inherent to the specific model developed. For example, the software was designed by DHI to disregard density variability within the flow medium. Flow movement is restricted in a direction parallel to the reach bottom. In the software, flow medium movement perpendicular to flow direction is disregarded.

Assumptions pertaining specifically to this case study are rooted in the lack of data available. For example, the ability of the model to simulate the hydrology and transport of mercury at the watershed scale is specifically limited at a subterranean level due to the geologic variability of the site and the lack of available data to characterize these matrix structures and thus the inability to characterize it at the present time. Per the DOE's 1994 Remedial Investigation Report: groundwater flow for a shallow interval extending to approximately 100 ft below ground surface, is dominated by interconnected fractures and solution conduits. In such case, groundwater flow and discharge occur rapidly therefore contaminants are predicted to be flushed through the system. At intermediate intervals between 100 and 328 ft below the surface, the zones are well interconnected possibly allowing plumes to develop. Furthermore, at a deep interval more than 328 ft in depth, flow zones are less frequent. Due to limited data availability, the model's geologic component was set for a 2 layer (upper and lower) aquifer as discussed in previous sections. This generalization does not account for fissure conduits common in sections of the watershed.

The heterogeneity of the surface or overland features within the domain area also serves as a limiting factor. Certain empirical parameters were set to apply over the entire watershed area. Another limitation of the model is that the precipitation data represents seasonal variability but is not reflective of the spatial variability to which the watershed may be subjected. Although the application of the rainfall time-series throughout the watershed is not highly reflective of the spatial dynamics of a hydrological event it represents the best means with which to simulate this item.

The capabilities of the mercury transport module within the EFPC watershed model are also limited as it pertains to the development of TMDL studies. It must be taken into account that the direct link between the importance of mercury speciation to the observed concentrations in fish tissue and water quality standards needs to be better established. Fish tissue concentration is related to methylmercury rather than total mercury. The differences in time and space patterns associated with methylmercury are ultimately dependent on intricate, interconnected and interacting transport and transformation processes. However, since the criteria have not yet been established, TMDL studies have not been conducted on this aspect by FIU.

An important model limitation is that errors are cumulative throughout the modules. For example, the differences between the observed and simulated flow in the MIKE SHE module is transferred throughout the rest of the modules. Therefore, the mercury mass rate curves generated take into account and thus accumulate errors carried over from flow and transport modules.

The modeling system consists of coupled MIKE SHE (a 3-dimensional saturated and unsaturated groundwater flow, 2-dimensional overland flow model), MIKE 11 (1-dimensional river flow model), and ECO Lab (1-dimensional water quality model).

MIKE SHE is a deterministic, physically based and fully distributed hydrological modeling system [79]. It consists of the Water Movement and Water Quality modules. The hydrological processes are described mostly by physical laws (laws of conservation of mass, momentum and energy). The 1-D and 2-D diffusive wave Saint Venant equations describe channel and overland flow, respectively. The Kristensen and Jensen methods are used for evapotranspiration, the 1-D Richards's equation for unsaturated zone flow, and a 3-D Boussinesq equation for saturated zone flow. These partial differential equations are solved by finite difference methods, while other methods (interception, evapotranspiration and snowmelt) in the model are empirical equations obtained from independent experimental research [94]. MIKE 11 is a one-dimensional modeling tool for the detailed analysis, design, management and operation of both simple and complex river and channel systems. The MIKE 11 Hydrodynamic (HD) module solves the depth integrated equations for the conservation of mass and momentum, i.e., the Saint Venant

equations [94]. The HD module is the nucleus of the MIKE 11 modeling system and forms the basis for most modules including Flood Forecasting, Advection-Dispersion, Water Quality and Non-cohesive sediment transport modules.

The present study was developed using ECO Lab, which is the water quality module of the DHI MIKE SHE – MIKE 11. The module has the capability of estimating dissolved and particulate mercury in the water column and in sediments. The module allows the selection of the integration method for the differential equations among Euler, Runge Kutta 4th order and Runge Kutta 5th order. It also requires the specification of the update frequency, which defines how often the ECO Lab processes are calculated in the simulation. These two parameters define the precision and the CPU time necessary to run simulations [93].

The ECO Lab template defined for the present study contains six state variables, sixteen constants, and three forcing variables, in addition to auxiliary variables and processes. The state variables (Table 29) are defined by the system of differential equations, the variables in the sediment have a fixed spatial position and variables in the water column are subject to transport by advection dispersion (AD) from MIKE11. The constants are parameters given to the model that are constant in time, some of them are calculated in the hydrodynamic model, while other constants have assigned default or measured values (e.g., molecular weight of mercury, density of dry sediment, porosity of the sediment), and some were subject to calibration (e.g., organic-carbon partition coefficient, desorption rate in water, desorption rate in sediment, fraction of organic carbon in suspended solids and fraction of organic carbon in sediment).

Table 29. ECO Lab State Variables

Variable	Transport	Units
Dissolved mercury in water column	AD	mg/l
Adsorbed mercury in water column	AD	mg/l
Dissolved mercury in sediment	No transport	g/m ²
Adsorbed mercury in sediment	No transport	g/m ²
Suspended solids	AD	mg/l
Mass of sediment	No transport	g/m ²

The forcing variables are external factors that influence the system and are calculated in the hydrodynamic model (e.g., thickness of the actual layer in the computational grid, total water depth, and current speed).

Auxiliary variables and processes serve as arguments for the equations describing the state variables.

Parameters Affecting Suspended Solids Transport in ECO Lab

Four main parameters define the total suspended solids (TSS) concentration: settling velocity (v_s), critical current velocity for initiation of the movement (v_c), resuspension rate (RR), and particle production rate (PPR). Those parameters are influenced by the level of sediments in the bed (X_{SED}), and the sizes of the material in suspension.

In ECO Lab the suspended solids concentration is given by the sum of production and resuspension minus the sedimentation rates [92],

$$\frac{dTSS}{dt} = pr_{ss} - sed_{ss} + res \quad \left[\frac{gDW}{m^3 bulk.d} \right] \quad (9)$$

The production of particles (pr_{ss}) is calculated as a function of the rate of particle production, which is a fix coefficient, as follows:

$$pr_{ss} = \frac{PPR}{dz} \quad \left[\frac{gDW}{m^3 bulk.d} \right] \quad (10)$$

Where: PPR is the particle production rate [$gDW/m^2/d$], in the present model defined after calibration as $10 g/m^2d$; and dz is the thickness of the actual layer in the computational grid [m], a forcing calculated by MIKE11.

Sedimentation (sed_{ss}) is calculated based on settling velocity by the following relationship [92], which takes into account that the adsorbed mercury will be transported with the suspended solids (DHI, 2009):

$$sed_{ss} = \frac{v_s \cdot TSS}{dz} \quad \left[\frac{gDW}{m^3 bulk.d} \right] \quad (11)$$

Where: v_s is the settling velocity of suspended solids [m/d], a value of 6 m/d was used in the present model as a calibration result; TSS is the suspended solids concentration in the water [g DW/m³ bulk]; and dz is the thickness of the actual layer in computational grid [m], calculated by MIKE11.

Resuspension (res) is determined from the following relationship [92], assuming that the current speed is higher than the critical value for initiation of the movement,

$$res = \frac{RR}{dz} \quad \left[\frac{gDW}{m^3 bulk.d} \right] \quad (12)$$

Where: RR is the resuspension rate [gDW/m²/d], in the present model defined as 650 g/m²/d; and dz is the thickness of the sediment layer in the computational grid [m].

Settling velocity (v_s)

Settling velocity reflects a balance between forces causing settling and forces resisting the settling. It varies as a result of changes in the density and in the apparent viscosity (sediment concentration) of the water. For the range of sediment sizes that we are considered in this work, as the concentration of suspended solids in the stream increases, the settling velocity decreases [107].

Once a particle enters the flow after being eroded from the floodplain or as a result of direct discharges to the water body, it can travel in suspension or be deposited in the bed. Coarser particles will move in suspension for shorter distances or might move as part of the bed load by sliding, rolling and bouncing. Settling velocity is then determined by characteristics of the water and by properties of the particles.

A characterization of suspended sediments for the EFPC was developed by the Tennessee Valley Authority (TVA), in 1984 [97]. Surface layer samples were collected along the creek from mile 0.23 (kilometer 0.37 from upstream) to mile 14.31 (kilometer 23 from upstream) and then sieved

and separated into fractions according to particles sizes of less than 0.0005mm, 0.002mm, 0.008mm, 0.016mm, 0.062mm, 0.125mm, 0.60mm and 2.0mm [97]. At the time of the study (1984), about 45% of the particles just upstream of Station 17 (km 23) had a sieve size of 0.062 mm or less and about 57% had a sieve size of 0.125 mm or less.

Table 30. Settling Velocity

Sediment	Particle Size^a (mm)	Particle Density^b (g/cm³)	Settling Velocity^c (m/d)
Coarse Silt	0.062-0.031	1.8	144.81-36.20
Medium Silt	0.031-0.016	1.8	36.20-9.64
Fine Silt	0.016-0.008	1.8	9.64-2.41
Very Fine Silt	0.008-0.004	1.8	2.41-0.60

^a Source Levine, Hargrove, & Forrest, 1995

^b Levine, Hargrove, & Forrest, 1995

^c Navier Stokes equation

Based on these data and using Stokes’ equation, the settling velocity is calculated for silt size particles, resulting in variation from 0.6 to 145 m/d (Table 30). In the model, a value of 6 m/d was used.

Critical current velocity for initiation of suspension (Vc)

When water is flowing in a channel, there are two major forces in action: the force of gravity moving the water down slope, and the force of friction of the water against the bed of the channel, slowing the water down. The interaction of these forces generates a shear stress field (τ) with higher values near the river bed.

The moment at which a particle is entrained from the bed and is transported in suspension is determined by the critical shear stress (τ_{cr}), which is the stress needed to mobilize a particle from the bed. When the shear stress and the critical shear stress are equal ($\tau = \tau_{cr}$), the channel is in equilibrium; if $\tau \gg \tau_{cr}$, degradation (erosion) of the channel occurs; and if $\tau \ll \tau_{cr}$, channel aggradations (deposition) will likely result [142].

In order for a particle to be transported in suspension, the particle’s velocity must be exceeded by the vertical component of the turbulent eddies velocity of the stream. Such values have been reported to be in the same order of magnitude as the critical bed shear velocity and, for this reason, the critical current velocity for initiation of suspension is often expressed in terms of the critical bed shear velocity [141].

Shields was the first in providing a dimensionless parameter (τ_{ci}) for the critical shear stress, based on specific density (s) of the sediment particles, critical bed shear velocity for initiation of the motion (μ_{*cr}), and average particle diameter (D_{50}) [90].

To calculate the critical current velocity, first, a dimensionless particle parameter (D^*) is calculated from the following equation.

$$D^* = D_{50} \left[\frac{(s-1)g}{\nu^2} \right]^{1/3} \tag{13}$$

where D_{50} is the average particle size, s is the specific density (particle density divided by fluid density), g is the acceleration due to gravity (981cm/s^2), and ν is the kinematic viscosity coefficient ($0.01 \text{ cm}^2/\text{s}$).

Table 31. Shields Dimensionless Parameters [141]

D^*	τ_{cr}
≤ 4	$0.24 \times D^{*-1}$
$4 < D^* \leq 10$	$0.14 \times D^{*-0.64}$
$10 < D^* \leq 20$	$0.14 \times D^{*-0.10}$
$20 < D^* \leq 150$	$0.14 \times D^{*0.29}$
$D^* > 150$	0.055

Then, the critical mobility parameter (τ_{cr}) is read from Shields curve according to the values presented in Table 31 and used in the calculation of the critical shear velocity (μ_{*cr}) from the following equation.

$$\tau_{cr} = \frac{(\mu_{*cr})^2}{(s-1).g.D_{50}} \tag{14}$$

Calculated values of critical current velocity varied between 0.01 – 0.10 m/s, for ranges of particles (D_{50}) between 0.004 mm and 0.125 mm, according to the suspended sediment characterization for the UEFPC. Particles' specific density, (s), is 1.8 g/cm³ [117].

In this work, a value of 0.135 m/s was used. The higher value used in the model is justified by the fact that Shields dimensionless parameter does not consider the entrainment of a particle from a bed of non-uniform size material; therefore, it does not account for the force needed to entrain a particle that is surrounded by larger particles is higher than the force needed to move a particle surrounded by smaller particles. This is known as the hiding effect [81]. In the case of the EFPC, the bed is made of gravel with particle sizes up to 38 mm.

Table 32. Mass of Sediment at Station 17 [130]

Sample	Fines kg/m ²	Rocks kg/m ²
1	85.2	196.9
2	23.0	152.6
3	7.3	158.6
4	36.9	103.9
5	45.7	259.0
6	15.8	152.3
7	111.0	204.3
8	54.3	270.8
9	305.0	89.1
Average	76.0	176.4

Mass of sediment (XSED)

Based on data collected by Southworth et al., 2010, the total mass of sediment available to be resuspended, per unit area, at a location close to Station 17 in the EFPC was estimated at an average of 76 kg/m² for the fines, and an average of 176 kg/m² for gravel (Table 32). In the model simulations, a value of 100 kg/m² was used for the mass of sediment available to be resuspended.

Resuspension rate (RR)

The resuspension of sediments occurs when the bottom shear stress exceeds the critical shear stress velocity. During the resuspension, particles that have been deposited in the bed of the stream are moved to the water column, providing an internal source of mercury. The availability of sediments for resuspension can be limited by the age of the deposits, the amount of particles available and the depth of the creek. The resuspension rate increases in the presence of turbulence in the water body.

In the case of the ECO Lab model, the resuspension rate is a constant parameter, used in the calculation of the sediments resuspended into the water column, therefore affecting the levels of suspended particles in the water column as well as the concentration of particulate mercury in the water.

During the sensitivity analysis, it was determined that this is the parameter that defines the peaks in the concentrations of suspended solids. After several simulations, a value of $650 \text{ g/m}^2/\text{d}$ was used in this study.

Particle production rate (PPR)

Particle production rate is the variable that simulates the production of particles in the stream due to primary production of algae and the photosynthesis. Species, composition and productivity of algae in natural streams are affected by factors like watershed area, levels of inorganic phosphorous, temperature, discharge, canopy cover, and light availability [143].

In open rivers, the algae production is more significant than in highly covered areas due to the availability of light. The periphyton uses sunlight to produce biomass from plant nutrients and dissolved inorganic carbon; this alga grows attached to sediments in the bed, and can be scoured out as a result of higher current velocities or as a result of bioturbation, generating suspended solids in the water column [112].

The effect of levels of microalgae in streams is also extended to the fate and transport of the contaminants due to periphyton's large surface area and sorptive nature, which increases the bioavailability of the contaminant as it is also a source of food for herbivores.

Inputs of inorganic nutrients, like phosphorus and nitrogen, stimulate periphyton growth, in the case of the EFPC, Hill et al. (2010) reported that levels of nutrients were over the boundary for eutrophication. A mean biomass of periphyton (data for years 1998 - 2002) was measured as $15 \mu\text{g}/\text{cm}^2$, and the primary productivity rate as an average of $7.5 \mu\text{g C}/\text{cm}^2/\text{h}$, an equivalent to $1.8 \text{ g C}/\text{m}^2/\text{d}$. If the fraction of organic carbon varies between 0.05 and 0.1, then the particle production rate can be estimated in the range of 18 to $36 \text{ g}/\text{m}^2/\text{d}$, using the average primary productivity rate, which means that there is a higher range of variation for the calculated PPR.

Parameters Affecting Mercury's Fate and Transport in ECO Lab

The main parameters in the ECO Lab module that define the concentrations of mercury in the water and sediment include the partition coefficients (organic carbon partition coefficient, soil-water partition coefficient), the fraction of organic carbon present in the suspended solids and sediments, and the desorption rate of mercury in the water and in the sediments.

Partition coefficients

Partition coefficients are empirically derived constants, and are used to describe the fate of contaminants in the environment, signifying how the contaminant is distributed among two phases (i.e., liquid-liquid, liquid-solid, and solid-solid) by indicating the affinity of the contaminant for a specific phase [116]. In the present study, the principal coefficients used are the soil-water partition coefficient (K_d), and the organic carbon partition coefficient (K_{oc}).

K_d describes the tendency of the chemical to be adsorbed by soil or sediment; it is a ratio of metal sorbed to the soil (mg of metal/ kg of soil) to metal dissolved in the liquid media (mg of metal/L of solution). High values of K_d indicate affinity of the chemical for soils and, consequently, lower values are indicative of the tendency to stay in solution. Allison et al.

(2005), based on an extensive literature review, proposed the partition coefficients presented in Table 33 for inorganic mercury, expressed as Log K_d (L/kg).

Table 33. Log K_d (L/kg) Values for Inorganic Mercury

Phase	Mean	Standard Deviation	Minimum	Maximum	Page
Soil/soil water	3.6 ^a	0.7	2.2	5.8	3-9
Sediment/pore water	4.9 ^b	0.6	3.8	6.0	3-12
Suspend solids/water	5.3 ^c	0.4	4.2	6.9	3-15

^a3,981 L/kg, ^b79,432 L/kg, and ^c199,526 L/kg

Values presented in Table 33, show a strong affinity of inorganic mercury to remain bound to soils, with higher affinity ($>K_d$) for suspended solids than for sediments. K_d for a particular stream and metal, will vary depending on the nature of the suspended solids and sediments, pH of the water, concentration of the metal in the particulate and dissolved phase, and presence and levels of metal complexing agents, among other factors [113]. In the case of the EFPC, a value of 1,796.7 L/kg was reported for the phase soil to soil water [99].

K_d can be calculated from the following relation [92],

$$K_d = f_{oc} \times K_{oc} \tag{15}$$

where: f_{oc} is the fraction of organic matter and K_{oc} is the organic carbon partition coefficient.

The fraction of organic carbon (f_{oc}) is a dimensionless parameter that measures grams of organic carbon over grams of soil; therefore, it gives the fraction of organic matter available for adsorbing the organic contaminant. Soils with high organic carbon content will adsorb more of the contaminant, consequently limiting the mobility to the water phase.

Values for f_{oc} in suspended sediments have been reported in the order of 0.05 – 0.1, with a mean of 0.075, and for soils in the range of 0.002-0.024, with a mean of 0.01 [135]. The USGS (2000)

reported f_{oc} in bed sediments in the range of 0.011 to 0.04, with mean of 0.02. In the case of the EFPC, f_{oc} for soil was reported in the range of 0.0002 – 0.014, with a median of 0.003 [101].

K_{oc} is the organic carbon partition coefficient, defined as the concentration of the chemical in the organic carbon component of the soil [μg adsorbed/kg organic C, or ppb] divided by the concentration of the chemical in water [$\mu\text{g/L}$]. High values of K_{oc} characterize less mobile organic chemicals.

Adsorption/desorption rates from suspended matter and sediments

The balance between adsorption and desorption processes define the concentration of mercury in the water. These processes are governed by factors like organic matter content of the sediments, pH of the water, levels of chloride ions, redox potential, and ionic strength [125].

In the formulation of ECO Lab, as well as in the literature, the role of organic matter in the sorption kinetics is vital. In general, high organic matter contributes to higher levels of adsorption [125, 143, and 118]. Also, the higher the organic carbon content of the soil (suspended matter and sediments), the “higher the fraction of Hg(II) that is resistant to desorption”[143]. This resistance of mercury to desorb from soils might be due to its diffusion within the micropores of the soil particles and to its affinity for sulfur sites.

Adsorption and desorption are reverse reactions that describe the transition, of mercury in this case, between the solute and the solid phases. With adsorption being the forward reaction occurring from the concentration in water to the concentration in soils, and desorption being the reverse reaction [92]. The partition coefficient (K_d) establishes a linear relationship between the concentration of a contaminant in soil and the concentration of that contaminant in water at equilibrium, therefore the adsorption and desorption rates are related to each other by K_d , as expressed in the equation below.

$$K_d = k_a / k_w \quad (16)$$

where: k_a is the adsorption rate [$\text{m}^3 \text{H}_2\text{O}/\text{gDW}/\text{d}$] and k_w is the desorption rate [d^{-1}].

K_d is different for suspended solids and sediment (Table 33); therefore, the rates are different.

The desorption rate of mercury from sediments was reported by Parkpoin et al. (2001) in the range of 0.0006 – 0.014/d with a median of 0.004/d, for sediments with f_{oc} of 0.02 to 0.03 and more than 50% clay content. Higher values for this rate correspond to sediments with higher levels of chloride ions (30%). During the model calibration, the best fit for this parameter was a value of 0.02/d.

The model domain defined for this project is the Upper East Fork Poplar Creek watershed, with a drainage area of about of 4.73 km². A total of 22 cross-sections were defined for the UEFPC.

The objective is to determine the sensitivity of model output to these input parameters:

1. Discharges of computed versus measured values at known points (NWT);
2. Groundwater level fluctuations will be compared with well data;
3. The resolution of overland flow will be compared in order to determine the flooding with sufficient accuracy.

The model components and the parameters which were used to analyze the uncertainties of the model are listed in Table 34 below.

Table 34. Model Components & Parameters Used for Uncertainty Analysis (from Table 27)

Model component	Calibration Parameters	Variation %
Saturated zone	Hydraulic Conductivity, vertical and horizontal	±50%
Vegetation	Leaf Area Index	±50%
Vegetation	Root Depth	±50%
Overland Flow	Manning's Coefficient	±50%
Evapotranspiration	Crop coefficient	±50%

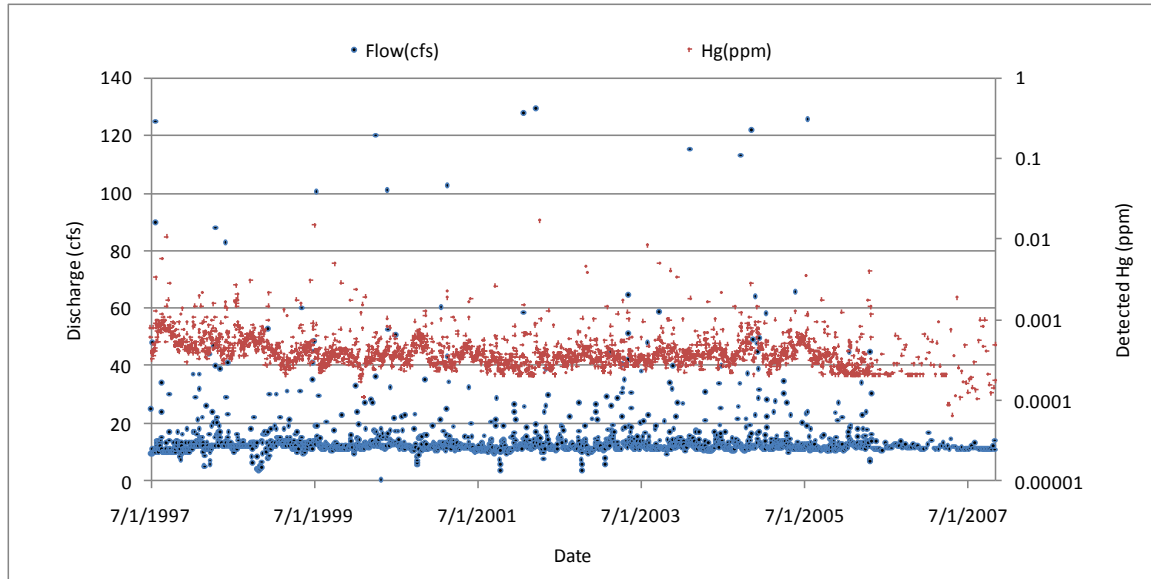


Figure 35. Measured concentrations of total mercury (mg/l) and discharges (cfs) at station 17 (EFK 23.4) on East Fork Poplar Creek.

The figure below shows a simulation of mercury concentrations in EFPC along the seven DOE stations. The data shows that the highest peak is observed at Station 17 (EFK 23.4) with gradual decreases downstream (caused by dilution of the tributaries).

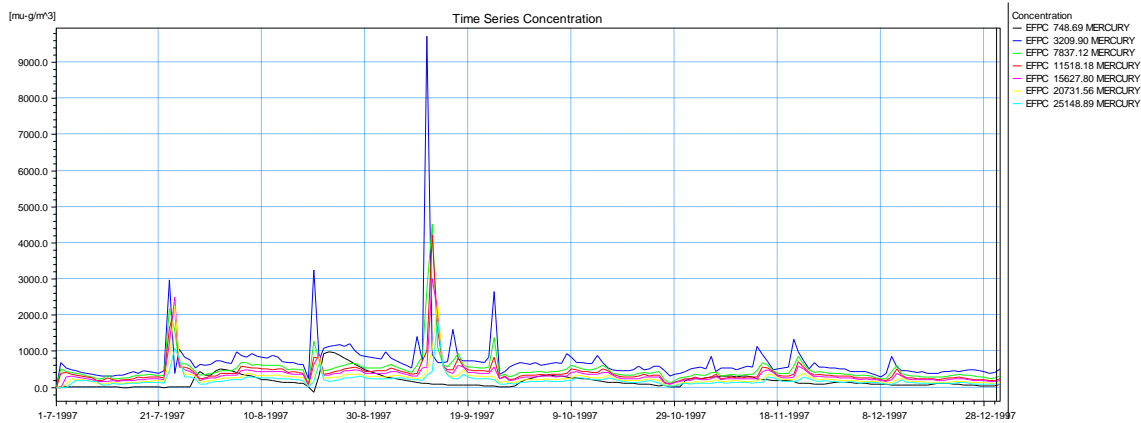


Figure 36. Simulation of mercury transport in EFPC (shown are Stations EFK 2.1, EFK 6.3, EFK 10.0, EFK 13.8, EFK 18.2, EFK 23.4, EFK 24.4).

Using the initial conditions shown in the figures below, the distribution of mercury was computed.

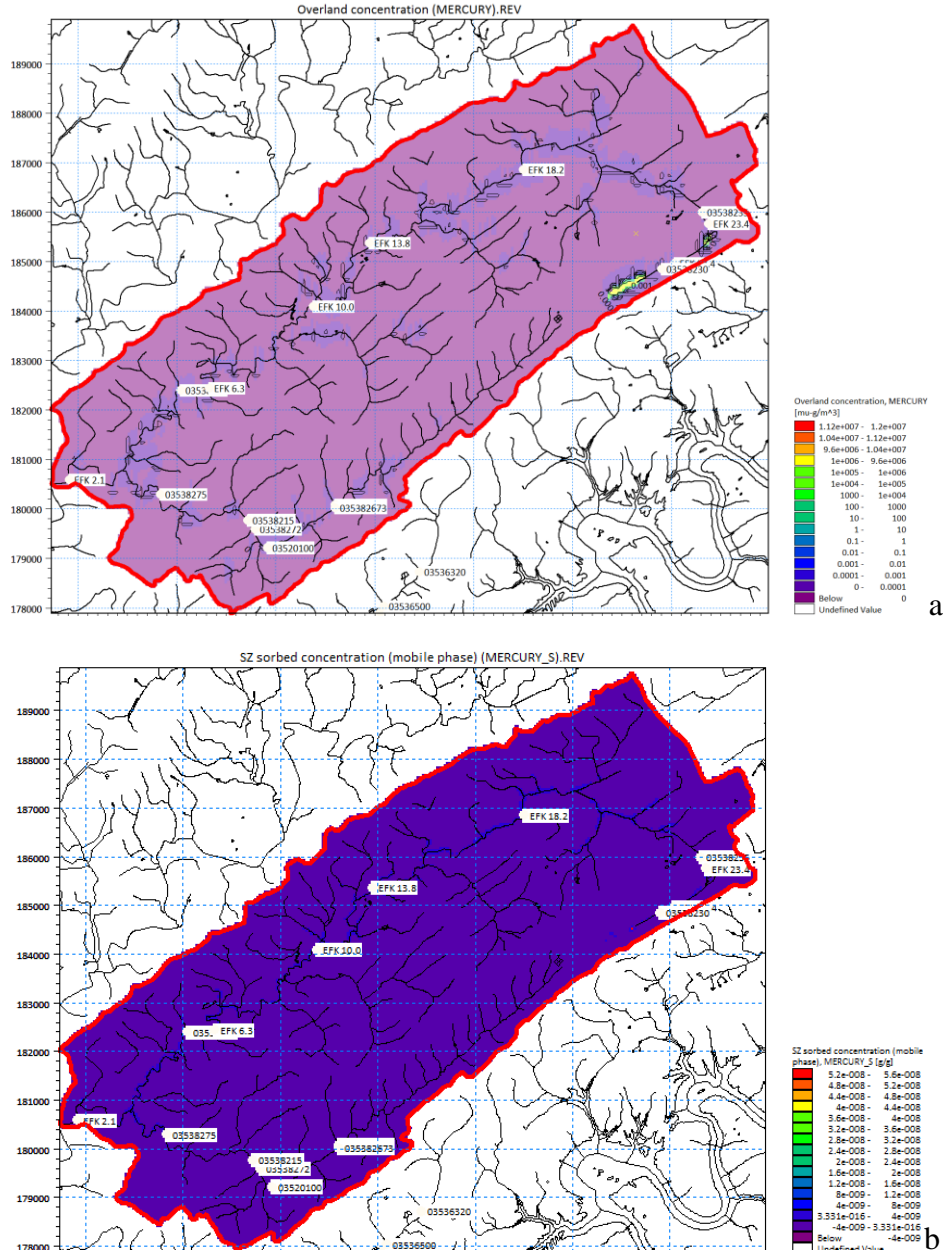


Figure 37. Simulated distribution of mercury transport a) mass per unit area and b) sorbed concentration in the saturated zone.

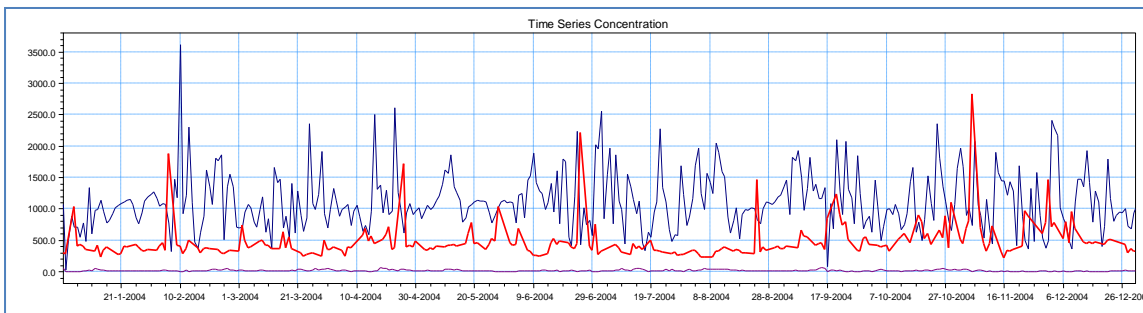


Figure 39. Observed and computed mercury concentration at Station 17.

The figure shows significant attenuation of mercury concentrations downstream EFPC (the result is consistent with dilution caused by downstream water addition), which may not be always valid considering that the model did not include sediment processes. The total mercury mass calculated for the year (in kg) is shown below.

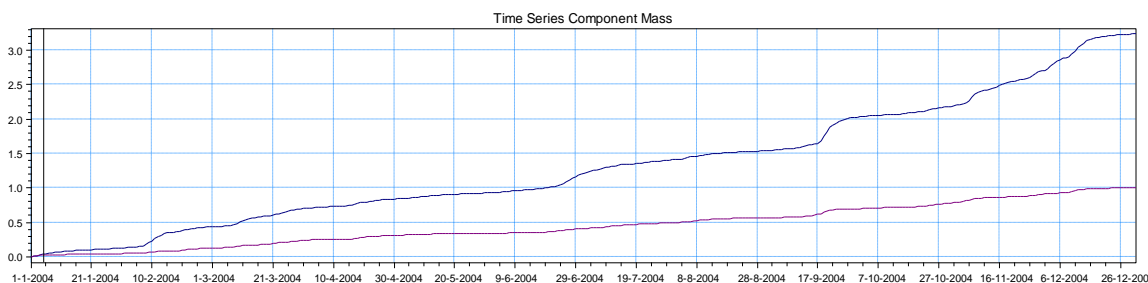


Figure 40. Observed and computed mercury leaving EFPC watershed.

The total mass accumulated at the watershed exit by river transport is lower by a factor of 3 when compared with the accumulated mass at Station 17. The mass balance shows that the difference is attributed to exchange with base flow and sorption downstream. These results are *ab initio*, which need to be correlated to measured data downstream. Furthermore, the model can be improved by considering sediment transport in the EFPC streams.

Modeling the Impact of Extreme Flood Events on Mercury Fate and Transport

In order to simulate and provide a better understanding of the flooding potential during extreme events and to determine the impact of flooding in the buildings, an integrated surface and subsurface watershed model will be developed which includes three-dimensional flow in the saturated and unsaturated zone, two-dimensional overland flow, and a one-dimensional hydraulic model of the river flow. This model will be evaluated under various management scenarios. The importance of delineating accurate floodplains under different flood events for East Fork Poplar Creek is critical for the analysis of the potential mobilization and dispersion of contaminants. The aim of this task is to provide decision makers with a state of the art numerical model which will support the selection of best management scenarios in terms of prioritizing remediation strategies based on the uncertainties related to extreme hydrological events at ORNL.

To simulate extreme events, data from Precipitation Frequency Data Server² was downloaded for Oak Ridge, TN for station OAK RIDGE ATDL according to NOAA’s Atlas 14 Precipitation frequency estimates (ARI is the Average Recurrence Interval).

Table 35. Precipitation Frequency Estimates (inches)

ARI*(years)	5 min	10 min	15 min	30 min	60 min	120 min	3 hr	6 hr	12 hr
1	9	14	17	23	29	34	37	46	58
2	10	16	20	28	35	41	44	55	69
5	12	19	24	34	44	51	55	67	84
10	13	22	27	39	51	60	65	78	97
25	15	25	31	47	62	73	78	93	114
50	18	28	35	53	72	84	89	106	129
100	19	31	39	59	82	96	101	120	145
200	21	34	42	66	92	108	114	135	162
500	24	38	47	76	108	127	134	156	185
1000	26	41	52	84	122	144	150	173	204

² http://hdsc.nws.noaa.gov/hdsc/pfds/orb/tn_pfds.html

Table 36. Precipitation Frequency Estimates (mm)

ARI*(years)	24 hr	48 hr	4 day	7 day	10 day	20 day	30 day	45 day	60 day
1	71	86	99	121	138	192	236	297	357
2	84	103	118	144	164	227	278	347	417
5	103	126	143	173	195	264	318	394	471
10	118	144	163	195	219	292	347	428	510
25	139	169	188	225	252	326	383	469	557
50	156	189	209	247	277	351	409	498	590
100	174	211	230	269	301	375	433	525	620
200	193	232	250	291	326	397	455	549	646
500	219	262	278	320	358	425	481	578	678
1000	240	287	300	342	382	445	499	598	699

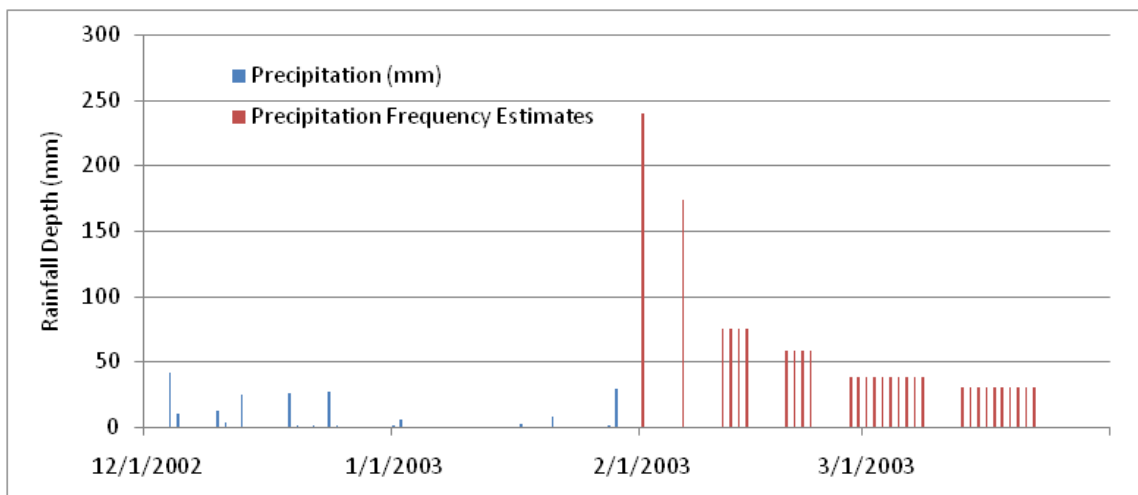


Figure 41. Simulated rainfall events.

Tests were performed for 24, 4-day, and 10 day rainfall event with frequency of 100 and 1000 years. Each of the rainfall events was added to the specified timeseries with 5 days distance between events.

Mercury TMDL of East Fork Poplar Creek

The Clean Water Act and associated regulations require each State to determine which waters do not meet water quality standards applicable according to their uses. Total maximum daily loads

(TMDLs) are required for pollutants violating these standards. To comply with these regulations the Tennessee Department of Environment and Conservation is developing the Mercury TMDLs in East Fork Poplar Creek [71]. The basis of that effort has been the development of a Load Duration Curve for Station 17 on the Y-12 complex using measured daily discharges and Total Mercury concentrations.

Although Hg concentration in water data is available in some stations, many stream reaches on the watershed have no time series discharge and concentration data that would support developing a similar TMDL analysis throughout the watershed. In order to extend the development of TMDLs to other locations on the watershed, FIU has developed the integrated model that after validation would be capable of generating discharges and Hg concentrations along the stream reaches of the East Poplar Creek watershed.

A number of other studies have reported use of models to support TMDLs in watersheds. Ambrose and Wool [70] have developed TMDLs for mercury in six south Georgia rivers and the Savannah River using the GIS-based Watershed Characterization System (WCS), a mercury delivery spreadsheet were developed and the water pollutant fate model WASPS. These models compute mercury buildup in watershed soils, loading and delivery through the watershed and mercury fate in the main stem streams. Results were compared against survey data gathered during drought conditions. Despite environmental variability and scientific uncertainties, calculated mercury concentrations in soils, sediment, and water compared reasonably well with the observed data.

The Environmental Protection Agency (EPA) has recently developed the TMDL Modeling Toolbox [72]. This set of software tools is a collection of models and databases that have been used independently in the past to develop TMDLs, including QUAL2K for Stream Water Quality, WAMView Watershed Assessment Model, Water Quality Analysis Simulation Program (WASP) and other tools. According to the EPA [72], the Toolbox models and databases have been used to develop TMDLs for a number of issues like pathogens, sediment, nutrients, dissolved oxygen, metals, temperature, and toxicants. Mercury TMDLs were developed in Georgia using WCS Mercury Tool and WASP.

The U.S. Geological Survey's Western Geographic Science Center, in collaboration with researchers at Stanford University, are developing an adaptive-management approach at the regional watershed scale to assist wastewater-treatment plants in meeting mercury discharge-permit requirements under TMDL guidelines [73]. Their study chose statistical models to explicitly state and reduce, where possible, inherent uncertainties in physical, chemical, and biologic processes controlling the fate and transport of Hg in aquatic environments. In addition, Wood et al. [73] developed and validated their approach with data from the Cache Creek sub-basin of the Sacramento River watershed, in north-central California.

North Carolina Department of Environment and Natural Resources developed Total Maximum Daily Load (TMDL) to address fish consumption advisories for mercury in the Cashie River, a tributary to Albemarle Sound (Roanoke River Basin) in Bertie County, North Carolina [75]. They used a linked-model approach to estimate the linkage between external mercury loads from the Cashie River watershed and MeHg exposure concentrations in the river. Loads from atmospheric and watershed sources were simulated with the WCS Mercury Load Estimation Tool. Transport processes in the river were modeled with the WASP-TOXI model. Using this model combination they studied the existing load and stream assimilative capacity, Waste Load and Load Allocations and proposed a TMDL implementation plan. The above examples indicate that there is a great potential in using modeling tools to support TMDL development in the Oak Ridge watersheds.

In this project we are applying the MIKE-SHE integrated hydrologic and water quality model to develop Hg Load Duration Curves for key locations and compare the results with the existing TMDL evaluations. This would extend the existing TMDL approach to other parts of the watershed where presently there is no possibility to have it for lack of adequate data. The MIKE-SHE model for the East Poplar Creek watershed was compiled with the objective to provide an assessment of the watershed assimilative capacity, critical conditions, and insight of future scenarios allowing evaluation of remediation options and environmental management plans for the East Poplar Creek Watershed. The proposed integrated approach will also provide a modeling tool to assist resource managers to assess point and non-point sources relative

contributions to mercury pollution in the watershed and in the evaluation of the effectiveness of TMDL proposals.

- Identify waters that do not meet water quality standards. In this process, the state identifies the particular pollutant(s) causing the water not to meet standards.
- Prioritize waters that do not meet standards for TMDL development (for example, waters with high naturally occurring "pollution" will fall to the bottom of the list).
- Establish TMDLs (set the amount of pollutant that needs to be reduced and assign responsibilities) for priority waters to meet state water quality standards. A separate TMDL is set to address each pollutant with concentrations over the standards.
- Develop a strategy to reduce pollution and assess progress made during implementation of the strategy. This is when a watershed partnership most likely will want to get involved. If the partnership has already developed a plan of action, it should be shared with the state. In fact, several states have incorporated watershed partnership plans into their state's strategy for specific TMDLs.

Section 303(d) of the Clean Water Act establishes the Total Maximum Daily Load (TMDL) program. A TMDL is a study that:

- Quantifies the amount of a pollutant in a stream,
- Identifies the sources of the pollutant, and
- Recommends regulatory or other actions that may need to be taken in order to lower pollutant levels to below TMDL for the stream.

Some of the actions that might be taken are:

Re-allocation of limits on the sources of pollutants documented as impacting streams. It might be necessary to lower the amount of pollutants being discharged under NPDES permits or to require the installation of other control measures, if necessary, to ensure that water quality standards will be met.

Data from Station 17 (EFK 23.4), which provided measurements of mercury and flow through the station, showed that both the load and the concentrations slowly declined to approximately 4 g/year.

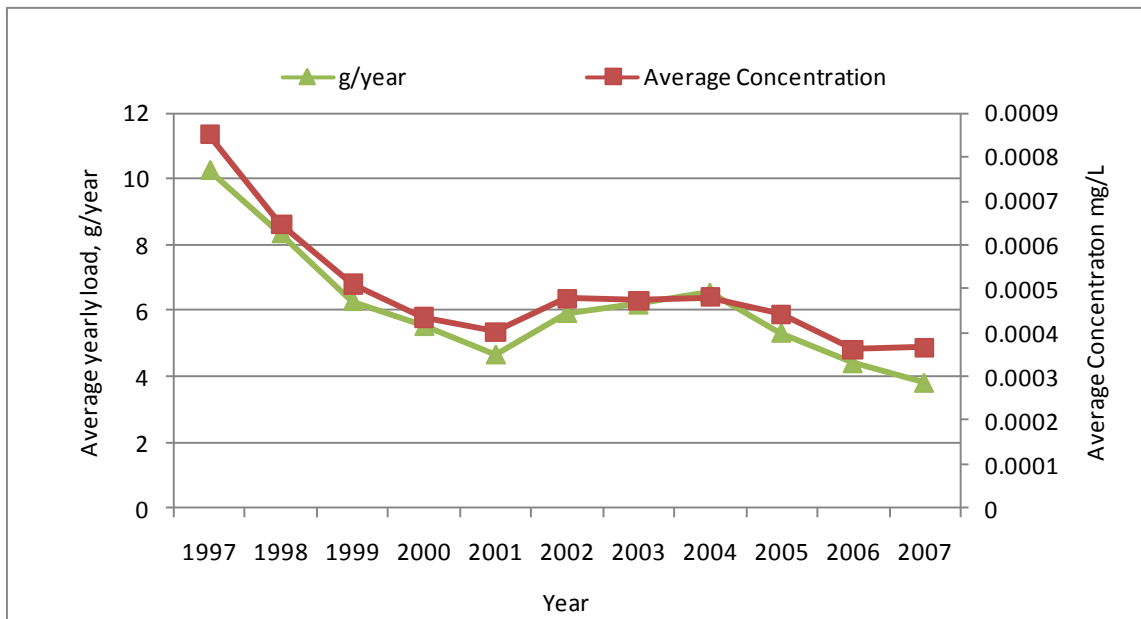


Figure 42. Average Concentration and average yearly load at Station 17 (EFK 23.4).

For sources the Tennessee Division of Water Pollution Control does not have regulatory authority over, such as ordinary agricultural or forestry activities, provide information and technical assistance to other state and federal agencies that work directly with these groups to install appropriate Best Management Practices. TMDLs can also be described by the following equation:

$$\text{TMDL} = \text{sum of nonpoint sources} + \text{sum of point sources} + \text{margin of safety} \quad (1)$$

Figure 43 depicts a flowchart of the TMDL studies currently conducted with the model.

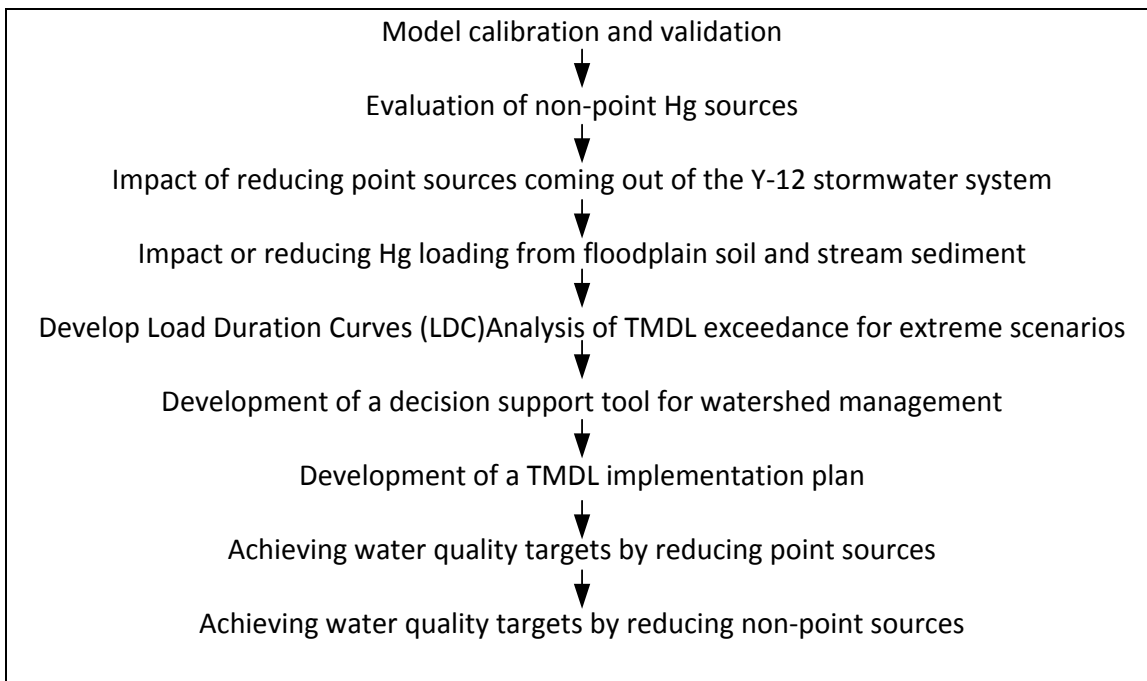


Figure 43. Flowchart of TMDL studies.

The Division of Water Pollution Control has structured monitoring and permitting activities on a rotating watershed basis. In keeping with this approach, Tennessee is developing TMDLs on a watershed basis, with each watershed examined at the appropriate time in the five-year. The integrated groundwater and surface water mode was used to construct a LDC for Y-12 Station 17 and compare with LDC from measured data. Once the model was calibrated and verified, LDC’s were developed for points along the stream with unavailable data. The models were used to compare the loads after storms during dry and wet periods.

The purpose of model calibration is to define optimum values for the parameters affecting the processes in the system, and implies the need to carry several simulations. Once the calibration parameters are identified, a sensitivity analysis is performed to gain insight into which assumptions are critical, to evaluate the effect on the process under simulation of changes in input parameters, and to determine the importance of each parameter in terms of its effect in the output [136].

For the sensitivity analysis, the input parameters are fixed during a simulation and are changed in different runs. A model parameter can be derived from observed or measured data, a constant that is characteristic of the process or region being modeled (e.g., porosity and density of the sediment), a quantity estimated from the physical formulation of the parameter (e.g., critical current velocity, settling velocity), or an estimated value from literature review (e.g., fraction of organic carbon).

Due to the wide range of variability that usually occurs in stream flows, and in order to effectively calibrate the variables for the model, flow and load duration curves constitute a valid tool for the analysis of data.

A flow duration curve (FDC) presents a relationship between the frequency and the magnitude of the flow in a particular stream. The daily main flow is presented on the Y-axis in cubic meters per second (cms). On the X-axis is the corresponding percent of time in which that flow value is met or exceeded. To construct it, the daily mean flow data for the given interval, is ranked from largest to smallest and a probability is assigned according to the rank using the following equation [136].

$$p_i = \frac{i}{n+1} \quad (17)$$

where: p_i is the exceedance probability, i is the rank number, and n is the number of observations.

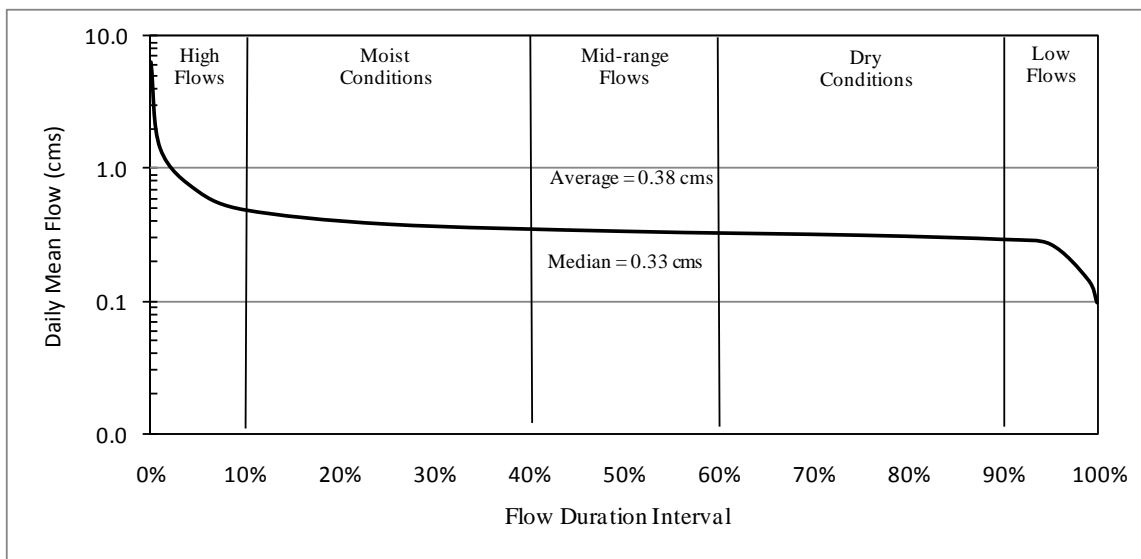


Figure 44. Flow duration curve UEFPC Station 17 (data from OREIS database years 1996-2008).

Figure 44 presents a flow duration curve for the UEFPC using observed data from the OREIS database for Station 17 for the years from 1996 to 2008. The highest observed flow value at this station for the studied period is 6.3 cm/s; the lowest observed flow is 0.1 cm/s, and the median flow (the 50 percent FDI) is 0.33 cm/s. Also, there were five levels of flow established according to the flow duration interval.

Table 37. Probabilistic Distribution of Observed Flow at UEFPC Station 17

Probability	Flow (cm/s)	Classification
0.01	1.4016	High flow
0.05	0.6658	High flow
0.10	0.4818	High flow
0.25	0.3767	Moist conditions
0.50	0.3329	Mid-range flow
0.75	0.311	Dry conditions
0.90	0.2891	Dry conditions
0.95	0.254	Low flow
0.99	0.1314	Low flow

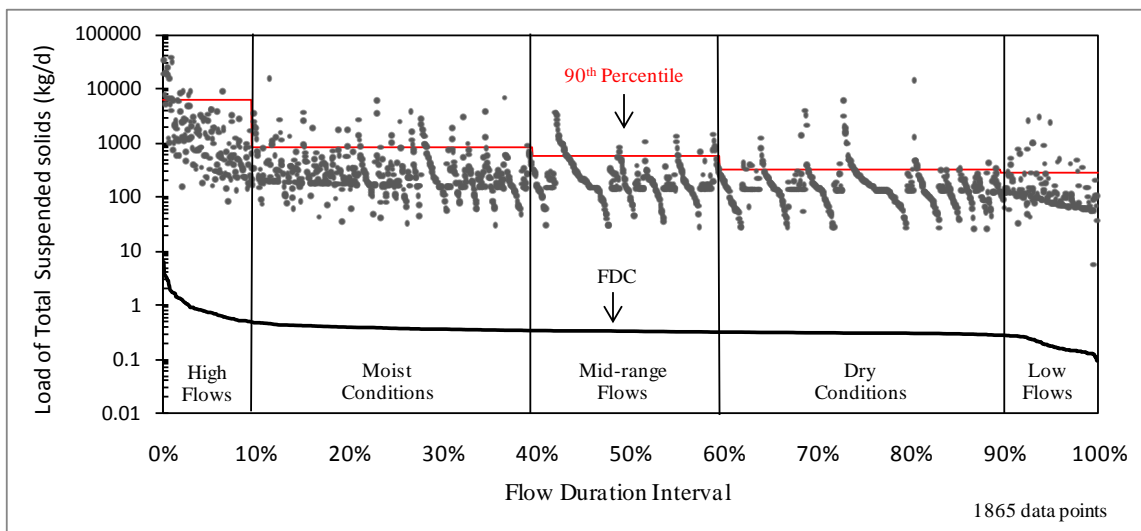


Figure 45. Load duration curve for suspended solids ranked by discharge at UEFPC Station 17 (data from OREIS database, years 1996-2009).

The load duration curve (LDC) was constructed by multiplying daily mean flow by the observed concentration of suspended solids in the water, as measured at Station 17. The results were ranked from highest to smallest flow and the probability per event was calculated from Equation 17. Figure 45 shows the results.

Table 38 presents the 90th and 50th percentile for TSS according to the level of flow, showing the relationship between discharge and levels of TSS, with higher concentrations of TSS occurring during high flows.

To show the relationship between suspended solids concentration and discharge, in Figure 46, suspended solids were ranked by flow: the 90th and 50th percentiles are presented in

Table 38.

Table 38. TSS, Load of TSS, Load of Hg, 90th and 50th Percentile, Under Different Flow Conditions (Data from OREIS Database, Years 1996-2008)

Flow	TSS 90th percentile mg/L	TSS 50th percentile mg/L	Load of TSS 90th percentile kg/d	Load of TSS 50th percentile kg/d	Load of Hg 90th percentile kg/d	Load of Hg 50th percentile kg/d
High Flows	59.0	12.4	6401.0	958.0	0.240	0.050
Moist conditions	24.5	6.4	827.0	218.0	0.035	0.013
Mid-range flow	19.3	5.8	569.0	169.0	0.027	0.011
Dry conditions	12.0	5.0	316.0	138.0	0.018	0.009
Low flow	15.2	5.0	276.0	95.0	0.019	0.009

The LDC for mercury was also constructed, by multiplying daily mean flow by the observed concentration of mercury in the water, as measured at Station 17. The results were ranked from highest to smallest flow (Figure 47). In this case, the observed concentration of total mercury is also higher during high flows, with a decrease of one order of magnitude (from 0.298 kg/d to 0.024 kg/d) from high flow to low flow conditions.

Table 38 presents the 90th and 50th percentiles for the load of mercury in kg/d, according to the level of flow.

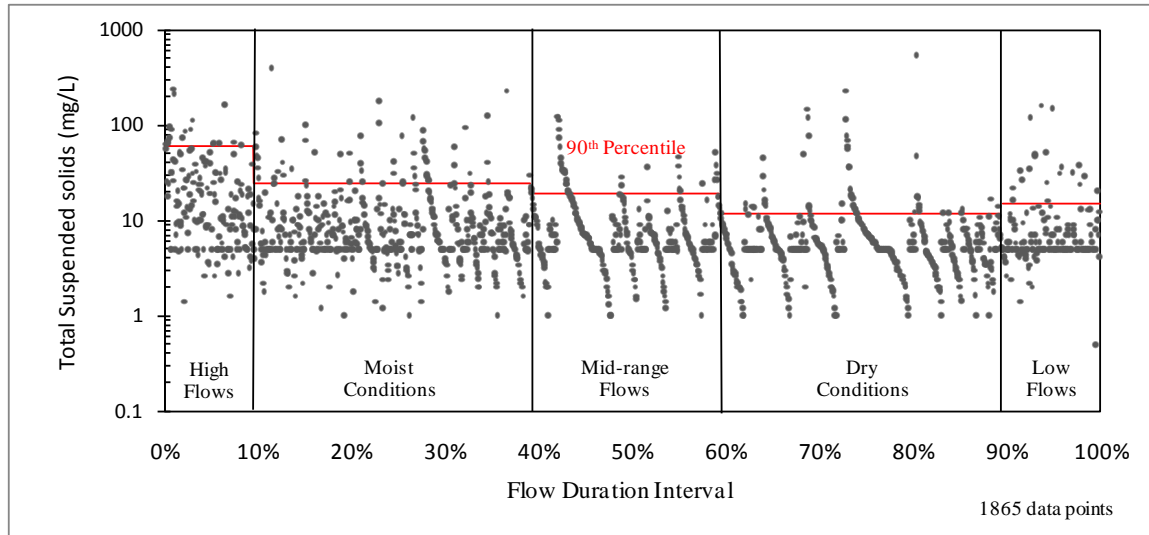


Figure 46. Total suspended solids by discharge at UEFPC Station 17 (data from OREIS database, years 1996-2009).

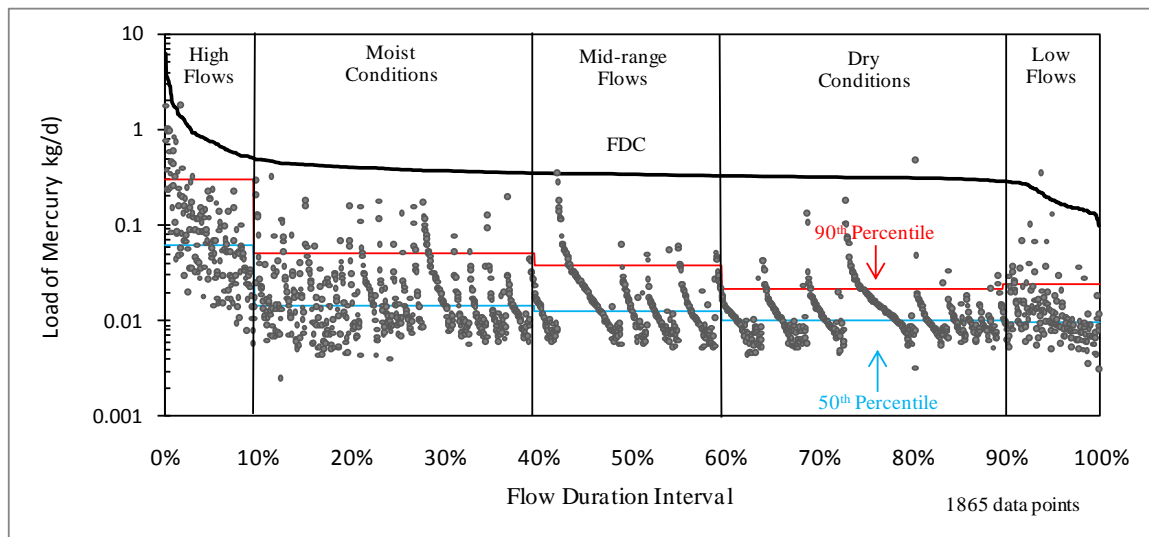


Figure 47. Load duration curve for mercury ranked by discharge at UEFPC Station 17 (data from OREIS database, years 1996-2008).

Calibration was carried out in two main steps. The first involved the parameters affecting the calculation of the total suspended solids in the system: the second step included the parameters affecting mercury concentrations and transport.

Sensitivity Analysis for Total Suspended Solids

The simulation of suspended particles at the UEFPC presents a challenge due to the high variability in the levels of suspended particles as shown in Figure 48, with daily observed values that vary between 1 and 177 mg/L, and have an average of 11 mg/L and a standard deviation of 21 mg/L.

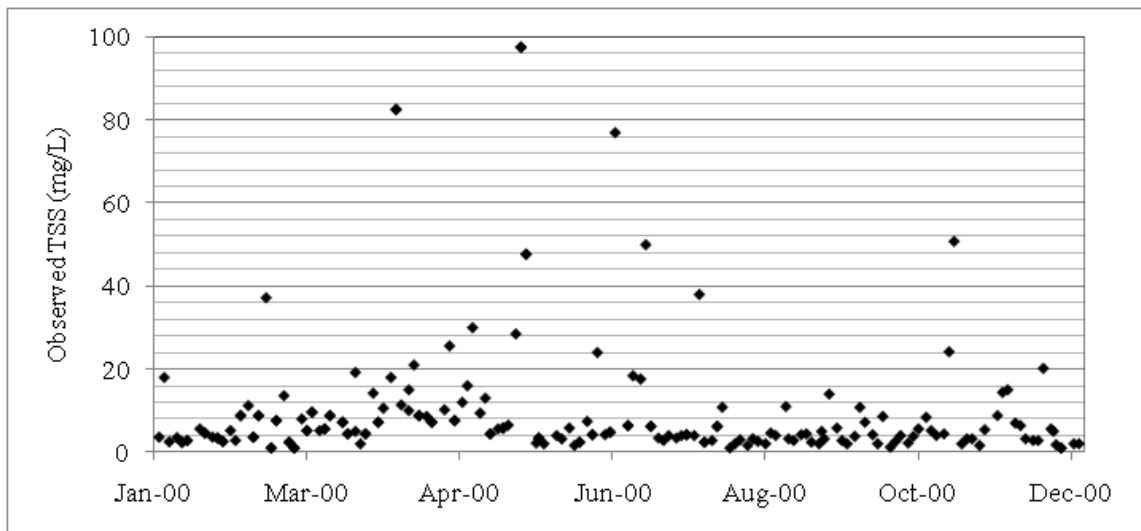


Figure 48. Total Suspended Solids at the UEFPC Station 17. Data from OREIS database year 2000.

There are four input parameters in ECO Lab that directly affect the concentration of total suspended solids (TSS): critical current velocity (v_c), settling velocity (v_s), resuspension rate (RR), and particle production rate (PPR). Simulations were run first for the year 2000 to find an acceptable range of parameters and then were extended for a period of 8 years (2000 to 2008) to finalize the calibration. The results are presented in the following sections, with an analysis based on load duration curves for both suspended solids and total mercury. Results are better

described by load duration curves due to a high dependence of suspended solids and mercury concentration on the level of discharge in the creek.

Critical Current Velocity (v_c)

Since the resuspension of particles from the bed occurs when the velocity of the stream is higher than the critical value for initiation of the movement (v_c), lower values of this parameter contribute to the resuspension of more particles, increasing the load of suspended solids in the water column (Figure 49).

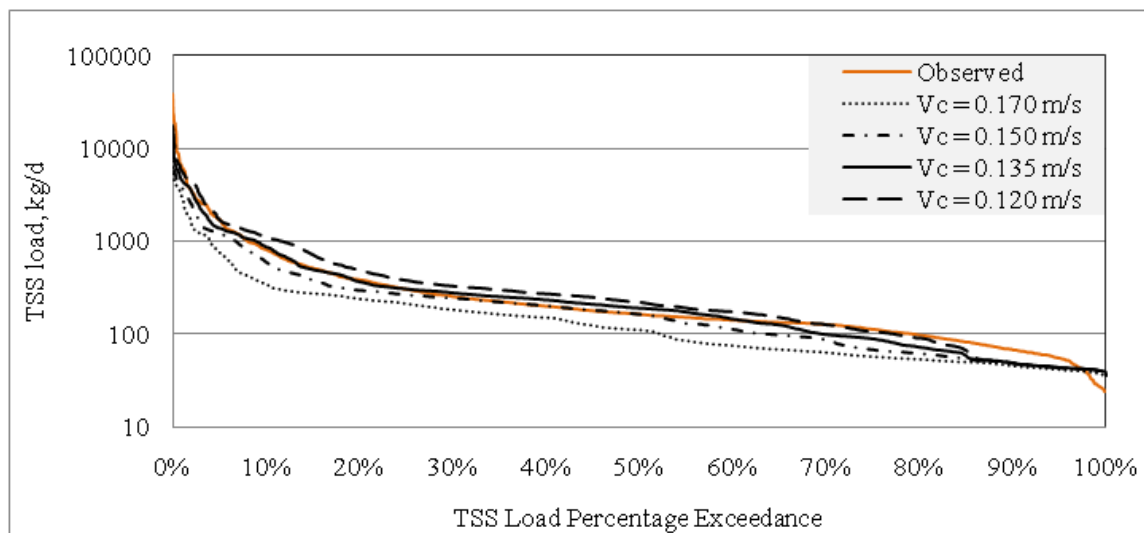


Figure 49. Effect of critical current velocity on the load of TSS.

The effect of v_c variations on TSS load is illustrated in Figure 50, where a 10% decrease in the critical current velocity (from 0.150 to 0.135 m/s and from 0.135 to 0.120 m/s) highly affects the TSS load in the high loads range while almost no change is produced in the lower loads (80% - 100% percentage exceedance). In general, the decrease of 10% in v_c increased the average TSS load by 26%. TSS shows the highest sensitivity to critical current velocity among all other effective parameters in the ECO Lab module of the model.

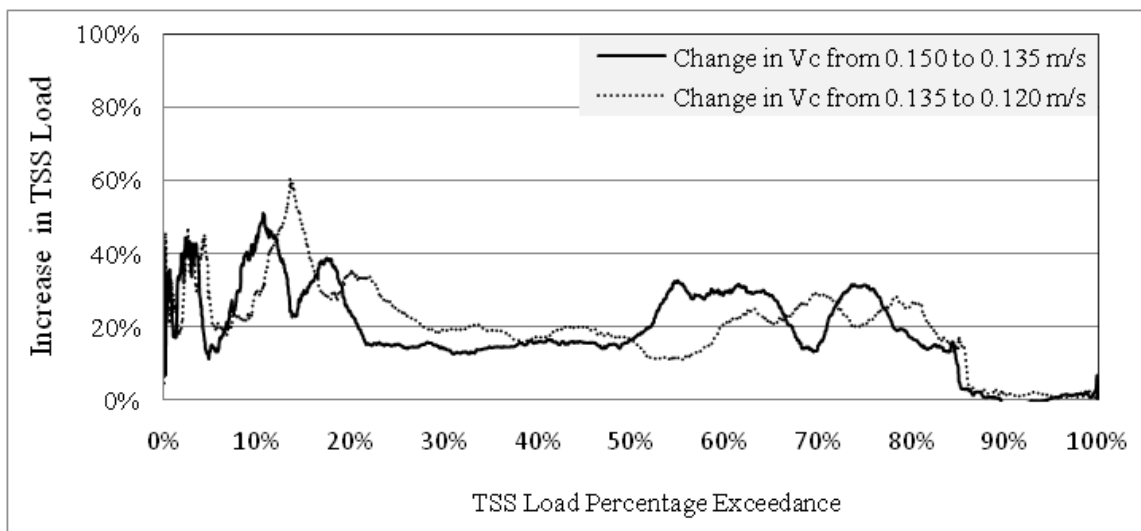


Figure 50. Effect on TSS load from decreasing critical velocity.

After the sensitivity analysis, a value of 0.135 m/s was chosen as the best value for this parameter, which makes the computed and observed data to be in the closest possible agreement (Figure 49).

Resuspension Rate (RR)

The resuspension rate is the most influential parameter on TSS peaks. The higher the resuspension rate, the higher the peak in the load of suspended solids, and in consequence, the higher the average concentration of TSS. Figure 51 shows the effect of RR variations on the TSS load. An increase in RR leads to a higher increase in larger values of TSS load and a lower increase in lower values of TSS and could even result in a decrease in the very low values of TSS as shown in Figure 52.

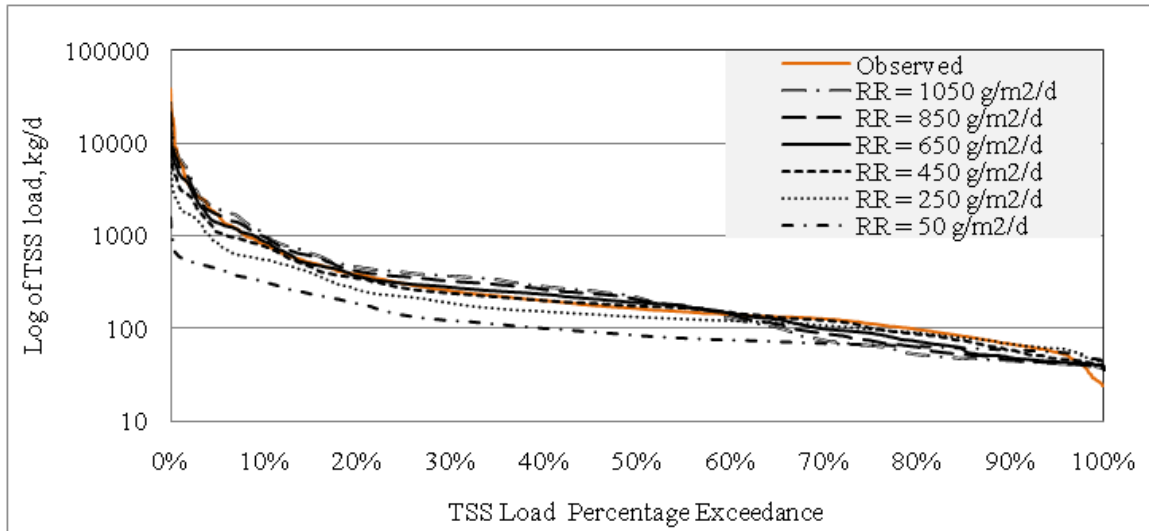


Figure 51. Effect of resuspension rate on the load of TSS.

After the sensitivity analysis on resuspension rate, the value of 650 g/m²/d was chosen as it gives the lowest error when comparing computed load to the observed load (Figure 51).

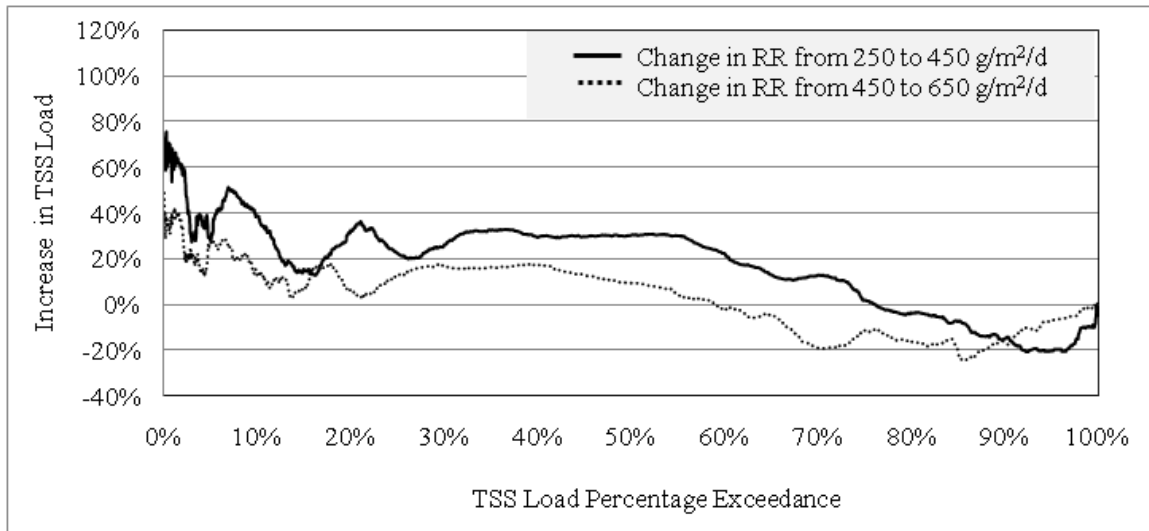


Figure 52. Effect on TSS load from increasing the resuspension rate.

Settling Velocity (V_s)

The lower the settling velocity, the longer it will take for particles to settle, therefore increasing the TSS in water. In general, the TSS load increases with decreasing settling velocity as illustrated in Figure 53.

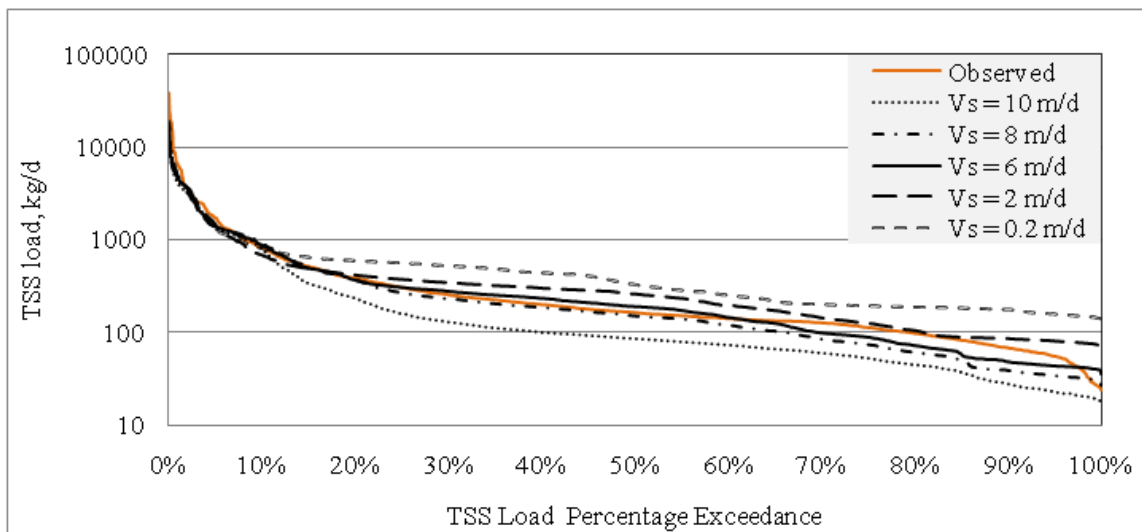


Figure 53. Effect of settling velocity on the load of TSS.

Changes in settling velocity have the least effect on high loads, which correspond to the 0 to 20 percentage exceedance, and cause higher changes on lower TSS loads. In Figure 54, a 25% decrease in the V_s increased the TSS load by about 20% in the mid-range loads, while affecting lower loads only by $\pm 10\%$. On average, during the 8-year period of the simulation, the load increased from 384 to 406 kg/d, about 6%, as a result of a 25% decrease in the settling velocity.

Sensitivity analysis on settling velocity has been performed within the ranges for very fine and fine silt, calculated in Table 30, which is in agreement with the sizes of suspended particles present in the creek. A value of 6 m/d was chosen as the best value which results in the best fit to the observed data.

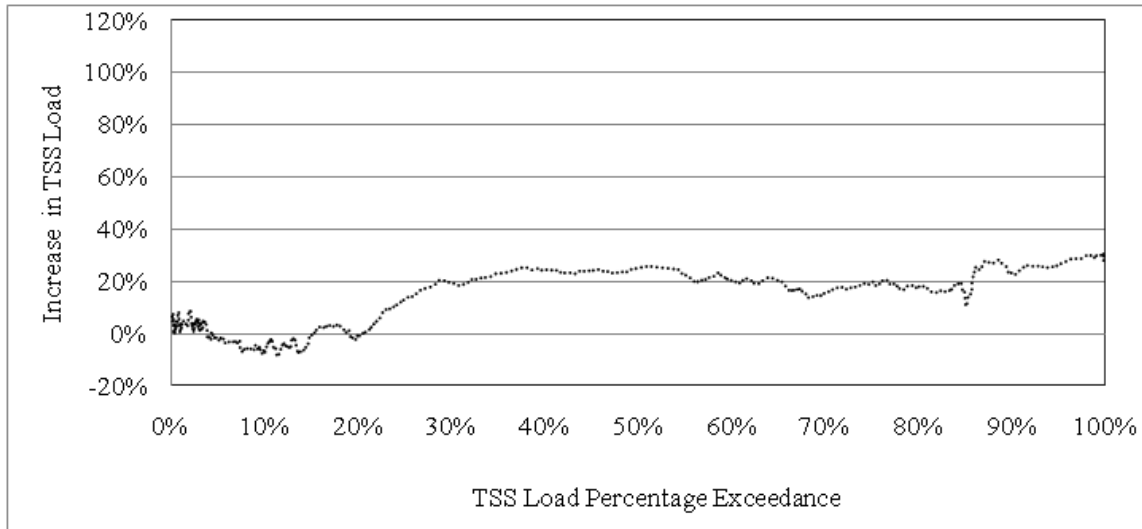


Figure 54. Effect on TSS load from decreasing settling velocity from 8 to 6 m/d.

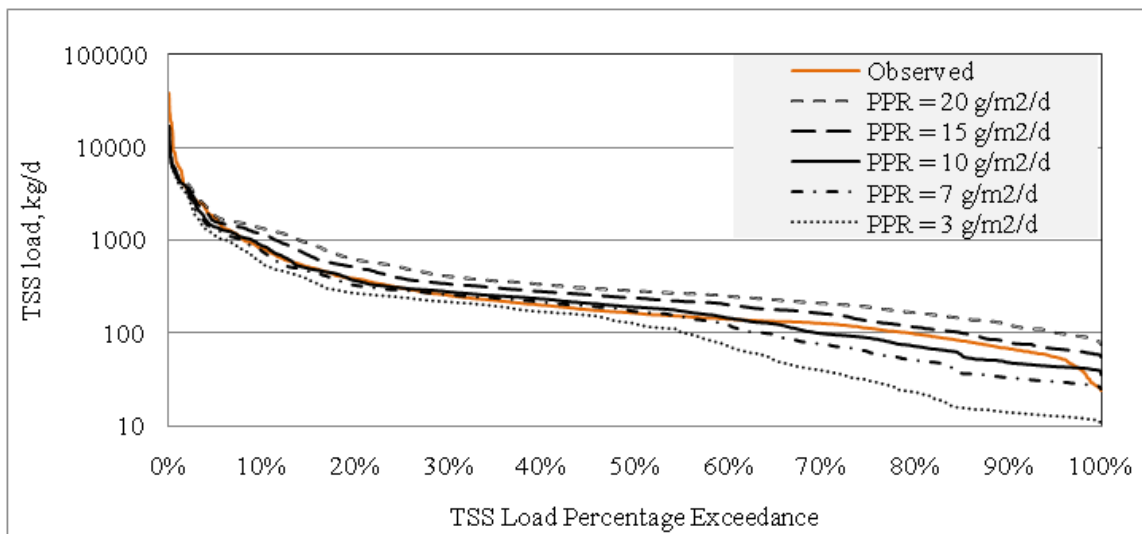


Figure 55. Effect of particle production rate on the load of TSS.

Particle Production Rate (PPR)

The particle production rate is a fixed coefficient that simulates waterborne particulate matter [92]. A series of simulations were run for different values of the parameter between 1 and 30 g/m²/d while other parameters were set at default values. As shown in Figure 55, increasing the

PPR increases the load of suspended solids in the water column, with higher effects on low loads (Figure 56).

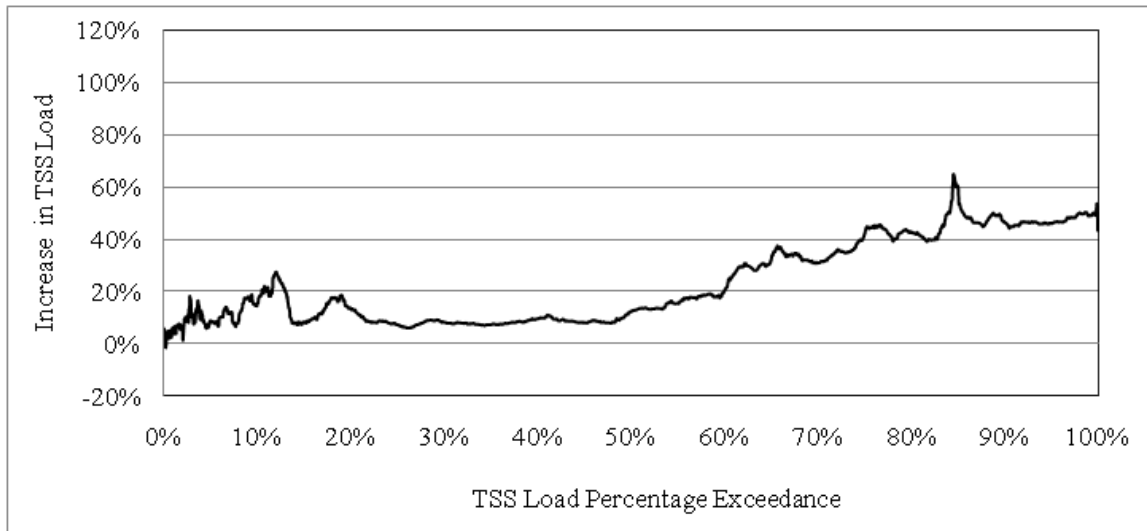


Figure 56. Effect on TSS load from increasing PPR from 7 to 10 g/m²/d.

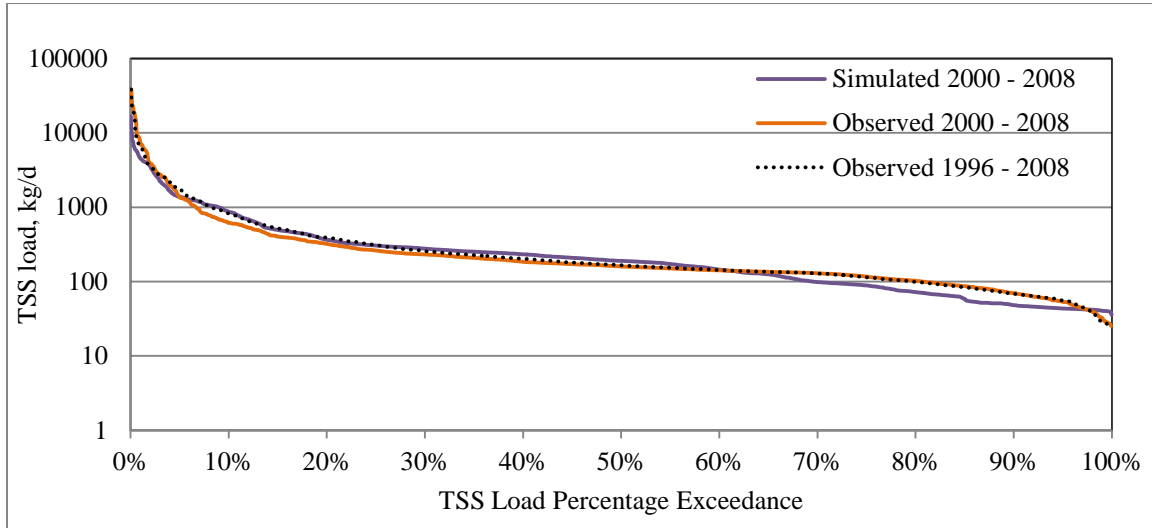


Figure 57. TSS load simulated and observed (2000 – 2008), UEFPC-Station 17.

Increasing the PPR by 43% (Figure 56) increased the average load of suspended solids during the 8-year simulation period by 10%, from an average of 370 kg/d (PPR = 7 g/m²/d) to 406 kg/d

(PPR = 10 g/m²/d). The average TSS increased from 10.17 to 11.36 mg/L during the same period.

A value of 10 g/m²/d was chosen as the best value for PPR following the sensitivity analysis as it creates the best agreement between the computed load and the observed load.

Figure 57 compares the computed and observed TSS load for a period of 8 years, including dry and wet years, with an average observed TSS of 11.72 g/m³ and an average computed TSS of 11.36 g/m³. Parameters for the simulation include particle production rate (10 g/m²/d), resuspension rate (650 g/m²/d), settling velocity (6 m/d), and critical velocity (0.135 m/s).

Sensitivity Analysis Mercury Variables

In the present study, mercury concentration is being analyzed in four sub-domains: dissolved in the water, adsorbed in the water (particulate), dissolved in the sediment pore water, and adsorbed in the sediment. At the Station 17 of the UEFPC, total mercury in the water column (dissolved plus particulate) is measured in a regular basis but there is no consistent observed data that reports dissolved and adsorbed mercury separately. For the purpose of the calibration, the average percentage of the dissolved and adsorbed mercury in the water column was calculated from data collected during the biological monitoring and abatement program during 1997 and 1998 [84], presented in the appendix section under.

For mercury in sediment, there were a few observed values from the OREIS database from data collected in 1996 during the UEFPC remedial investigation. Data for dissolved mercury in pore water can be found in the Appendix section in and has an average concentration of 0.00067 mg/L and a standard deviation of 0.00096 mg/L. Data for adsorbed mercury in the sediment is presented in and has an average concentration of 33.90 mg/L and a standard deviation 32.56 mg/L.

There are four input parameters in ECO Lab that directly affect the concentration of mercury in the water column and/or the sediment: organic-carbon partition coefficient (k_{oc}), fraction of organic carbon in suspended solids (f_{ocss}), fraction of organic carbon in sediments (f_{ocsed}),

desorption rate in water (k_w) and desorption rate in sediments (k_s). Since mercury in water is mainly (about 80%) in the particulate form, the level of suspended solids in the water also plays an important role in the simulation of mercury concentration.

Organic Carbon Partition Coefficient and Fraction of Organic Carbon

The organic carbon partition coefficient (k_{oc}) defines the concentration of mercury in the organic carbon component of the soil. As k_{oc} refers to the organic carbon content of the soil, the parameter can be calculated from the relationship between the fraction of organic carbon (f_{oc}) and the soil-water partition coefficient (k_d) presented in equation (22). In the case of the EFPC, for the phase soil to water, a k_d of 1796.7 L/kg was reported for mercury, and an average f_{oc} in soil of 0.003 [99], which lead to a calculated k_{oc} of 590,000 L/kg.

Following the sensitivity analysis, a value of 500,000 L/kg was chosen as the best value for k_{oc} , as it creates the best agreement between the computed mercury concentrations and the observed values.

The major effect of k_{oc} in the ECO Lab formulation is in the dissolved mercury in the sediment (Table 39). In general, as k_{oc} decreases, the dissolved mercury in the sediment increases. If the fraction of organic carbon is kept constant, decreasing k_{oc} results in a lower partition coefficient for the sediment (k_{dse}). This represents an increasing affinity of the contaminant for the liquid phase, resulting in a higher concentration of dissolved mercury in the sediment.

No major effect was detected in the computed dissolved mercury in the water column, because the major parameter controlling it is mercury's desorption rate in water.

The fraction organic carbon coefficients were defined from average values for suspended solids and sediments in streams, presented by USEPA (2008) as 0.05 for suspended solids, and 0.02 for sediment.

Table 39. Effect of Changes in k_{oc} on Mercury Concentrations in Water and Sediment

k_{oc}	Diss. Hg water mg/L	Ads. Hg water mg/L	Diss. Hg sediment mg/L	Ads. Hg sediment mg/kg
1,000,000	0.000217	0.000447	0.000237	29.55
700,000	0.000221	0.000445	0.000337	29.54
500,000	0.000224	0.000444	0.000472	29.53
50,000	0.000232	0.000434	0.004700	29.16
5,000	0.000232	0.000434	0.046370	29.16

The above parameters resulted in a k_d of 25,000 L/kg for the phase suspended solids/water column, and k_d of 10,000 L/kg for the phase sediment/pore water.

Desorption Rate in Water

The desorption rate of mercury in water (k_w) is one of the most important parameters in the simulation of dissolved and adsorbed mercury in the water, along with the level of suspended solids in the system. Simulations were carried out varying the parameter between 0.0003/d and 30/d. As k_w decreases the dissolved mercury in the water column decreases and the adsorbed mercury increases, generating also a decrease in the total mercury.

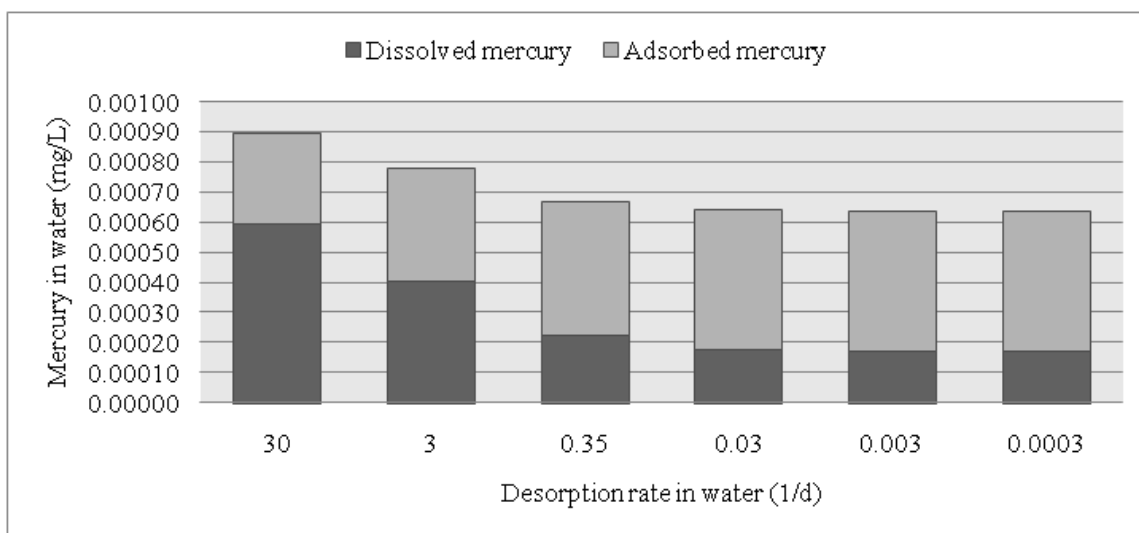


Figure 58. Effect on mercury concentration in water from changing k_w .

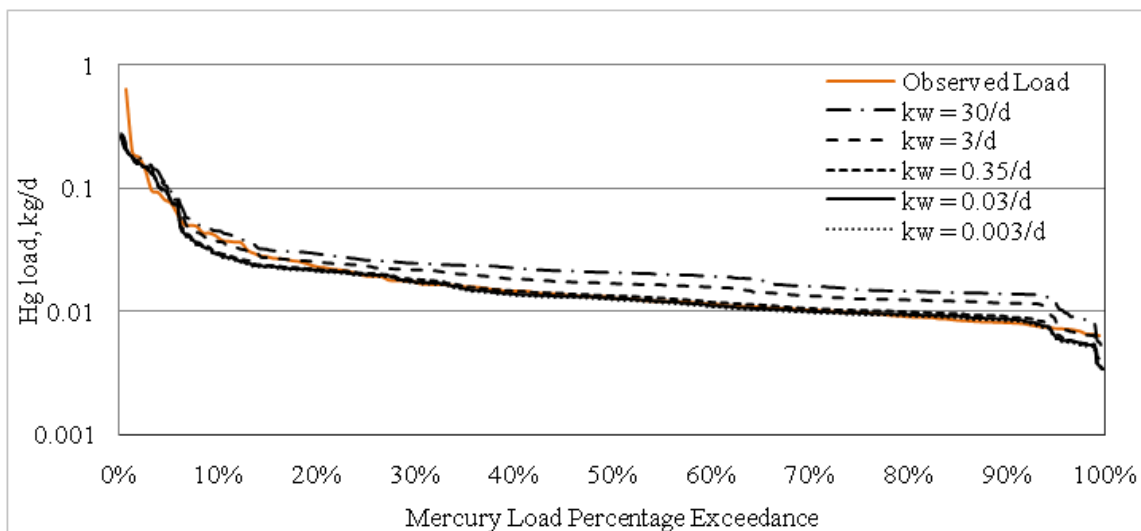


Figure 59. Effect on load of mercury as desorption rate in water changes.

A decrease in k_w generates a decrease in the load of total mercury in the water column as shown in Figure 59, with no noticeable effect in rates below 0.003/d. After the sensitivity analysis, a value of 0.03/d was chosen as the best value for the parameter, as it makes the computed mercury (dissolved and adsorbed) concentrations and the load of total mercury to be in the best agreement with the observed values.

Suspended Solids Concentration

The level of suspended solids in the system is a determinant factor in the total mercury in the water. The observed adsorbed mercury represents about 85% of the total mercury in the water column, which explains the sensitivity of the model to the concentration of suspended solids.

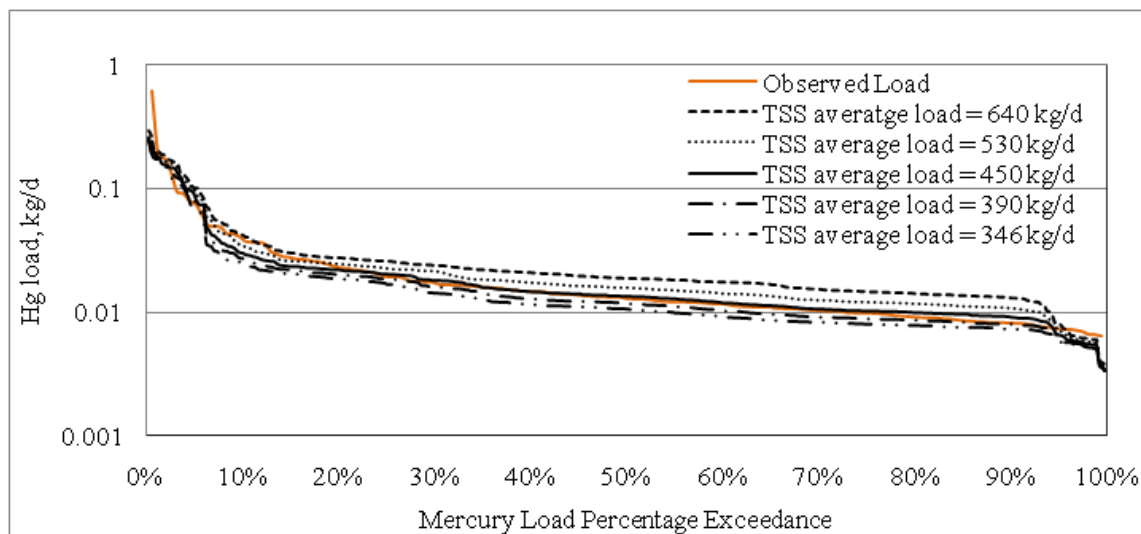


Figure 60. Effect on load of mercury as TSS load changes.

The dissolution mechanism of the mercury beads within the EFPC watersheds was reviewed and the competitive absorption on the EFPC sediment between the major cations contained in EFPC water (Ca^{2+} , Mg^{2+} , etc.) and Hg^{2+} were investigated. An extended mercury thermodynamic database relevant to EFPC environmental conditions was developed and further utilized integrated into the coupled flow and transport models already developed for the site (PHREEQC, XPSWMM, MIKE). The task relied on a thermodynamic equilibrium software and reaction kinetic software to characterize the most dominant species and processes for the environmental conditions of ORR. The model was developed using ECO Lab, which is a kinetic and reaction solver implemented as a separate module.

A set of equations were implemented in the kinetic solver which provide distribution between total mercury and methylmercury species based on observed distribution coefficients (as fraction). This is an initial approximation to ensure that the model can correctly calculate distribution of species.

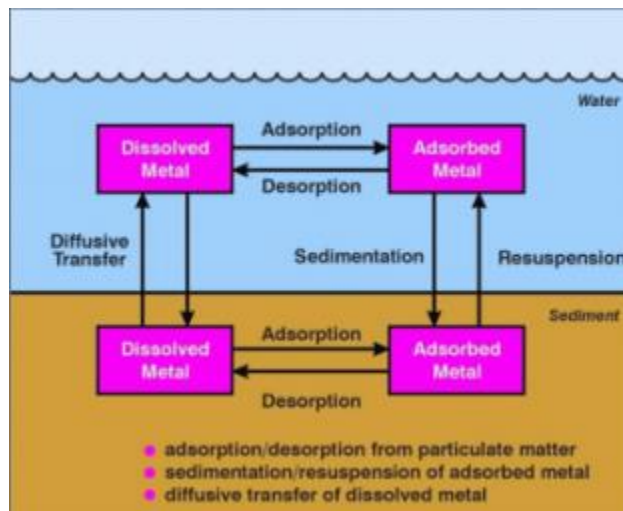


Figure 61. A summary of the processes which are currently included for modeling total mercury and methylmercury.

The mercury transport processes which were developed and incorporated in ECO Lab are defined by specifying:

- Dissolved mercury concentration in the water (SHM).
- Adsorbed mercury concentration on suspended matter (XHM).
- Dissolved mercury concentration in the sediment pore water (SHMS).
- Adsorbed mercury concentration in the sediment (XHMS).
- Dissolved methylmercury concentration in water (MeM)

The mercury exchange between suspended solids and the water column is represented by the variable SHM. This exchange is mainly driven by the organic carbon partitioning coefficient, indicating the contaminant’s affinity towards the soil phase. Dissolved mercury is computed using the following set of coupled equations [33]:

$$\frac{dS_{HM}}{dt} = -adss + dess + difv \tag{18}$$

$$adss = k_w K_d S_{HM} TSS \tag{19}$$

$$d_{ess} = k_w X_{HM} \tag{20}$$

$$d_{ifv} = \frac{f_{biot(difw)} \left(\frac{S_{HMS}}{(pors)(dzds)} - S_{HMS} \right)}{(dzwf + dzds) dz} \tag{21}$$

The equations above represent the relation between adsorption (*adss*), desorption (*dess*), and diffusive transfer (*difv*). The variables k_w , K_d , TSS , $f_{biot(difw)}$, $pors$, $dzwf$ and dz are equivalent to the desorption rate (d^{-1}), partitioning coefficient for mercury ($m^3 H_2O/gDW$), total suspended solids concentration ($g DW/m^3$ bulk), factor for diffusion due to bioturbation (dimensionless), thickness of diffusion layer in sediment (m), and thickness of the computational grid layer (m) respectively.

The methylmercury concentration is represented using a simple distribution coefficient which is based on observed distribution between total dissolved mercury and methylmercury concentrations:

$$MeM = Kmm * SHM \tag{22}$$

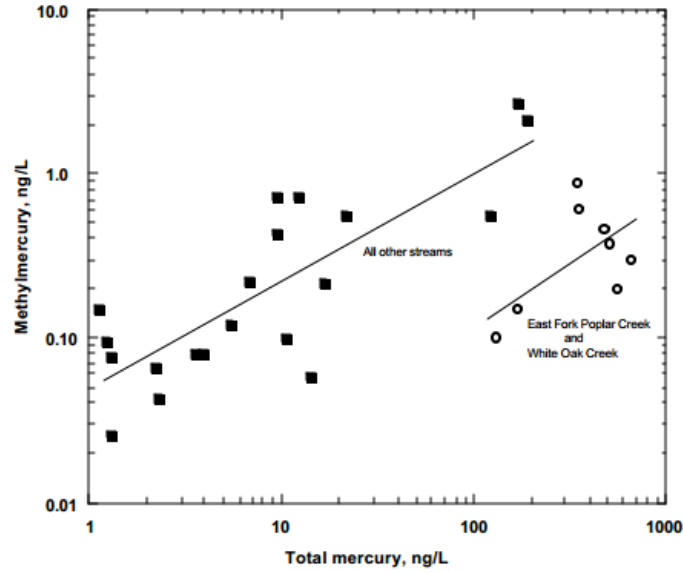


Figure 62. Relation between total mercury and methylmercury at ORR from experimental data.

The adsorbed mercury concentration on suspended matter within the water column results from mercury being absorbed by both the suspended solids and particles re-suspended by the river bed layer, and eliminating the mercury desorbed from suspended solids into water column, and also those adsorbed by settling particles.

$$\frac{dX_{HM}}{dt} = ad_{ss} - de_{ss} - se_{v} + re_{sv} \tag{23}$$

$$se_{v} = \frac{v_s X_{HM}}{dz} \tag{24}$$

$$re_{sv} = \frac{RR \frac{X_{HMS}}{X_{SED}}}{dz} \tag{25}$$

In the equations above, se_{v} and re_{sv} represent the sedimentation and re-suspension of particles. The settling velocity (m/d) of suspended solids is defined by v_s . RR is the re-suspension rate (gDW/m²/d). X_{SED} is the sediment mass (gDW/m²). The equations assume that the current speed

is greater than the critical speed responsible for initiating movement. S_{HMS} is calculated based on the equations below:

$$\frac{dS_{HMS}}{dt} = -ads + dess - dif \quad (26)$$

$$ads = k_s K_{ds} S_{HMS} \frac{X_{SED}}{dz_s \cdot por_s} \quad (27)$$

$$dess = k_s X_{HMS} \quad (28)$$

The desorption rate in sediment (d-1), metal partitioning coefficient between particulates and water ($m^3 H_2O/gDW$), and sediment porosity ($m^3 H_2O/ m^3 bulk$), are given by k_s , K_{ds} , and por_s . The variables in the above equations have been defined earlier in this section. X_{HMS} is calculated using the following relations:

$$\frac{dX_{HMS}}{dt} = ads - dess - sev + resv \quad (29)$$

$$ads = k_s K_{ds} S_{HMS} \frac{X_{SED}}{dz_s \cdot por_s} \quad (30)$$

$$sev = v_s X_{HM} \quad (31)$$

$$resv = \frac{RRX_{HMS}}{X_{SED}} \quad (32)$$

These above kinetic and thermodynamic equations were implemented within the MIKE 11 and MIKE SHE model and provide better understanding of the coupling of hydrology and mercury fate and transport with conversion to methylmercury. The equations provide the distribution

between total mercury and methylmercury species based on observed distribution coefficients (as fractions).

The mercury transport processes which were developed and incorporated in ECO Lab are defined by specifying dissolved mercury concentration in the water column and the sediment pore water, the adsorbed mercury concentration on suspended matter and in the sediment. For this initial phase of development of the template, the methylmercury concentration was added in the template as dissolved species only. The template has been completed and implemented in the hydrologic and transport model. Initial testing of the template has been conducted to calibrate the model using observed ratios of total mercury and methylmercury concentrations.

Based on observed data for the ORR watersheds (EFPC and WOC), the ratios between methylmercury to total mercury ranged between $K_{mm} = 1:500$ to $1:1000$. The initial results showed that the template predicts as expected the ratio between total mercury and methylmercury concentrations.

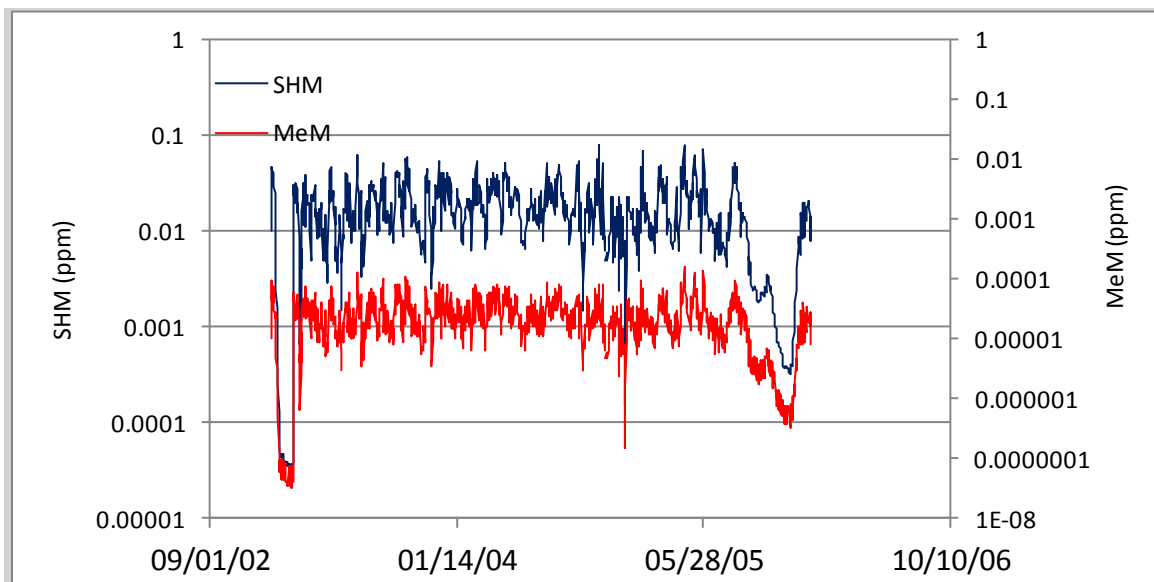


Figure 63. Nearly proportional distribution between dissolved mercury (SHM) and methylmercury species (MeM) is shown (based on the ECO Lab kinetic model)

The ECO Lab kinetic provides coupling between hydrology and mercury fate and transport with conversion to methylmercury. Additional factors are required (sorption to TSS,

photodegradation) to provide better understanding of the methylmercury's behavior in the environment. A literature review was conducted to determine the distribution coefficient between dissolved methylmercury species and methylmercury species sorbed on organic material present in water or in sediments and this process will be implemented in the ECO Lab template. A literature review served to provide understanding of recent experimental work on the distribution coefficients between dissolved methylmercury species and methylmercury species sorbed on organic material present in water or in sediments to aid in sensitivity analysis using the ECO Lab template in coupling with the MIKE SHE hydrological model. Simulations were conducted to determine the sensitivity of the kinetic parameters to the final results.

The numerical model was updated to reflect additional data obtained from the OREIS, USGS, and TDEC. Water flow is simulated in MIKE 11 via a 1-dimensional engine directly linked to the network geometry. The network developed for the EFPC model consists of reaches, nodes, grid points, and cross-sections. The river and stream network for the domain area was revised as shown below and currently it consists of 142 branches or MIKE SHE links, and 1288 nodes. Cross-sections are set to allow for overbank spilling. The left and right bank elevations and bed layer are consistent with topography files. Resistance (Manning's M) values range between 1 and 20 throughout the domain.

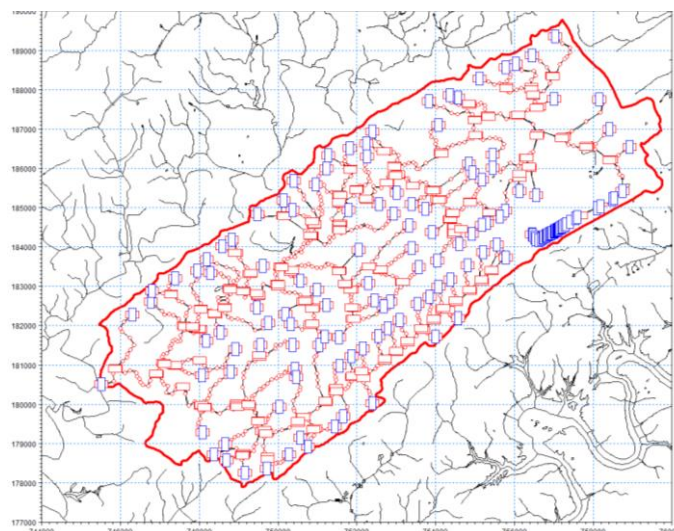


Figure 64. River network in the model indicating point nodes, boundary conditions and cross-sections.

In addition, the boundary conditions were updated in the watershed model and the open boundary conditions were coupled with additional boundary point sources to simulate the hydrology of the natural environment as well as the most significant anthropological alterations to the site. Preliminary simulations were conducted to ensure the model has expected performance. The EFPC model was modified by adding outfalls (point sources) to the boundary file in both the HD and AD module. The newly developed boundary conditions file for the modules consist of the previously existing EFPC Model boundary file and the Y-12 Model. The new boundary condition file consists of a total of 176 branches of which 42 were defined as point sources.

The advection-dispersion of solutes is coupled to the simulated flows and fluxes calculated by the MIKE SHE flow model. After the modifications to the AD simulations were made (through the ECO Lab module), additional calibrations were conducted to improve the calibration of the flow model and to calibrate the simulated concentrations and mass fluxes to the measured concentrations by tuning only the solute transport model. The purpose of the calibration was to tune the model to better match measured conditions for the most recent period. Additional factors that were taken into account are:

- Uncertainty in the measurements (time, space, equipment)
- Representativeness of measurements (point/average grid values)
- Differences between the conceptual model and nature
- Uncertainty in other model parameters and data (source description etc.)
- Additional refinements that were made to account for the dual porosity parameters

Using the revised model, the mercury concentrations along East Fork Poplar Creek were summarized and compared to observed data.

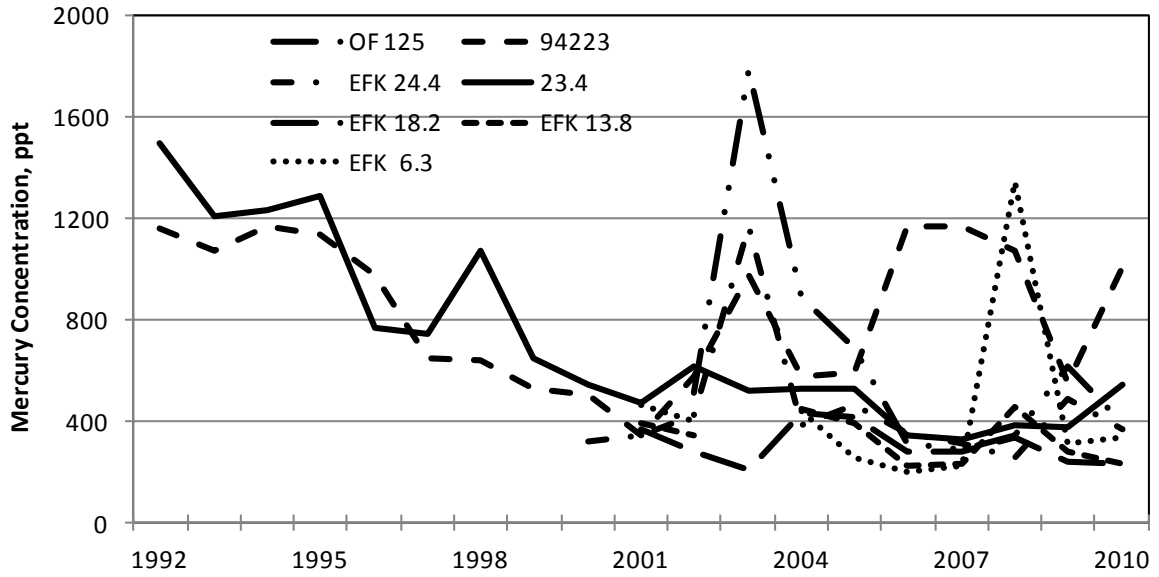


Figure 65. Monthly-based variations of average mercury concentration at selected stations along EFPC.

A SURFACE WATER MODEL FOR THE ORNL 4500 AREA

Study Area

The specific system of interest and its drainage area, herein referred to as the stormwater collection system up to Outfall 211, are located within the red circle as shown in Figure 1 and in more detail in Figure 2. It is approximately 4.5 acres and encompasses the following ORNL buildings: 4500N Wings 1, 2, and part of Wing 3, 4500S Wings 1, 2, and part of Wing 3, 4501, 4505, 4507, 4508, and 4556. The system is bounded by mostly impervious land cover (due to roof top runoff through storm drains and pavement to the north, south, east, and west); however, there are minor pervious areas throughout the drainage area.



Figure 66. Area of Interest and Building Identification.



Figure 67. Area of Interest Boundary.

A stormwater model for the contributing drainage areas to Outfall 211 has been developed and consists of 51 link/52 nodes of closed circular conduits discharging into a free surface creek. The node elevations range from 793 ft, NAD to 803 ft, NAD respectively. The system is composed of multiple sub-drainage areas with up to five sub-catchment areas for one inlet. The sub-catchment areas are defined by imperviousness, slope, width, and area. They are linked to a node so that once the rainfall is simulated it is routed into and through the system. Model inputs include topography, pervious and impervious drainage areas of each sub-catchment area, infiltration parameters, slope of sub-catchment areas, length and diameter of pipes, and Manning's coefficient for pipe roughness.

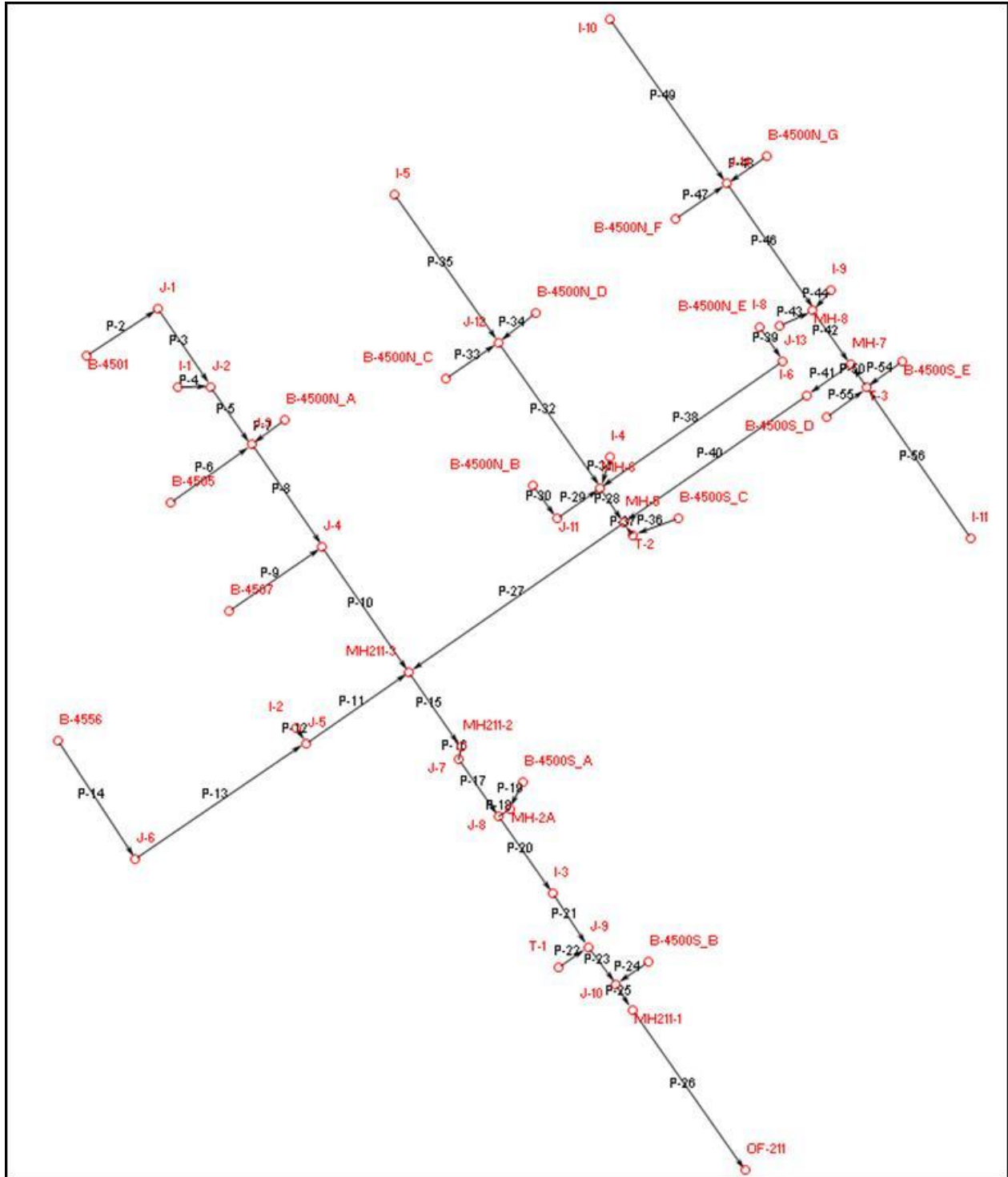


Figure 68. Stormwater Collection System.

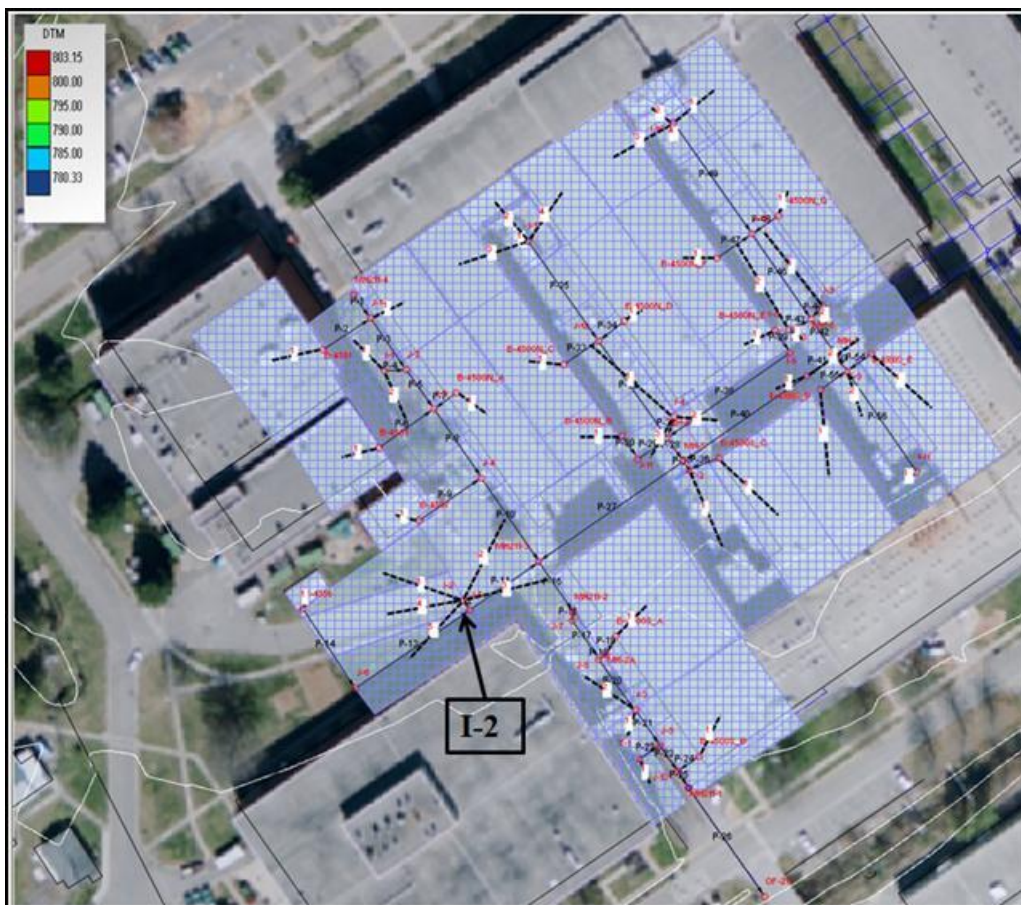


Figure 69. Sub-catchment Delineation of System.

The system was modeled as one-dimensional steady flow where a steady uniform rainfall event will be modeled. One-dimensional unsteady non-uniform flow was also modeled where the rainfall varies with time. Both synthetic and actual rainfall data from the Oak Ridge area was modeled through the system.

The storm system is unique in that sources from the adjacent buildings, such as cooling water and condensate from various AC units contribute to the Outfall 211 drainage system as well as process water from the Creep Laboratory (Building 4500S). ORNL receives their water supply, public drinking water and process water, from the Oak Ridge Water Treatment Plant where it is chlorinated for disinfection purposes. Thus, a dechlorinator has been added after Outfall 211 for dechlorination prior to its discharge into WOC.

From Building 4556 a 4" VP connects to a 10" VP which conveys water into MH211-3. MH211-3 is located at the northwest corner of Building 4500S. The main storm line runs west of 4500N and 4500S and contains MH211-1, MH211-2, MH211-2a, MH211-3, MH211-4, and Outfall 211. It begins at MH211-4 and ends at Outfall 211. From MH211-4 to MH211-3, the main storm line is constructed of 15" RCP. South of MH211-3, the line is 30" RCP. Outfall 211 is a culvert located under a bridge. However, prior to its release during dry periods, the water is held back by a 65" long, 13.5" high metal plate accompanied by an 8" PVC orifice. The 8" PVC conveys the water into the dechlorinator. Just prior to the dechlorinator the 8" PVC splits into two 4" PVC as it is directed through the dechlorinator for disinfection prior to its final release into WOC. It seems that only one of the two 4" PVC conveys water through the dechlorinator where the other is closed via a ball valve. This immediately impacts the system by restricting flow from an 8" PVC to a 4" PVC. Thus, for this project the dechlorinator was not modeled and the point of discharge for the system is immediately after Outfall 211.



Figure 70. Outfall 211.



Figure 71. WOC East of Outfall 211.



Figure 72. Dechlorinator in WOC.

As an industrial area, ORNL is composed of mostly impervious area with sparse pervious areas and lies within the Tennessee State Plane North American Datum (NAD) 1983. The area bordering the area of interest ranges in elevation from 780 ft NAD to 855 ft NAD as shown on the digital terrain model (DTM). However, the area of interest is relatively flat ranging from 780 ft NAD to 810 ft NAD.

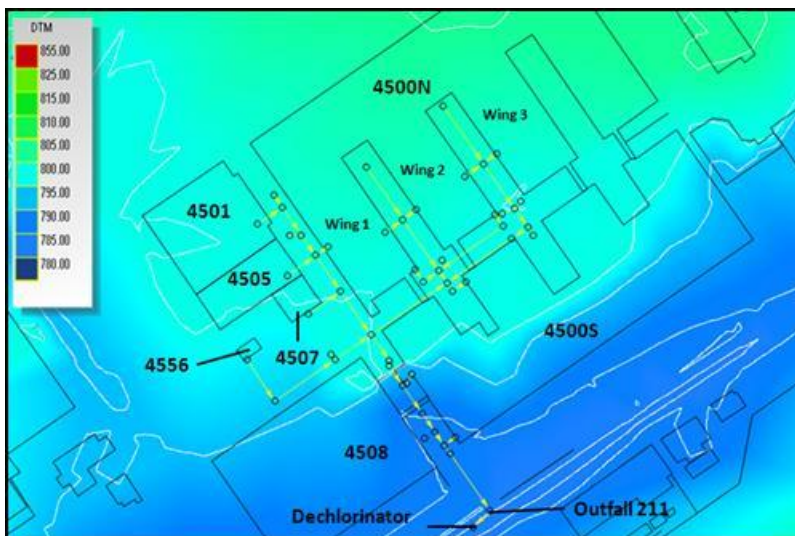


Figure 73. XPSWMM Digital Terrain Model.

Research Objective

In order to effectively assess the transport of contaminants within the system, it is first important to best understand the flow of water within the system of interest. Thus, the main research objective of this study was to develop a hydrologic-hydraulic model of the stormwater collection system that was properly calibrated and verified for both steady uniform flow and unsteady non-uniform flow local conditions. Successful development will mean that the model is capable of supporting an analysis of the system for the following types of simulations in support of decision-making related to design, operation and maintenance of the system:

1. To produce a valid surface water model for ORNL's future use in the prediction of water stages and flow rates.
2. To produce hydrographs and probability of exceedance (PE) curves in order to predict water stages and flow rates for various storm events.
3. To provide a transport analysis by introducing and tracking a conservative contaminant through the system. Furthermore, characterize the data by fitting it to its best fit probability distribution.

Site Analysis

The model is based upon two sets of drawings: 1) the original drawings from the 1950's, and 2) the ATLAS drawings, which are more recent sketches based on what is believed to be underground. Neither set of drawings contained all of the pertinent information for the model. The following assumptions and notes were made based on the information found from the two sets of drawings.

The original drawings indicate that the Outfall 211 drainage system begins from the east between 4500N and 4500S Wings 2 and 3. However, the ATLAS drawings show it interconnected with the drainage system to the east. This model is in accordance with the original drawings where Outfall 211's drainage system stands alone and begins from the east at the manhole (B-4500S_E) located between 4500N and 4500S Wings 2 and 3.



Figure 74. Location of MH B-4500S_E.

The ATLAS drawings do not show the existing inlet (I-2) to the west of MH211-3.



Figure 75. Location of Inlet I-2.

The ATLAS drawings indicate that the inlet east of 4500N Wing 1 is shown to the west of the manhole located at the north-south centerline; however, it is located to the east of the north-south centerline (I-4).



Figure 76. Location of Inlet I-4.

The ATLAS drawings do not show the two inlets (I-8 and I-9) located east of 4500N Wing 2.



Figure 77. Location of I-8 and I-9.

There are unknown inverts, manhole elevations, and inlet elevations throughout the system so reasonable assumptions were made from analysis of surrounding or like data. Assumptions were made for the building area contributing to the roof drains.

Model Development

Models are used today as an efficient, effective way to simulate theoretical and actual data. The program chosen to develop the stormwater model is XPSWMM, which is the Microsoft Windows version of the Environmental Protection Agency (EPA) stormwater modeling (SWMM) tool (USEPA, 2012). This model was chosen because of its ability to achieve the research objectives of the study. XPSWMM uses a spatially distributed link/node network to analyze the hydraulic, hydrologic, and quality of a stormwater or wastewater system. The model is known for simulating the rainfall-runoff process including infiltration, evaporation, and depression storage as well as groundwater interaction. XPSWMM is equipped with three modes, the hydraulic, runoff, and sanitary modes, of which only the hydraulic and runoff modes will be utilized in this model (Jacobson, 2011; Elliott and Trowsdale, 2007). The dialogs request certain information depending on which mode is active. The XPSWMM link/node system is shown

below. XPSWMM is equipped with GIS and CAD, and imagery interaction. This may be seen below where a GIS shapefile containing the locations of the storm system was uploaded with an aerial photograph of the area of interest.

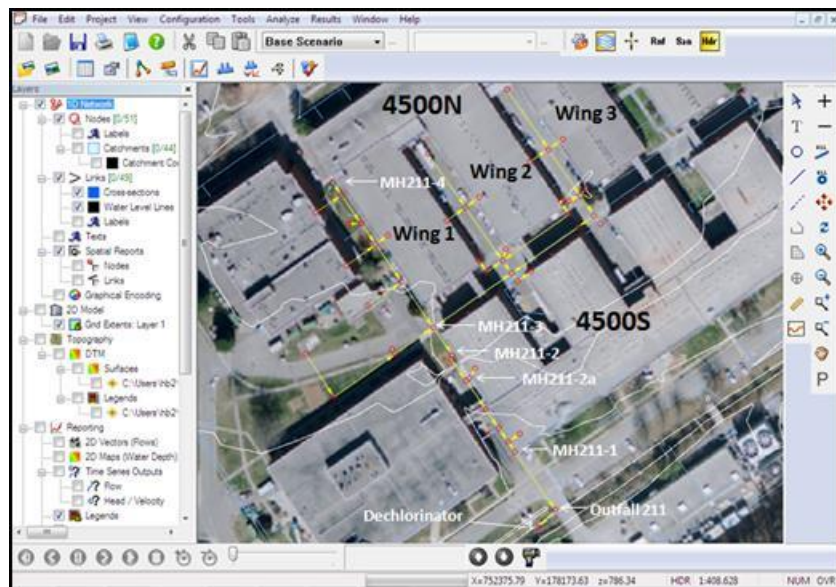


Figure 78. XPSWMM Model Main Storm Line.

Basic Theory

The system is modeled as one-dimensional (1D) steady uniform flow as well as unsteady non-uniform flow. The water flow within the storm sewer is simulated to operate as partially filled open channel flow because the gravity system is open to atmospheric pressure. However, it is possible that during a large storm event that some pipes will operate at capacity and encounter full flow. The simulations demonstrated by this study involve various types of flow within the system: steady and unsteady, uniform and non-uniform, and laminar and turbulent. Steady flow has a constant flow rate with respect to time. If the flow rate varies with respect to time then the flow is considered unsteady. Uniform flow is defined by the velocity remaining constant with respect to space and non-uniform flow by the velocity changing with respect to space. Lastly, laminar flow occurs when water particles follow straight and parallel streamlines within the pipe.

Turbulent flow, being the opposite type of flow, meanders across what would be considered streamlines. These terms may be coupled together to further describe the type of flow such as steady uniform, steady non-uniform, unsteady uniform, and unsteady non-uniform flow. Although flow rates occur as one-, two-, and three-dimensional, the simulations presented within this study pertain to 1D routing.

During steady open channel flow, steady-uniform and steady non-uniform flow can occur. Uniform flow is not common and may rarely exist; however, given a small margin of error in depth it may be considered uniform for simplicity. The depth of flow within a channel having uniform flow is considered normal depth. For calibration purposes the study provides a steady uniform flow simulation by introducing a constant precipitation into the system at two isolated locations, and a mass balance of the system is taken using the conservation of mass, also known as the continuity equation, as follows:

$$m = \rho * A * v \quad \text{(Equation 33)}$$

If inflow and outflow of the system is being examined, then mass in equals mass out. This is considered mass balance.

$$m_1 = m_2 \quad \text{(Equation 34)}$$

The total energy conveyed between the links within the system is accounted for by solving the Bernoulli's equation. Bernoulli's equation may be applied to pressurized systems and gravity systems and assumes that the fluid is incompressible, in-viscid, and steady flow occurring along a streamline. It considers two points along a streamline, one upstream and one downstream, where the energy upstream is equal to the energy downstream plus the energy losses during conveyance. Bernoulli's equation written in terms of specific energy is as follows:

$$E_1 = E_2 + E_f \quad \text{(Equation 35)}$$

where E_1 represents the specific energy upstream, E_2 represents specific energy downstream, and E_f represents the total specific energy lost downstream.

Specific energy is the total energy of the water body relating to the channel bottom as its datum. The upstream and downstream total specific energy or head, E_1 and E_2 , in the Bernoulli's equation accounts for pressure, kinetic, and potential energy of the fluid as follows:

$$E = \frac{p}{\gamma} + \frac{v^2}{2g} + z \quad \text{(Equation 36)}$$

The equation above also represents the energy grade line (EGL) of the water surface where the hydraulic grade line (HGL) only accounts for the first and last term, the pressure and elevation heads. Therefore, the EGL will always be equal to or larger than the HGL by a difference of the second term, the kinetic energy.

The total energy losses due to friction, E_f , may be from a combination of head loss from pipe friction and from minor losses such as entrance and exit losses within the system. Bernoulli's equation written in terms of pressure, kinetic, and potential energy as well as friction losses is as follows:

$$\frac{p_1}{\gamma} + \frac{v_1^2}{2g} + z_1 = \frac{p_2}{\gamma} + \frac{v_2^2}{2g} + z_2 + h_f + h_m \quad \text{(Equation 37)}$$

where p is the atmospheric pressure, γ is the density of the fluid, v is the velocity, g is the gravity constant, z is the elevation from the datum, h_f is head loss due the friction of the pipe, and h_m is the minor friction loss.

Within the system of interest (with control volume as a whole or segments of pipe), the inflow must equal the outflow as the law of conservation of mass:

$$Q = A_1 * v_1 = A_2 * v_2 \quad \text{(Equation 38)}$$

The friction losses between the pipes are calculated by using the Manning's formula, solving for the slope, S , and plugging it into the second equation as follows:

$$Q = \frac{1.486}{n} A * R^{2/3} * S^{1/2} \quad \text{(Equation 39)}$$

$$h_f = L * S \quad \text{(Equation 40)}$$

where Q is the flow rate, n is the Manning's roughness coefficient, A is the area in flow, R is the hydraulic radius equaled to the area in flow divided by the wetted perimeter of the pipe, S is the slope of the pipe, and L is the length of pipe.

Minor losses due to entrance and exit losses are computed as follows:

$$h_m = k + \frac{v^2}{2g} \quad \text{(Equation 41)}$$

where k is the typical loss coefficient and was assumed to be 0.5 for entrance loss and 1 for exit loss.

When uniform depth exists, normal depth occurs and Manning's formula may be rearranged to solve for normal depth, d_n :

$$D = d_n = 1.335 \left(\frac{nQ}{\sqrt{S}} \right)^{\frac{3}{8}} \quad \text{(Equation 42)}$$

When there is a variation of elevation or change in width of the channel, there will be a change in the depth. The specific energy of the reach may be used in order to determine the new depth of flow in the pipe. From Equation 2, the specific energy may also be expressed as:

$$E = d + \frac{Q^2}{2gA^2} \quad \text{(Equation 43)}$$

where d is the depth or critical depth.

There are three possible depths for the water elevation. One depth will be negative which is not valid. The other two are plausible depths which will provide the same energy and are known as alternate depths.

The flow rate during this period may be categorized as subcritical, supercritical, or critical. Subcritical meaning that the flow is tranquil having a low velocity and a high depth. Supercritical means that rapid flow occurs with high velocity and low depth. Critical depth is the depth that minimizes the energy of flow; however, it does not minimize the depth. On the contrary, for a unique slope it would maximize the quantity of flow through its cross section. Critical flow and critical depth may be computed for a circular pipe as follows:

$$\frac{Q^2}{g} = \frac{A^3}{T} \quad \text{(Equation 44)}$$

The boundary condition chosen for this study is free outfall outlet control, which implies that the receiving water body's (i.e., WOC's) elevation is lower than OF211's discharge elevation; thus, no backwater would occur in the system at OF211. Furthermore, a depth criterion of using a minimum of critical depth or normal depth is applied to modeling computations.

Where there are multiple pipes entering an inlet, transient conditions (unsteady flow) occur. XPSWMM uses a hydraulic flow model known as EXTRAN for dynamic flow analysis. EXTRAN computes the St. Venant equations which represent 1D non-uniform, turbulent flow for open channel and closed conduit flow which would occur when multiple pipes are connected to one manhole. Backwater conditions may occur at these locations producing the non-uniform, turbulent flow within the pipes. The St. Venant equations are as follows, where the first equation below is based on the continuity equation and the next equation on the conservation of momentum principle (Chanson, 2004):

$$\frac{\partial A}{\partial t} + \frac{\partial Q}{\partial x} = 0 \quad \text{(Equation 45)}$$

$$\frac{\partial Q}{\partial t} + \frac{\partial}{\partial x} (V^2 A) + gA \frac{\partial d}{\partial x} = gA(S_0 - S_f) \quad \text{(Equation 46)}$$

Per Chanson 2004, the St. Venant equations assume the following conditions apply: the flow is 1D; the pressure distributions are hydrostatic; the flow resistance and turbulent losses are the same as for a steady uniform equilibrium flow for the same depth and velocity, regardless of trends of depth; the channel slope is small; the water density is constant; sediment motion neglected for fixed boundary conditions.

XPSWMM uses the Modified Euler technique to solve the equations via numerical method when solving the St. Venant equations. The computations are completed via standard step method which means each pipe is a segment of known length where the depth is calculated by either knowing or assuming a depth at one end of the segment. The computations are completed by a 1D-analytical engine in three phases: Phase 1 – downstream analysis, Phase 2 – upstream analysis, Phase 3 – combined profile of downstream and upstream. The program continues the calculation via iterative approximation which is trial and error process. If the sequence of equations is convergent the model will continue; however, if there are significant errors within the calculations then a warning message will appear notifying the user of the error. At that time the model will stop all simulations and the model input should be reviewed.

Model Input

Hydraulics Mode Input

The network is made up of a series of links and nodes, a link being a conduit such as a storm drain, storm pipe, or culvert that conveys water from one node to another. Nodes are considered to intake stormwater runoff or other discharges, and in this case would be the A/C units' condensate and cooling water or the chlorinated discharge water from the Creep Laboratory in Building 4500S. The required input data for the conveyance through the conduits are the Manning's roughness coefficient, slope, downstream invert, upstream invert, pipe length, and spill crest elevations.

Node data, conduit shapes, control structures and weirs may be modeled in the hydraulic mode. The node dialog requests the spill crest elevation where it can be the manhole elevation for a manhole, inlet elevation for an inlet, or top of pipe for a junction box. For the purpose of this project, a junction box is considered as a point where the storm pipe changes direction without a manhole or inlet, or where the storm drain enters the main storm line. Below is the node data dialog box indicating the spill crest and invert elevations. Also, within this dialog the user inflow was incorporated for the transport analysis where timeseries flow rate and concentration data were added.

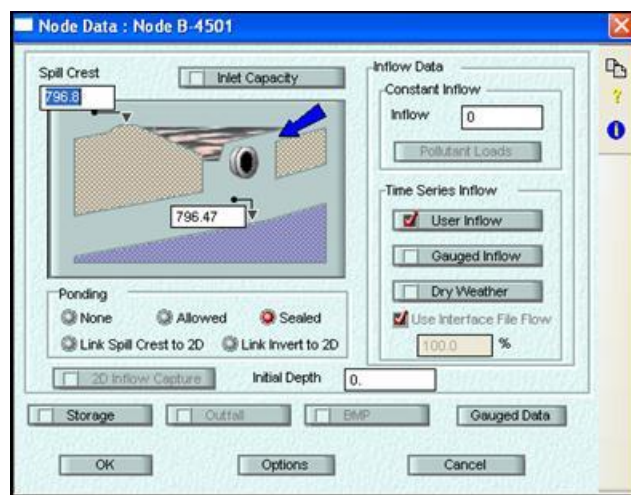


Figure 79. XPSWMM Node Data Dialog.

The node input data table indicating the information that was entered into the system is shown below.

Table 40. XPSWMM Node Data Entry

Name	Sub-catchment	Spill Crest (ft)	Invert Elevation (ft)	Width (ft)	Slope (ft/ft)	Area (ac)	Impervious Percentage (%)
B-4500N_A	1	799.75	799.2	15.3	0.01	0.161	100
B-4500N_B	1	799.6	799.1	13	0.01	0.043	100
B-4500N_C	1	800.15	798.6	24.1	0.02	0.129	100

B-4500N_D	1	800.15	798.6	47	0.03	0.183	100
B-4500N_E	1	799.2	798.7	12.5	0.01	0.054	100
B-4500N_F	1	802	799.6	32	0.01	0.14	100
B-4500N_G	1	802	799.6	22.4	0.01	0.14	100
B-4500S_A	1	789.6	785.5	37.1	0.05	0.269	100
B-4500S_B	1	786.5	786	26.7	0.05	0.183	100
B-4500S_C	1	797	796.5	48.6	0.01	0.129	100
B-4500S_D	1	797.4	796.9	64	0.01	0.14	100
B-4500S_E	1	797.4	796.9	52.5	0.01	0.14	100
B-4501	1	796.8	796.47	32.2	0.01	0.183	100
B-4505	1	797.7	796.8	19	0.02	0.086	100
B-4507	1	793.55	793	16.7	0.05	0.032	100
B-4556	1	796.1	795.75	10.6	0.01	0.011	100
I-1	1	800.57	795	43.3	0.05	0.065	5
I-1	2			52.2	0.05	0.108	5
I-10	1	803.15	795.7	20.3	0.01	0.075	100
I-10	2			12.8	0.01	0.032	100
I-10	3			20.3	0.01	0.075	100
I-10	4			14	0.02	0.032	100
I-11	1	798.2	797.5	50	0.015	0.054	100
I-2	1	799	795.8	18	0.02	0.065	80
I-2	2			40	0.02	0.237	80
I-2	3			5	0.02	0.065	95
I-2	4			10.2	0.02	0.086	100
I-2	5			13.2	0.01	0.108	5
I-3	1	790.4	782.3	14.9	0.015	0.022	90
I-3	2			9.9	0.015	0.075	95
I-4	1	799	795.5	14	0.01	0.161	100
I-4	2			17.9	0.02	0.054	95
I-4	3			15.5	0.02	0.075	95
I-5	1	802.21	795.4	18.4	0.01	0.054	100
I-5	2			15.6	0.01	0.022	100

I-5	3			22.3	0.01	0.075	100
I-5	4			22.5	0.01	0.075	100
I-6	1	800	791	12.15	0.02	0.043	95
I-6	2			7.7	0.02	0.065	95
I-8	1	798.2	793.8	12	0.02	0.003	100
I-8	2			12	0.02	0.03	100
I-9	1	798	793.8	5.3	0.015	0.065	100
I-9	2			5.3	0.02	0.011	100
I-9	3			21	0.02	0.011	100
I-9	4			21	0.02	0.011	100
J-1	1	802.5	791.4	22.6	0.01	0.086	100
J-10		788	781.8	0	0	0	0
J-11		799	797.7	0	0	0	0
J-12		796.6	795.3	0	0	0	0
J-13		798.8	798.3	0	0	0	0
J-14		802	793.75	0	0	0	0
J-2		800	790.4	0	0	0	0
J-3		797	789.9	0	0	0	0
J-4		799.5	789	0	0	0	0
J-5		795.2	793.7	0	0	0	0
J-6		795.8	795.45	0	0	0	0
J-7		801	783.5	0	0	0	0
J-8		792.94	782.7	0	0	0	0
J-9		789	782	0	0	0	0
MH-2A		793.16	785.5	0	0	0	0
MH-5		799	790.4	0	0	0	0
MH-6		800	795.2	0	0	0	0
MH-7		800	791.3	0	0	0	0
MH-8		797.2	792.3	0	0	0	0
MH211-1		789	781.7	0	0	0	0
MH211-2		800.4	783.6	0	0	0	0
MH211-3		799.5	786.85	0	0	0	0

OF-211		786.44	780.74	0	0	0	0
T-1	1	786	784.2	9.5	0.15	0.043	100
T-2	1	800	796	52.9	0.015	0.151	100
T-3	1	800	796	18	0.1	0.14	100

XPSWMM provides a dialog for the conduit characteristics where a variety of pipe shapes are available along with an aid to visualizing the conduit profiles. The study only includes circular pipes.

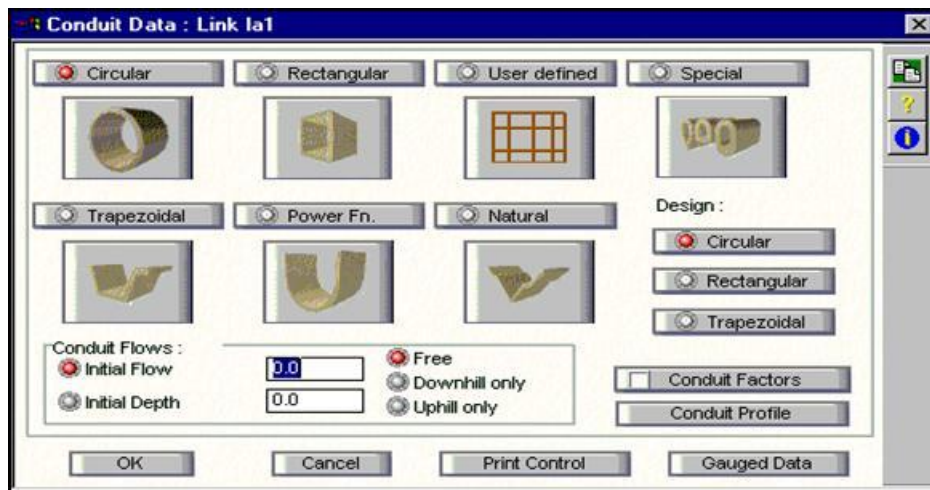


Figure 80. XPSWMM Conduit Shapes.

Additional pipe characteristics such as the diameter, slope, length, and Manning’s roughness coefficient are input in the conduit profile dialog as shown below.

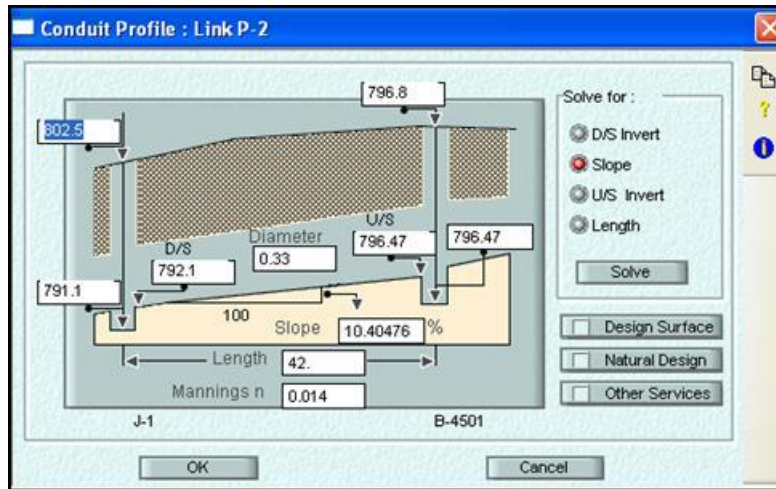


Figure 81. XPSWMM Conduit Profile.

The link data table indicating the information that was entered into the system is shown below.

Table 41. XPSWMM Link Data Entry

Name	Shape	Length (ft)	Manning's Roughness Coeff.	Conduit Slope (ft/ft)	Diameter (in)
P-10	Circular	78.4	0.015	1.148	15
P-11	Circular	64.3	0.015	8.709	15
P-12	Circular	8.8	0.015	23.864	15
P-13	Circular	106.6	0.015	0.563	3.996
P-14	Circular	72.55	0.015	0.414	3.996
P-15	Circular	45.3	0.015	7.174	30
P-16	Circular	5.6	0.015	1.786	30
P-17	Circular	35.3	0.015	2.266	30
P-18	Circular	6.6	0.015	12.121	6
P-19	Circular	16.1	0.015	0	6
P-2	Circular	43.95	0.015	9.488	3.96
P-20	Circular	45	0.015	0.889	30
P-21	Circular	29.1	0.015	1.031	30
P-22	Circular	18.27	0.015	1.095	6
P-23	Circular	20.2	0.015	0.99	30

P-24	Circular	20.37	0.015	10.8	6
P-25	Circular	11.7	0.015	0.855	30
P-26	Circular	100.3	0.015	0.957	30
P-27	Circular	135.3	0.015	2.217	24
P-28	Circular	21.8	0.015	10.55	15
P-29	Circular	27.9	0.015	6.452	6
P-3	Circular	46.6	0.015	2.146	15
P-30	Circular	21.35	0.015	6.557	6
P-31	Circular	17	0.015	1.765	15
P-32	Circular	88.5	0.015	0.113	15
P-33	Circular	32.6	0.015	10.123	6
P-34	Circular	24.7	0.015	13.36	6
P-35	Circular	90.1	0.015	0.111	15
P-36	Circular	24.6	0.015	2.033	6
P-37	Circular	7.8	0.015	1.282	6
P-38	Circular	115.9	0.015	2.071	6
P-39	Circular	21.1	0.015	1.896	6
P-4	Circular	16.4	0.015	26.829	12
P-40	Circular	115.9	0.015	0.518	24
P-41	Circular	28.14	0.015	1.066	24
P-42	Circular	34.37	0.015	2.037	15
P-43	Circular	19	0.015	7.895	15
P-44	Circular	14.1	0.015	10.638	15
P-46	Circular	80.29	0.015	1.806	15
P-47	Circular	32.34	0.015	15.77	6
P-48	Circular	25.3	0.015	20.158	6
P-49	Circular	104.7	0.015	1.862	15
P-5	Circular	35.4	0.015	1.412	15
P-50	Circular	14.5	0.015	23.448	8.04
P-54	Circular	22.8	0.015	3.07	6
P-55	Circular	25.3	0.015	2.767	6
P-56	Circular	108.2	0.015	1.386	8.04
P-6	Circular	51.5	0.015	12.621	9.996
P-7	Circular	21.6	0.015	39.815	6
P-8	Circular	62.3	0.015	1.4	15

P-9	Circular	58.2	0.015	5.584	6
-----	----------	------	-------	-------	---

Runoff Mode Input

In the runoff mode, drainage areas are delineated for the inlets via sub-catchments. One inlet can have up to five sub-catchment areas where each sub-catchment may have varying areas, impervious percentage, width, and slope. The various sub-catchments make up the node catch basins incorporating the higher elevation contour surrounding the node. The sub-catchments are areas that are assigned an inlet. The runoff from the sub-catchment is routed into the inlet and through the network system.

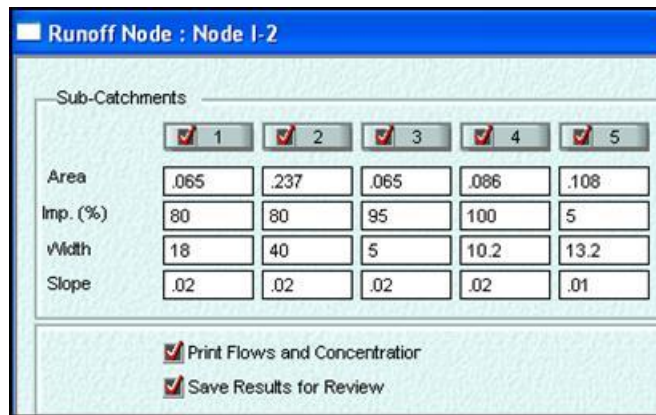


Figure 82. Runoff Node Dialog.

Within the runoff node sub-catchment dialog the routing method, rainfall, and infiltration methods are determined as shown below.

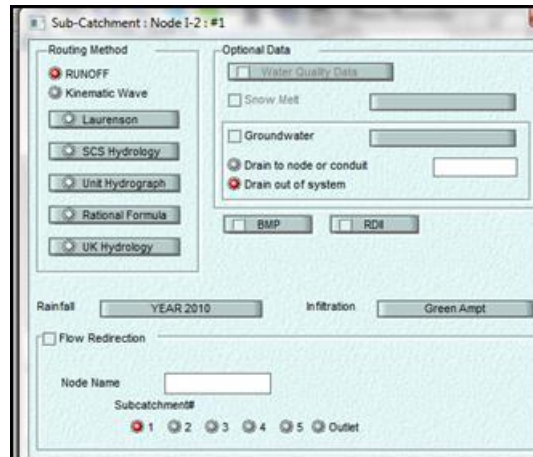


Figure 83. Runoff Node Sub-catchment Dialog.

Routing Method

The SWMM Runoff Non-linear Reservoir Method further known as the runoff routing method was chosen for the simulations as it allowed for the rainfall-runoff process for single rainfall events and continuous rainfall simulations. The Runoff method is a deterministic method where the calculations are of known relationships thus producing precise values. The runoff method simulates rainfall, snowmelt, infiltration, evaporation, and groundwater interaction. The surface water runoff is the rainfall amount minus losses. This study accounts for infiltration and evaporation losses. The runoff is conveyed via overland flow from divided drainage areas and sub-catchments. Overland flow is computed by taking into account the drainage area, percent impervious, basin width and slope, rainfall, and evaporation and infiltration method.

Rainfall

Both single rainfall events and continuous rainfall events are used within the study. Single event simulations are for a short period time such as 24 hours. The calibrations and design storm simulations were single event runs. The sensitivity analysis and transport analysis utilized actual rainfall data from the year 2010 which contain continuous rainfall events retrieved from ORNL's Tower C monitoring station. The rainfall distribution data is entered as a hyetograph which is time series data of the intensity of the rainfall event with either 15 or 60 minute intervals.

The first rainfall event simulated was for steady uniform flow calibration of the model where a single 24-hour rainfall event (hypothetical) having a uniform intensity was entered into the system. The next sets of rainfall data simulated were used to calibrate the model under unsteady non-uniform flow conditions. These simulations utilized single rainfall events also retrieved from ORNL's Tower C monitoring station. They also varied in the date collected and timeframe analyzed; however, all hyetographs had intervals of 60 minutes. The next set of simulations was run for the 5, 10, 25, and 100 year design storm events. The design storms utilized the SCS Type II unit-hyetograph which was multiplied by a factor corresponding to the magnitude of the design storm. The sensitivity analysis and the transport analysis simulate yearly continuous rainfall data from January 1, 2010, through December 31, 2010.

Infiltration Parameters

Green Ampt Infiltration Method

Green Ampt and the Horton's infiltration methods were chosen for the infiltration sensitivity analysis. The sensitivity analysis simulates the Year 2010 continuous rainfall data. The ORNL site is composed of buildings, pavement, and minor pervious areas. It is surrounded by ORR's wooded lands. Soils in the area are a mixture of reddish-brown clays and silts resulting from in-situ weathering of shaley limestone bedrock.

The Green Ampt infiltration method was chosen for all of the simulations within the hydrology and transport analyses – Manning's roughness coefficient variations, design storm events, steady uniform flow and unsteady non-uniform flow calibrations, and the three variations within the transport analysis because it is known to simulate unsteady continuous rainfall events. XPSWMM calculates the infiltration rates by utilizing the Green Ampt – Mein Larson equations, the first being the Mein-Larson equation where the soil has yet to become saturated and the Green Ampt equation once saturation of the soil has occurred. The Mein Larson calculations assume that the infiltration rate approaches the rainfall intensity rate then calculates the unsaturated soil's infiltration rate as if the cumulative infiltration volume is less than the required cumulative infiltration volume for the soil to become saturated.

The cumulative infiltration volume is then determined by the following formula:

$$F_s = \frac{(S_u * IMD)}{\frac{i}{K_s} - 1} \tag{Equation 47}$$

where, F_s = cumulative infiltration volume required to cause surface saturation, ft; S_u = average capillary suction at the wetting front, ft water; IMD = initial moisture deficit, ft/ft; i = rainfall intensity, ft/sec; and K_s = saturated hydraulic conductivity of soil, ft/sec.

If the soil has been saturated where the infiltration rate approaches the infiltration capacity then the following scenario is run through XPSWMM:

$$F_p = K_s * \left(1 + S_u * \left(\frac{IMD}{F} \right) \right) \tag{Equation 48}$$

where, F_p = infiltration capacity, ft/sec; K_s = saturated hydraulic conductivity of soil, ft/sec; S_u = average capillary suction at the wetting front, ft water; IMD = initial moisture deficit for the event, ft/ft; and F = cumulative infiltration volume, ft.

The Green Ampt parameters and their values based on clay loamy soil consistent with the ORNL 4500 area are shown in the figures below.

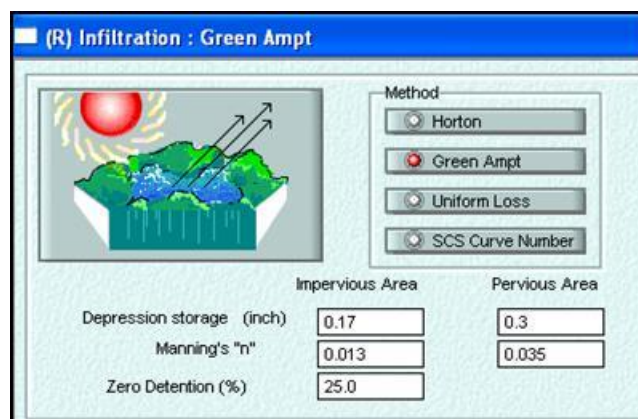


Figure 84. Infiltration Parameters.

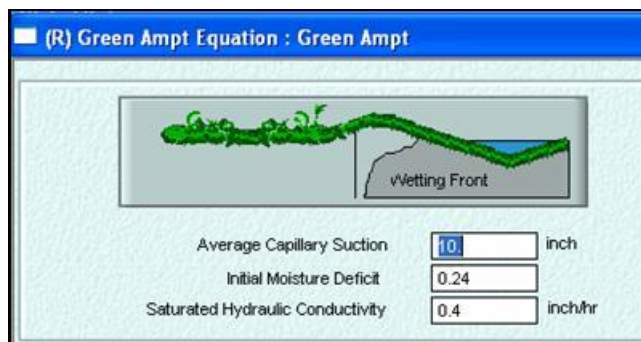


Figure 85. Green Ampt Parameters.

Horton Infiltration Method

The Horton Infiltration Method was chosen as the infiltration method to be compared to the Green Ampt simulations as it may also simulate unsteady continuous rainfall events. The Horton equation indicates infiltration capacity as a function of time is as follows (Verma, 1982):

$$F_p = F_c + (F_0 - F_c)e^{-kt} \tag{Equation 49}$$

where, F_p = infiltration rate into soil, in./hr (mm/hr); F_c = minimum or asymptotic value of F_p , in./hr (mm/hr); F_0 = maximum or initial value of F_p , in./hr (mm/hr); t = time from beginning of storm, sec; and k = decay coefficient, 1/sec.

Horton’s Infiltration Method is known to calculate infiltration rates for single storm events. However, XPSWMM has an option for Horton’s infiltration calculations to be regenerated, which is equal to the regeneration specified multiplied by the decay specified. For the Horton simulation a regeneration of 0.01 was used with a decay rate of 0.001.

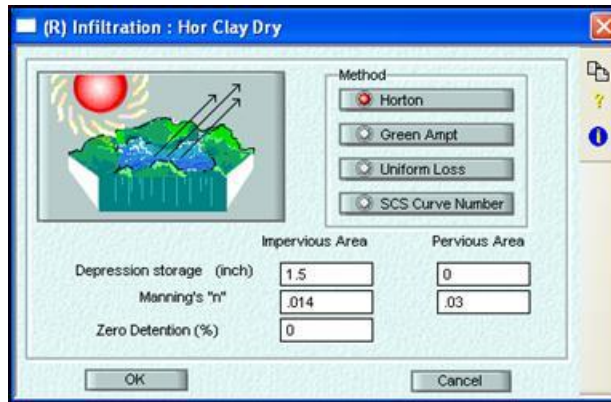


Figure 86. Horton Infiltration Dry Clay Parameter.

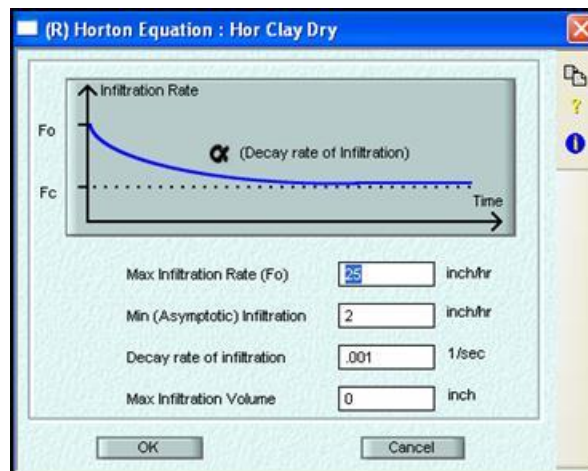


Figure 87. Horton Equation Dry Clay Parameter.

Hydrology Analysis

A hydrology analysis was performed on the model beginning with a calibration of the model using both synthetic storm events for steady uniform flow conditions and unsteady non-uniform conditions and actual rainfall data. The results of the simulations using actual rainfall data are compared to OF-211 data provided by ORNL in order to validate the model. The hydrology analysis of the model includes the following:

1. Calibration
 - a. Calibration of Steady Uniform Flow Conditions

- b. Calibration of Non-steady Non-Uniform Flow Conditions
- 2. Sensitivity Analysis
 - a. Manning's Roughness Coefficients
 - b. Green Ampt and Horton's Infiltration Methods
 - c. Percent Imperviousness
- 3. Design Storm Analysis
 - a. 5 Year – 24 Hour Design Storm Event
 - b. 10 Year – 24 Hour Design Storm Event
 - c. 25 Year – 24 Hour Design Storm Event
 - d. 100 Year – 24 Hour Design Storm Event

Steady Uniform Flow Calibrations

The model was calibrated for steady uniform flow conditions where the rainfall intensity remained constant for the duration of the storm event. For the steady uniform flow simulation a hypothetical 24 hour rainfall having an intensity of 0.5 inch/hour as shown in Figure 88. Rainfall Hyetograph for Steady Uniform Flow was simulated through two inlets on the main line.

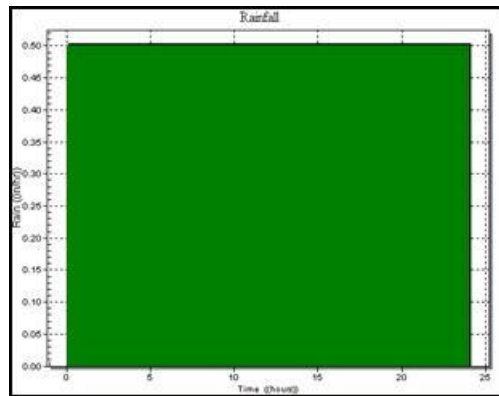


Figure 88. Rainfall Hyetograph for Steady Uniform Flow.

Only inlet 1 and the nodes on the main trunk line were active. All other nodes and links were disabled so that flow only entered into inlets 1 and 3 (I-1 and I-3) in order to calibrate the model for steady uniform flow.

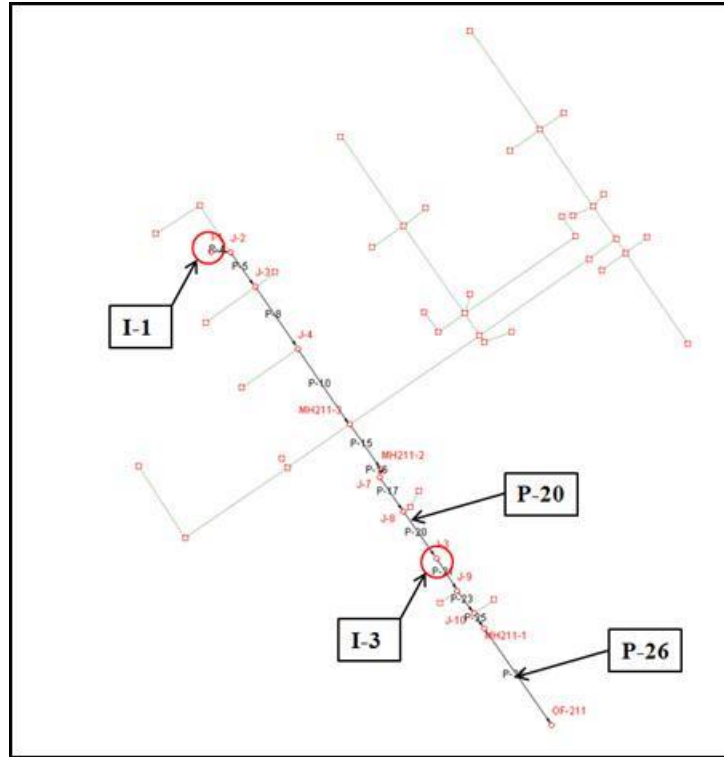


Figure 89. Stormwater Collection System for Steady Uniform Flow.

From the conservation of mass equation, mass flow rate in equals mass flow rate out, the system was analyzed.

$$m = \rho * Q \tag{Equation 50}$$

$$\rho_{I-1} * Q_{I-1} + \rho_{I-3} * Q_{I-3} = \rho_{out} * Q_{out} \tag{Equation 51}$$

Where ρ is the density of the surface water in pounds per square foot (lb/sf) and Q is the flow rate of the surface water in cubic feet per second (cfs). Knowing that the density of the

surface water is constant, the density can be cancelled out leaving the flow rate of I-1 plus the flow rate of I-3 to equal the flow rate out.

$$Q_{I-1} + Q_{I-3} = Q_{out} \quad \text{(Equation 52)}$$

where

$$Q = c * i * A \quad \text{(Equation 53)}$$

where c is the dimensionless runoff coefficient, i is the rainfall intensity in inches per hour (in./hr), and A is the area of the sub-drainage area in acres (ac). The flow is in cfs and represents the peak flow rate.

Unsteady Non-Uniform Flow Calibration

In order for the ORNL surface water model of the 4500 Area to be considered a valuable source to assess flow rates within the network, it must be calibrated with existing OF-211 data. The non-uniform flow calibration was conducted by simulating actual rainfall that occurred during the timeframe that ORNL provided outfall 211 (OF-211) flow rate data to XPSWMM predicted flow rates. ORNL monitored the OF-211 flow rate discharge from October 21, 2012 11:00 AM to December 19, 2012 9:00 AM. ORNL noted dates and times that precipitation occurred. After review of the ORNL data, the following dates and timeframes (hereby referred to as trials) were used for the calibration based upon peak flow rates indicated by the ORNL hydrographs provided:

1. November 12, 2012 1:00 PM – 10:10 PM
2. November 26, 2012 10:15 PM – November 27, 2012 5:50 AM
3. December 10, 2012 3:25 AM – 6:30 PM
4. December 15, 2012 9:45 PM – December 16, 2012 8:55 PM

For the calibration trials a Manning's n coefficient of 0.015, the Green Ampt infiltration method, and evaporation default of 0.1"/day were used. The calibrations are based on 24-hour simulations and were conducted by analyzing the ORNL observed flow rate data at OF-211. Rainfall data was retrieved around the time that the data produced peak flow rates. Once the base flow rate was subtracted from the ORNL observed data, the XPSWMM P-26 results were overlain. A timeframe was chosen where the beginning and end times corresponded to flow rates that were zero. Peak flow rates and their corresponding times are noted as well as a summation of flow rates for both the ORNL data and the XPSWMM results during the time of calibration for comparison.

Calibration of Model Trial 1

Sixty-minute interval rainfall data was retrieved from ORNL Tower C and indicates that precipitation occurred on November 12, 2012 between the hours of 12:00 AM and 7:00 PM. The rainfall data was simulated through the network. The timeframe for calibration purposes was chosen as November 12, 2012 from 1:00 PM to 10:10 PM. XPSWMM produced the hyetograph shown below based upon the rainfall data entered into the model.

Table 42. Rainfall Data for Calibration Trial 1

Tower C Rainfall Data 60 min Intervals			
Time	Rain (in)	Time	Rain (in)
11/12/2012 11:00	0	11/12/2012 16:00	0.12
11/12/2012 12:00	0.01	11/12/2012 17:00	0.08
11/12/2012 13:00	0.04	11/12/2012 18:00	0.06
11/12/2012 14:00	0.07	11/12/2012 19:00	0.03
11/12/2012 15:00	0.24	11/12/2012 20:00	0

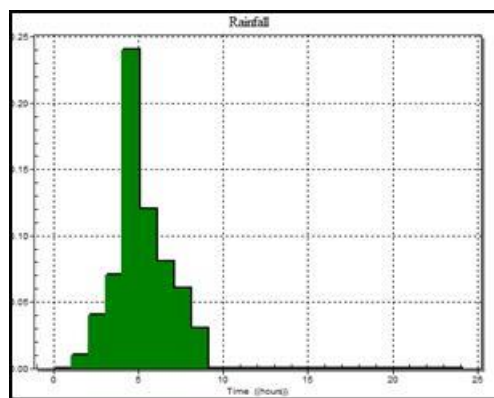


Figure 90. Rainfall Hyetograph for Calibration Trial 1.

Calibration of Model Trial 2

The precipitation data beginning on November 26, 2012 at 9PM thru November 27, 2012 at 6AM is shown below and was simulated through the network. The timeframe for calibration purposes was chosen as November 26, 2012 10:15 PM - November 27, 2012 6:05 AM. XPSWMM produced the hyetograph below based upon the rainfall data entered into the model.

Table 43. Rainfall Data for Calibration Trial 2

Tower C Rainfall Data 60 min Intervals			
Date & Time	Rain (in)	Date & Time	Rain (in)
11/26/2012 21:00	0	11/27/2012 3:00	0.04
11/26/2012 22:00	0.07	11/27/2012 4:00	0
11/26/2012 23:00	0.07	11/27/2012 5:00	0
11/27/2012 0:00	0.12	11/27/2012 6:00	0.01
11/27/2012 1:00	0.04	11/27/2012 7:00	0
11/27/2012 2:00	0.02		

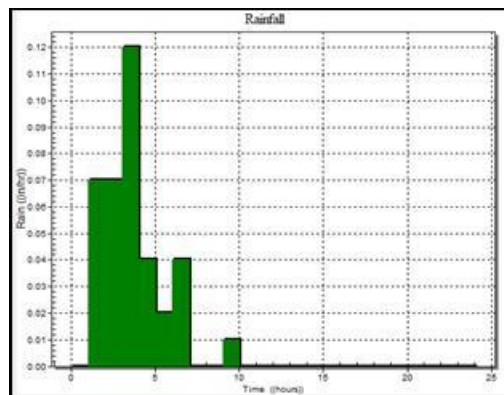


Figure 91. Rainfall Hyetograph for Calibration Trial 2.

Calibration of Model Trial 3

Sixty-minute interval rainfall data was retrieved from ORNL Tower C and indicates that precipitation occurred on December 10, 2012 between the hours of 3:00 AM and 4:00 PM. The rainfall was simulated through the network. ORNL OF-211 data provided for calibration is shown in the hydrograph below. The timeframe for calibration purposes was chosen as December 10, 2012 3:25 AM – 6:30 PM. XPSWMM produced the hyetograph shown below based upon the rainfall data entered into the model.

Table 44. Rainfall Data for Calibration Trial 3

Tower C Rainfall Data 60 min intervals					
Time	Rain (in)	Time	Rain (in)	Time	Rain (in)
12/10/2012 2:00	0	12/10/2012 8:00	0.1	12/10/2012 14:00	0
12/10/2012 3:00	0.03	12/10/2012 9:00	0.1	12/10/2012 15:00	0
12/10/2012 4:00	0.12	12/10/2012 10:00	0.05	12/10/2012 16:00	0.01
12/10/2012 5:00	0.02	12/10/2012 11:00	0.02	12/10/2012 17:00	0
12/10/2012 6:00	0.31	12/10/2012 12:00	0.04		
12/10/2012 7:00	0.08	12/10/2012 13:00	0.04		

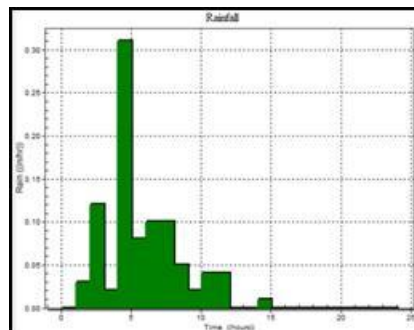


Figure 92. Rainfall Hyetograph for Calibration Trial 3.

Calibration of Model Trial 4

Sixty-minute interval rainfall data was retrieved from ORNL Tower C and indicates that precipitation occurred on December 15, 2012 between the hours of 9:00 PM and 8:00 PM. The rainfall was simulated through the network. The timeframe for calibration purposes was chosen as December 15, 2012 9:45 AM – 8:55 PM. XPSWMM produced the hyetograph shown below based upon the rainfall data entered into the model.

Table 45. Rainfall Data for Calibration Trial 4

Tower C Rainfall Data 60 min intervals					
Time	Rain (in)	Time	Rain (in)	Time	Rain (in)
12/15/2012 20:00	0	12/16/2012 6:00	0.12	12/16/2012 14:00	0
12/15/2012 21:00	0.01	12/16/2012 7:00	0.06	12/16/2012 15:00	0
12/15/2012 22:00	0.1	12/16/2012 8:00	0.09	12/16/2012 16:00	0
12/15/2012 23:00	0.06	12/16/2012 9:00	0.04	12/16/2012 17:00	0.01
12/17/2012 0:00	0.01	12/16/2012 8:00	0.09	12/16/2012 18:00	0.01
12/16/2012 1:00	0.01	12/16/2012 9:00	0.04	12/16/2012 19:00	0.02
12/16/2012 2:00	0	12/16/2012 10:00	0.05	12/16/2012 20:00	0.01
12/16/2012 3:00	0.01	12/16/2012 11:00	0.03	12/16/2012 21:00	0
12/16/2012 4:00	0.26	12/16/2012 12:00	0		
12/16/2012 5:00	0.34	12/16/2012 13:00	0.01		

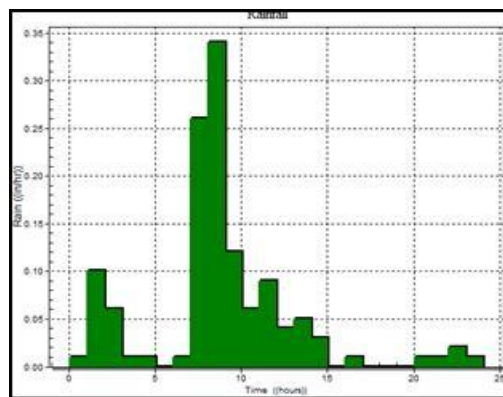


Figure 93. Rainfall Hyetograph for Calibration Trial 4.

Sensitivity Analysis

Multiple sensitivity analyses were completed and analyzed in order to understand the impact of the various parameters on the system. They were conducted where actual continuous rainfall data from year 2010 (January 1, 2010 thru December 31, 2010) was simulated as well as the Manning’s roughness coefficients, infiltration parameters, and percent imperviousness. Year 2010 rainfall data was retrieved from ORNL’s Tower C monitoring station in 15 minute intervals as shown below.

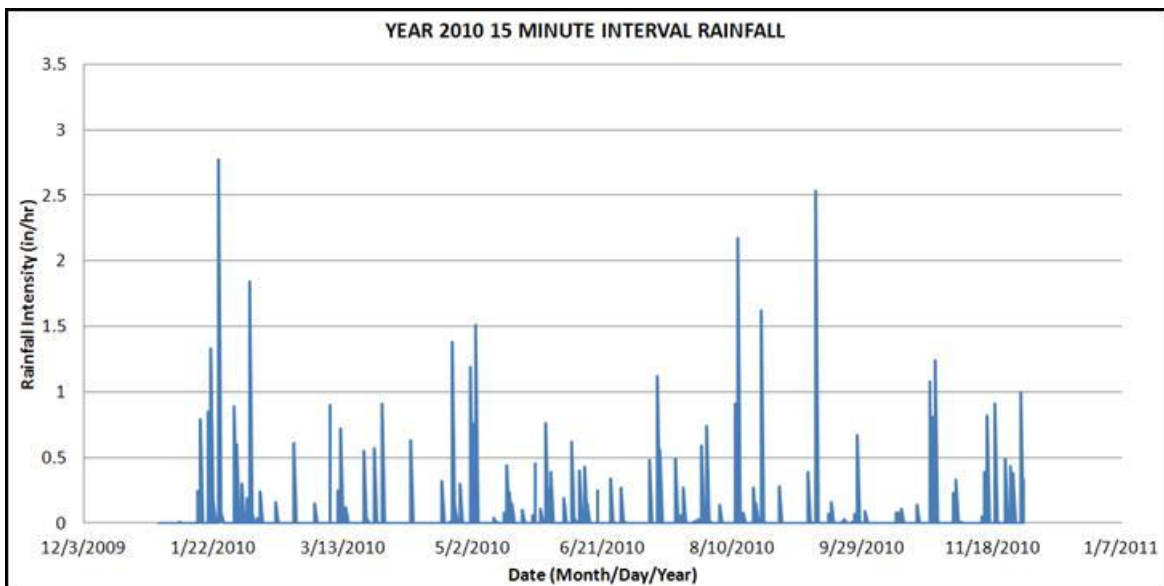


Figure 94. Year 2010 Rainfall Data.

For the purpose of demonstrating the effects the various parameters have on the network, the nodes MH211-3 and OF-211 and the links P-10, P-11, P-15, P-27, and P-26 will be used. However, not all are used in each section to avoid redundancy.

MATLAB was chosen for the task. MATLAB produced plots for each variable versus time and their probability of exceedance (PE) curves.

The simulations were run where the data was saved every 300 minutes throughout the yearly simulation. Thus, 1 year saved every 300 minute interval gives 1748 intervals. When analyzing a peak flow rate for a specified pipe it may be difficult to sort through the 1748 intervals of flow rates for that single pipe. Thus, the PE has been calculated for all pipes and nodes within the remaining simulations in order to find the maximum flow rate within a pipe and for what percent of the time it remains at that flow rate. For instance, if a node meets or exceeds its inlet elevation (link flow rate) for 90% of the duration of the storm event, then it may be necessary for improvements to be considered. When producing PE curves, time is not a factor and is calculated as follows, where the rank from largest to smallest and the number of intervals which equals 1748 for the sensitivity analysis and transport analysis, are considered:

$$\text{Probability Exceedance} = \text{Rank} / (\text{Total Number of Values} + 1) \quad \text{(Equation 54)}$$

Probability Distribution (PD) Fitting

It is known that hydrological data follow a pattern (Hanson, 2008; Kroll, 2002; Mahdavi, 2010; Vogel, 1996). More specifically, low stream flow and rainfall depth are two hydrological data types that are continually analyzed and fit to probability distributions to better understand their patterns (Hanson, 2008; Kroll, 2002; Vogel, 2002). The resulting XPSWMM data are fit to suitable PDs. Hydrological timeseries data can be lengthy and numerous; thus, fitting the data allows the data to be characterized by its high and low distributions, which reduces the level of risk and uncertainty of results and allows for better understanding of data parameters when they are analyzed as a whole and fitted to a PD. This permits the extrapolation of data, for example in special situations such as defective monitoring equipment, on the basis or assumption the hydrological parameters at that given location are consistent with nearby outfalls, and may permit an educated guess with some certainty the data is realistic. Thus, the hydrograph and pollutograph timeseries data from the transport simulations were entered into the EasyFit 5.5 tool where it fit the data to numerous probability distribution functions and ranked them according to

Komogorov Smirnov, Anderson Darling, and Chi-Squared methods. The distribution fits were ranked highest by the Komogorov Smirnov method for this study.

Design Storm Simulations

The U.S. Natural Resources Conservation Service (NRCS), formerly known as the U.S. Soil Conservation Services (SCS) method, is used to compute rainfall distributions. NRCS has divided the United States into four main regions where Type II distribution represents rainfall for the Tennessee Valley (Fiuzat, 1991; City of Knoxville, 2012). For the design storms, the SCS Type II unit-hyetograph (shown in the figure below) will be multiplied by a precipitation corresponding to its storm event in order to duplicate flow rates and water elevations corresponding to the magnitude of the storm event throughout the site for analysis.

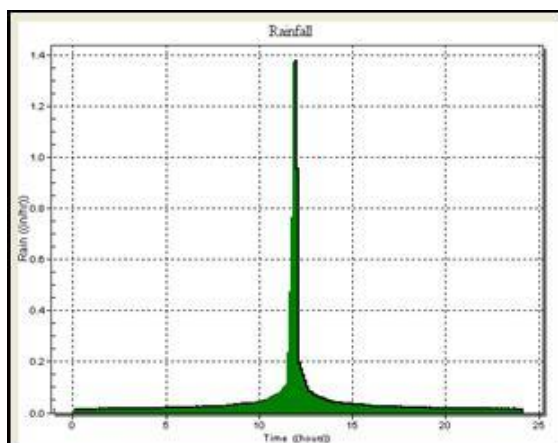


Figure 96. SCS Type II Unit Hyetograph.

When a piece of land is developed, design storms are simulated for pre-development and post-development conditions to ensure that the post conditions do not exceed the pre-conditions. If they did, then during a heavy rainfall they would flood their neighbor. The 5 year storm event is run to assess the parking lot elevation, the 10 year storm event for roadways, the 25 year storm event for the properties berm elevation (to keep the excess rain on their property so that they would not flood their neighbor), and the 100 year storm event for the building's finish floor. It is

dependent on which municipality the land resides under as to the duration (24 hour or 72 hour) of the storms required for analysis. For this reason, these design storms have been simulated over the network. The design simulations are based on a Manning’s roughness coefficient of 0.015, Green Ampt infiltration method, and the estimated percent imperviousness from site visits. The table below indicates the single design storm events and their corresponding precipitation that the unit-hyetograph will be multiplied by in order to run the design storm specific to its region (NOAA, 2006).

Table 46. NOAA Precipitation

Storm Event	Precipitation
5 year - 24 hour	4.1”
10 year - 24 hour	4.7”
25 year - 24 hour	5.5”
100 year - 24 hour	6.8”

Transport Analysis

The transport analysis has been conducted by introducing a hypothetical conservative contaminant into the system. Examples of conservative contaminants are bromine, nitrate, technetium-99, and dye, as opposed to a non-conservative contaminant where adsorption/desorption would occur. The conservative contaminant (described as ‘pollutant’ by XPSWMM) may be routed via the Hydraulics or the Runoff mode within XPSWMM. Introducing the pollutant via the Hydraulics mode may be interpreted as having a residual contaminant within an existing pipe and/or inlet within the system. Four variations of the Hydraulics mode simulations were run. This study focuses on injecting a pollutant into the Hydraulics mode specifically as user timeseries inflow at various nodes, as shown in the interface below.

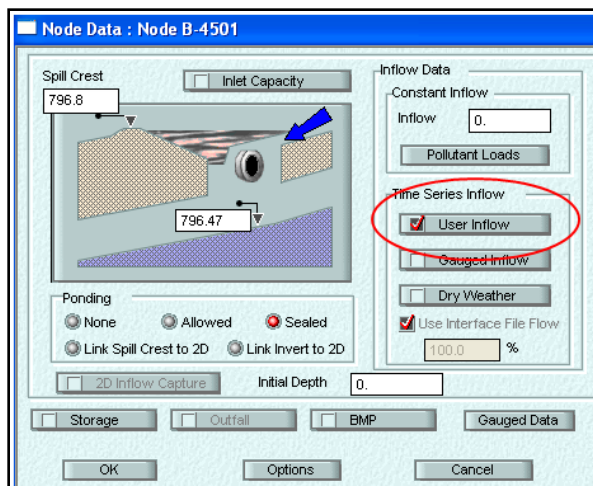


Figure 97. XPSWMM User Inflow.

Similarly to the sensitivity analysis, the simulations were run using the following parameters: actual 15 minute interval rainfall data, year 2010; Manning’s roughness coefficient, n , of 0.015; Green Ampt infiltration parameters for loamy clay soil; an evaporation default of 0.1”/day; and estimated percent imperviousness from site visits. The following describes the various simulations run in order to assess the effects of a hypothetical pollutant entering the system as a residual contaminant existing within the pipes. Four timeseries were used for the simulations (one steady flow and concentration, and three varied flow and concentration).

The first is the timeseries containing a constant flow of 0.17 cfs and a constant pollutant concentration of 0.1 mg/L, which from here onwards will be referred to as the ‘steady timeseries’ followed by three varied flow rate and concentration timeseries for a duration of 24 hours. The pollutant concentrations are hypothetical; however, the flow rates resemble the base flow rate found during the calibration of the model which is approximately 0.17 cfs in the system due to the once through cooling water for the AC units. The hypothetical scenarios used for the simulations are listed below:

1. HYD Scenario 1: Steady timeseries A was introduced into the system at both locations B-4501 and B-4500N_G

2. HYD Scenario 2: Steady timeseries A was introduced into the system at B-4556 and varied timeseries B into I-5
3. HYD Simulation 3: Varied timeseries B was introduced into the system at I-11 and varied timeseries C at I-10
4. HYD Scenario 4: Varied timeseries C was introduced into the system at B-4500S_C and varied timeseries D at T-1

The following table depicts the steady timeseries (A) and the three varied timeseries (B), (C), and (D) that were introduced into the system for the four various simulations.

Table 47. Transport Simulations Hypothetical Timeseries

(A)			(B)			(C)			(D)		
Time (hr)	Q (cfs)	C (mg/L)	Time (hr)	Q (cfs)	C (mg/L)	Time (hr)	Q (cfs)	C (mg/L)	Time (hr)	Q (cfs)	C (mg/L)
0	0.17	0.1	0	0.14	0.1	0	0.11	0.2	0	0.17	0.5
1000	0.17	0.1	2220	0.15	0.5	500	0.13	0.3	4	0.14	0.2
2000	0.17	0.1	3210	0.16	0.7	2100	0.12	0.1	9	0.13	0.4
3000	0.17	0.1	4320	0.17	0.4	3400	0.15	0.25	16	0.15	0.15
4000	0.17	0.1	5555	0.13	0.2	4990	0.18	0.5	18	0.16	0.6
6000	0.17	0.1	6000	0.15	0.15	6230	0.16	0.4	20	0.18	0.15
7000	0.17	0.1	7000	0.14	0.3	7110	0.15	0.35	22	0.11	0.3
8448	0.17	0.1	8448	0.13	0.1	8000	0.14	0.1	24	0.13	0.25

The following table summarizes the location and which timeseries (steady or varied) were introduced into the system. Two timeseries were entered for each simulation.

Table 48. Transport Simulation Scenarios

Hydraulics Mode Simulation	Node 1	Input 1	Node 2	Input 2
HYD 1	B-4501	A	B-4500N_G	A
HYD 2	B-4556	A	I-5	B
HYD 3	I-11	B	I-10	C
HYD 4	B-4500S_C	C	T-1	D

The simulations ran in the Hydraulics mode take into account an assumed event mean concentration of 0.1 mg/L, with a standard deviation of 0.01 mg/L and an assumed initial pollutant concentration of 0.1 mg/L. No buildup is assumed for these simulations, only washoff of the pollutant which is calculated via the event mean concentration rating curve approach with a coefficient of 1. The event mean concentration approach assumes that the quantity of the pollutant plus or minus its standard deviation is proportional to the quantity of runoff.

Transport Analysis Simulation 1

The flow and pollutant steady timeseries (A) was injected at the two nodes B-4501 and B-4500N_G as shown below. A pollutant load is expected to occur within P-10 as a result from the flow and concentration timeseries data entered into node B-4501. Similarly, a pollutant load should occur within to the east P-27 due to the flow and concentration timeseries introduced into node B-4500S_G. No pollutant or additional flow was introduced to the east; therefore, no pollutant load should appear to the east within P-11. Only the runoff from continuous yearly rainfall events is routed through the system to the east. The load within P-15 will depict a combination of the two loads from P-10 and P-27.

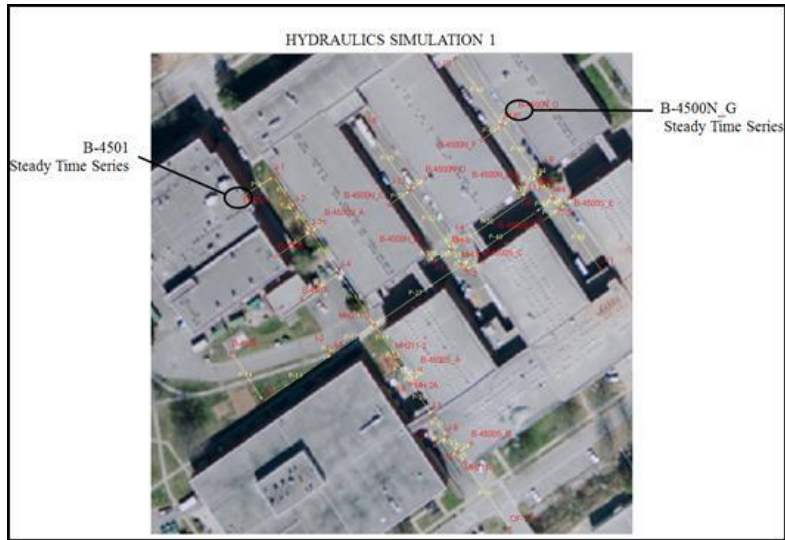


Figure 98. Transport Scenario 1 Entrance of Pollutant Location.

Transport Analysis Simulation 2

The second simulation introduces a steady timeseries flow and concentration into node B-4556 and a varied timeseries in node I-5. A pollutant load is expected to occur from the east within P-11 due to the introduction of the steady timeseries into node B-4556. Similarly, a pollutant load is expected to occur from the west within P-27 due to the introduction of the steady timeseries into node I-5.

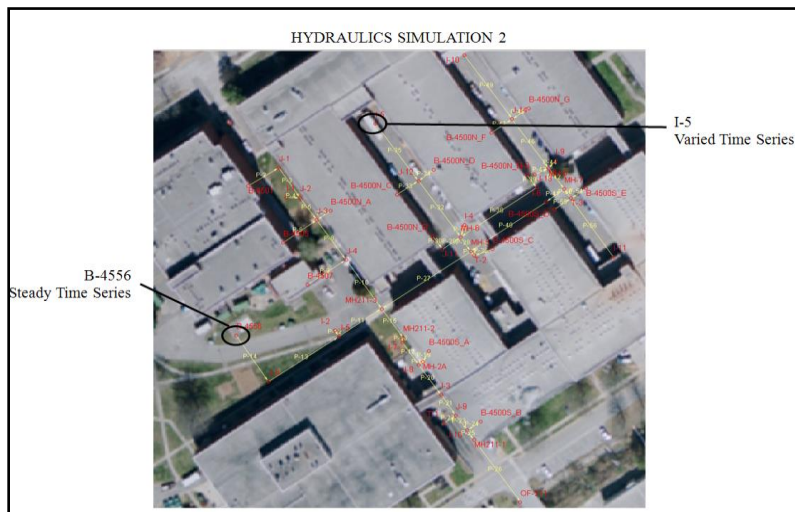


Figure 99. Transport Analysis Scenario 2 Pollutant Entrance Locations.

Transport Analysis Simulation 3

Scenario 3 introduces varied flow and concentration timeseries (B) into node I-11 and varied flow and concentration data (C) into node I-10. No pollutant was introduced into the north and west wings of the system; therefore, no pollutant load should appear in links P-10 and P-11.

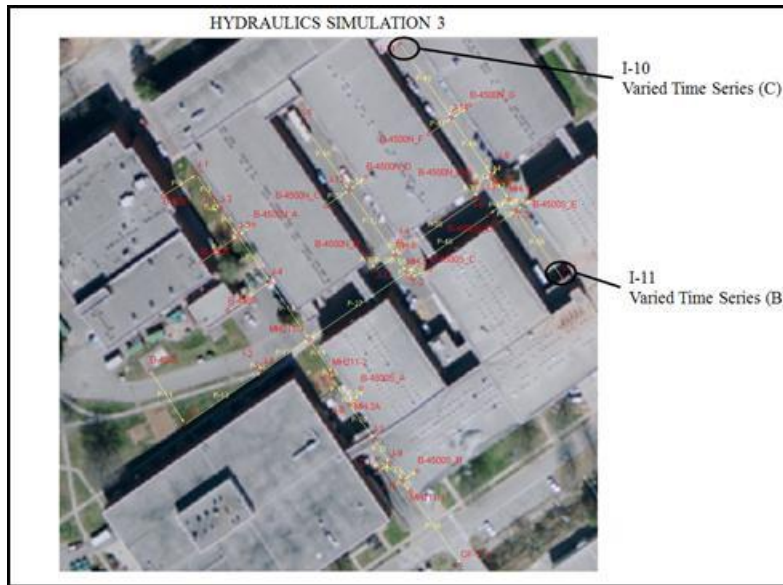


Figure 100. Transport Analysis Scenario 3 Entrance of Pollutant.

Transport Analysis Simulation 4

The last scenario introduces varied flow and concentration timeseries (C) into node B-4500S_C, and varied flow and concentration (D) data into node T-1. Similar to simulation 3, no pollutant was introduced into the north and west wings of the system; therefore, no pollutant load should appear in links P-10 and P-11.

The mass balance calculation for the flow rate entering I-1 was calculated as follows:

$$Q_{I-1} = 0.05 * 0.5 \left(\frac{\text{in}}{\text{hr}}\right) * (0.173 \text{ ac}) \tag{Equation 55}$$

$$Q_{I-1} = 0.004 \text{ cfs} \tag{Equation 56}$$

The sub-drainage areas are mostly green space with an estimated impervious area of 5%. A rainfall intensity of 0.5 in./hr and a sub-drainage area total of 0.173 ac were used. A rational runoff coefficient may be estimated as 0.05 to 0.35 for lawns. The rational method runoff coefficient is shown in the table below.

Table 49. Rational Method Runoff Coefficients

Rational Method Runoff Coefficients (Chow, 1988)	
Ground Cover	Runoff Coefficient, c
Lawns	0.05 - 0.35
Forest	0.05 - 0.25
Cultivated land	0.08-0.41
Meadow	0.1 - 0.5
Parks, cemeteries	0.1 - 0.25
Unimproved areas	0.1 - 0.3
Pasture	0.12 - 0.62
Residential areas	0.3 - 0.75
Business areas	0.5 - 0.95
Industrial areas	0.5 - 0.9
Asphalt streets	0.7 - 0.95
Brick streets	0.7 - 0.85
Roofs	0.75 - 0.95
Concrete streets	0.7 - 0.95

Based on the flow rate produced by XPSWMM, a runoff coefficient of 0.05 would satisfy the simulation. Dense grass is present in this area. This should be considered as an acceptable approximation for the runoff coefficient. Thus, the peak flow rate in P-20 should be equal to that of Q_{I-1} . The XPSWMM hydrograph results in Figure 103. Conduit P-20 Results for Steady Uniform Flow indicate that the peak flow rate is 0.004 cfs, which complies with the mass balance equation for Q_{I-1} that equals 0.004 cfs.

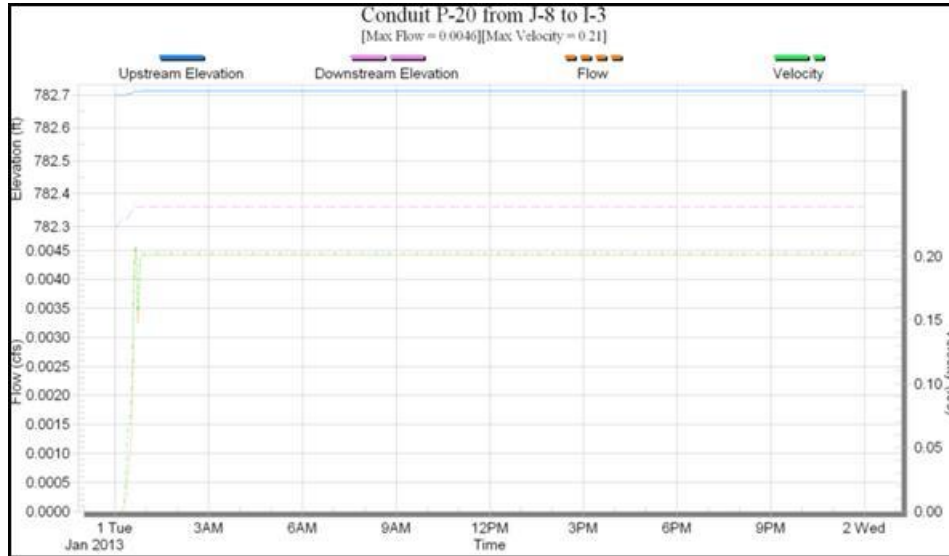


Figure 103. Conduit P-20 Results for Steady Uniform Flow.

The mass balance calculation for the flow rate entering I-3 was calculated as follows:

$$Q_{I-3} = 0.95 * 0.5 \left(\frac{\text{in}}{\text{hr}} \right) * (0.097 \text{ ac}) \tag{Equation 57}$$

$$Q_{I-3} = 0.046 \text{ cfs} \tag{Equation 58}$$

$$Q_{out} = Q_{I-1} + Q_{I-3} = 0.05 \text{ cfs} \tag{Equation 59}$$

I-3 sub-catchments total 0.097 ac, a steady uniform rainfall of 0.5 in./hr, and an assumed rational runoff coefficient of 0.95 for asphalt streets was used as this is an asphalt driveway resulting in a flow rate of 0.046 cfs.

Link P-26 is located immediately before Outfall 211; therefore, the peak flow rate in P-20 should equal that of Q_{out} . The XPSWMM hydrograph results in Figure 104. Conduit P-26 Results for Steady Uniform Flow indicate that the peak flow rate is 0.05 cfs, which complies with the mass balance equation for Q_{out} .

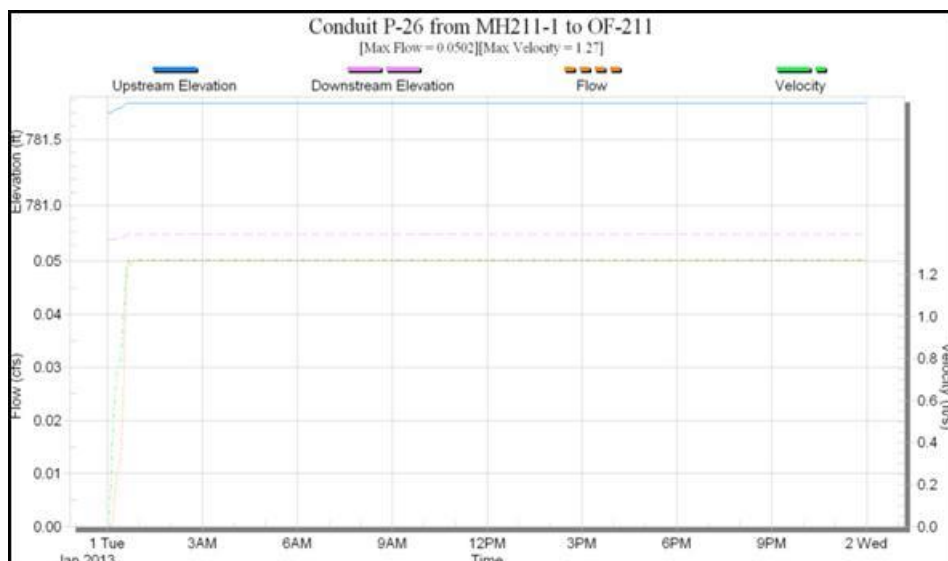


Figure 104. Conduit P-26 Results for Steady Uniform Flow.

Unsteady Non-Uniform Flow Calibration Results

The unsteady non-uniform calibration was performed by simulating actual rainfall events and comparing the model results of OF-11to OF-211 monitored data. After analyzing the OF-211 flow rate data provided by ORNL, an approximate 0.17 cfs base flow was observed. It is known that the OF-211 storm system contains base flow and is defined as once-through cooling water and steam condensate from the adjacent buildings’ AC units; however, their exact quantities and locations are unknown. Therefore, a 0.17 cfs has been extracted from the ORNL flow rate data in order to compare the XPSWMM results for calibration purposes due to the fact that exact base flow quantities and locations of entry into the system are unknown. The XPSWMM model

introduces actual 60-minute interval rainfall data that was retrieved from ORNL Tower C monitoring station for calibration purposes.

XPSWMM provides resulting flow rates within each pipe and resulting elevations at each node after the model is solved; thus, flow rates from pipe 26 (P-26), which is the pipe immediately prior to OF-211, were analyzed. The data provided by ORNL is in 5-minute intervals; thus, the XPSWMM P-26 resulting flow rates were extracted in 5-minute intervals, and both data are presented as hydrographs for comparison. The calibration is based on flow rates presented in cubic feet per second (cfs). ORNL provided data in gallons per minute (gpm). A conversion factor of 0.002228 cfs per gpm was used.

Calibration of Model Trial 1 Results

The rainfall event that occurred on November 12, 2012 between the hours of 12:00 AM and 7:00 PM was utilized for the calibration trial 1. The figure below is a hydrograph of the ORNL OF-211 data provided during the time the precipitation occurred and includes the 0.17 cfs base flow which was later extracted for calibration purposes.

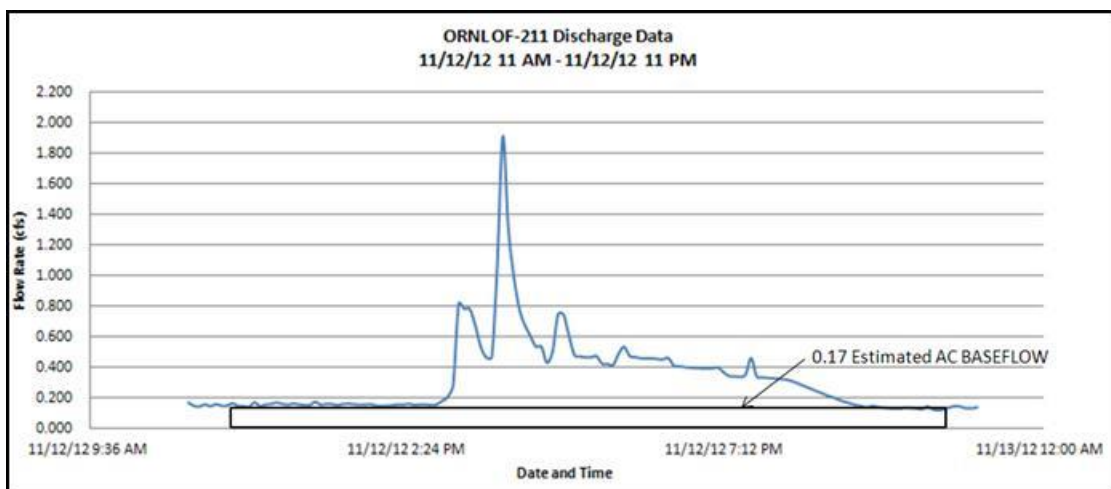


Figure 105. ORNL Data with Base Flow.

The figure below shows that the ORNL observed flow rate data has a peak flow rate of 1.73 cfs (excluding 0.17cfs base flow) on November 12, 2012 at 3:50 PM. The XPSWMM hydrograph does not indicate as large of a peak as the ORNL data, however the summation of flow rates under the curve are very similar. The lag time for the model to simulate the rainfall is approximately 25 minutes. This may be considered a successful calibration as the summation of flow rates during the calibration duration are equal, which is shown in the second figure below. The figure is the cumulative flow rate versus time which indicates more clearly the two sets of data summation of flow rates.

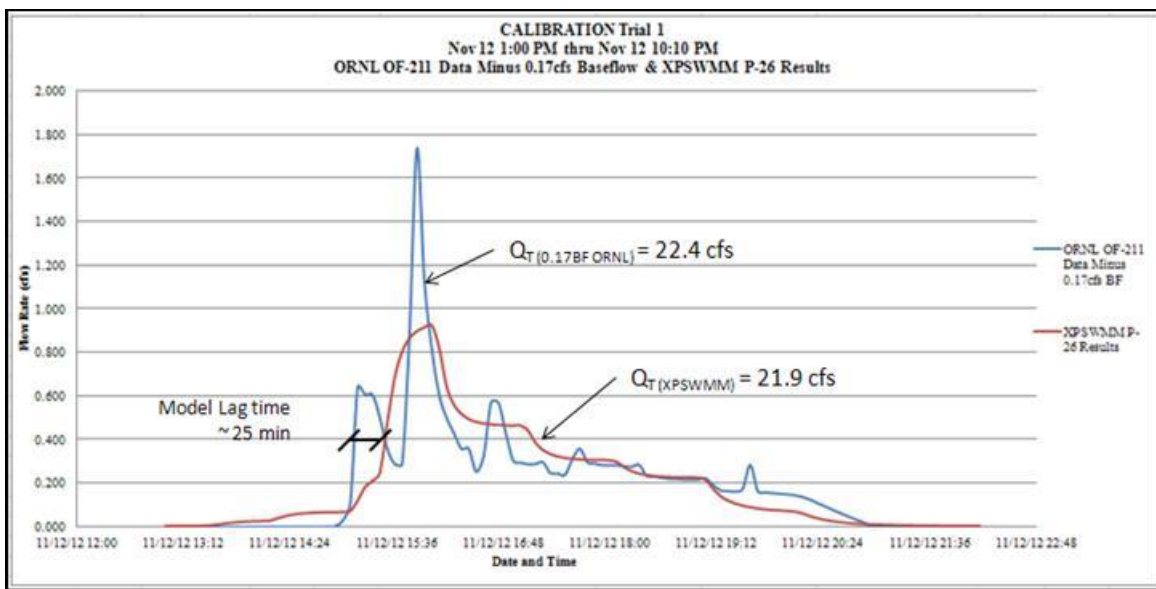


Figure 106. ORNL Data and XPSWMM Results Hydrograph.

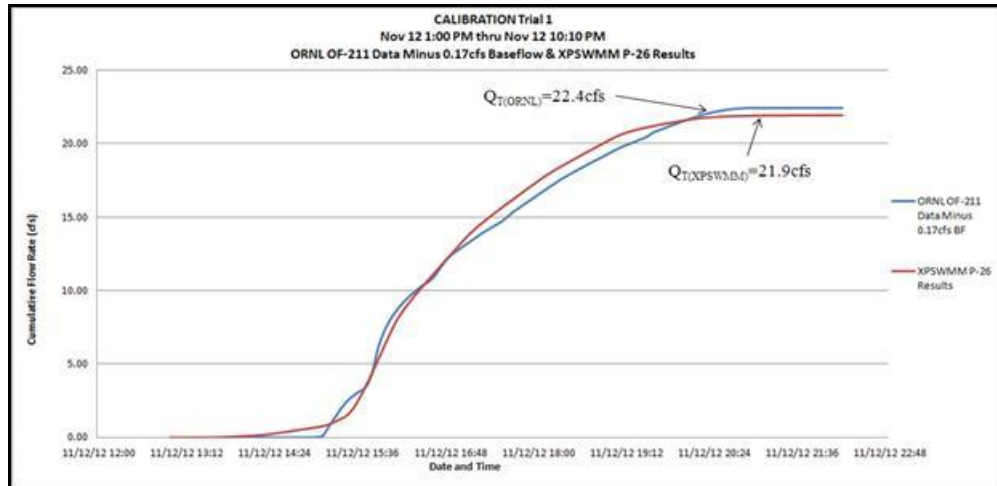


Figure 107. ORNL Data and XPSWMM Results Cumulative Flow Rates.

Calibration of Model Trial 2 Results

The rainfall event that occurred on November 26, 2012 at 9PM thru November 27, 2012 at 6AM was utilized for the calibration trial 2. The figure below is a hydrograph of the ORNL OF-211 data provided during the time the precipitation occurred and includes the 0.17 cfs base flow which was later extracted for calibration purposes.

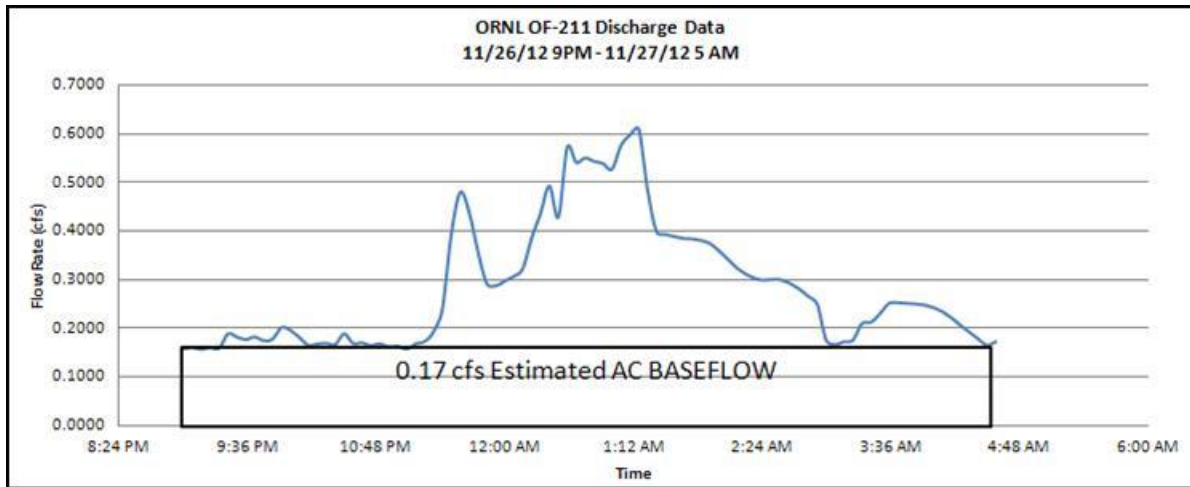


Figure 108. ORNL Data with Base Flow.

The ORNL observed data indicates a peak flow rate of 0.44 cfs (excludes 0.17 cfs base flow) on November 27, 2012 at 1:15 AM. The XPSWMM hydrograph indicates a peak flow rate of 0.44 cfs at 1:00 AM. A summation of the ORNL OF-211 flow rates and the XPSWMM results are also depicted in the figure below. The peak flow rates are consistent if one accepts that a 0.17 cfs base flow occurs during that timeframe. ORNL’s peak falls behind the model results by 15 minutes. However, the XPSWMM model lags behind ORNL data by approximately 55 minutes. The lag time is the difference in time between the two sets of data where the first rainfall interval has been routed through the system. The summation of the flow rates during the calibration timeframe is similar. Below that is a figure indicating the cumulative flow rate versus time which indicates more clearly the two sets of data summation of flow rates during the calibration duration.

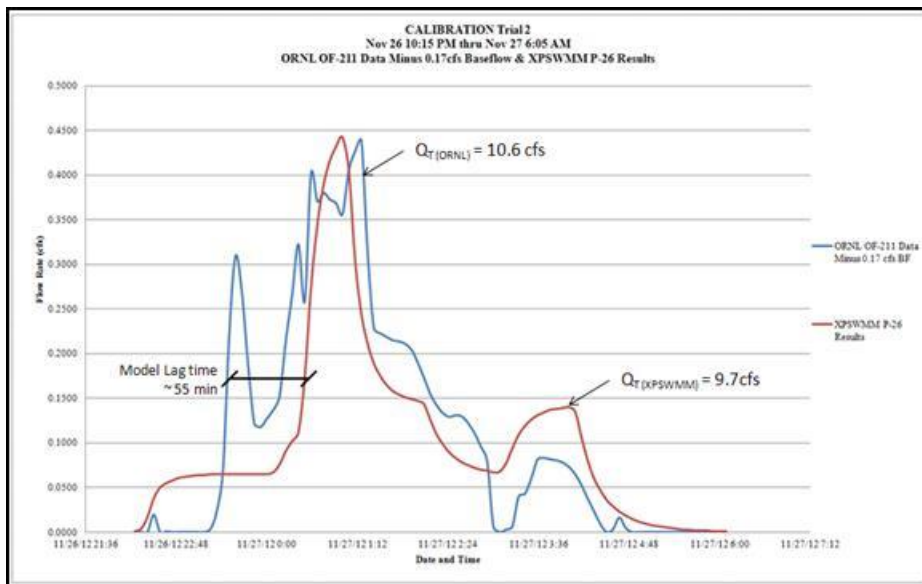


Figure 109. ORNL Data and XPSWMM Results Hydrograph.

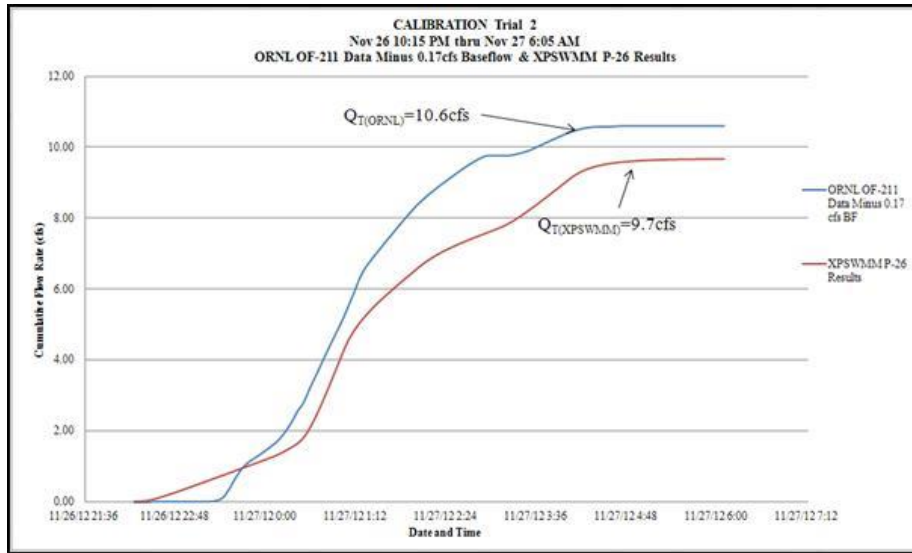


Figure 110. ORNL Data and XPSWMM Results Cumulative Flow Rates.

Calibration of Model Trial 3 Results

The rainfall event that occurred on December 10, 2012 between the hours of 3:00 AM and 4:00 PM was utilized for the calibration trial 3. The figure below is a hydrograph of the ORNL OF-211 data provided during the time the precipitation occurred and includes the 0.17 cfs base flow which was later extracted for calibration purposes.

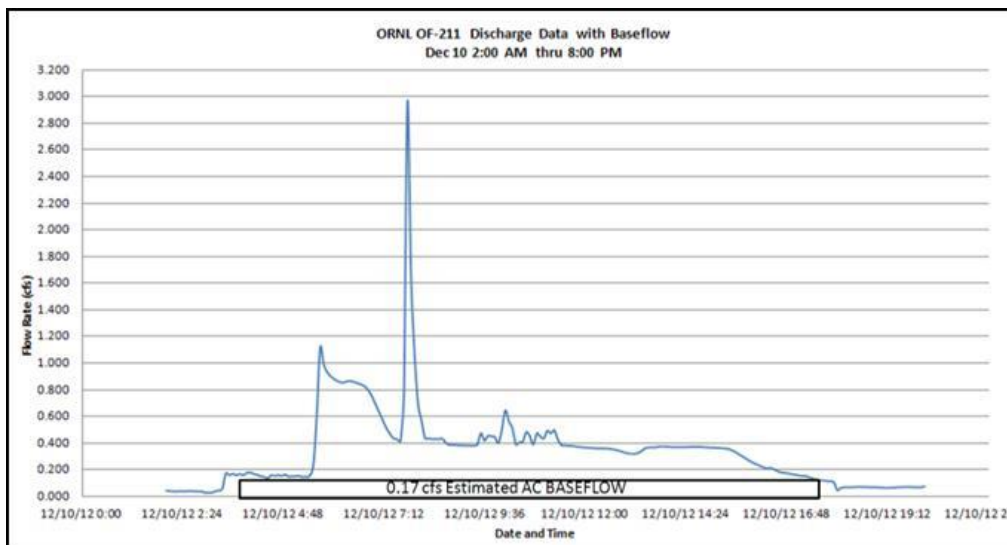


Figure 111. ORNL Data with Base Flow.

ORNL noted that the 3 cfs peak flow rate may be a faulty reading from the flow rate monitor. The figure below is an overlay of the ORNL data (minus 0.17 cfs base flow) and XPSWMM results. ORNL observed data indicates a peak flow rate of 2.79 cfs (excludes 0.17 base flow) on December 10, 2012 at 7:45 AM. Below that is a figure indicating the cumulative flow rate versus time which indicates more clearly the two sets of data summation of flow rates during the calibration duration. The hydrograph produced by XPSWMM portrays a peak flow rate of 1.22 cfs at 7:00 AM. The lag between the two sets of data is approximately 40 minutes. The total flow rate summation results are relatively close.

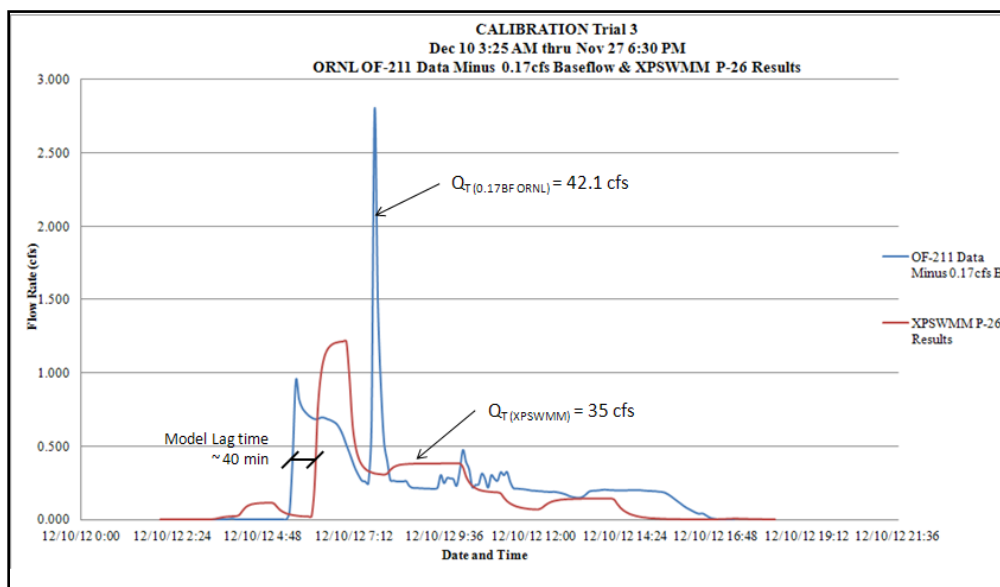


Figure 112. ORNL Data and XPSWMM Results Hydrograph.

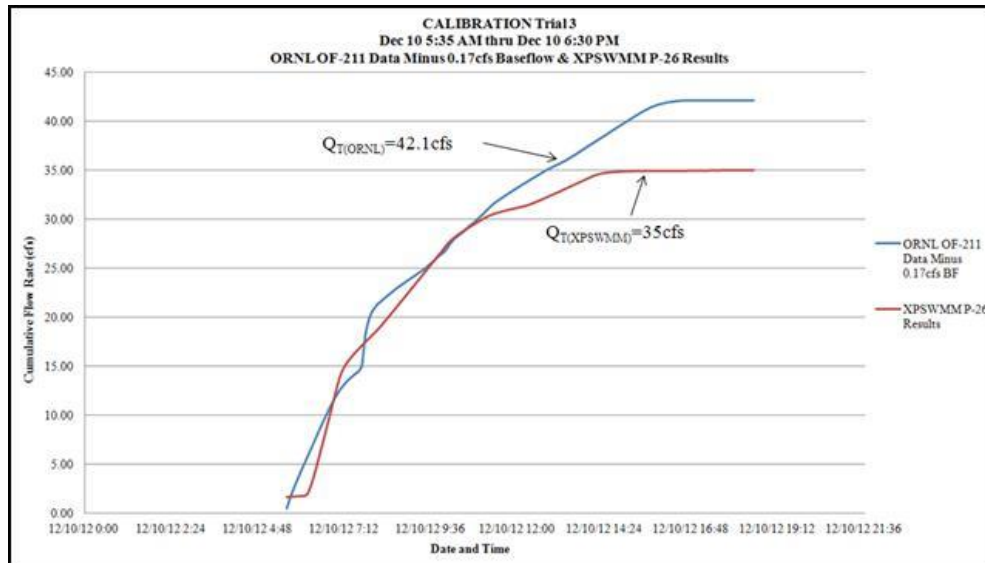


Figure 113. ORNL Data and XPSWMM Results Cumulative Flow Rates.

Calibration of Model Trial 4 Results

The rainfall event that occurred on December 15, 2012 between the hours of 9:00 PM and 8:00 PM was utilized for the calibration trial 4. The figure below is a hydrograph of the ORNL OF-211 data provided during the time the precipitation occurred and includes the 0.17 cfs base flow which was later extracted for calibration purposes.

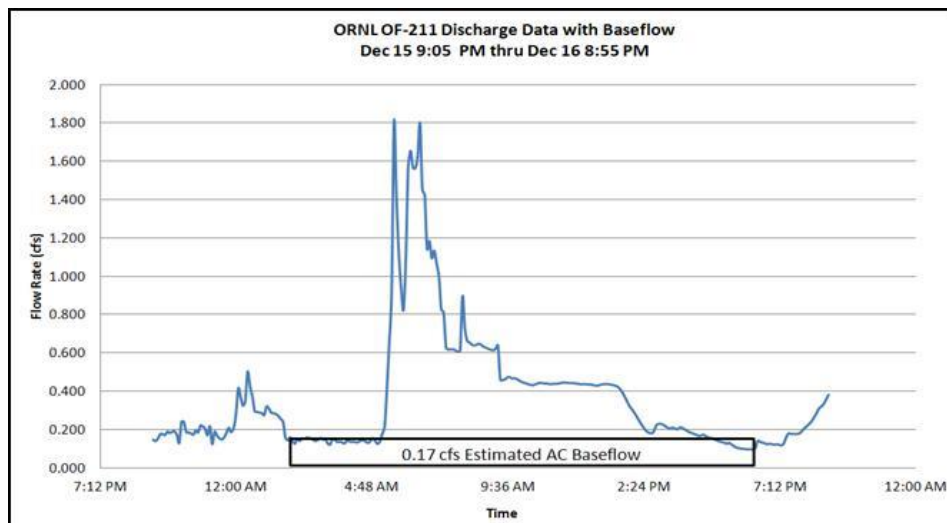


Figure 114. ORNL Data with Base Flow.

The figure below shows that the ORNL observed flow rate data has a peak flow rate of 1.64 cfs (excluding base flow) on December 16, 2012 at 5:35 AM. Similarly, the XPSWMM hydrograph specifies a peak flow rate of 1.34 cfs at 5:50 AM. The lag between the two sets of data is approximately 35 minutes. The total flow rates are relatively close and may be considered that the two sets of data do correlate. Below that is a figure indicating the cumulative flow rate versus time which indicates more clearly the two sets of data summation of flow rates during the calibration duration.

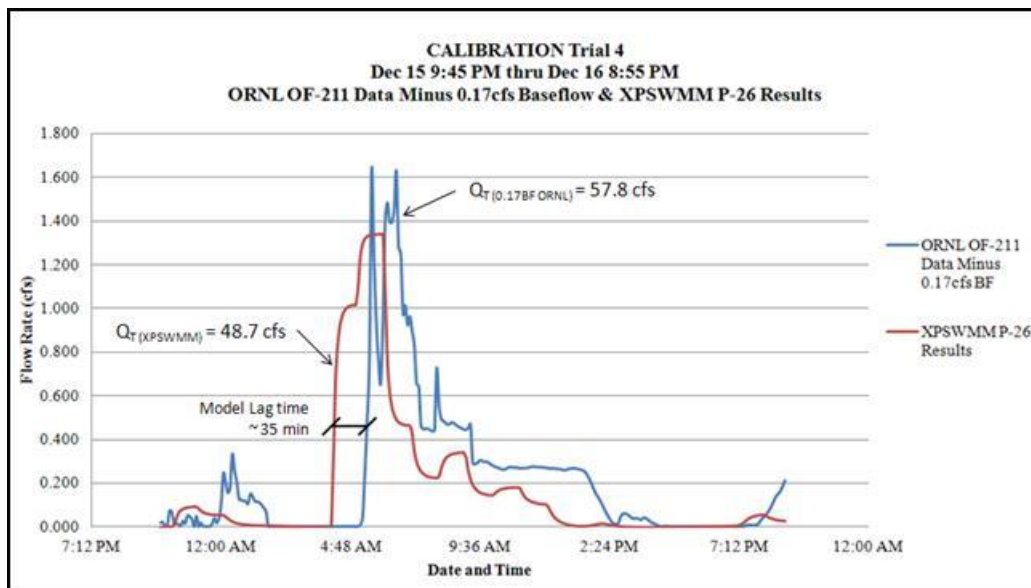


Figure 115. ORNL Data and XPSWMM Results Hydrograph.

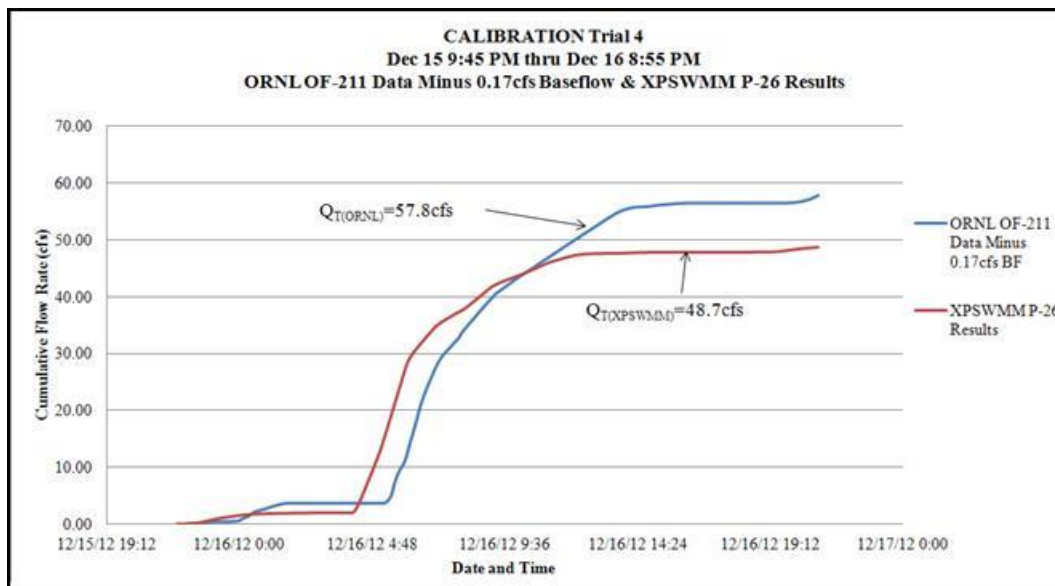


Figure 116. ORNL Data and XPSWMM Results Cumulative Flow Rates.

Sensitivity Analysis Results

Manning’s Roughness Sensitivity Analysis Results

The Manning’s roughness coefficient is based on the material of the pipe or the type of channel. It is inversely proportional to the flow rate where the smaller the coefficient the larger the flow due to the friction caused by the channels roughness. The network contains the following types of pipes: wrought iron (WI), vitrified clay pipe (VP), concrete pipe (CP), reinforced concrete pipe (RCP), and polyvinyl chloride (PVC).

The following are the results from varying the Manning’s roughness coefficient, n, by 0.011, 0.013, 0.05, 0.017, and 0.035 where continuous rainfall of year 2010 was simulated, the Green Ampt method used, and an evaporation default of 0.1”/day assumed. The following are the resulting hydrographs for MH211-3 and OF-211 with their PE curves:

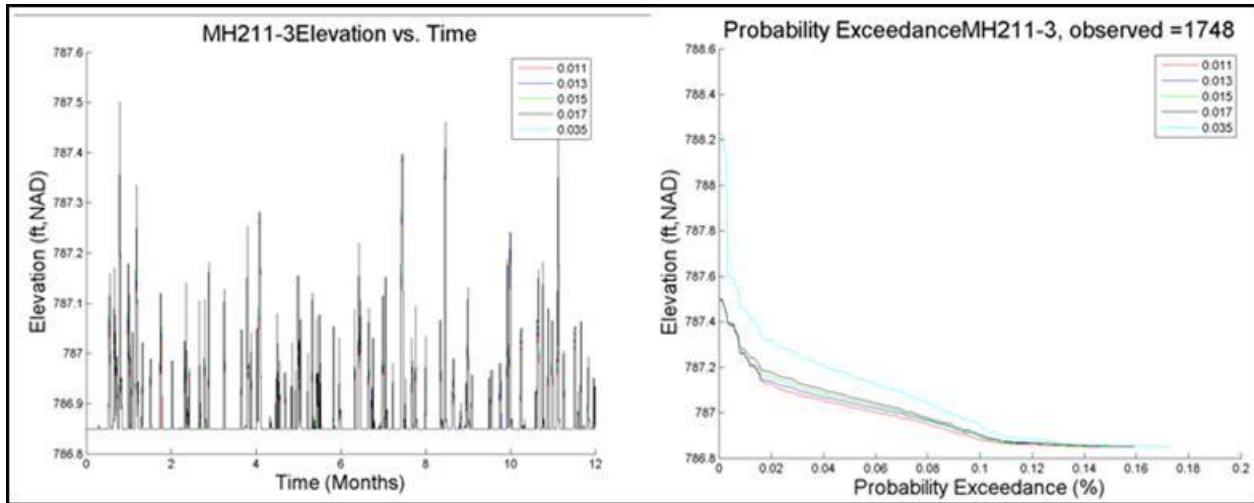


Figure 117. MH211-3 Hydrograph and PE Curves for Manning's Roughness Coefficient Sensitivity Analysis.

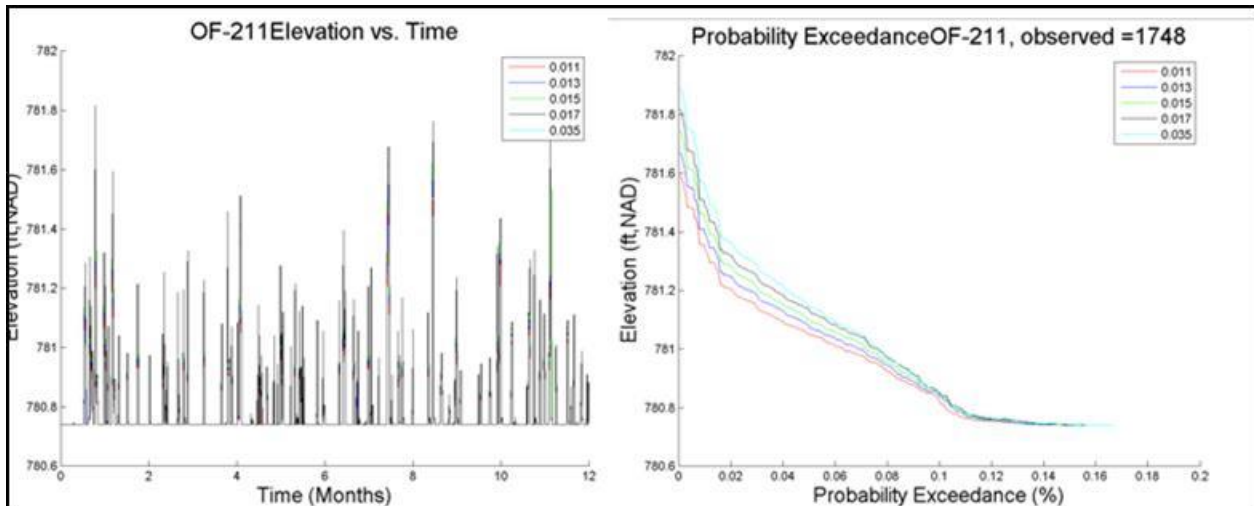


Figure 118. OF-211 Hydrograph and PE Curves for Manning's Roughness Coefficient Sensitivity Analysis.

The results indicate minor changes (if any) in the flow rate through the specified pipes; however, node elevations are shown to vary via the hydrographs and vary more on the probability of exceedance curves. Although Manning's coefficient of 0.035 is specific to grassy areas, it was

used in order to assess the sensitivity of the simulation. As one would expect, it does have a larger impact than the 0.017, 0.015, etc. Also note the PE x-axis was decreased from 1 (100%) to 0.2 (20%) with the purpose of demonstrating that the roughness coefficients do make a difference; however, too minor to take into account for this study. Thus, the coefficient 0.015 for the remaining simulations was chosen due to the fact that the typical value for closed conduits flowing through partly full concrete sewer gravity pipes is 0.015, as indicated in the Manning's n for concrete pipe closed conduits flowing partly full table located below.

Table 50. Manning's n for Concrete Pipe

Manning's n for Concrete Closed Conduits Flowing Partly Full Table			
(Chow, 1988)			
Type of Conduit and Description	Minimum	Normal	Maximum
Concrete:			
Culvert, straight and free of debris	0.010	0.011	0.013
Culvert with bends, connections, and some debris	0.011	0.013	0.014
Finished	0.011	0.012	0.014
Sewer with manholes, inlet, etc., straight	0.013	0.015	0.017
Unfinished, steel form	0.012	0.013	0.014
Unfinished, smooth wood form	0.012	0.014	0.016
Unfinished, rough wood form	0.015	0.017	0.020

Infiltration Sensitivity Analysis Results

Yearly simulations were run where the Manning's roughness coefficient of 0.015 was held constant, and an evaporation default of 0.1"/day was assumed. Green Ampt and the Horton's infiltration methods were used and the results are compared.

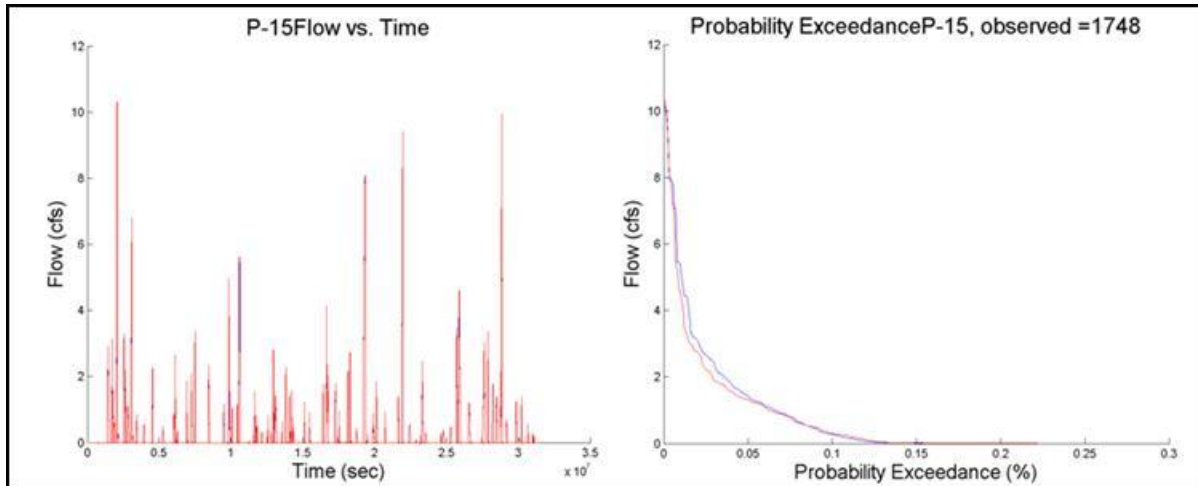


Figure 119. P-15 Hydrograph and PE Curves for Infiltration Sensitivity Analysis.

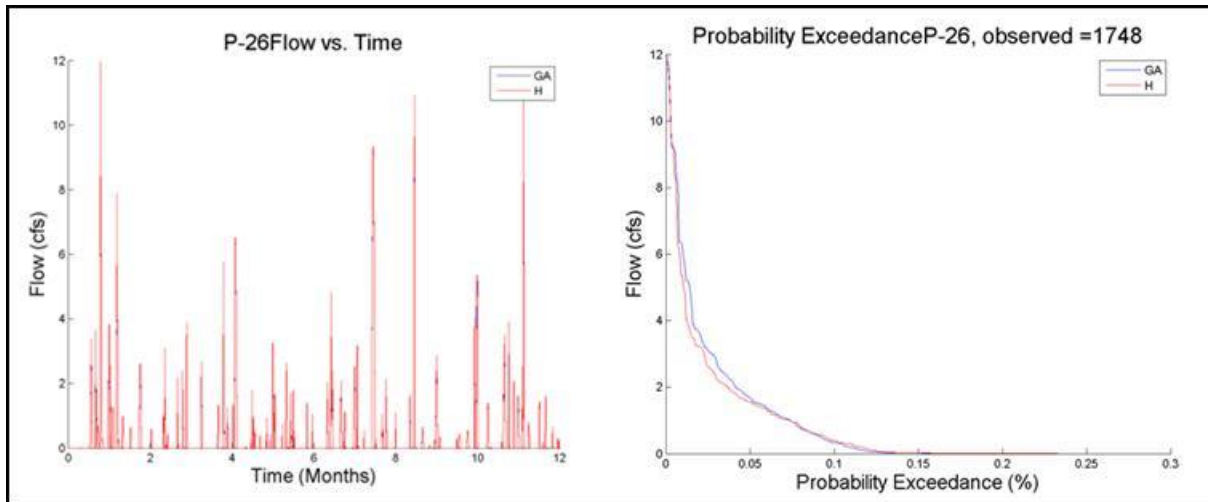


Figure 120. P-26 Hydrograph and PE Curves for Infiltration Sensitivity Analysis.

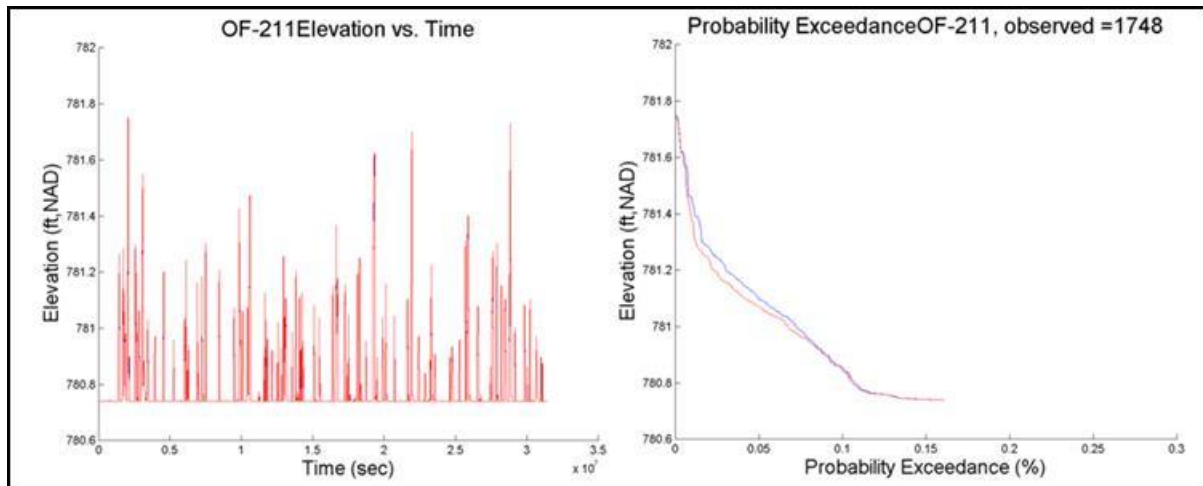


Figure 121. OF-211 Hydrograph and PE Curves for Infiltration Sensitivity Analysis.

The results indicate minor differences in the hydrographs and minor differences in the node elevations. This could be that the Horton's default regeneration rate of 0.01 and/or decay rate of 0.001 were not large enough to produce a significant regeneration throughout the continuous rainfall. Studies have found that the Green Ampt method simulates one dimensional unsteady continuous rainfall events effectively and due to the fact there are only minor differences in the two methods, Green Ampt infiltration parameters have been chosen for the remaining simulations (Risse, 1994).

Percent Impervious Sensitivity Analysis Results

The assumed percent imperviousness was obtained from visual inspection during the site inspections. An increase of imperviousness on a basin will impact the surface water runoff as there will be a larger quantity of runoff due to less infiltration. The time of concentration will also lessen and impact the peak of the hydrographs as the runoff will approach the inlet at an increased speed.

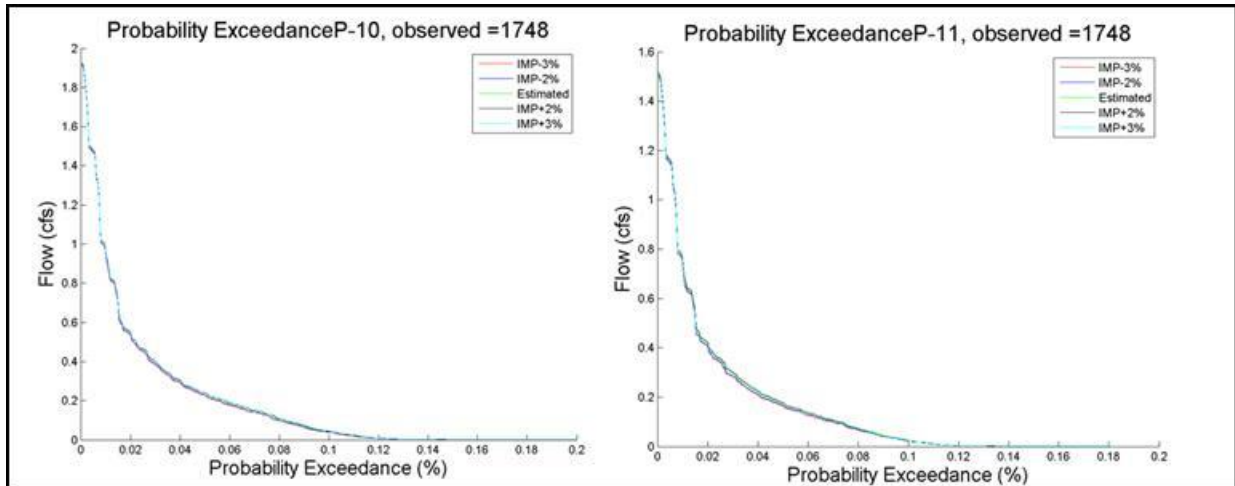


Figure 122. P-10 and P-11 PE Curves for Percent Imperviousness Sensitivity Analysis.

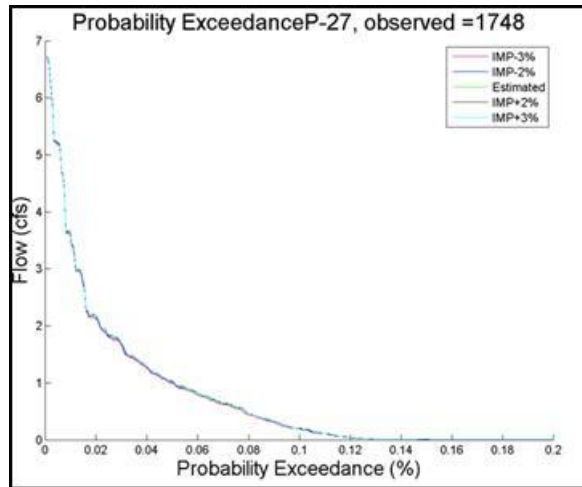


Figure 123. P-27 PE Curves for Percent Imperviousness Sensitivity Analysis.

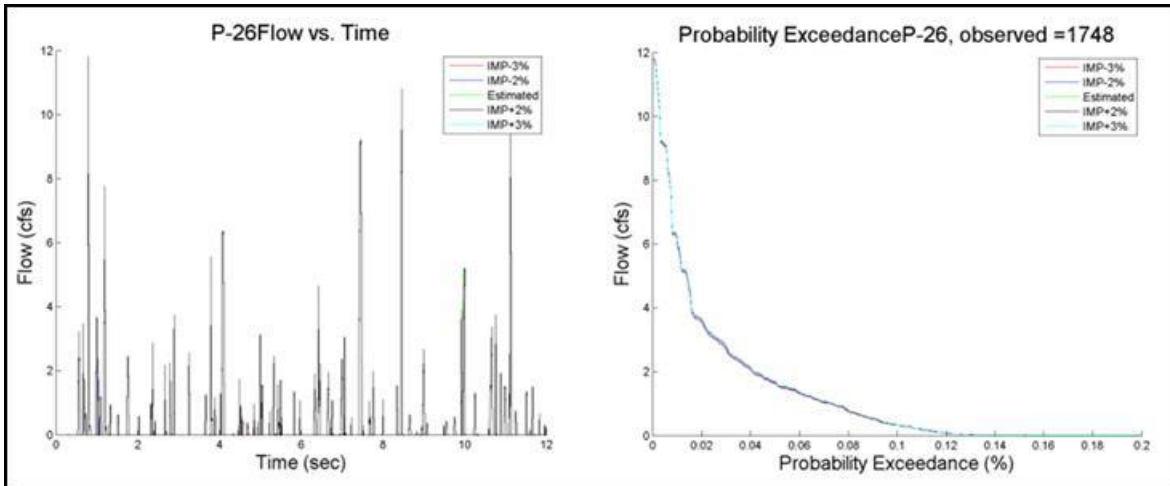


Figure 124. P-26 Hydrograph and PE Curves for Percent Imperviousness Sensitivity Analysis.

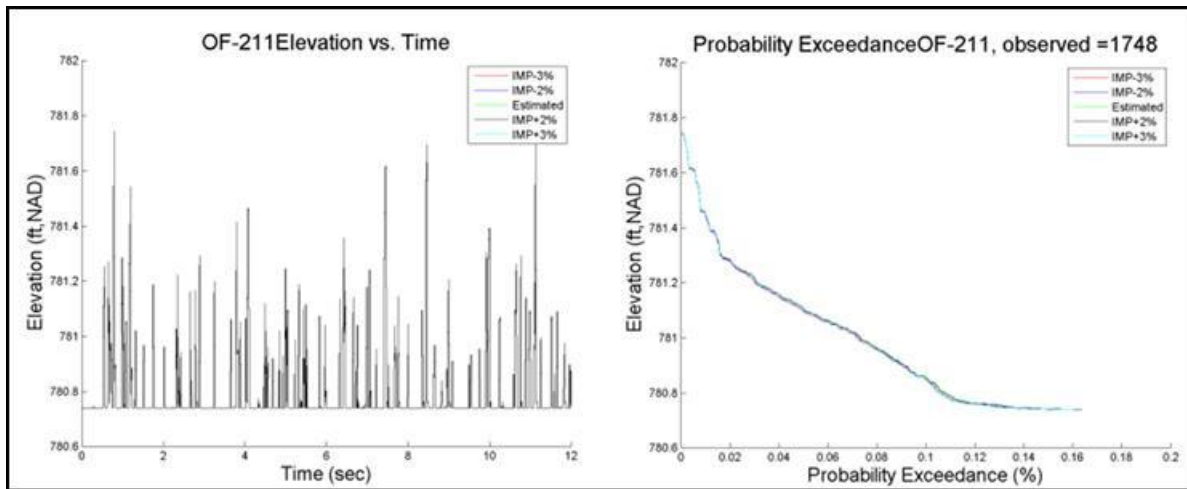


Figure 125. OF-211 Hydrograph and PE Curves for Percent Imperviousness Sensitivity Analysis.

The amount of imperviousness a basin has is directly connected to the volume of runoff. There are only subtle differences between the variations of percent imperviousness. When an increase in imperviousness occurs, the PE curves falls flatter, which indicates that a higher flow rate will occur for a longer time.

One base simulation was held consistent through all three sensitivity analyses and is used for the base of the simulations in the transport analysis, which was the simulation using Manning’s n roughness coefficient of 0.015, the Green Ampt infiltration parameters, evaporation default of 0.1”/day, and the estimated percent imperviousness. The figure below is a snapshot of the north-south main trunk line which includes the following pipes: P-2, P-3, P-4, P-5, P-8, P-10, P-15, P-16, P-17, P-20, P-21, P-23, P-25, and P-26 and indicates that the system on day 23 hour 23:00:00 which encounters its first peak throughout the yearly continuous rainfall events. The first pipe, P-2, is a 4” diameter storm lateral from building 4501 and nearly reaches capacity due to the peak in rainfall intensity. Also to be noted, according to the rainfall intensity simulated through the system, the first peak occurs on January 24, 2010 at hour 20:00:00 which is a day after the model predicts its first peak.

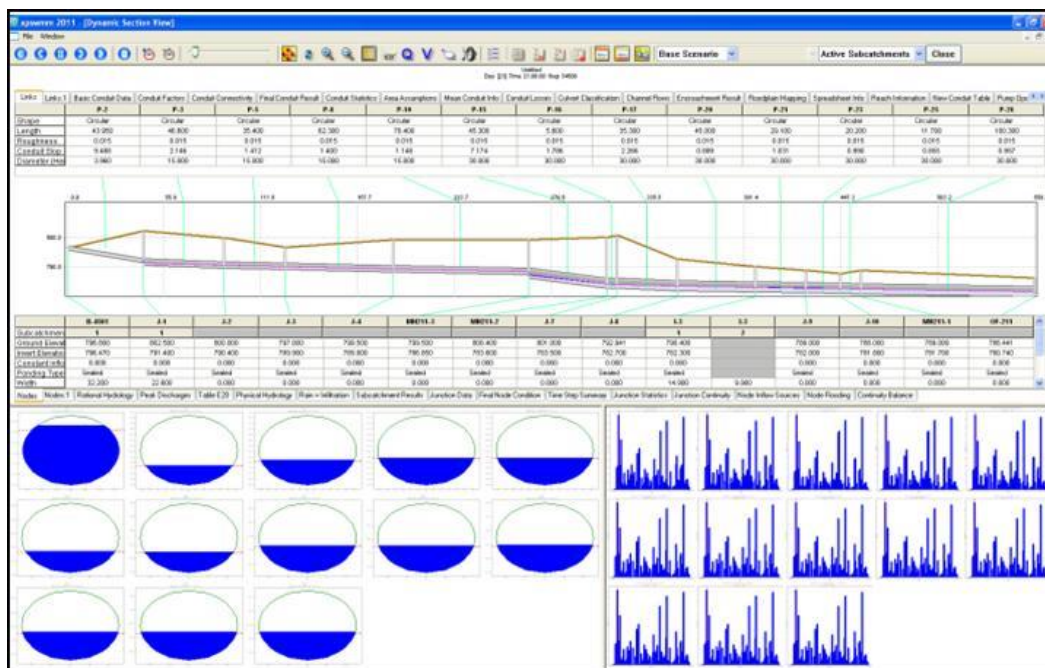


Figure 126. XPSWMM North-South Storm Line Results for Base Conditions.

Similarly to the north/south main trunk line, XPSWMM estimates a peak to occur in the east-west trunk lines (I-10 thru B-4556) on day 23; however at the 18:00:00 hour. The east/west main trunk line is defined as the following pipes: P-14, P-11, P-27, P-40, P-41, P-42, P-46, and P-49 and is shown in the figure below.

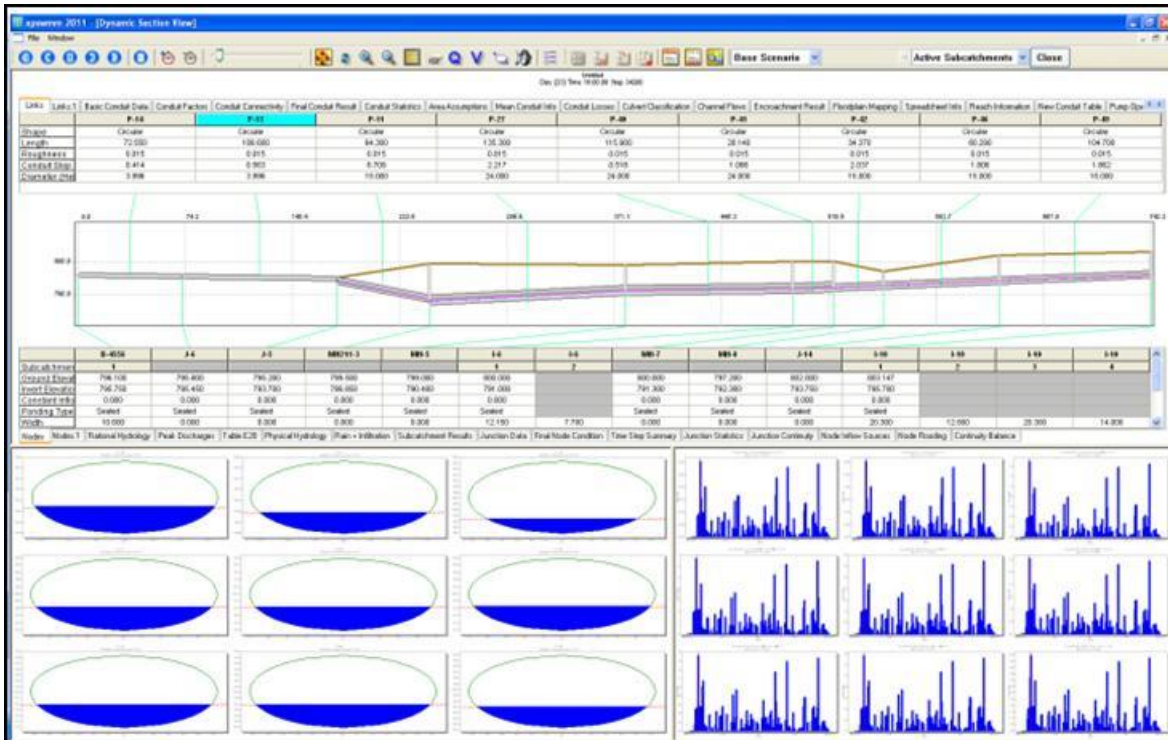


Figure 127. XPSWMM East-West Storm Line Results for Base Conditions.

The system does indicate during the first peak in rainfall intensity that minor flooding occurs between nodes I-3 to OF-211 as the hydraulic grade line approaches the ground elevation, as shown in the figure below.

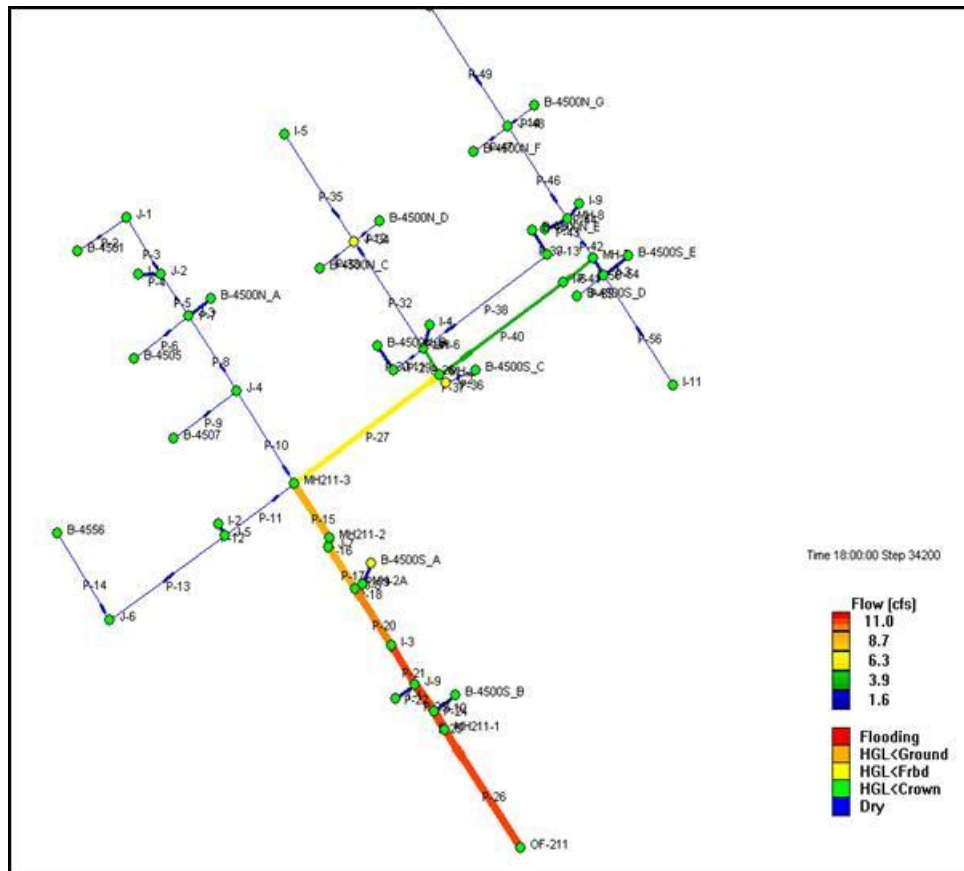


Figure 128. XPSWMM Results for Base Conditions.

Design Storm Simulation Results

The design simulations are based on a Manning’s roughness coefficient of 0.015, Green Ampt infiltration method, and the estimated percent imperviousness from site visits. Below are the hydrographs and PE curves for nodes MH211-3 and OF-211 and for links P-10, P-11, P-26, and P-27.

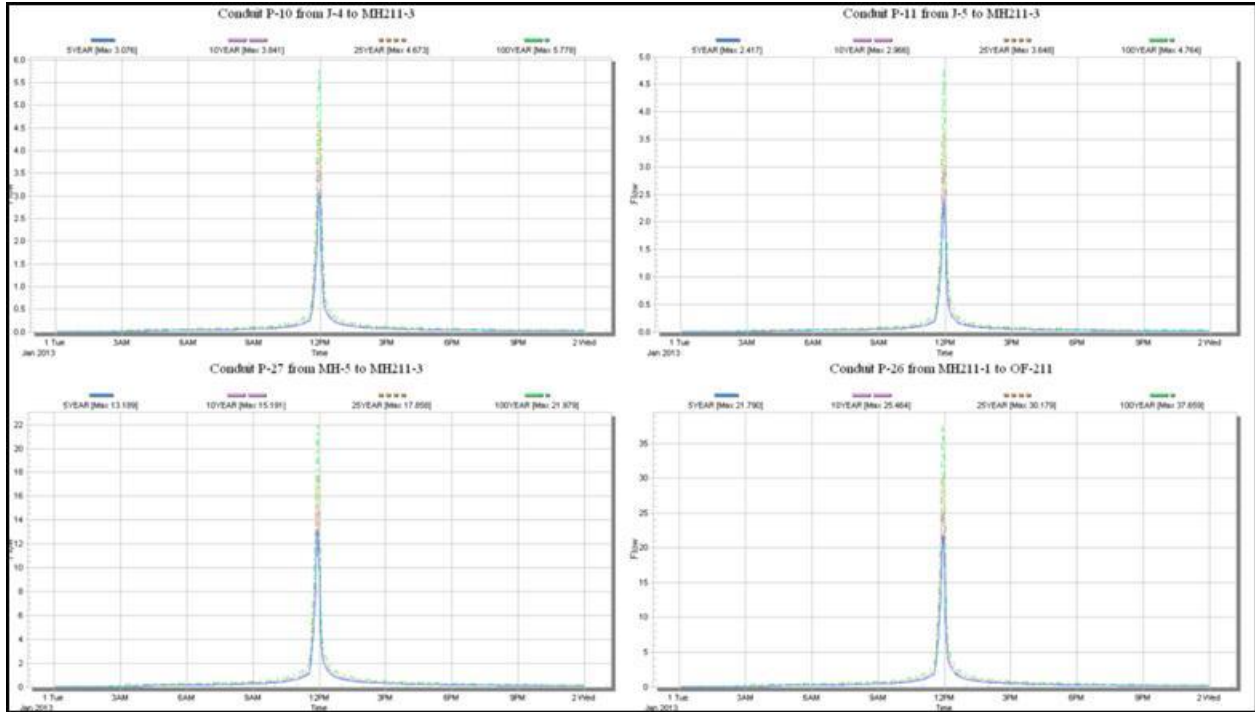


Figure 129. XPSWMM Design Storm Hydrographs.

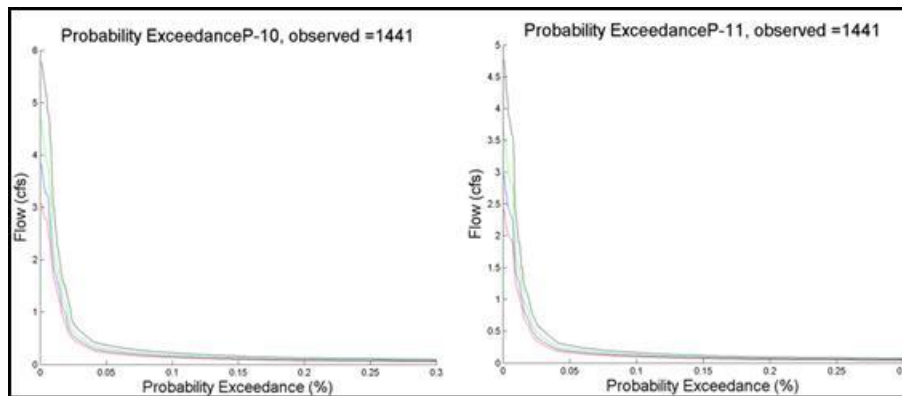


Figure 130. P-10 PE Curves for Design Storm Events.

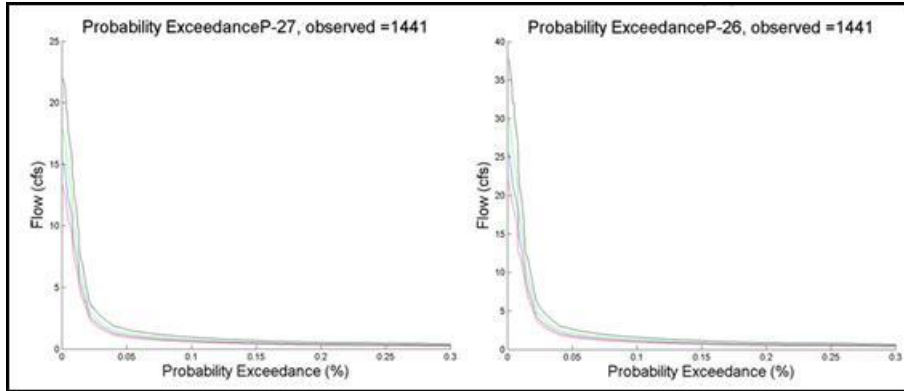


Figure 131. P-27 PE Curves for Design Storm Events.

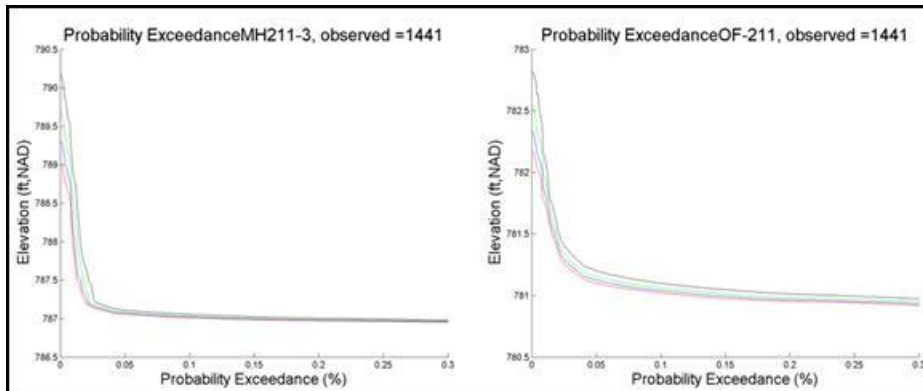


Figure 132. MH211-3 PE Curves for Design Storm Events.

The table below is a summary of the maximum stages (elevations) and flow rates for the chosen nodes and links. Due to the fact that the design storms precipitation amounts vary in magnitude almost an inch, a difference in node elevations and link stages throughout the events are observed as shown in the hydrographs and PE curves.

Table 51. Design Storm Stage and Flow Rate Results

Design Storm	Peak Stage (ft, NAD)		Peak Flow Rate (cfs)			
	MH211-3	OF-211	P-10	P-11	P-26	P-27
5 yr - 24 hour	789	782.2	3.1	2.4	21.8	13.2
10 yr - 24 hour	789.3	782.3	3.8	3	25.5	15.2
25 yr - 24 hour	789.7	782.5	4.7	3.6	17.9	30.2
100 yr - 24 hour	790.2	782.8	5.8	4.8	22	37.7

For the simulations, the hydraulic grade line (HGL) and flow quantities and capacities of the main conduits have been evaluated to determine the extent of overflow. The 5 year and 10 year – 24 hour storm events do not encounter flooding. The HGL is shown in the figure below for the main trunk line beginning at P-10 to P-26. The HGL rose higher for the 10 year model’s storm event than the 5 year model’s storm event due to the fact that less precipitation was simulated over the site. The figures below indicate that the water does not exceed the top of the pipe; thus, no flooding is expected to occur as the water is contained within the pipes for both the 5 year and 10 year – 24 hour storm events.

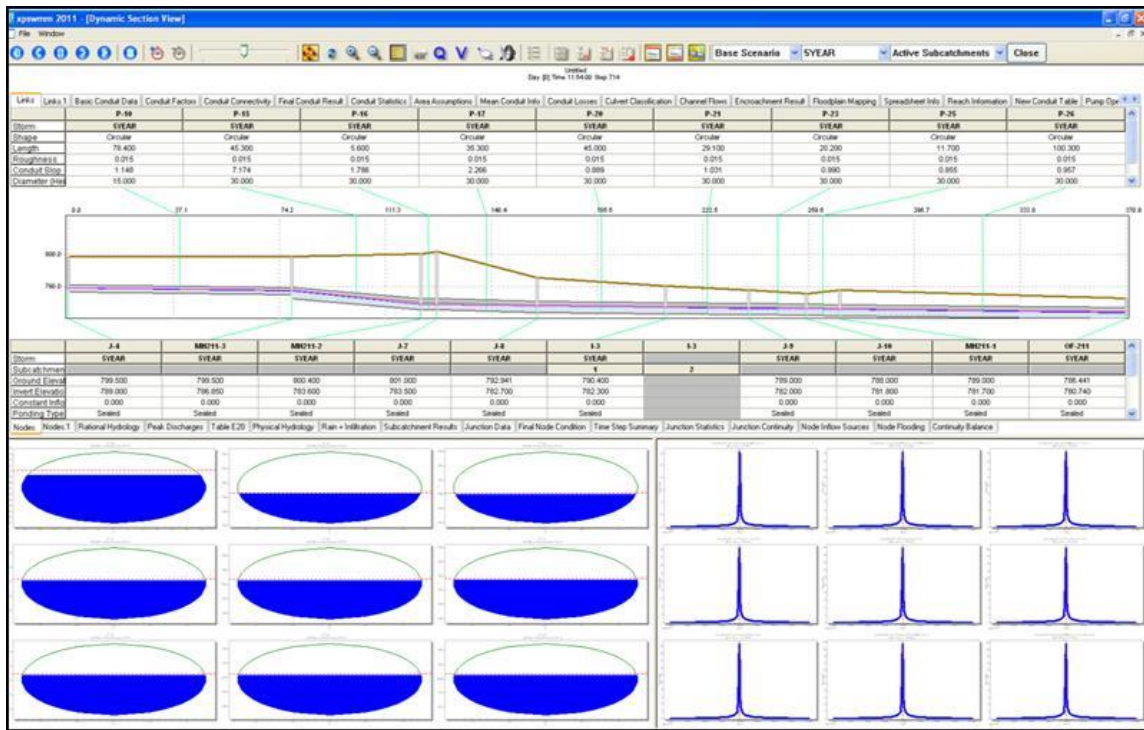


Figure 133. XPSWMM 5-Year 24-Hour Storm Event.

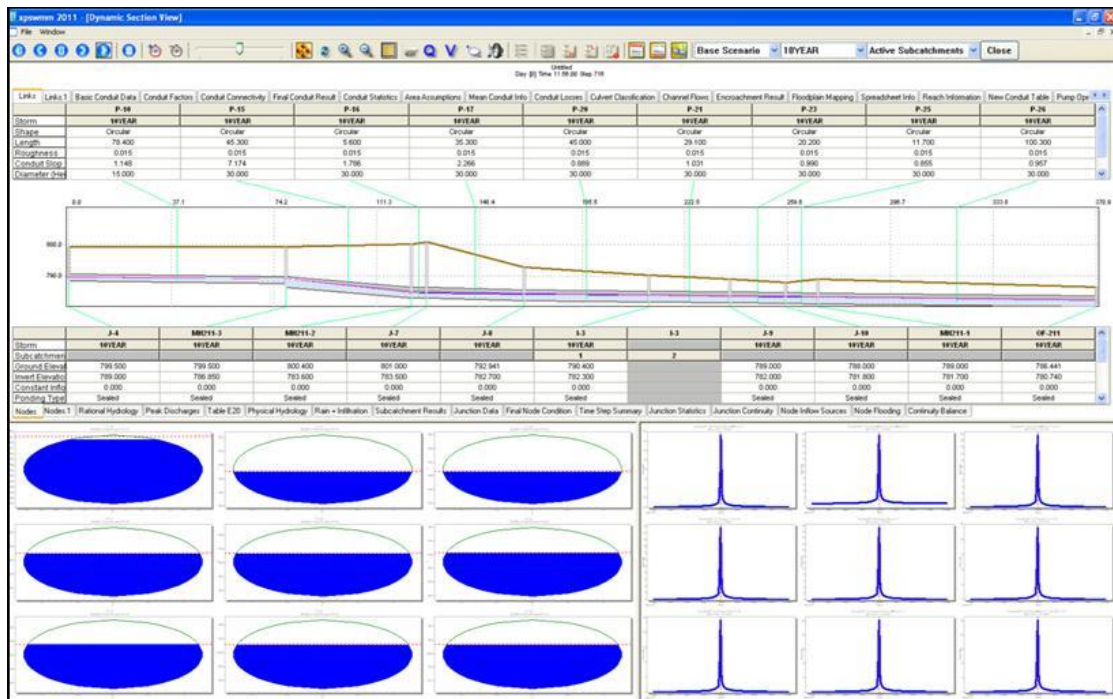


Figure 134. XPSWMM 10-Year 24-Hour Storm Event.

However, for the 25 year and 100 year models – 24 hour storm events do cause flooding to occur within the system. As would be expected, the 100 year model’s storm produced a larger runoff excess than the 25 year model’s storm event. The figures below indicate that P-10 exceeds its maximum capacity, which indicates there would be ponding on the pavement.

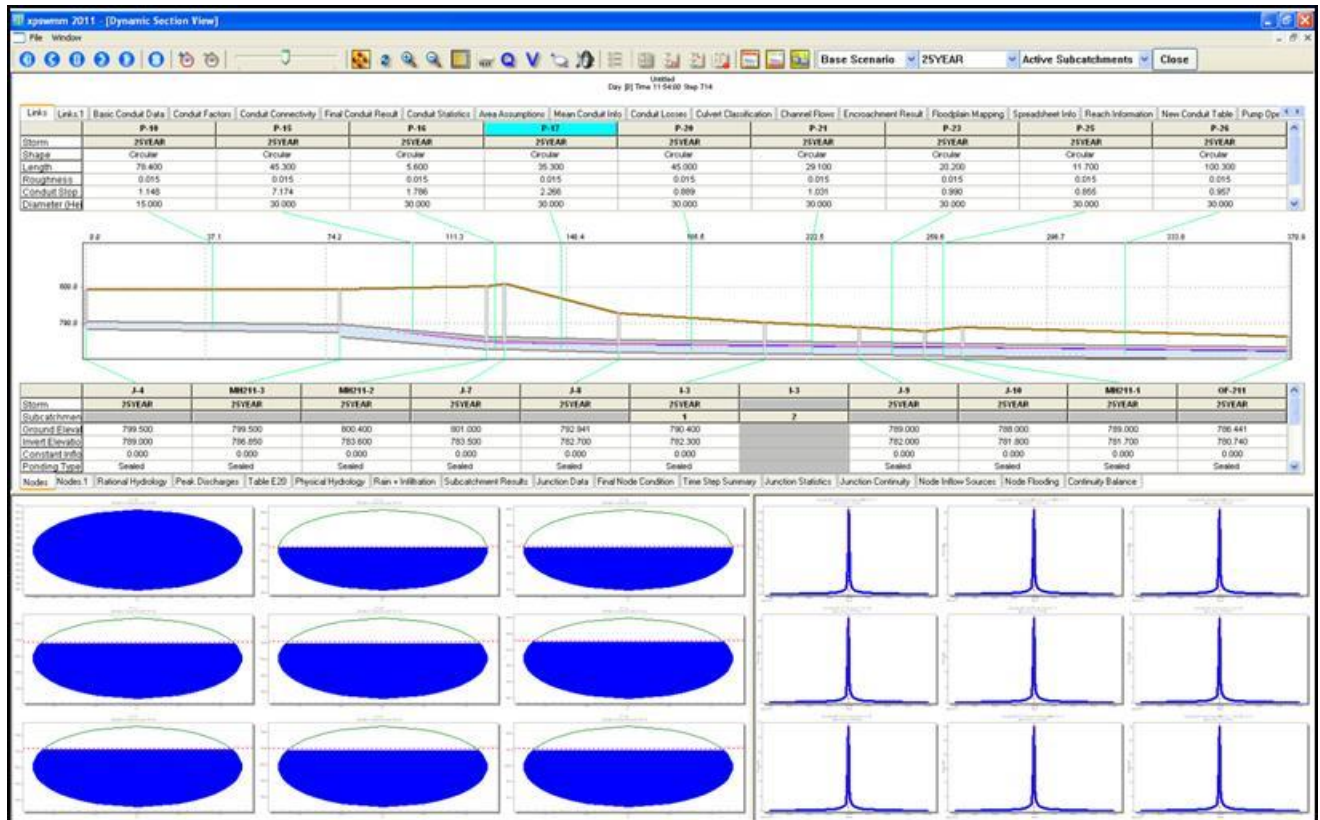


Figure 135. XPSWMM 25-Year 24-Hour Storm Event.

The figure below is a schematic of the system indicating where the flooding occurred and its quantity. The links (P-21, P-22, and P-26) that are red represent that the flow rate has met or exceeded 28.2 cfs, and the nodes (B-4501, J-12, B-4500_S, B-4500S_D, and B-4500S_E) that are red represent flooding in which the HGL was exceeded and there was insufficient capacity within the pipes.

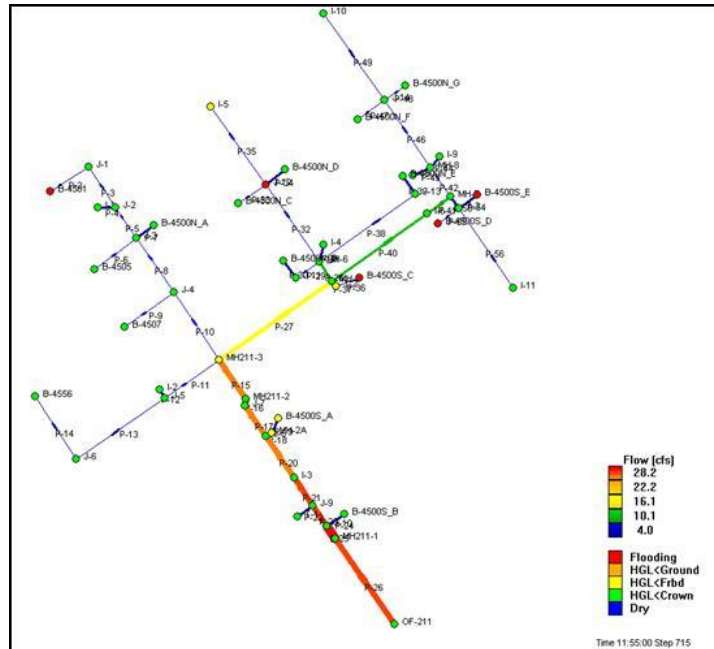


Figure 136. XPSWMM 25-Year 24-Hour Storm Event Areas of Flooding.

Below are the 100 year – 24 hour design storm event results which are similar to the 25 year storm results. The major difference is that the flow rate is higher, reaching up to 35.1 cfs in the pipes leading up to OF-211. In addition, flooding occurs in the storm lateral, B-4500S_A.

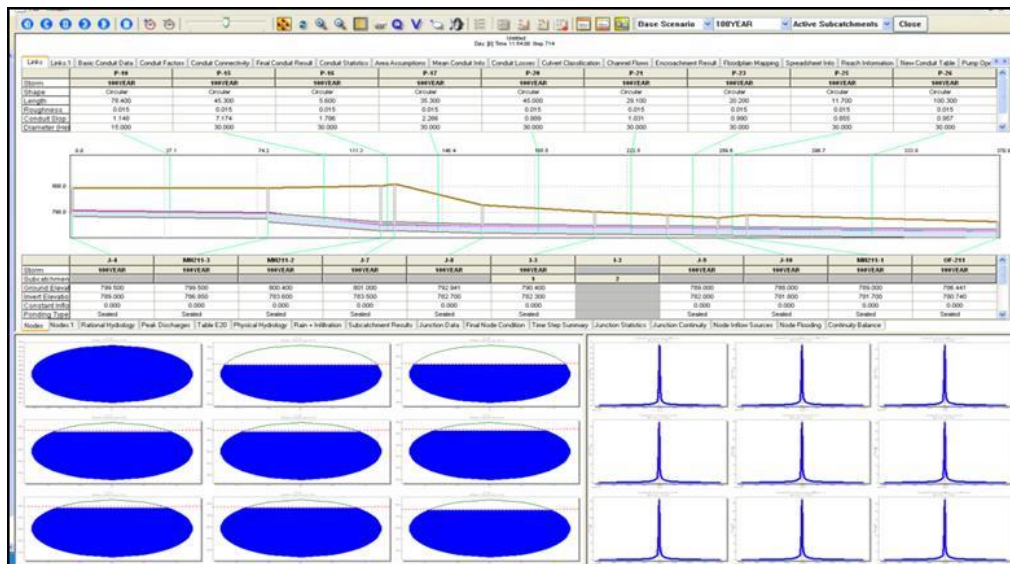


Figure 137. XPSWMM 100-Year 24-Hour Storm Event.

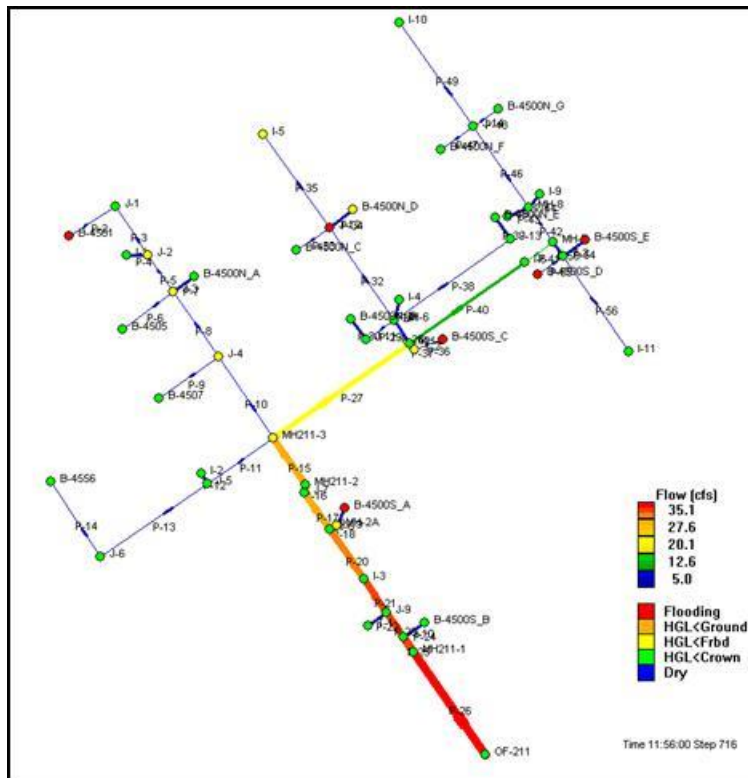


Figure 138. XPSWMM 100-Year 24-Hour Storm Event Areas of Flooding.

Transport Analysis Results

The model’s accuracy is indicated by the convergence of the numerical calculations which is demonstrated via the continuity check. The continuity check is performed for each simulation and is displayed to the user after each simulation completion. The model provides results as a cumulative depth for each simulation for precipitation, infiltration, evaporation, surface runoff from watersheds, and water in surface storage. These numbers are consistent for the four simulations because they simulate the same rainfall events and the additional flow rates introduced are minor. The table below represents the continuity results from the model for the transport scenarios.

Table 52. Continuity Results

Continuity Results over Entire Basin for Transport Simulations	
Surface Water	Depth (in.)
Total Precipitation	603.798
Total Infiltration	33.725
Total Evaporation	16.988
Surface Runoff from Watersheds	553.096
Total Water remaining in Surface Storage	-
Infiltration over the Pervious Area	415.946

The continuity check is calculated by the following equations:

$$\text{Precipitation} - \text{Infiltration} - \text{Evaporation} - \text{Surface Runoff from Watersheds} - \text{Water in Surface Storage} \tag{Equation 60}$$

where the losses are the last four terms.

$$((1 - (\text{Precipitation} / \text{Losses})) * 100) \tag{Equation 61}$$

The continuity check result for the simulations is -0.19%. XPSWMM considers a continuity error of less than 1% excellent, 1% to 2% is great, and 2% to 5% is good. All of the simulations executed for this study resulted in less than 1% error.

Transport Analysis Simulation 1 Results

As expected, loads were present in links P-10, P-15, P-26, and P-27; however, none was present in P-11 as no load was introduced west of MH211-3. The constant 0.1 mg/L concentration entered into B-4501 and B-4500N_G appears as the maximum concentration of 0.1 mg/L. The concentration lessens as runoff is introduced into the system as it responds to the yearly rainfall. Links P-10 and P-27 hydrographs and pollutographs respond to the steady flow rate timeseries entered. This is shown to be the minimum constant base flow of 0.17 cfs. No additional flow was

entered into the system west of P-11; thus, no base flow is indicated. P-15 flow rate agrees with the flow rates entered into node MH211-3, and indicates a base flow of 0.34 cfs which agrees with the 0.17 cfs from P-10 and P-27. P-26 also indicates a base flow of 0.34 cfs and has a larger flow rate than in P-15, as it should due to the runoff entering the system south of P-15. The simulation results accurately respond to the first scenario. The maximum flow rate within link P-26 is 12.1 cfs and the maximum elevation in node OF-211 is 781.8 ft, NAD. The cumulative load in P-26 is estimated to be 65 lb.

The following are the hydrographs and pollutographs (concentration versus time and load versus time) for the first simulation for links P-10, P-11, P-15, P-26 and P-27. Link P-10 collects water from the north, P-11 from the east, and P-27 from the west, then the water is conveyed via MH211-3 into P-15, then P-26 and into OF-211. In addition, the XPSWMM model specifies the velocity on the hydrographs. These velocities are cumulative velocities hence their magnitude. In addition, the loads shown on the pollutographs are also cumulative load values represented by a diagonal line.

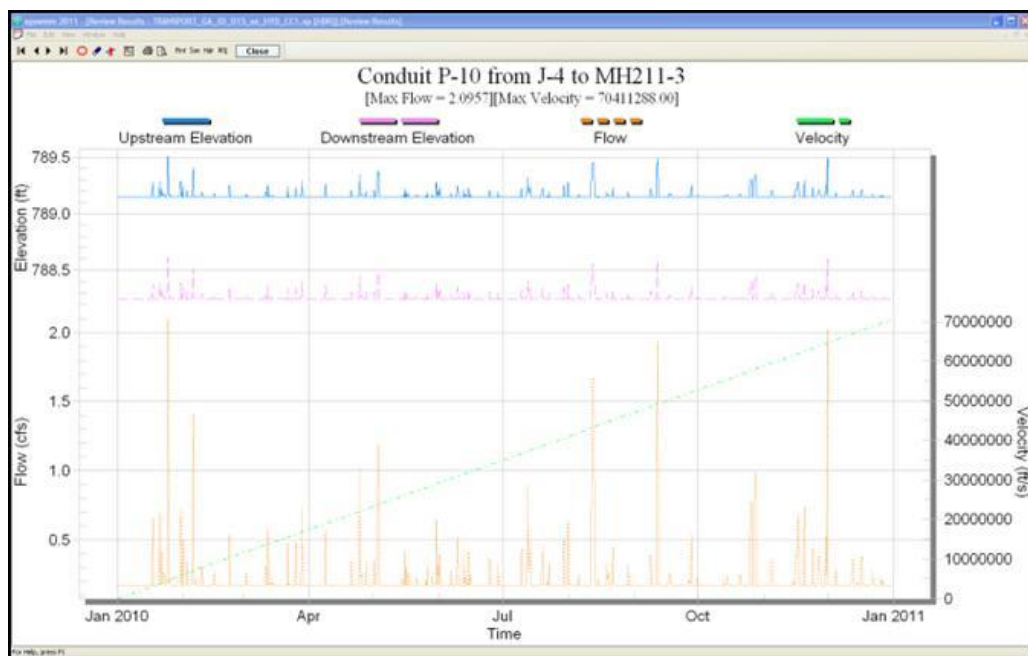


Figure 139. XPSWMM P-10 Hydrograph.

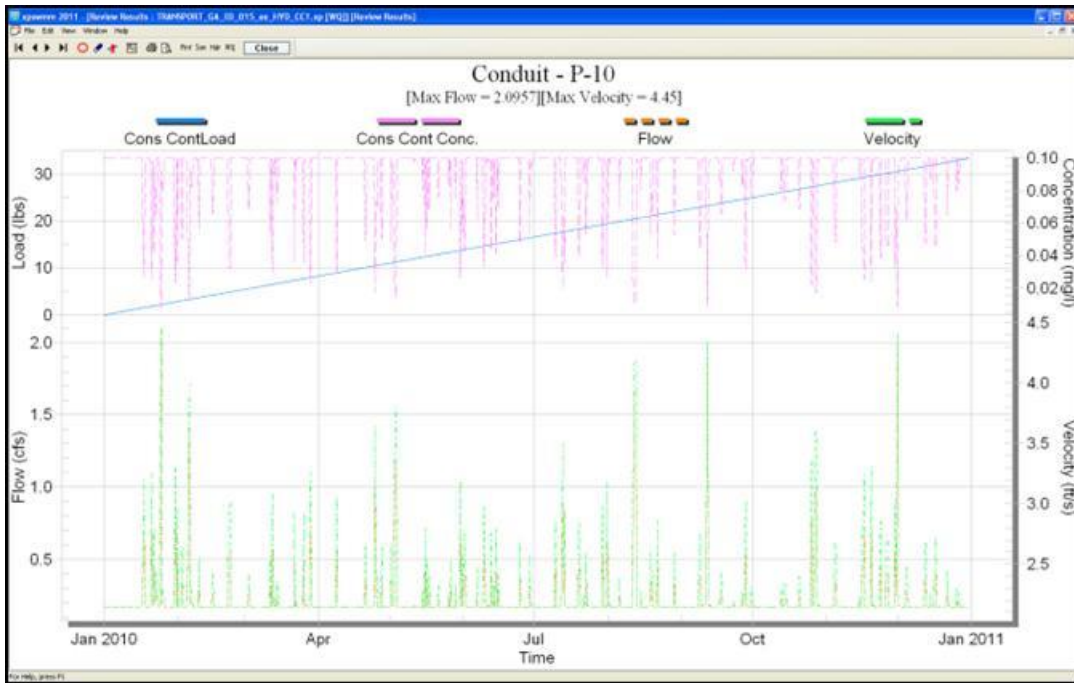


Figure 140. XPSWMM P-10 Pollutograph.

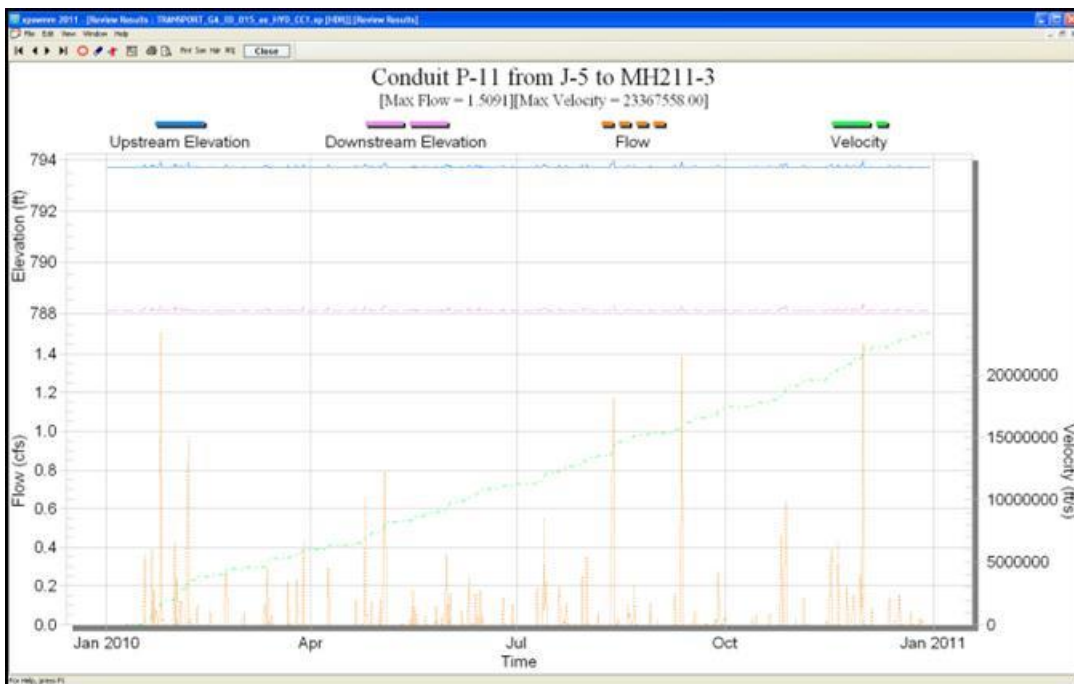


Figure 141. XPSWMM P-11 Hydrograph.

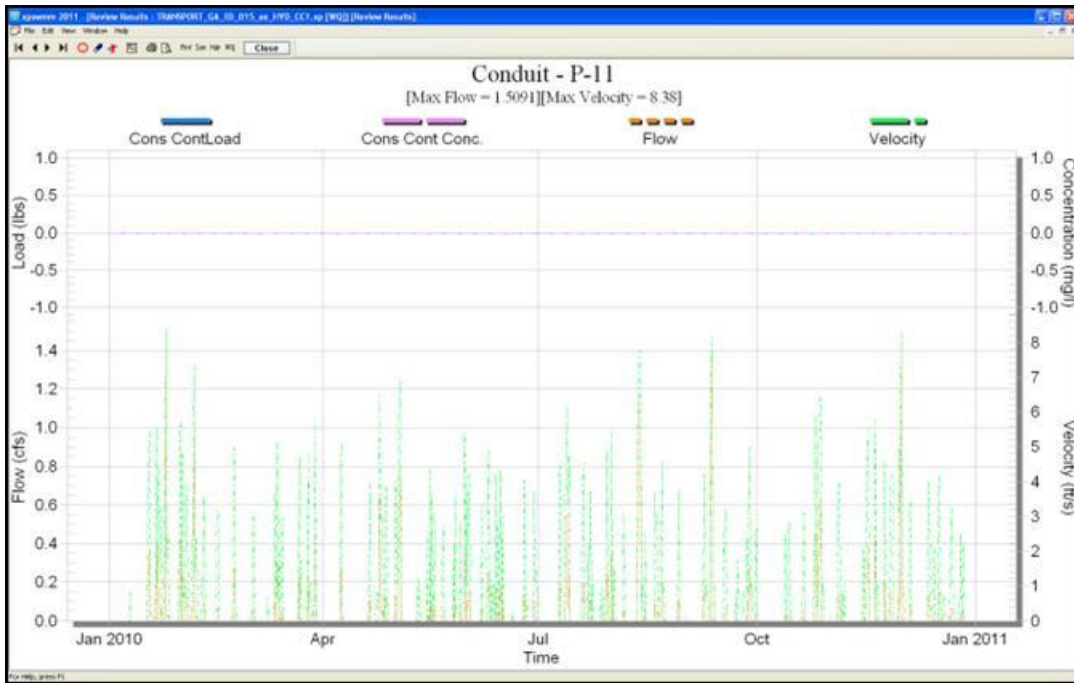


Figure 142. XPSWMM P-11 Pollutograph.

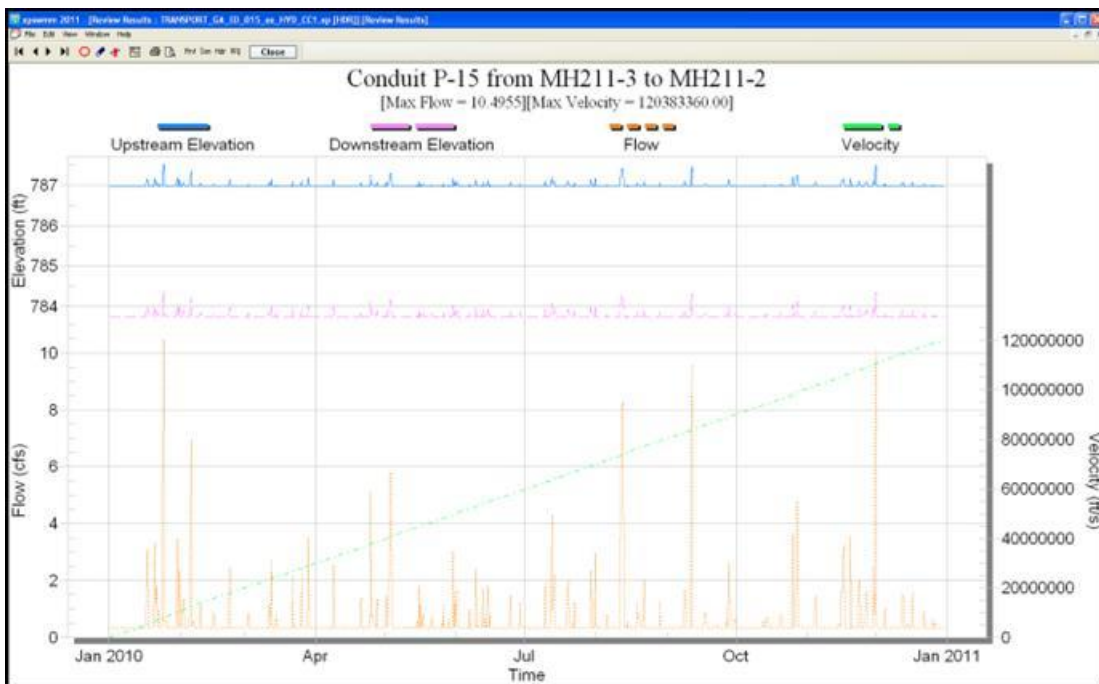


Figure 143. XPSWMM P-15 Hydrograph.

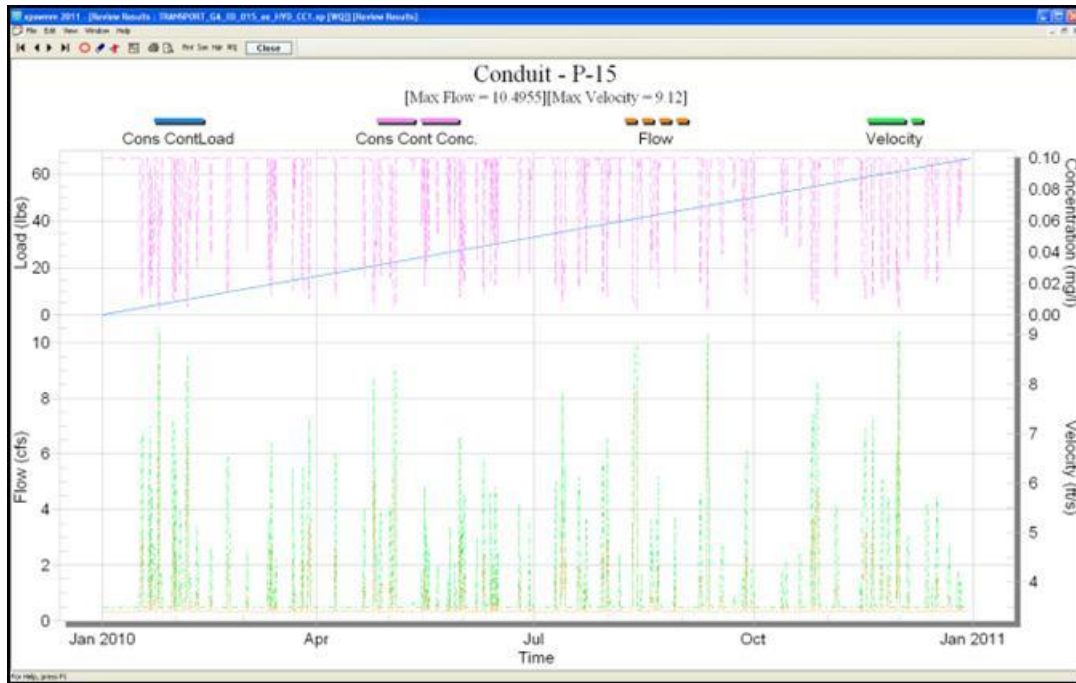


Figure 144. XPSWMM P-15 Pollutograph.

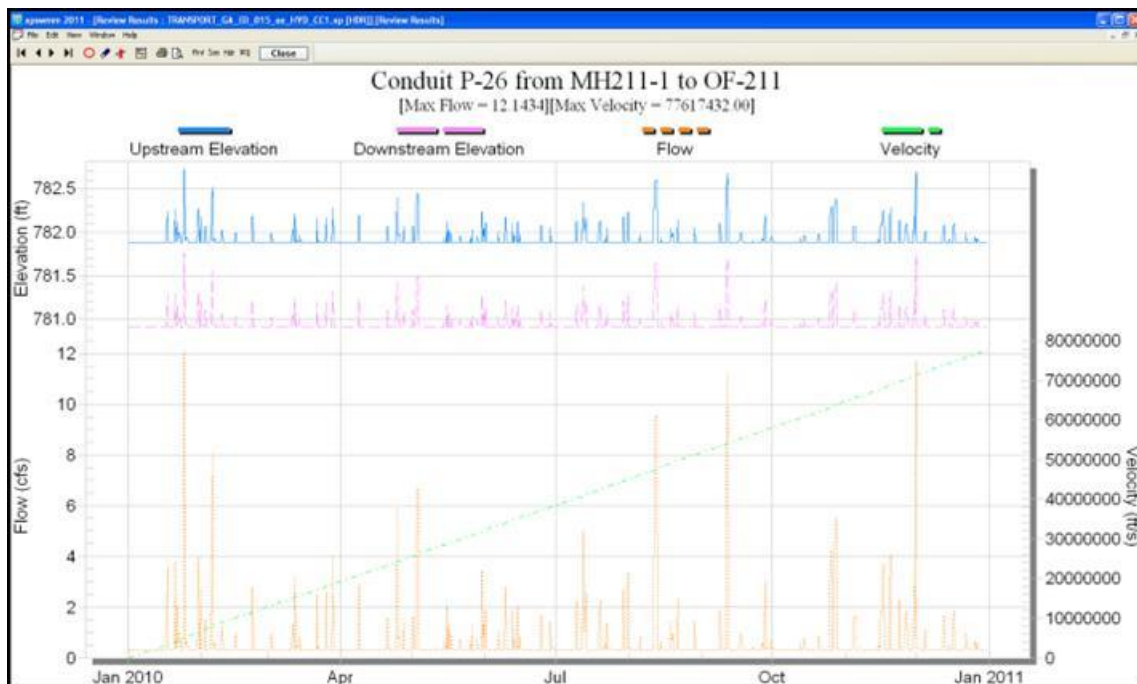


Figure 145. XPSWMM P-26 Hydrograph.

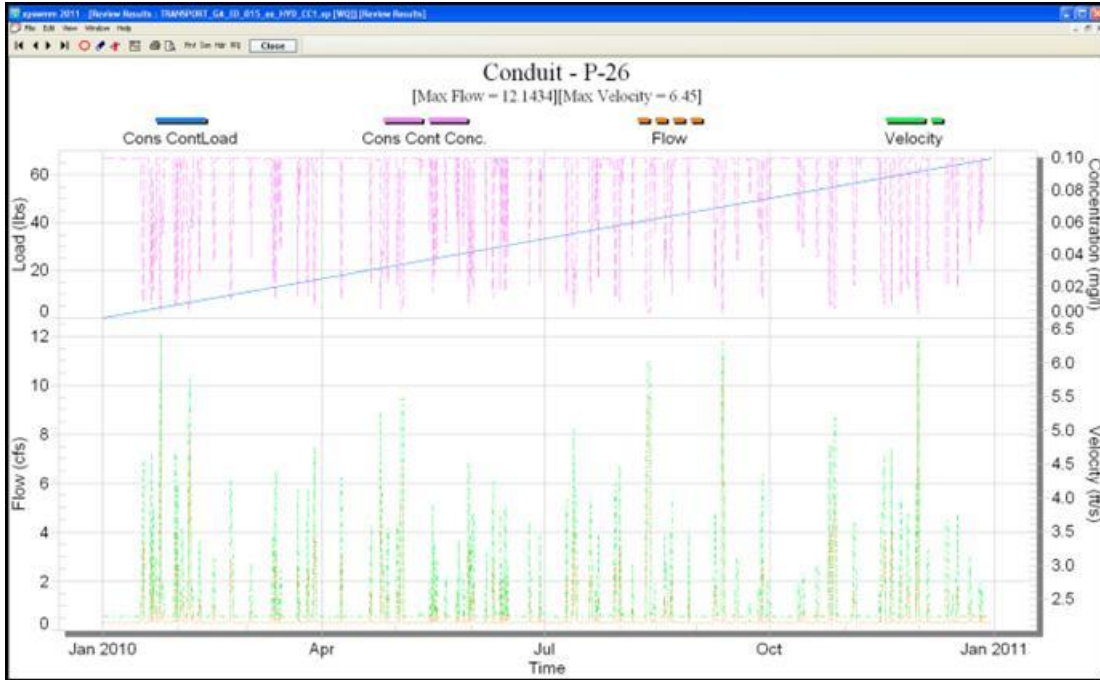


Figure 146. XPSWMM P-26 Pollutograph.

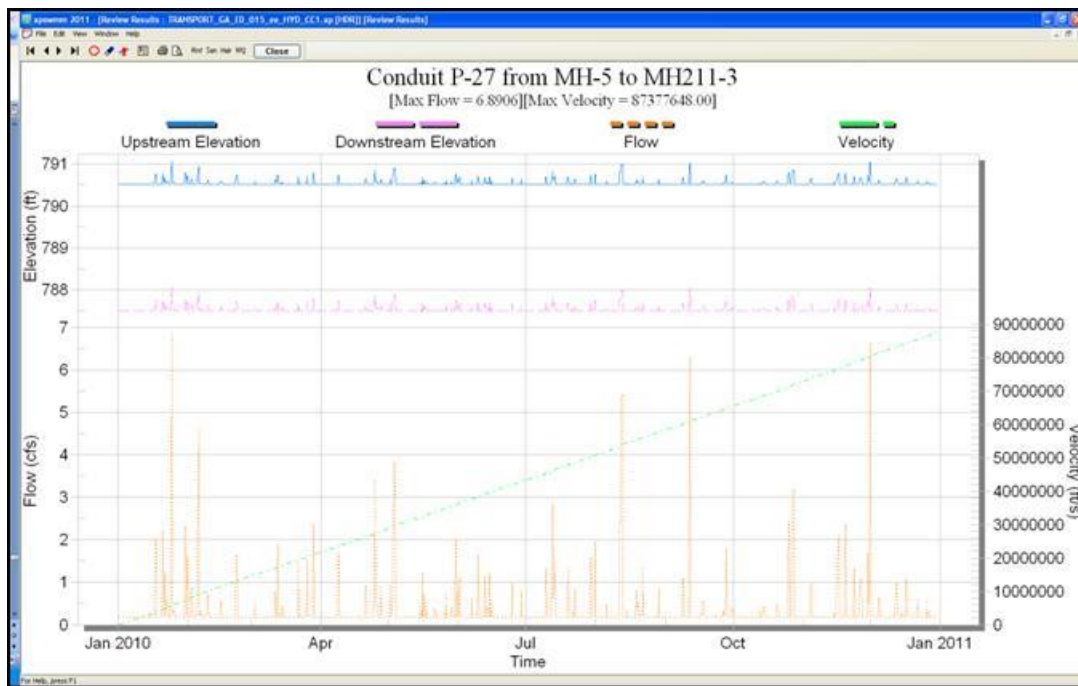


Figure 147. XPSWMM P-27 Hydrograph.

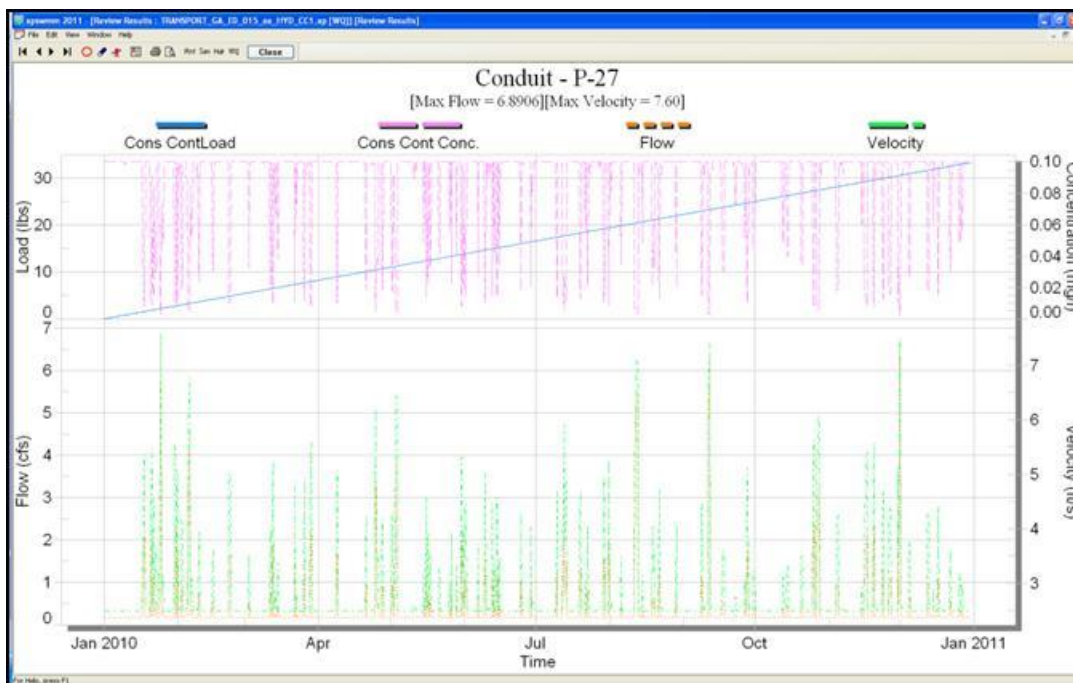


Figure 148. XPSWMM P-27 Pollutograph.

Transport Analysis Simulation 2 Results

Scenario 2 varies from Scenario 1 as steady timeseries is entered at the west and varied timeseries to the east. As expected, P-10 does not indicate a pollutant load and P-11, P-15, P-26, and P-27 do. Similar to Scenario 1, a constant concentration of 0.1 mg/L is entered into the system; the pollutograph indicates a maximum concentration of 0.1 mg/L. The concentration remains constant during the event except when runoff is encountered and then the concentration is decreased. Link P-27 spikes at the concentration of 0.63 mg/L at the beginning of the pollutograph, which responds to the varied timeseries (B) entered. The timeseries (B) ends at hour 24 with a concentration of 0.1 mg/L. The model holds the concentration constant at 0.1 mg/L throughout the remaining storm event except when runoff is encountered, then the concentration is decreased. A base flow rate of 0.17 cfs is represented in P-11 and a base flow rate of 0.13 cfs in P-27. P-15 and P-26 indicate a base flow of 0.1 cfs from the yearly rainfall and the additional flow rates entered into the system. The maximum flow rate within link P-26 is 12.1 cfs and the maximum elevation in node OF-211 is 781.8 ft, NAD. The cumulative load is estimated to be 26 lbs.

The following are the resulting hydrographs and pollutographs for simulation 2.

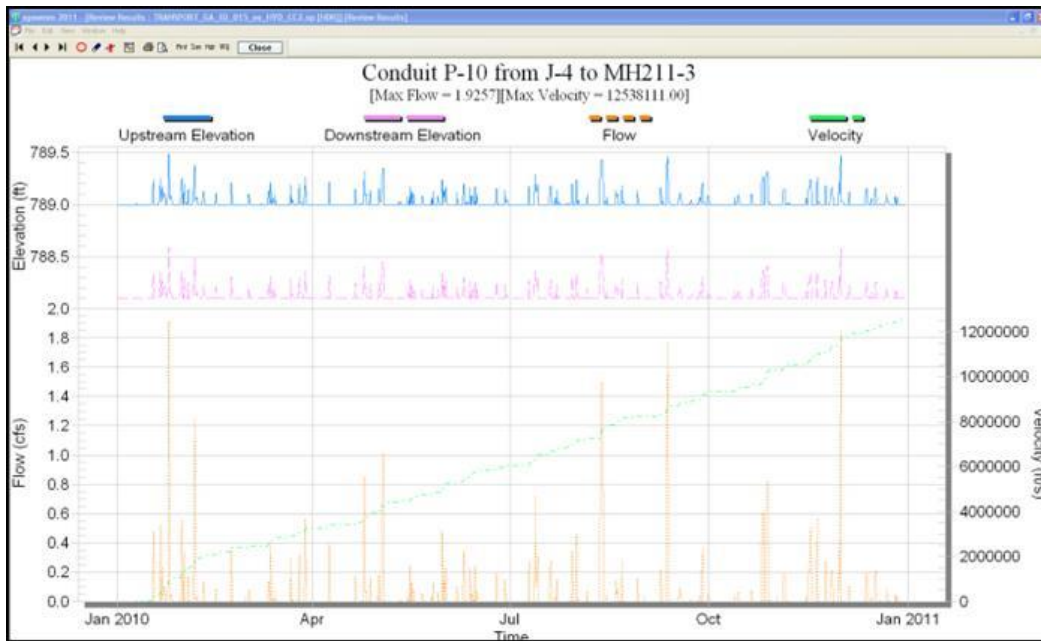


Figure 149. XPSWMM P-10 Hydrograph.

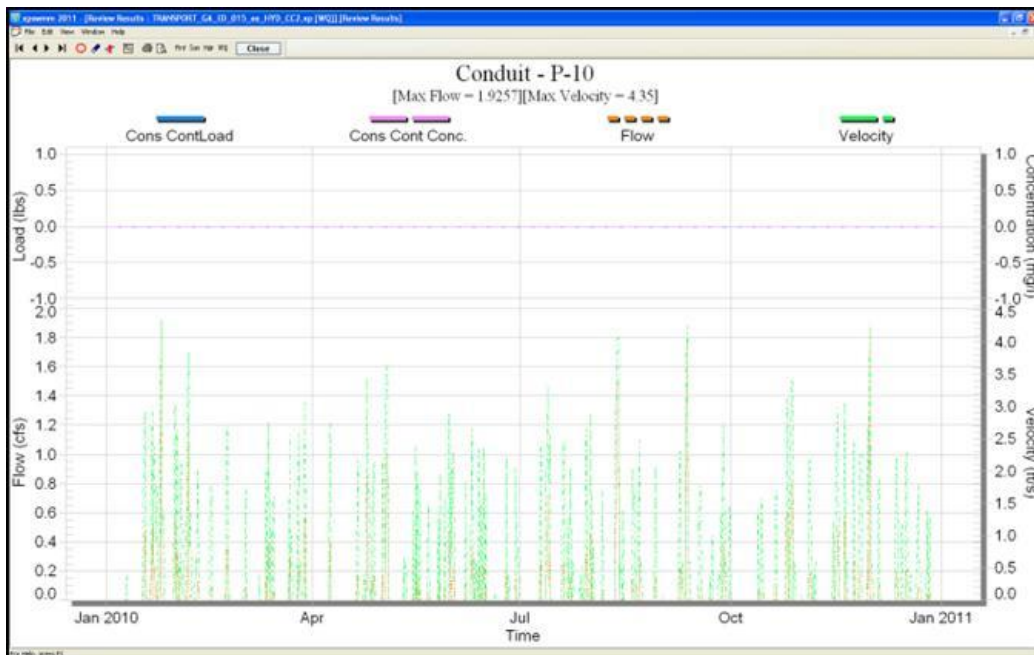


Figure 150. XPSWMM P-10 Pollutograph.



Figure 151. XPSWMM P-11 Hydrograph.

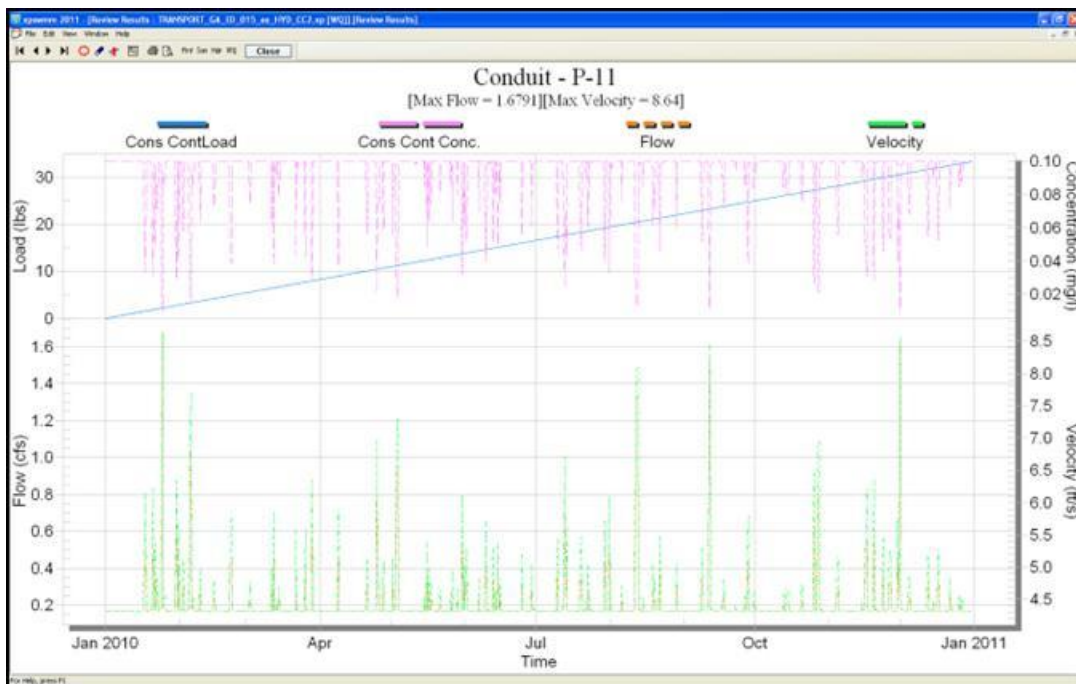


Figure 152. XPSWMM P-11 Pollutograph.

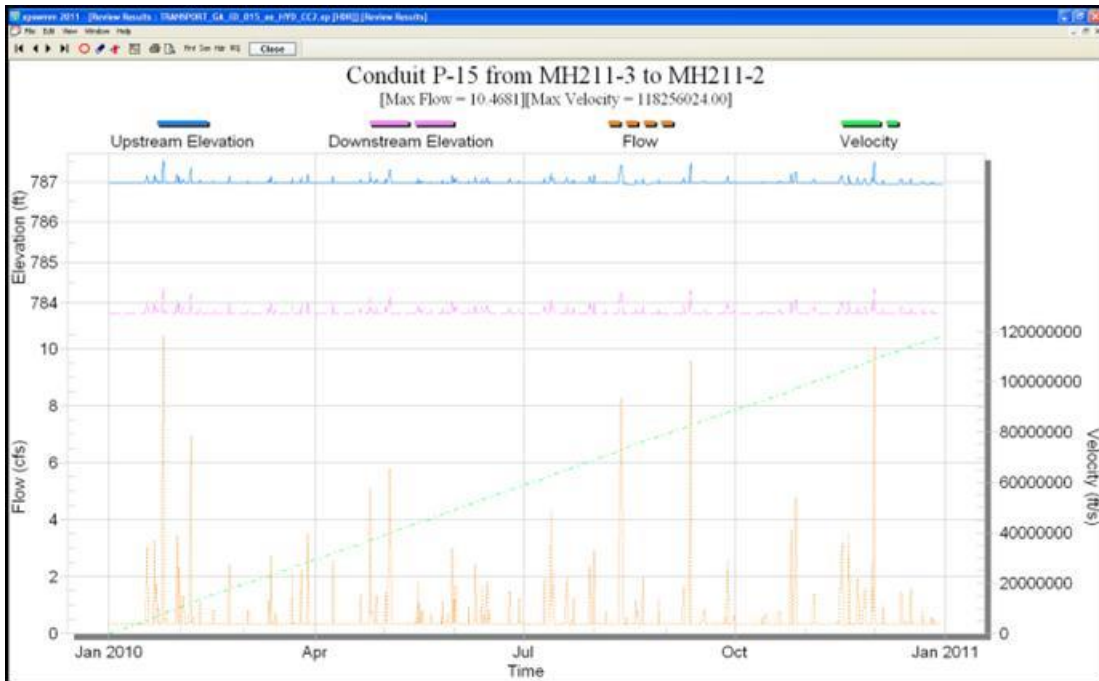


Figure 153. XPSWMM P-15 Hydrograph.

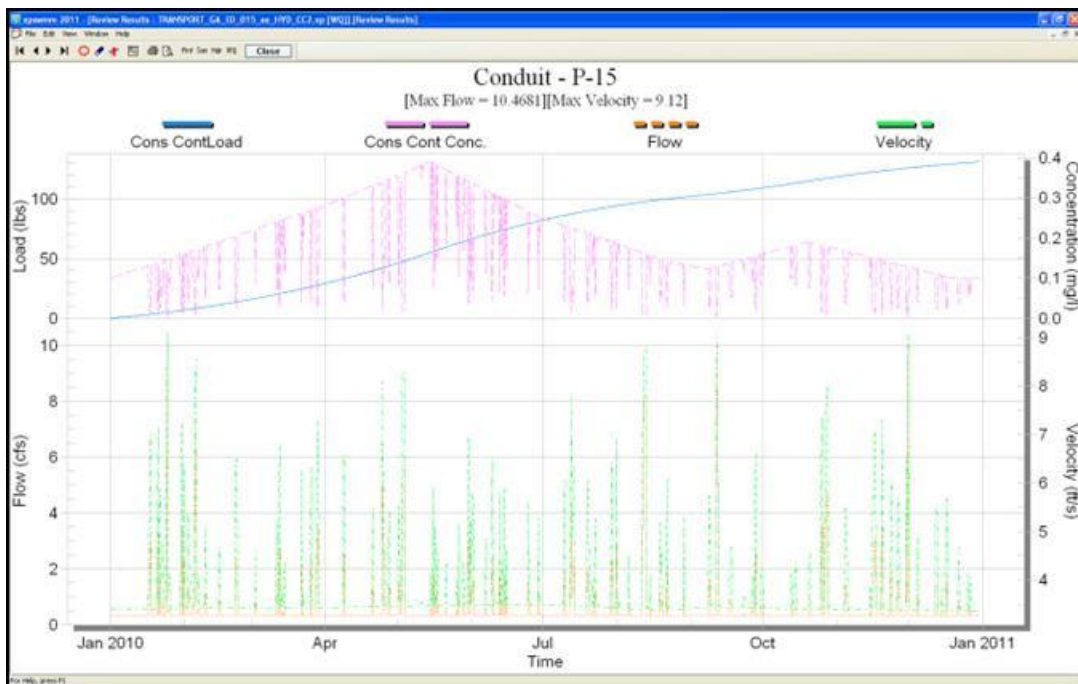


Figure 154. XPSWMM P-15 Hydrograph.

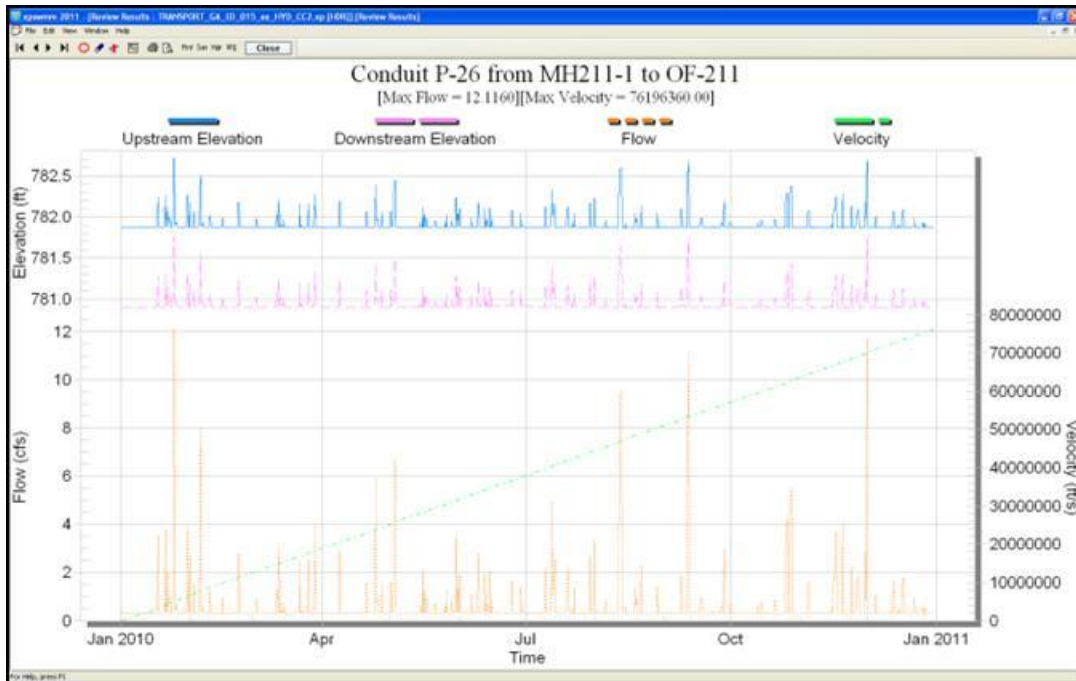


Figure 155. XPSWMM P-26 Hydrograph.

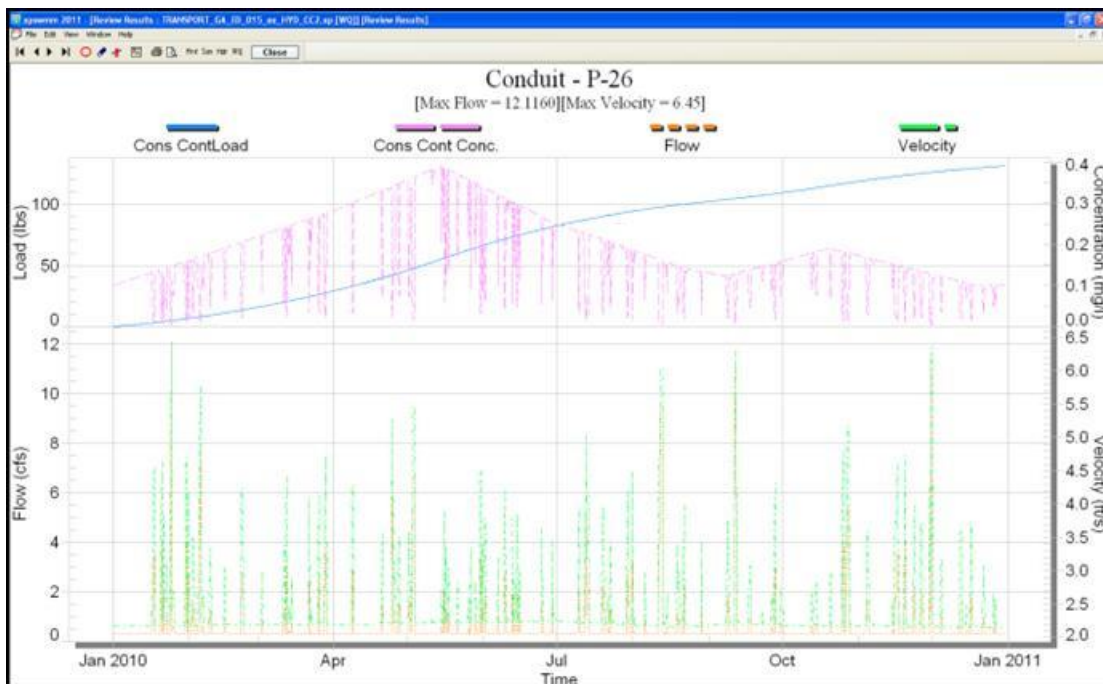


Figure 156. XPSWMM P-26 Pollutograph.

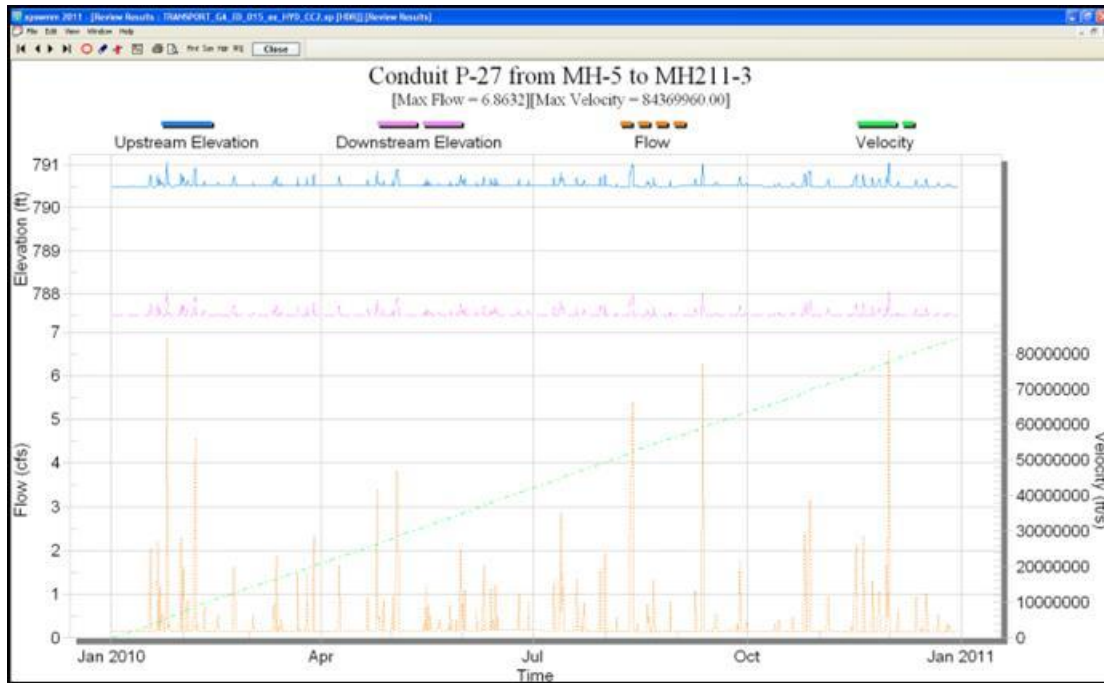


Figure 157. XPSWMM P-27 Hydrograph.

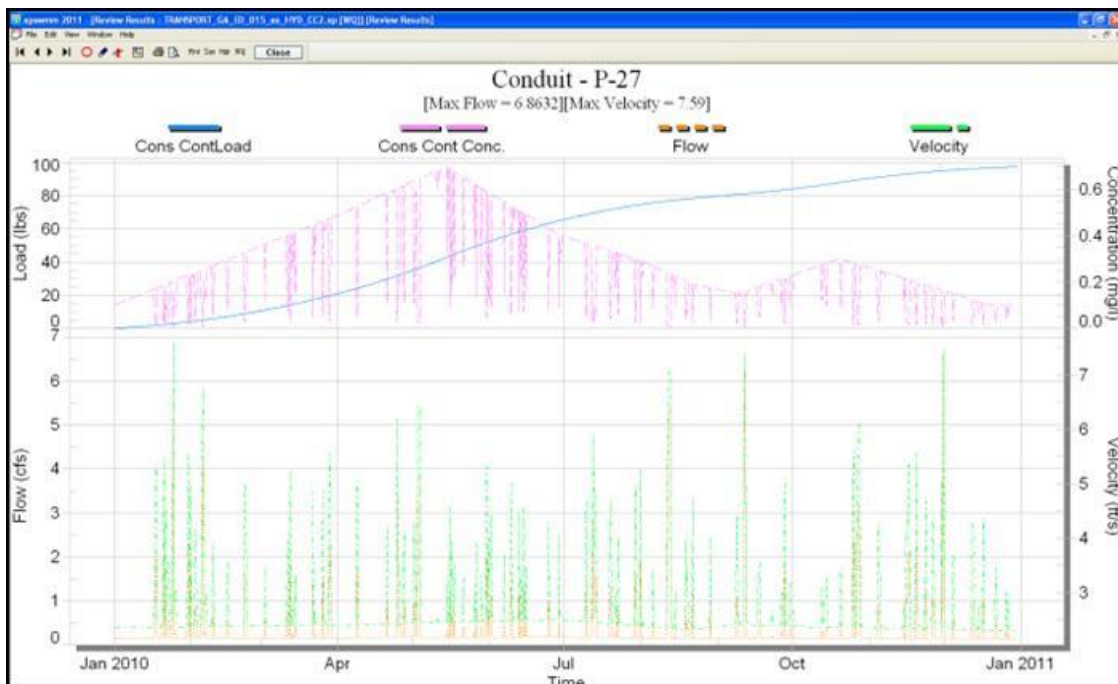


Figure 158. XPSWMM P-27 Pollutograph.

Transport Analysis Simulation 3 Results

Scenario 3 is focused on the system to the west and south of MH211-3. Link P-27 represents the combination of the two varied timeseries (B) and (C) in I-11 and I-10. Links P-15, P-26, and P-27 indicate a base flow of 0.27 cfs and a base pollutant of 0.1 mg/L from the two. The flow rate within the links increases as runoff enters the system and the concentration decreases as expected. The maximum flow rate within link P-26 is 12.1 cfs and the maximum elevation in node OF-211 is 781.8 ft, NAD. The cumulative load is estimated to be 50 mg/L. The following are the resulting hydrographs and pollutographs for simulation 3.

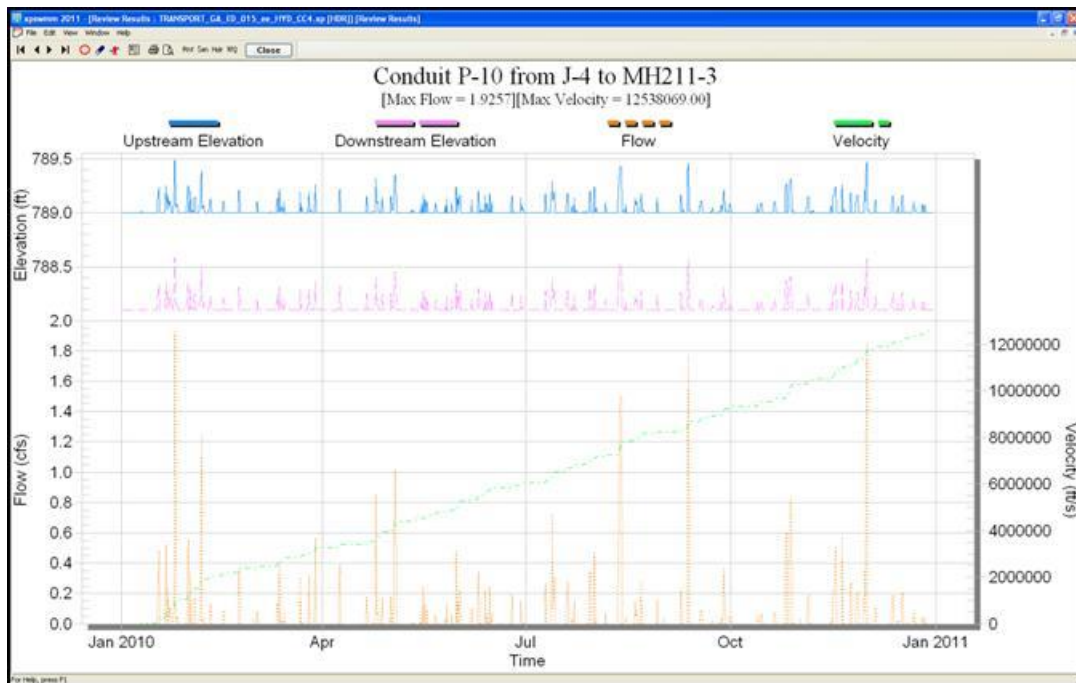


Figure 159. XPSWMM P-10 Hydrograph.

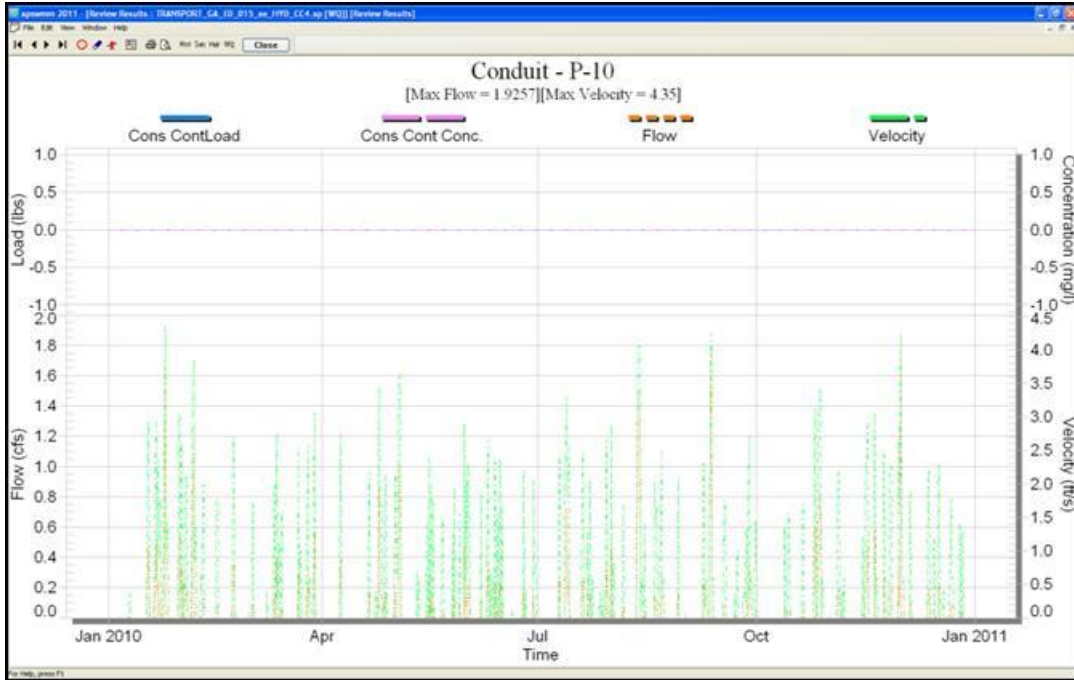


Figure 160. XPSWMM P-10 Pollutograph.

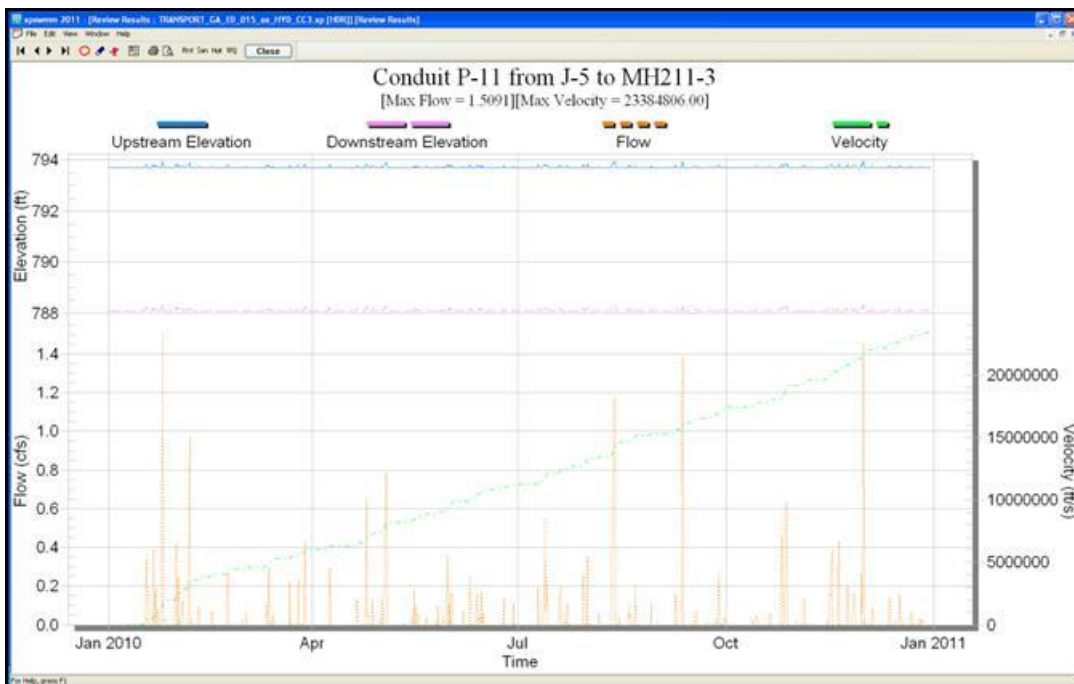


Figure 161. XPSWMM P-11 Hydrograph.

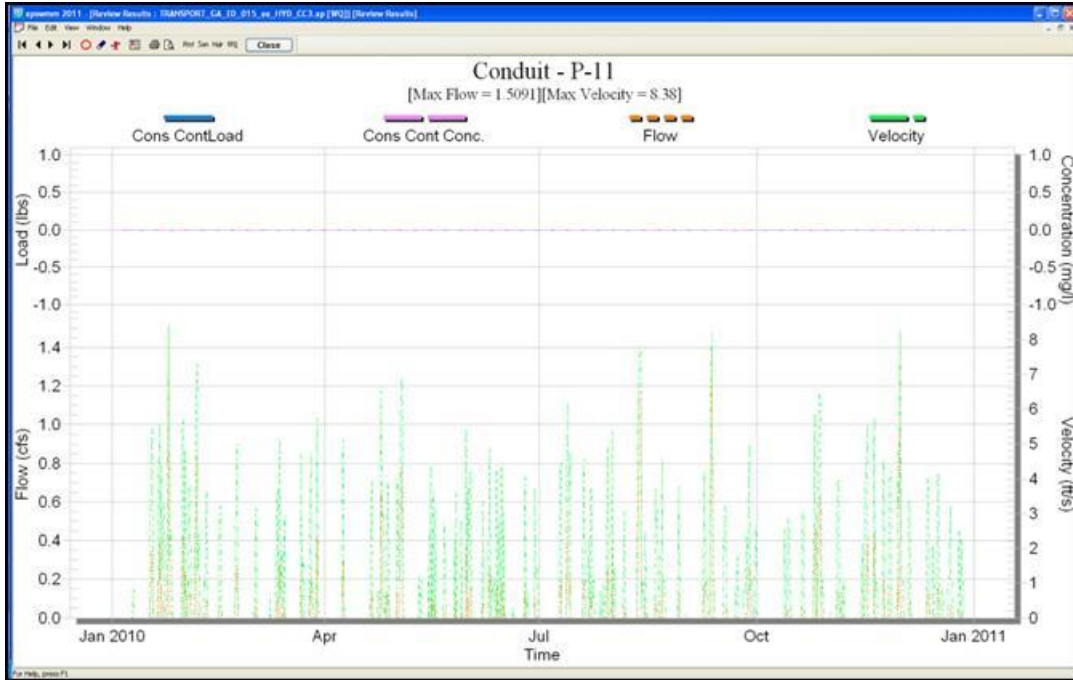


Figure 162. XPSWMM P-11 Pollutograph.

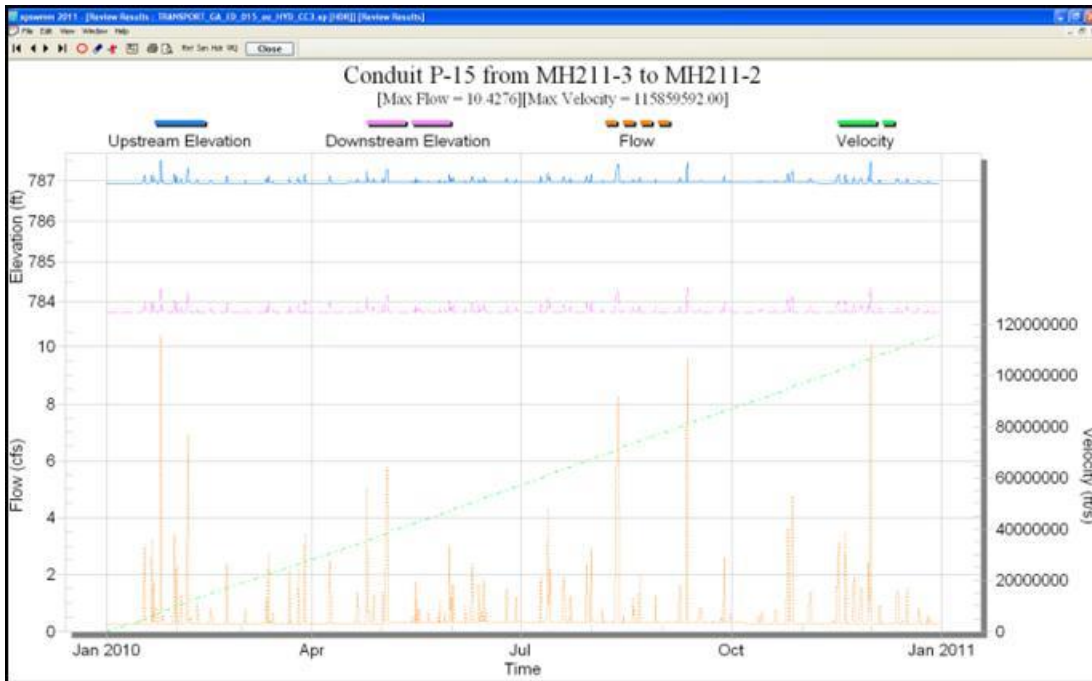


Figure 163. XPSWMM P-15 Hydrograph.

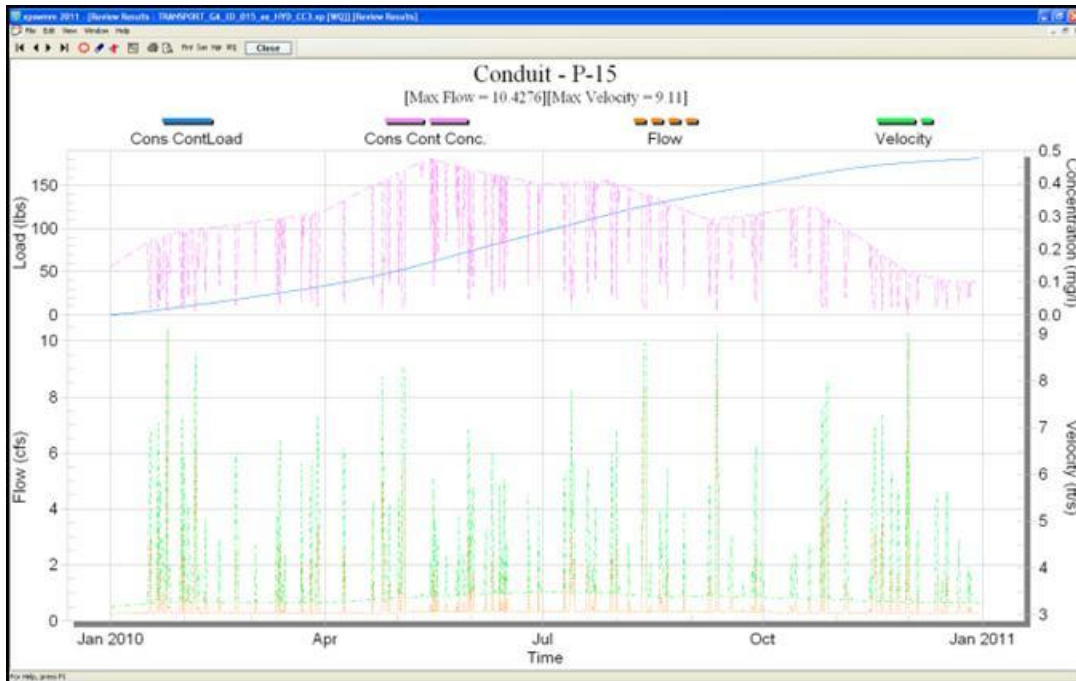


Figure 164. XPSWMM P-15 Pollutograph.

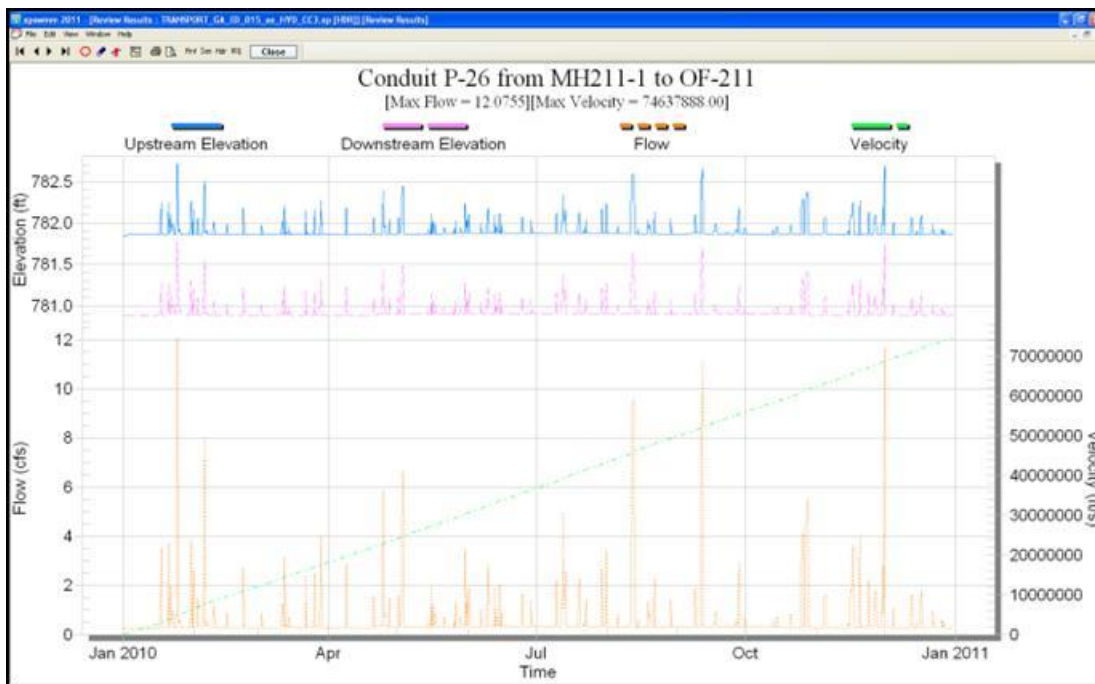


Figure 165. XPSWMM P-26 Hydrograph.

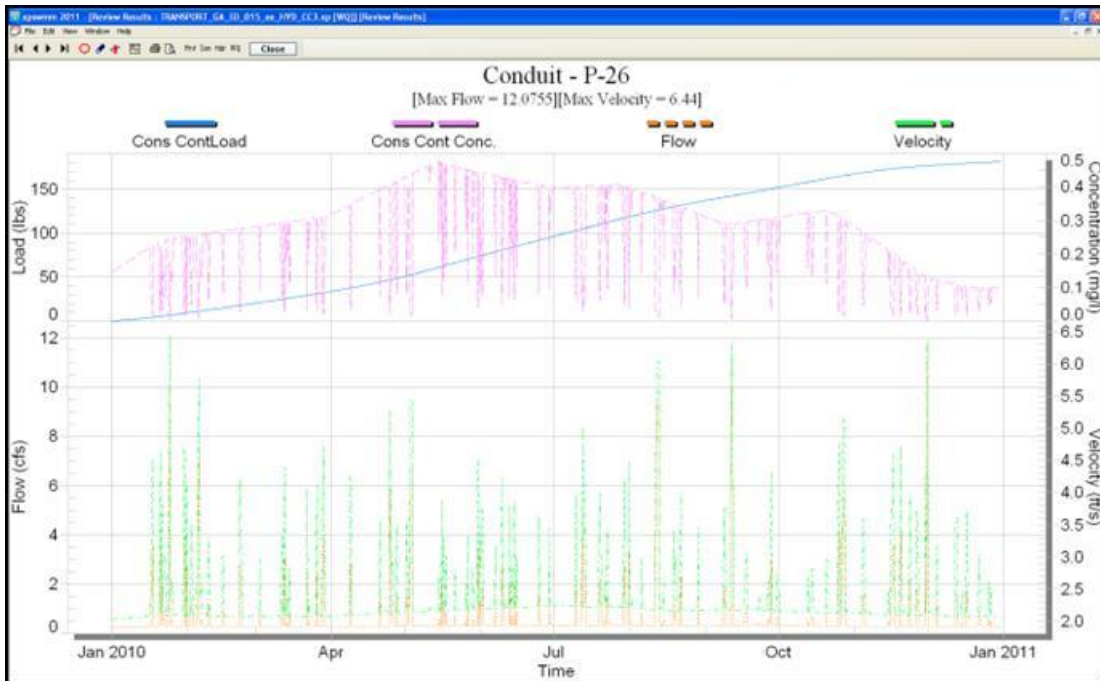


Figure 166. XPSWMM P-26 Pollutograph.

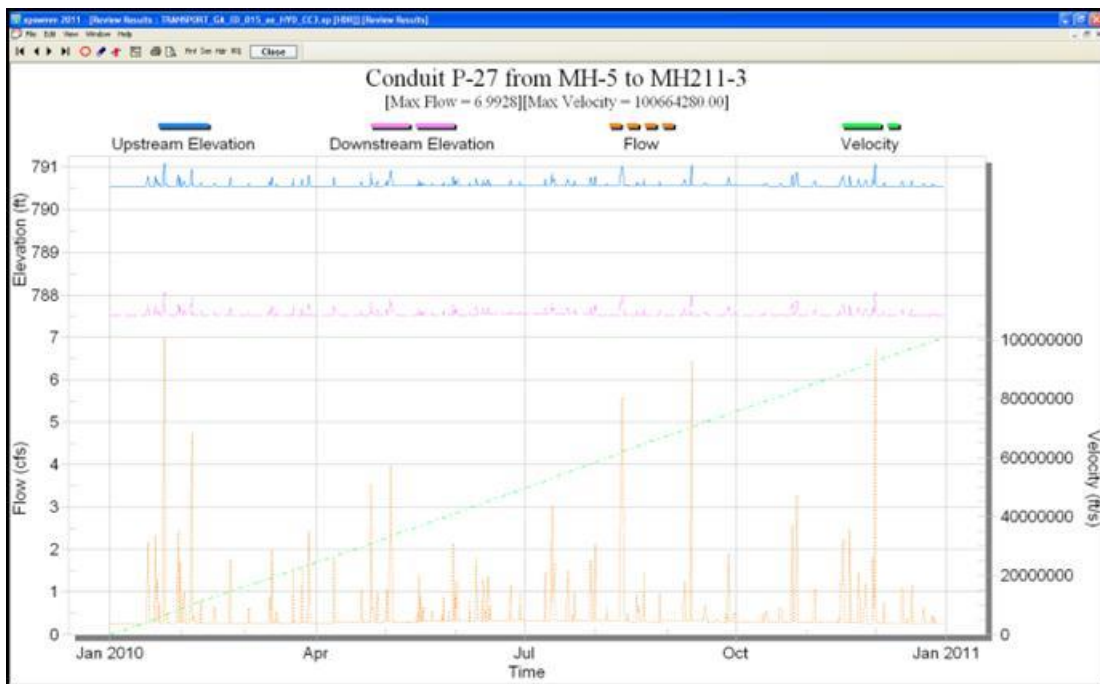


Figure 167. XPSWMM P-27 Hydrograph.

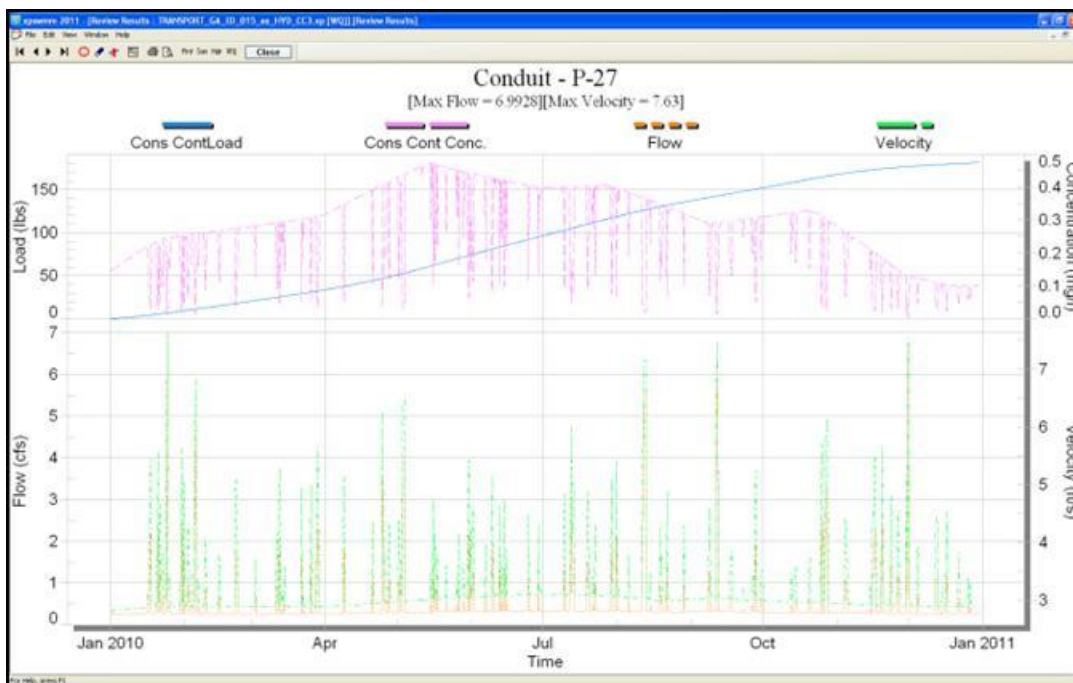


Figure 168. XPSWMM P-27 Pollutograph.

Transport Analysis Simulation 4 Results

Similar to simulation 3, simulation 4 introduces varied timeseries in two different locations and P-27 represents the combination of the two. A 0.14 cfs base flow and a 0.1 mg/L pollutant base concentration are indicated in links P-27 and P-15. Link P-26 estimates a base flow rate of 0.27 cfs and a 0.172 mg/L base pollutant concentration throughout the event. The maximum flow rate within link P-26 is 12.1 cfs and the maximum elevation in node OF-211 is 781.8 ft, NAD. The cumulative pollutant load for the year is estimated at 90 lbs. The following are the resulting hydrographs and pollutographs for simulation 4.

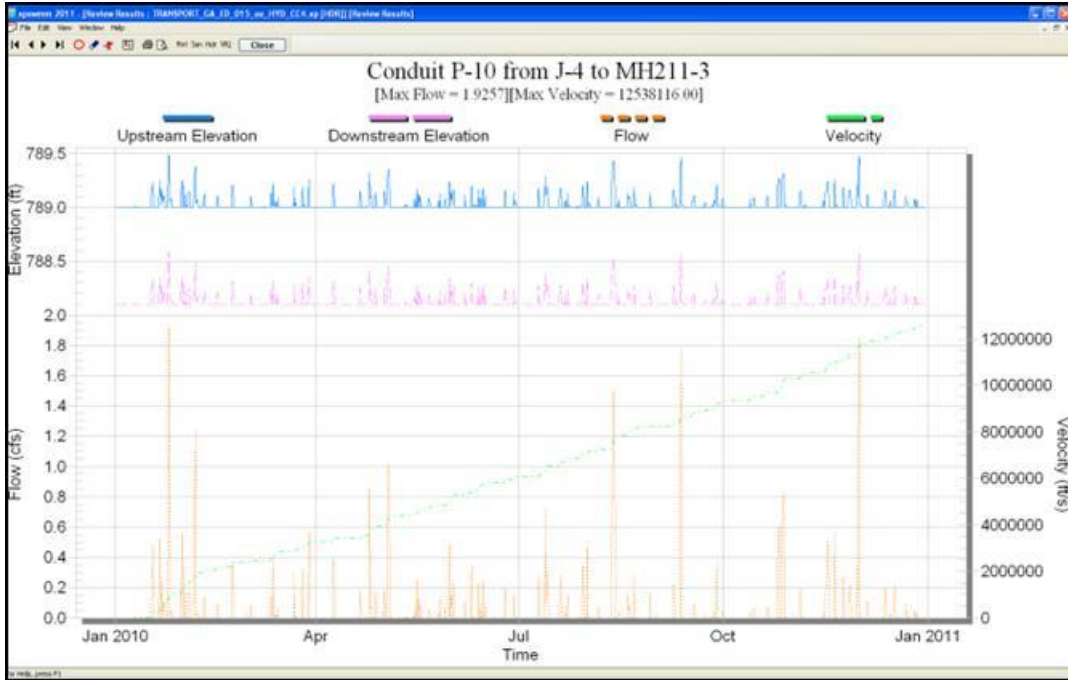


Figure 169. XPSWMM P-10 Hydrograph.

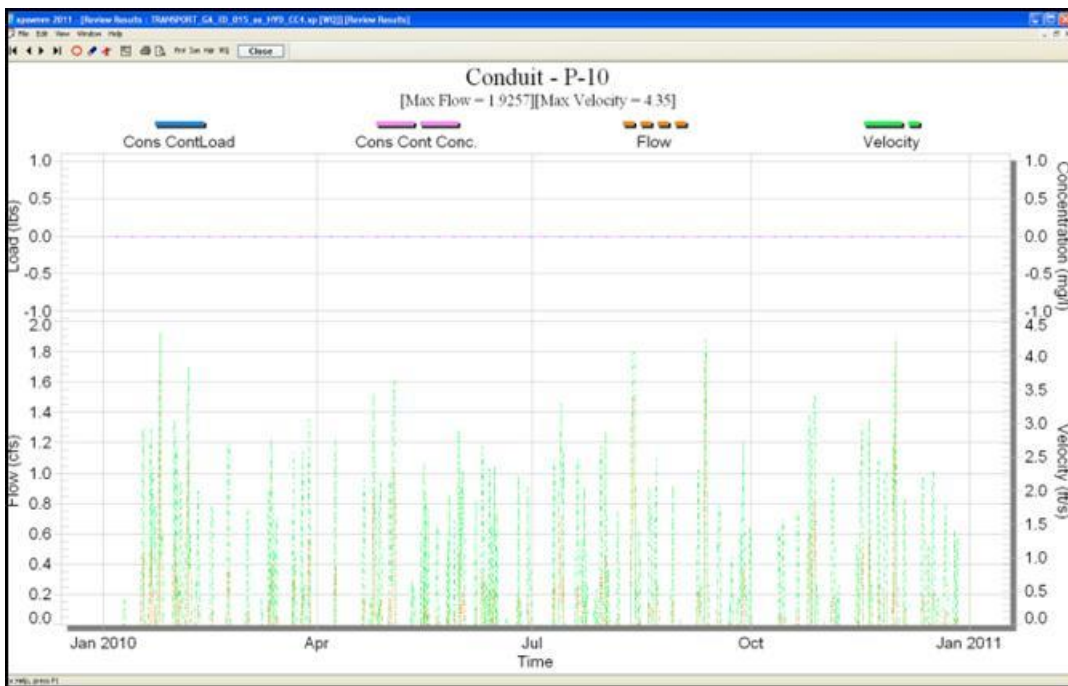


Figure 170. XPSWMM P-10 Pollutograph.

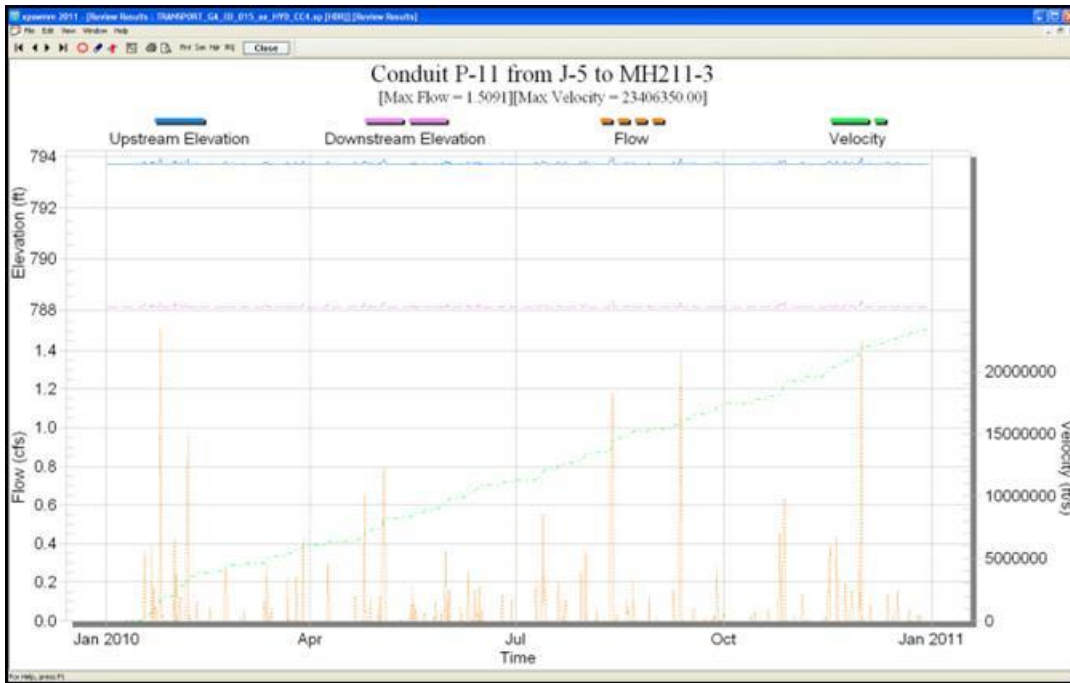


Figure 171. XPSWMM P-11 Hydrograph.

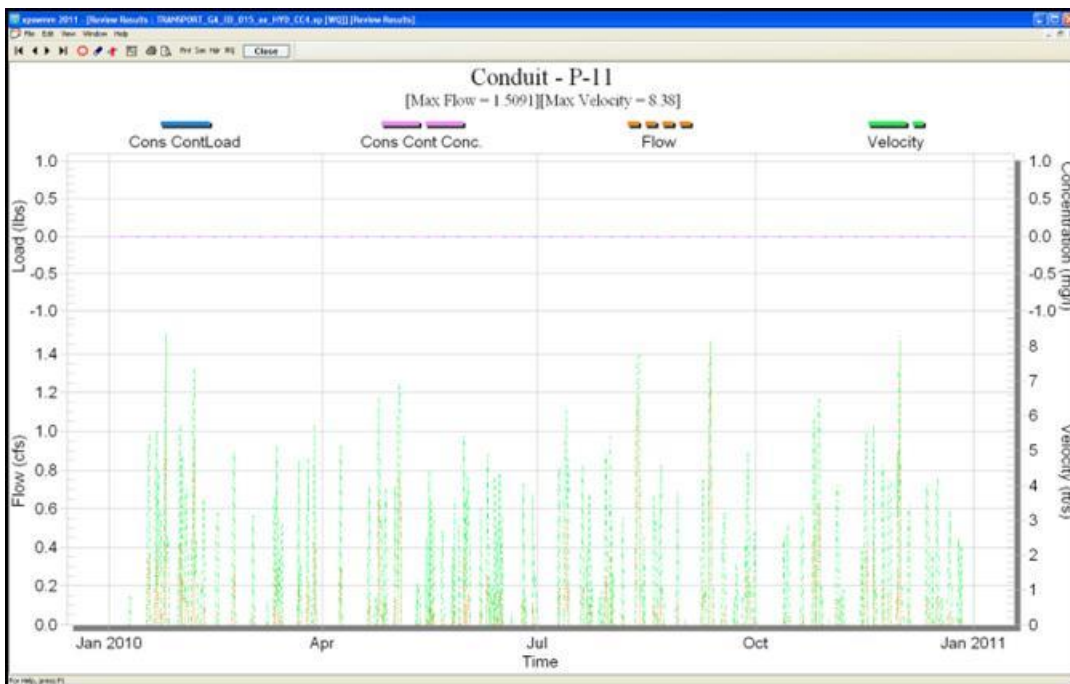


Figure 172. XPSWMM P-11 Pollutograph.

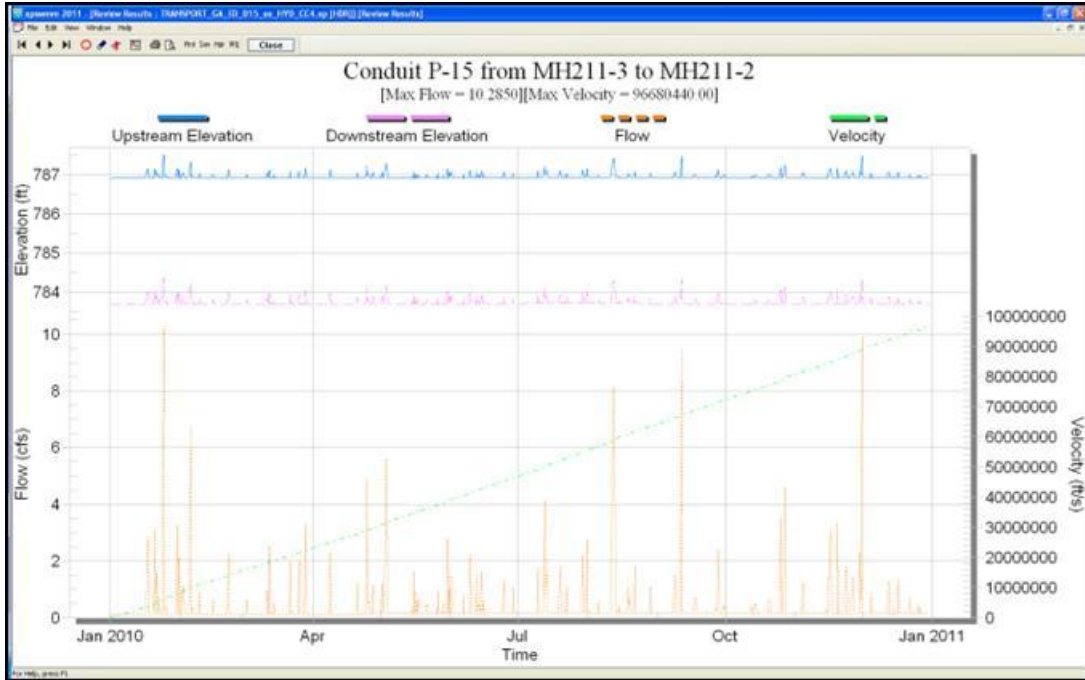


Figure 173. XPSWMM P-15 Hydrograph.

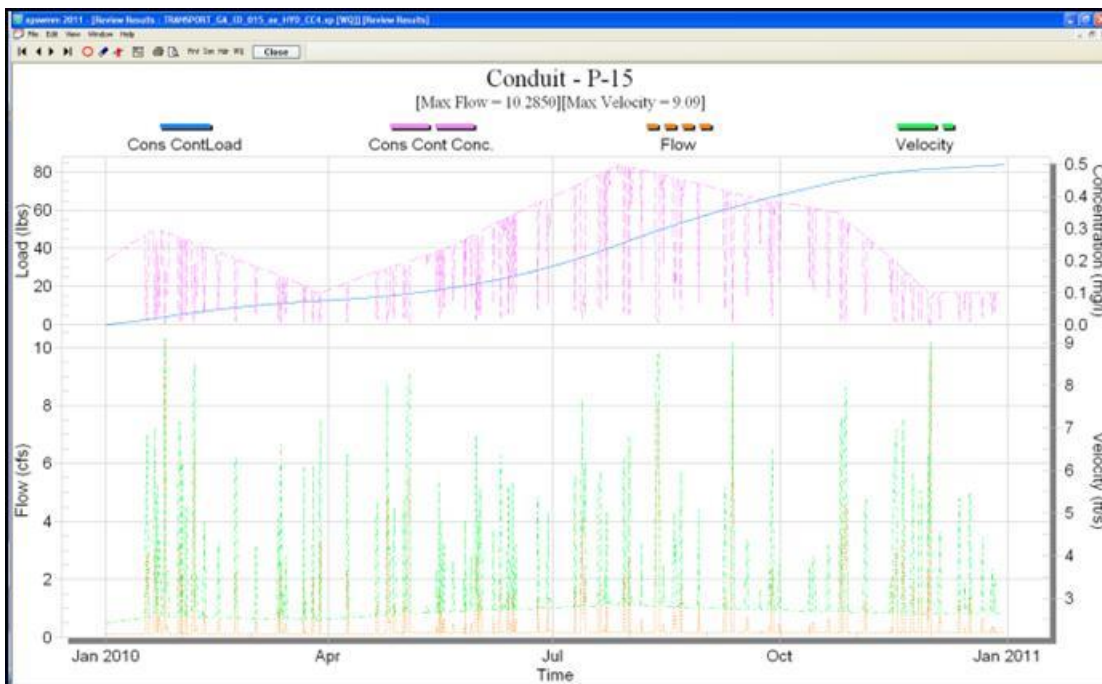


Figure 174. XPSWMM P-15 Pollutograph.

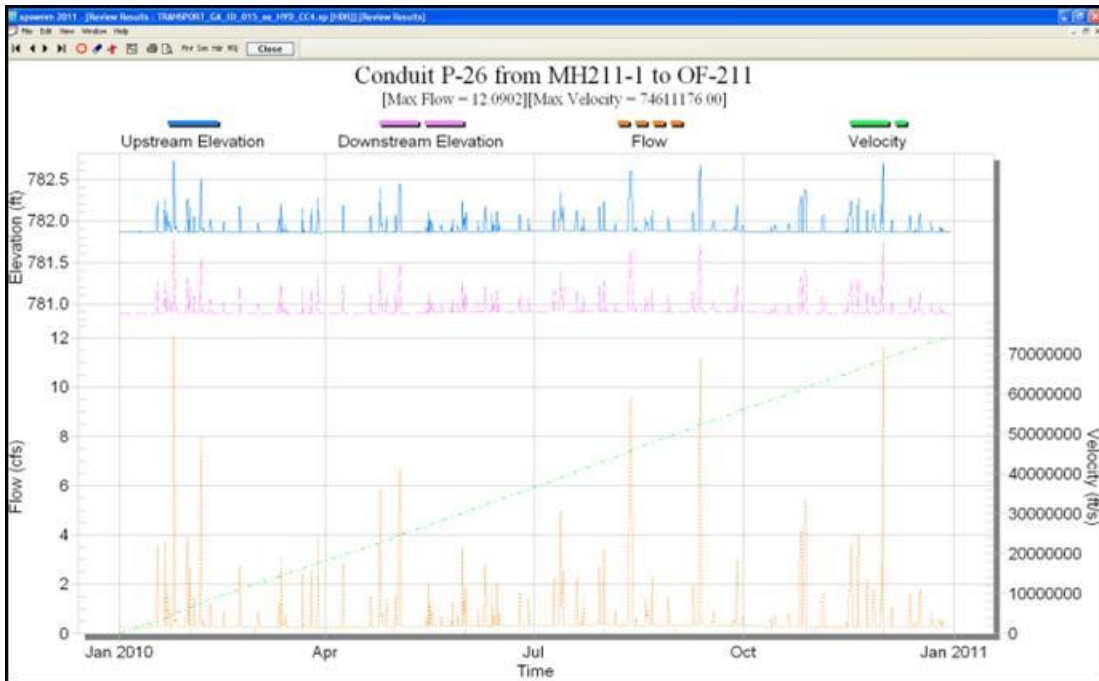


Figure 175. XPSWMM P-26 Hydrograph.

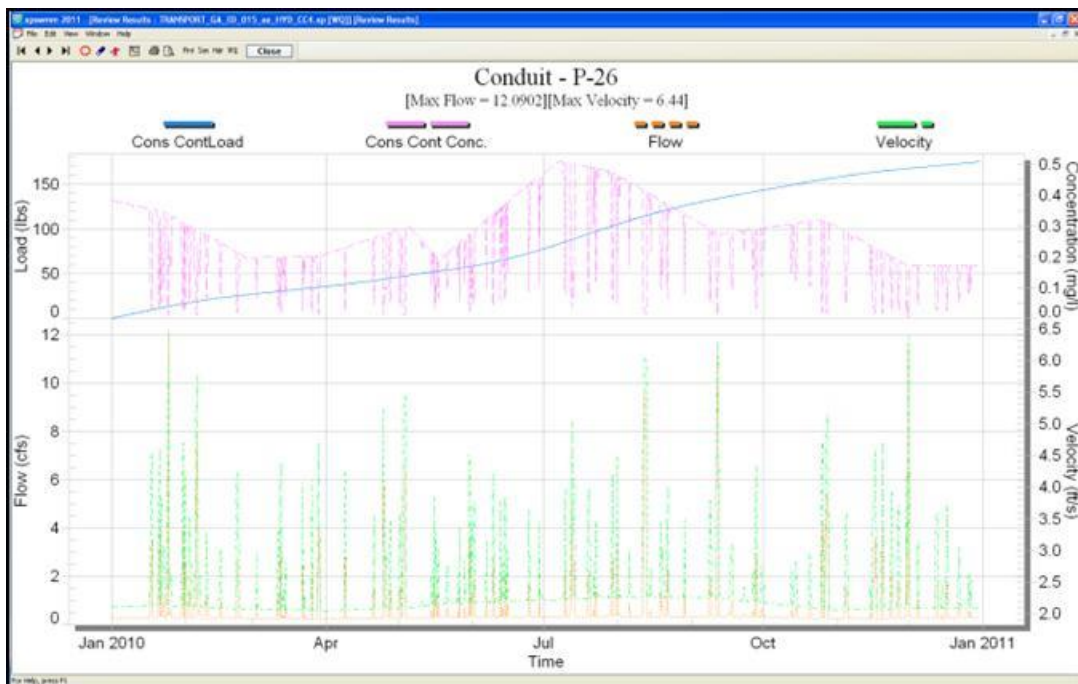


Figure 176. XPSWMM P-26 Pollutograph.

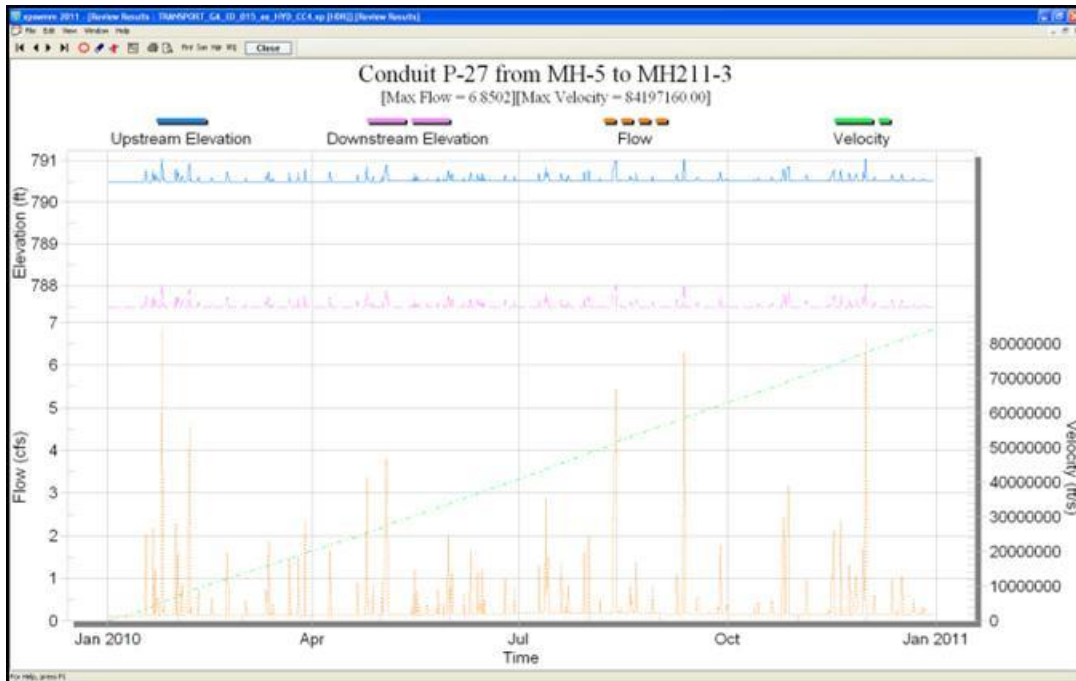


Figure 177. XPSWMM P-27 Hydrograph.

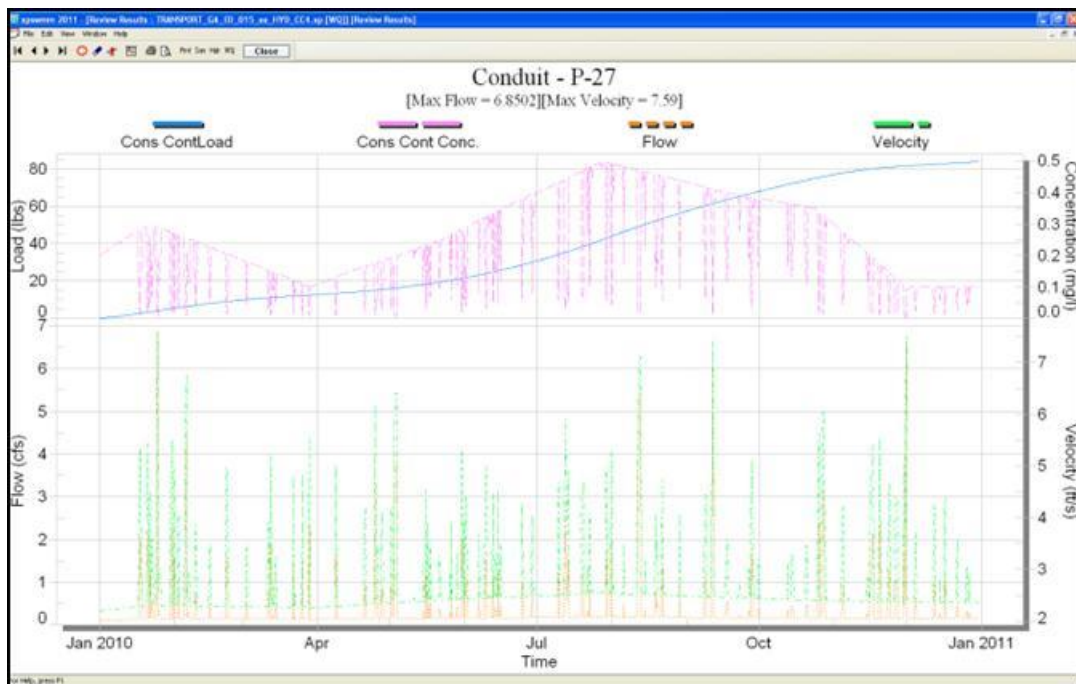


Figure 178. XPSWMM P-27 Pollutograph.

Transport Analysis - Probability of Exceedance Results

The following figures are hydrographs representing all four scenarios and to the right are their probability of exceedance curves. P-10 and P-11 show a larger variance in PE compared to the other links. These are minor changes in flow rate due to the introduction of base flow.

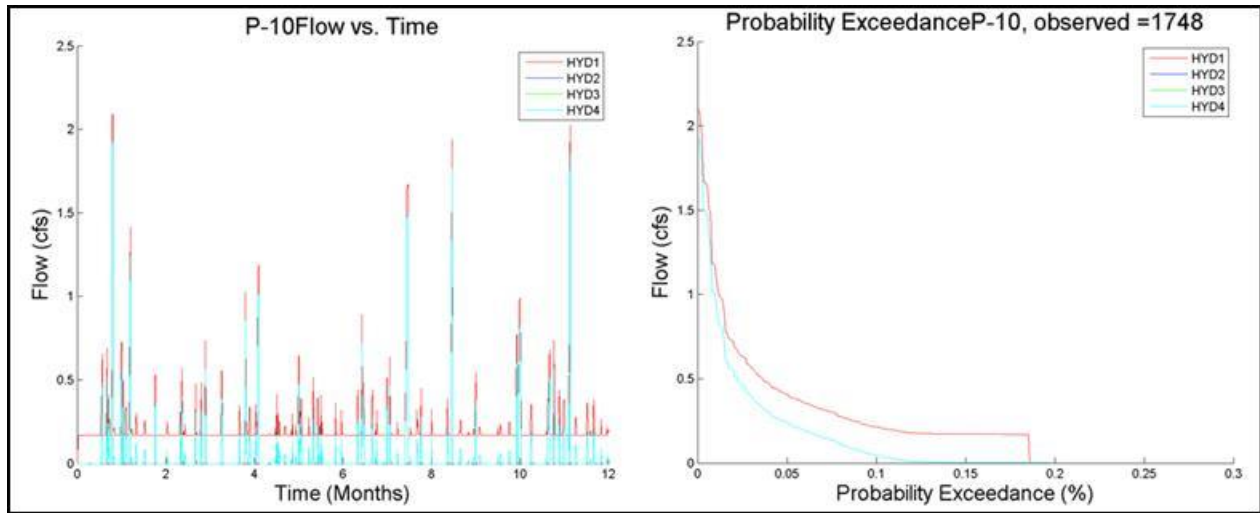


Figure 179. P-10 Hydrographs Indicating Simulations 1-4 and their PE Curves.

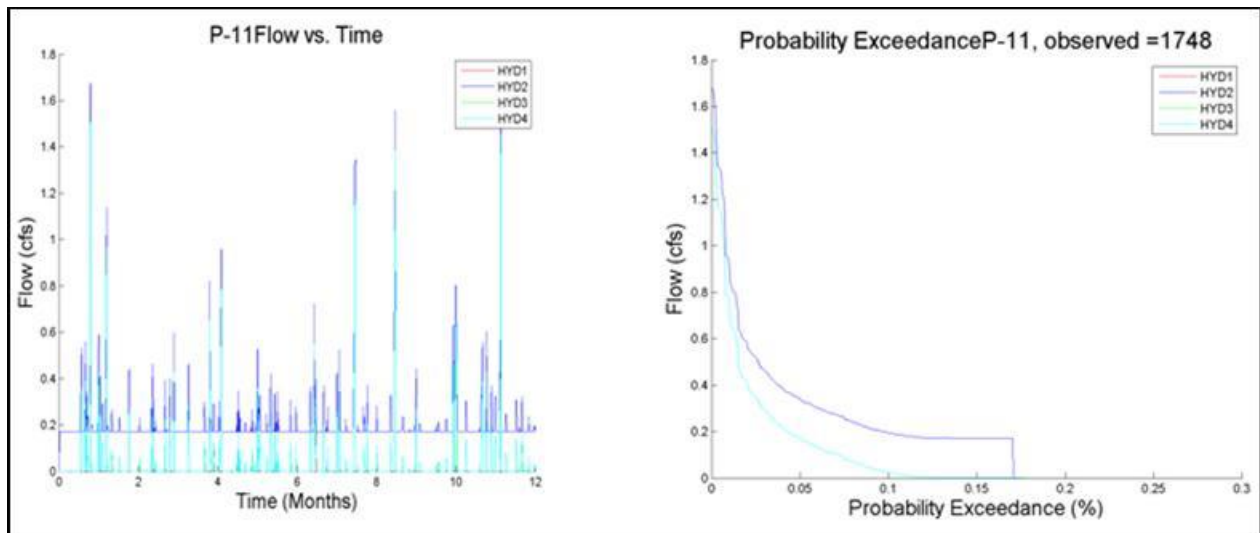


Figure 180. P-11 Hydrographs Indicating Simulations 1-4 and their PE Curves.

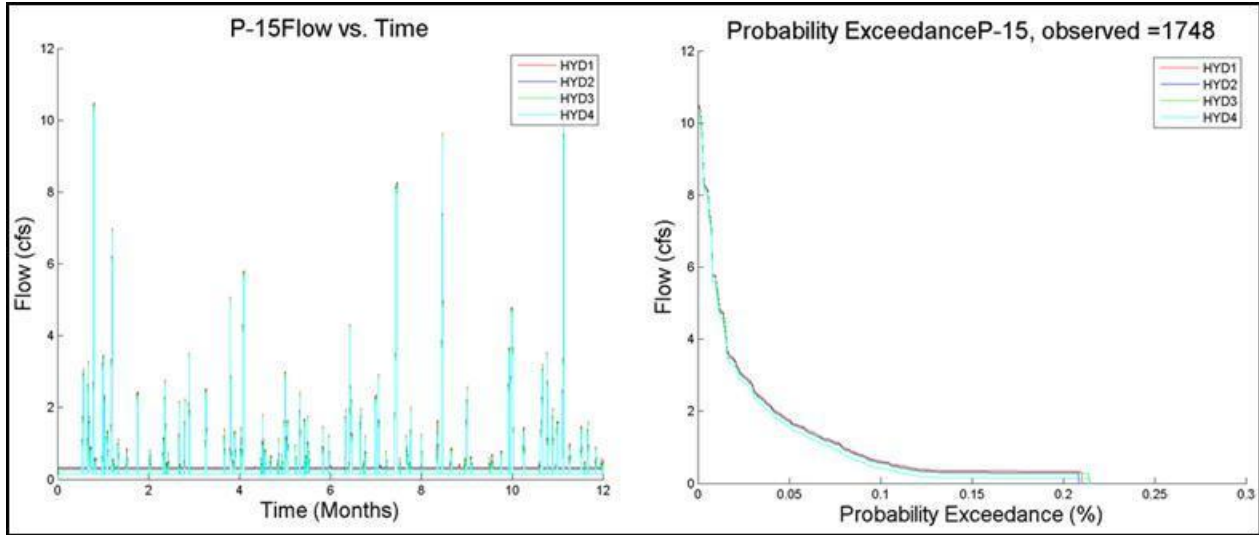


Figure 181. P-15 Hydrographs Indicating Simulations 1-4 and their PE Curves.

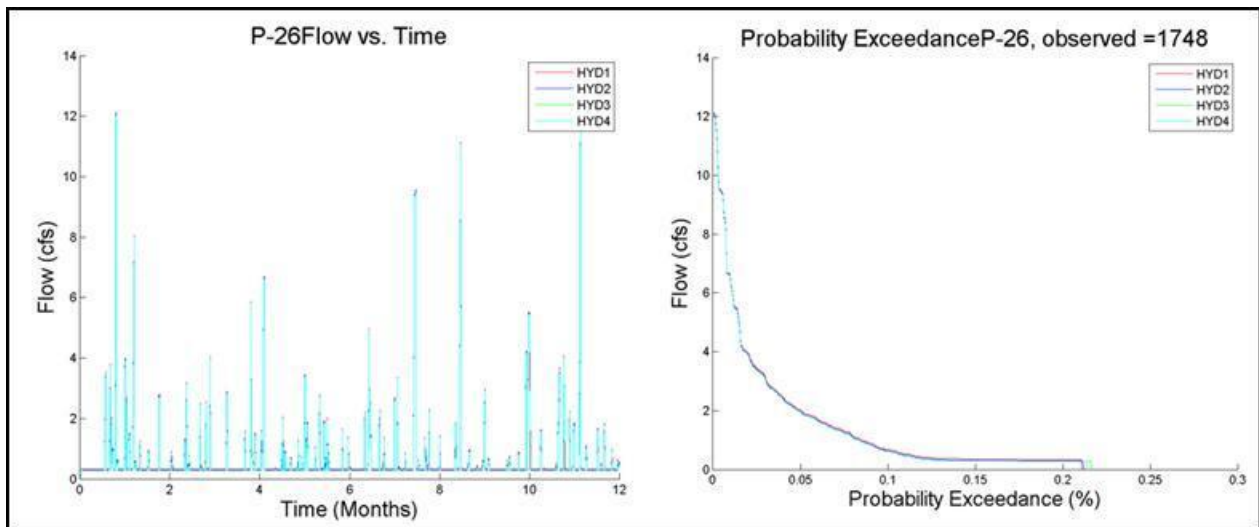


Figure 182. P-26 Hydrographs Indicating Simulations 1-4 and their PE Curves.

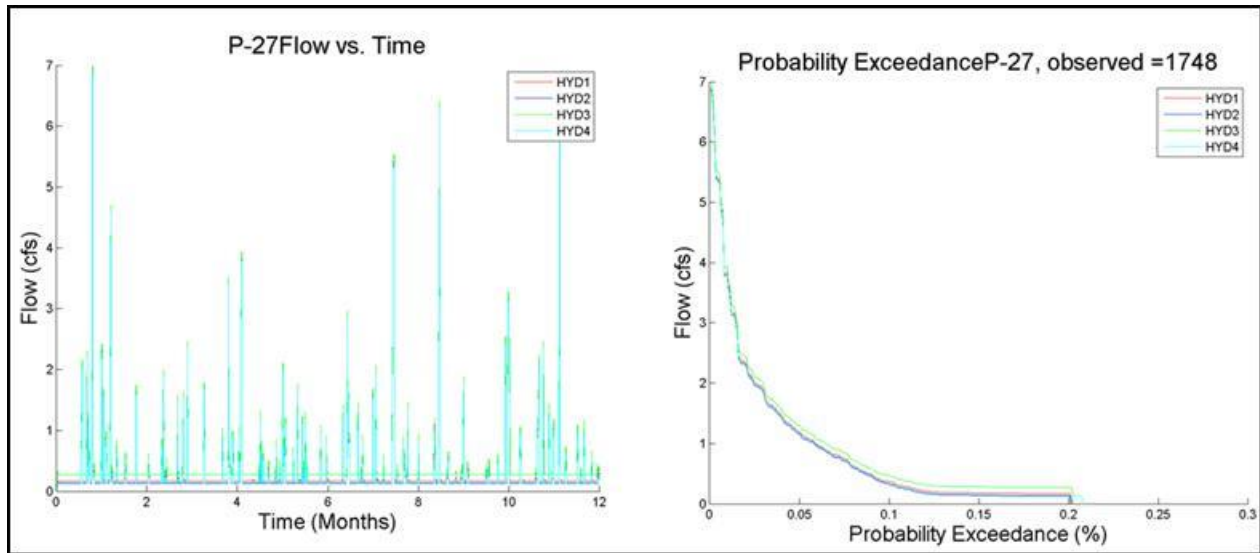


Figure 183. P-27 Hydrographs Indicating Simulations 1-4 and their PE Curves.

Probability Distribution Fitting Results

The first ranked distributions were chosen for the majority of the parameters, but were not chosen for all due to the fact that the best fit distributions were not widely known. For instance, for Scenario 1, P-11 concentration was best fit to the generalized gamma (4P) distribution. Thus, for the purpose of this study the following widely used probability distributions were chosen for analysis: Log-normal, Log-Logistic, Logistic, Generalized Extreme Value (GEV), Inverse Gaussian, and Exponential.

The following tables display the resulting distributions out of the six chosen probability distributions from the ‘goodness of fit’ test for the four scenarios. The not applicable (N/A) label is indicated where no contaminant or load should be found due to the fact that it was not introduced into the system upstream of that location.

Table 53. Scenario 1 ‘Goodness of Fit’ Results

HYDRAULICS SIMULATION 1			
GOODNESS OF FIT RESULTS			
Pipe	Q	C	L
P-10	Log-normal	Log-Logistic	Log-Logistic
P-11	Logistic	N/A	N/A
P-15	Exponential	Log-Logistic	Logistic
P-26	Log-Logistic	Log-Logistic	Logistic
P-27	GEV	GEV	Log-Logistic

Simulation 1 flow rates do not follow one distribution but all vary between the distributions. The contamination concentration data fit the log-logistic distribution. The load contaminant concentration data is split in half between log-logistic and logistic.

Table 54. Scenario 2 ‘Goodness of Fit’ Results

HYDRAULICS SIMULATION 2			
GOODNESS OF FIT RESULTS			
Pipe	Q	C	L
P-10	Logistic	N/A	N/A
P-11	Lognormal	GEV	Logistic
P-15	GEV	GEV	Lognormal
P-26	GEV	Log-Logistic	Lognormal
P-27	GEV	GEV	Lognormal

The ‘goodness of fit’ for Simulation 2 shows that the flow rate and contaminant concentration may be characterized by the GEV and the contaminant load is represented by the log-normal distribution.

Table 55. Scenario 3 ‘Goodness of Fit’ Results

HYDRAULICS SIMULATION 3			
GOODNESS OF FIT RESULTS			
Pipe	Q	C	L
P-10	Logistic	N/A	N/A
P-11	Logistic	N/A	N/A
P-15	GEV	GEV	GEV
P-26	GEV	GEV	GEV
P-27	GEV	Lognormal	GEV

Simulation 3 links, P-10 and P-11, contain runoff only and share the Logistic distribution fit; however, three out of five links share the generalized extreme value distribution. The concentration data and contaminant load is characterized by the generalized extreme value distribution.

Table 56. Scenario 4 ‘Goodness of Fit’ Results

HYDRAULICS SIMULATION 4			
GOODNESS OF FIT RESULTS			
Pipe	Q	C	L
P-10	Logistic	N/A	N/A
P-11	Logistic	N/A	N/A
P-15	GEV	GEV	Log-Logistic
P-26	Log-Logistic	GEV	Log-Logistic
P-27	GEV	GEV	Log-Logistic

Lastly, simulation 4 indicates the combination of runoff and additional flow rate is characterized by the generalized extreme value distribution as shown in links P-15 and P-27. The contaminant

concentration also fits the generalized extreme value distribution. Lastly, the contaminant load fits the log-logistic distribution.

CONCLUSIONS

The hydrology of the East Fork Poplar Creek watershed has been analyzed using MIKE-SHE/MIKE-11 software, which is an integrated surface and subsurface finite difference model. The model integrates the main components of a hydrological cycle, and includes groundwater flow (3D saturated modeling was used to analyze the mercury cycle in the environment and to determine the fate and transport of contamination within the watersheds containing mercury contaminated sites. The model simulates one-dimensional flow within the river; once the flow rate exceeds the corresponding conveyance capacity, the rivers flood and the software applies a two-dimensional simulation to compute the flow stages and rates. The integrated modeling of river, surface and groundwater helps provide an understanding of the mechanisms of mercury transport within the watershed. The model was applied to determine the complex water dynamics that occur through the interactions between surface and groundwater flow patterns in the vicinity of the study site. These interactions include evapotranspiration and precipitation.

The dissolution mechanism of the mercury beads within the EFPC watersheds was implemented into the hydrological model and the competitive absorption on the EFPC sediment between the major cations contained in EFPC water (Ca^{2+} , Mg^{2+} , etc.) and Hg^{2+} was also investigated. A mercury thermodynamic database relevant to EFPC environmental conditions was developed and integrated into the coupled flow and transport models already developed for the site using an enhanced PHREEQC database. The inclusion of thermodynamic equilibrium and reaction kinetics allowed for the characterization of the most dominant species and processes for the environmental conditions of ORR.

The integrated model was extended by implementing an ECO Lab model which was used to simulate the exchange of Hg between the creek and river, the distribution of mercury species within pore water, sorbed mercury within pores, sorbed mercury on suspended particles and "free" mercury which includes dissolved and chelated mercury species (natural organic matter). The development of a mercury/methylmercury template provided improved fate and transport model which can be used for analysis of remediation scenarios to address the complexity of total mercury transport and also the reactions which lead to generation or degradation of

methylmercury. The reaction and kinetic model was calibrated using the observed ratio between total mercury and methylmercury.

The model provides a better understanding of the series of complex interactions between the flow and transport in the hydrological subdomains, which are not completely understood and lead to higher environmental risks caused by elevated concentrations of mercury and methylmercury in East Fork Poplar Creek. The model will support the needs for systematic consideration, evaluation and proper coordination and sequencing of the remediation technologies in order to accomplish the cleanup objectives without increasing the environmental risks downstream. This work will provide stakeholders and decision-makers with a tool to review the technical alternatives in a robust and logically consistent manner.

The environment in the vicinity of the Y-12 Plant and Lower East Polar Creek watershed (LEFPC), the X-10 Plant and White Oak Creek watershed (WOC) at the Oak Ridge Reservation (ORR) has been contaminated by thousands of pounds of mercury as a result of nuclear materials processing activities. To comply with the regulatory standards of mercury concentrations in streams and total maximum daily loads (TMDL), a significant reduction of the mercury levels will be required, particularly in the natural waters, with target levels in the low parts per trillion. Using the site characterization data, an integrated surface and groundwater flow and transport model of EFPC has been developed using MIKE-SHE and MIKE-11 models. The models were used to simulate the hydrology and mercury fate and transport within the LEFPC watershed. In addition, the LEFPC model was used to provide hydrologic and mercury transport data with focus on TMDL. The model developed in this work provides a tool with predictive capabilities for simulating mercury fate and transport that accounts for unique surface-subsurface characteristics and reactive processes. The research work has developed the following areas:

Data characterization and review: A review was completed of historical (1950 to present) hydrologic (groundwater levels, precipitation, evapotranspiration, flow and stages in creeks), water quality (pH, ORP, dissolved oxygen) and contamination data (mercury and methylmercury concentrations in soil and water) available at OREIS, USGS, NOAA, and EPA, and within a summary document for East Fork Poplar Creek. The review provided critical information about

the hydrology and mercury fate and transport that can be useful for site conceptual and numerical models. The outcome of this work was data collection, integration and analysis of the physical and chemical characteristics of the watersheds, including the spatial and temporal variations of relevant hydrological characteristics

Integrated numerical model of the EPFC watershed. An integrated surface and groundwater flow model has been developed which incorporated the entire hydrological cycle: precipitation, evapotranspiration, overland and river flow, and flow in the groundwater saturated and unsaturated zones. The model includes a transport component which uses advection, dispersion, sorption/desorption to provide high resolution information about water and contaminant fluxes between various hydrologic components. Standard GIS data are used and each model is readily extendable to provide state of the art simulation and visualization of the hydrology and transport within the watershed. The objective of the numerical models was to provide an improved understanding of the multiphase transport of mercury species in saturated and variably saturated zones, including physical, bio- and chemical transformation under environmental conditions relevant to the Oak Ridge Site and fate and transport of mercury within ORR watersheds with a focus on determining the regional aspects of mercury plumes and defining strategies for reducing the mercury load and releases in the ecosystem. The outcome of modeling was a set of tools that can be used to forecast the effectiveness of different remediation scenarios and the short- and long-term patterns of migration and fate of mercury within the EFPC watershed.

One source of mercury in East Fork Poplar Creek is contamination of soil due to post-WWII activities at Y-12, between 1950 and 1963. About 230,000 lbs of elemental mercury from the West End Mercury Area was lost from process spills and was released to EFPC via building drains and as process discharges in the form of dilute acidic wastes. Contamination exists in soil and shallow groundwater in and around the buildings and in former process equipment. Long-term deposition has led to a secondary source in sediments and bank soils.

Numerical simulations outlined in this report consider the entire hydrological cycle and include flow in rivers, overland flow, groundwater flow in the saturated and unsaturated zones, evapotranspiration and precipitation time series. The model requires standard GIS input for the

boundaries and for the watershed parameters, which considerably shortens model development and testing. Stochastic parameters and hydrologic conditions over a given five year period of historical hydrological data are used to analyze the hydrological cycle and to determine the prevailing mercury transport mechanism within the watershed.

A surface water model for the ORNL 4500 Area was developed for this study which stores basin and sub-basin characteristics and may be used in predicting flow rates and elevations for specified storm events, continuous rainfall events or single design storm events. The model was calibrated and validated based on monitored time series data provided by ORNL and actual rainfall events that occurred during that timeframe.

The calibration was conducted by routing the rainfall which was retrieved from ORNL Tower C that occurred during those times through the model. It is known that the OF-211 system contains a base flow rate which is defined by once-through AC unit condensate from adjacent buildings that discharges into WOC via OF-211. The XPSWMM model does not simulate this base flow only the runoff produced by the rainfall. Thus, the data provided by ORNL was analyzed and an estimated base flow rate of 0.17 cfs was observed and subtracted in order to calibrate the data and verify the model. The XPSWMM results and the ORNL data were compared. The first calibration was successful as both the data provided and the model results corresponded to an approximate cumulative flow rate of 22 cfs during the calibration timeframe. The remaining three calibration trials resulted in a relative percent error of 20% or less. For the purpose of this study a relative percent error of 20% or less is considered successful. Thus, the model was demonstrated to be an effective tool, properly responding to rainfall data as shown by the calibration.

A sensitivity analysis was conducted wherein five variations of the Manning's roughness coefficients (0.011, 0.013, 0.015, 0.017, and 0.035) were run in order to analyze the impact the parameter had on the system. Continuous rainfall events were run for the year 2010. Yearlong rainfall events in 15 minute intervals produces a large amount of data, thus, the results were analyzed by fitting the data to probability of exceedance curves. The PE curves provide insight into the percentage of time that any node's elevation (link's flow rate) will be met or exceeded

during a storm event. Similarly, infiltration methods (the Green Ampt and Horton's infiltration parameters) were simulated as well as changing the impervious areas within the sub-catchment areas to analyze their impact on the system. The changes within parameters did indicate the model's sensitivity to the parameters, although minor, resulted in variations in flow rate and water stages throughout the events.

As one might surmise, flooding within the system does occur during the 25 year and 100 year – 24 hour storm events due to the fact that the storm event scenarios are for designing of a system and do not resemble ordinary precipitation events throughout the year. If future drainage or building improvements within the 4500 Area are proposed, then the model may be adjusted to the proposed conditions and flow rates, and water stages may be predicted for the design-based storm events.

The transport analysis has provided insight into how a conservative contaminant would react within the system if introduced at the various locations. The flow rates, concentration, and loads were fit to a probability distribution in order to characterize the data. When only runoff from the continuous rainfall events during 2010 was routed the data clearly follows the logistic distribution. Link P-27 receives flow from the system to the east and four out of the four simulations are characterized by the GEV distribution. The minor flow introduced into the system does not affect the amount of flow received from the main storm trunk and laterals. GEV and log-logistic distributions best represent the conservative contaminant concentration data when routed through the chosen links. The contaminant load data timeseries varied at each simulation. The trend shown is within each simulation not within specific flow distribution and contaminant distribution; the flow rate distribution and concentration distribution within the simulation do not determine consistent load distributions.

Ultimately, ORNL is concerned with residual contamination within the area. Understanding the flow characteristics within the study area is fundamental to estimating contaminant transport which directly correlates to the flow rate. The resulting flow rate quantities from this model may also be used in support of other models where flow rates and soil concentrations may be coupled in order to assess the pollutant loads within the soils. This information will assist in locating

areas where remediation is necessary. These models can be used to predict the effectiveness of remediation strategies and to optimize them.

REFERENCES

1. Aastrup, M, Johnson, J., Bringmark, E., Bringmark, I and A. Iverfeldt. 1991. Occurrence and transport of mercury within a small catchment area. *Water, Air, and Soil Pollution* 56, 155-167.
2. Abbott M. B. and J. C. Refsgaard. 1996. *Distributed Hydrological Modeling*. Kluwer Academic: Dordrecht.
3. Agency for Toxic Substances and Disease Registry (ATSDR), Federal Facilities Assessment Branch and Division of Health Assessment and Consultation. 2006. *Public Health Assessment: Evaluation of Potential Exposures to Contaminated Off-Site Groundwater from the Oak Ridge Reservation (USDOE) Oak Ridge, Tennessee*.
4. Akçay, H., Kilin, S. and C. Karapire. 1996. A comparative study on the sorption and desorption of Hg, Th and U on clay. *Journal of Radioanalytical and Nuclear Chemistry*. V. 214, N. 1, 51-66.
5. Allison J, D. and T. L. Allison. 2005. Partition coefficient for metals in surface water, soil, and Waste. EPA/600/R-05/074.
6. <http://support.esri.com/index.cfm?fa=downloads.dataModels.filteredGateway&dmid=15>. ArcHydro tools, Available from URL:
7. Bibler, J. P. and D. B. Marson. 1992. Behavior of mercury, lead, cesium, and uranium ions on four SRS soils. Report WSRC-RP-92-326, p.50. Available at <http://www.osti.gov/bridge/servlets/purl/7064035-hwmdrD/7064035.pdf>.
8. Carsel, R. F. and R. S. Parrish. 1988. Developing Joint Probability Distributions of Soil Water Retention Characteristics. *Water Resources Research*, V. 24, N. 5, P 755-769.
9. ChemRisk. (1999a). Radionuclide releases to the Clinch River from White Oak Creek on the Oak Ridge Reservation—an assessment of historical quantities released, off-site radiation doses, and health risks, task 4. Reports of the Oak Ridge dose reconstruction, volume 4. Tennessee Department of Health. July 1999. Available from URL: <http://www2.state.tn.us/health/CEDS/OakRidge/WOak1.pdf>.
10. <http://www2.state.tn.us/health/CEDS/OakRidge/Screen.pdf> ChemRisk. 1999b. Screening-level evaluation of additional potential materials of concern, task 7. Reports of the Oak Ridge dose reconstruction, volume 6. Tennessee Department of Health. July 1999.
11. Chow, V.T., 1959. *Open-Channel Hydraulics*. McGraw-Hill, New York, NY.
12. Clapp, R., and G. Hornberger (1978), Empirical Equations for Some Soil Hydraulic Properties, *Water Resour. Res.*, 14(4), 601-604.
13. DHI, 2008. MIKE 11 Short Descriptions, Danish Hydraulic Institute, Hørsholm, Denmark.
14. Fröberg, M., Jardine, P. M., Hanson, P. J., Swanston, C. W., Todd, D. E., Tarver J. R., and C. T. Garten, Jr. 2007. Low Dissolved Organic Carbon Input from Fresh Litter to Deep Mineral Soils. *Soil Sci Soc Am J.*, 71, p. 347-354.
15. <http://data.geocomm.com/catalog/US/61084/1914/group4-3.html> GeoCommunity website
16. Glass, G. E, Sorenson, J. A., Schmidt, K. W. and G.R. Rapp. 1990. New source identification of mercury contamination in the Great Lakes, *Environmental Science and Technology*, 24 (7), 1059-1069.
17. Hatcher, R. D. et al. 1989. *Field Guide and Perspective on the Geology and Hydrology of the Oak Ridge Reservation*. Oak Ridge National Laboratory /University of Tennessee, Oak

- Ridge, Tennessee.
18. Hatcher, R. D., Lemiszki, P. J., Dreier, R. B., Ketelle, R. H., Lee, R. R., Leitzke, D. A., McMaster, W. M., Foreman, J. L., and S. Y. Lee. 1992. Status Report on the Geology of the Oak Ridge Reservation, ORNL/TM-12074. Prepared for the Office of Environmental Restoration and Waste Management.
 19. Hornberger, G. M., J. P. Raffensperger, P. L. Wiberg, K. N. Eshelman, 1998: Elements of Physical Hydrology, Johns Hopkins University Press, Baltimore, pp.302. DHI, 2008. MIKE SHE User Manual, Danish Hydraulic Institute, Hørsholm, Denmark.
 20. <http://sti.srs.gov/fulltext/ms2002056/ms2002056.html> Kaplan, D. I. Knox, S. and J. Myers. 2002. Mercury Geochemistry in a Wetland and its Implications for In-situ Remediation
 21. Kaplan, D. I., and S. M. Serkiz. 2000. In-situ Kd Values and Geochemical Behavior for Inorganic and Organic Constituents of Concern at the TNX Outfall Delta. WSRC-TR-99-00488. Aiken, SC.
 22. Kaplan, D. I., and G. M. Iversen. 1999. Material and Methods for the Ford Building Sediment Hg-Kd Study. Report WSRC-TR-99-00357 prepared for DOE under the contract number DE-AC09-96SR18500.
 23. Lee, Y., Borg, G. C., Iverfeldt, A. and H. Hultberg. 1994. Fluxes and turnover of methylmercury mercury pools in forest soils. In Mercury Pollution: Integration and Synthesis.
 24. Lietzke, D. A., S. Y. Lee, T. Tamura. 1986. Resource Management Plan for the Oak Ridge Reservation, Volume 20: Soil Conservation Plan for the Oak Ridge Reservation. ORNL/ESH-1/V20.
 25. Lyon, B. F., Ambrose, R., Rice, G. and C. J. Maxwell. 1997. "Calculation of Soil- Water and Benthic Sediment Partition Coefficients for Mercury", Chemosphere, Vol.35, No. 4, pp. 791-808.
 26. Martin (1988) In: Seiler G. and Siegel H. (Eds), Handbook of toxicity of inorganic compounds. New York: Marcel Dekker, p 14.
 27. Moore, G. K. 1988. Concepts of Groundwater Occurrence and Flow near Oak Ridge National Laboratory, Tennessee. ORNL/TM-10969, Martin Marietta Energy Systems, Inc., Oak Ridge, Tennessee.
 28. Moore, G. K. 1988. Groundwater parameters and flow systems near Oak Ridge National Laboratory, ORNL/TM-11368. Oak Ridge National Laboratory.
 29. Moore, J. W. and S. Ramamodora. 1984. Heavy Metal in Natural Waters- Applied Monitoring in Impact Assessment, Springer-Verlag, New York.
 30. NOAA (National Oceanic and Atmospheric Administration). 2006. Local Climatological Data Annual Survey with Comparative Data, Oak Ridge, Tenn. National Oceanic and Atmospheric Administration, National Climatic Data Center, Asheville, NC.
 31. Oakes, T. W. to Wing, J. F. (Letter). 1983a. Department of Energy/Oak Ridge Operations. Mercury in Soil and Sediment at ORNL.
 32. Oakes, T. W. to Wing, J. F. (Letter). 1983b. Department of Energy/Oak Ridge Operations. Mercury in Soil Samples at ORNL.
 33. ORNL, Oak Ridge Y-12 Plant, and East Tennessee Technology Park. 2006. Oak Ridge Reservation Annual Site Environmental Report for 2005. Prepared for the U.S. Department of Energy. September 2006. Report#DOE/ORO/2218. Available from URL: <http://www.ornl.gov/aser>.

34. Parr, P. D. and J. F. Hughes. 2006. Oak Ridge Reservation Physical Characteristics and Natural Resources. ORNL/TM-2006/110.
35. Refsgaard, J. C. and B. Storm. 1995. In: Singh, V. P., (Ed.), Computer Models of Watershed Hydrology, Water Resources Publications, Englewood, USA, pp. 809–846.
36. Rivers, J. M., Nyquist, J. E., Roh, Y., Terry, D. O. and W. E. Doll. 2004. Investigation into the Origin of Magnetic Soils on the Oak Ridge Reservation, Tennessee. *Soil Sci. Soc. Am. J.* 68, p.1772–1779.
37. Robinson, K. G. and M. S. Shuman. 1989. Determination of mercury in surface waters using an optimized cold vapor spectrophotometric technique. *International Journal of Environmental Chemistry*, 36, 111-123.
38. Sarkar, D., M. E. Essington, et al. (1999). "Adsorption of Mercury (II) by Variable Charge Surfaces of Quartz and Gibbsite." *Soil Science Society of America Journal*, 63: 1626-1636.
39. Sarkar, D., M. E. Essington, et al. (2000). "Adsorption of Mercury (II) by Kaoline." *Soil Science Society America Journal*, 64: 1968-1975.
40. Schlüter, K. 1997. Sorption of Inorganic Mercury and Monomethyl Mercury in an Iron-Humus Podzol Soil of Southern Norway Studied by Batch Experiments. *Environmental Geology*, 30(3/4), p. 266-279.
41. Scurlock, J. M. O., Asner, G. P. and S. T. Gower. 2001. Worldwide historical estimates of Leaf Area Index, 1932–2000. Office of Scientific and Technical Information, Oak Ridge, TN, USA, Report ORNL/TM-2001/268.
42. Solomon, D. K., Moore G. K., Toran, L. E., Dreier, R. B., and W. M. McMaster. 1992. Status report. A Hydrological Framework for the for the Oak Ridge Reservation. ORNL/TM/12026.
43. Taylor, Jr., F. G. 1989. Mercury Assessment for Water and Sediment in Oak Ridge National Laboratory Streams. U.S. DOE Oak Ridge National Laboratory, Oak Ridge, Tennessee. Report # ORNL/M-713.
44. http://www.tngis.org/frequently_accessed_data.htmlTennessee Spatial Data Server, Available from URL:
45. Tennessee Valley Authority (TVA). 1972. Upper Bear Creek Experimental Project: A Continuous Daily Streamflow Model. Research Paper No. 8, Tennessee Valley Authority Division of Water Control Planning, Knoxville, Tennessee.
46. US DOE. 1999. Remedial Investigation/Feasibility Study for Bethel Valley Watershed at Oak Ridge National Laboratory, Oak Ridge, Tennessee. Report# DOE/OR/01-1748/V1&D2.
47. <http://www.epa.gov/ORD/NRMRL/Pubs/600R01043/600R01043chap2.pdf>. US EPA. 2004. Basic Concepts of Open Channel Flow Measurement. Available from URL:
48. Van Genuchten, M., Th. 1976. A closed-form equation for predicting the hydraulic conductivity of unsaturated soils. *Soil Sci Soc. J.*, 44(5), 892-898.
49. <http://public.ornl.gov/nabirfrfc/other/frcconmod.pdf> Watson, D. B., Kostka, J. E., Fields, M. W. and P. M. Jardine. 2004. The Oak Ridge Field Research Center Conceptual Model. NABIR Field Research Center Technical Report, Oak Ridge, Tennessee.
50. Yin, Y., H. E. Allen, et al. (1996). "Adsorption of Mercury (II) by Soil: Effects of pH, Chloride, and Organic Matter." *Journal of Environmental Quality*, 25: 837-844.
51. <http://tnmap.state.tn.us/portal/GISLinks.aspx>
52. <http://streamstats.usgs.gov/tstreamstats/index.asp>

53. <http://water.usgs.gov/osw/streamstats/tennessee.html>
54. Geologic Map of Tennessee, William D. Hardeman, Tennessee Division of Geology, Published by the Tennessee Division of Geology, 1966, at a scale of 1:250,000.
55. http://nwis.waterdata.usgs.gov/nwis/inventory/?site_no=03537000
56. http://nwis.waterdata.usgs.gov/nwis/inventory/?site_no=03536550
57. http://nwis.waterdata.usgs.gov/nwis/inventory/?site_no=03536440
58. http://nwis.waterdata.usgs.gov/nwis/inventory/?site_no=03519650
59. http://nwis.waterdata.usgs.gov/nwis/inventory/?site_no=03536380
60. http://nwis.waterdata.usgs.gov/nwis/inventory/?site_no=03536500
61. http://nwis.waterdata.usgs.gov/nwis/inventory/?site_no=03536320
62. http://nwis.waterdata.usgs.gov/nwis/inventory/?site_no=03538272
63. Imported from Basin Characteristics file
64. 41 Wolock, D.M., 2003, Flow characteristics at U.S. Geological Survey streamgages in the conterminous United States: U.S. Geological Survey Open-File Report 03-146, digital data set, available on World Wide Web at URL <http://water.usgs.gov/lookup/getspatial?qsitesdd>
65. 42 Wolock, D.M., 2003, Base-flow index grid for the conterminous United States: U.S. Geological Survey Open-File Report 03-263, digital data set, available on World Wide Web at URL <http://water.usgs.gov/lookup/getspatial?bfi48grd>
66. 43 Law, G.S., and Tasker G.D., 2003, Flood-Frequency Prediction Methods for Unregulated Streams of Tennessee, 2000: U.S. Geological Survey, Water-Resources Investigations Report 03-4176, 79p.
67. Guide for Selecting Manning's Roughness Coefficients for Natural Channels and Flood Plains United States Geological Survey Water-supply Paper 2339.
68. <http://www.y12.doe.gov/about/factsheet.php>
69. <http://tapestry.usgs.gov/features/06valleyridge.html>
70. Ambrose, R. & Wool, T. Modeling Tools Used for Mercury TMDLs in Georgia Rivers. Proceedings of the 2001 Georgia Water Resources Conference, March 26-27, 2001, at the University of Georgia. Kathryn. J. Hatcher, editor, Institute of Ecology, The University of Georgia, Athens, Georgia.
71. PROPOSED TOTAL MAXIMUM DAILY LOAD (TMDL) for Mercury in East Fork Poplar Creek Lower Clinch River Watershed (HUC 0601 0207) Anderson and Roane Counties, Tennessee, Preliminary 2nd Draft, October 2008.
72. Scurlock, J. M. O., Asner, G. P. and S. T. Gower. 2001. Worldwide historical estimates of Leaf Area Index, 1932–2000. Office of Scientific and Technical Information, Oak Ridge, TN, USA, Report ORNL/TM-2001/268.
73. Wood, A. W., Bernknopf, R., Rytuba, J., Singer, D.A., Champion, R. 2005. Offset-based Decision Support Models for Mitigating Mercury Sources in the Cache Creek Watershed, North Central California. Proceedings of the Water Environment Federation, National TMDL Science and Policy 2005 , pp. 1496-1516(21).
74. <http://www.state.tn.us/environment/wpc/tmdl/approved.shtml>
75. NC DENR. 2004. North Carolina Department of Environment and Natural Resources. Total Maximum Daily Load for Mercury in the Cashie River, North Carolina. Public Review Draft 7/28/2004.
76. EPA, 2008. TMDL Modeling Toolbox, <http://www.epa.gov/athens/wwqtsc/html/tools.html>.
77. Wolock, D.M., 2003, Flow characteristics at U.S. Geological Survey streamgages in the

- conterminous United States: U.S. Geological Survey Open-File Report 03-146, digital data set, available on World Wide Web at URL <http://water.usgs.gov/lookup/getspatial?qsitesdd>
78. Wolock, D.M., 2003, Base-flow index grid for the conterminous United States: U.S. Geological Survey Open-File Report 03-263, digital data set
 79. Abbott, M. B., and J. C. Refsgaard. "Distributed Hydrological Modeling." Kluwer Academic: Dordrecht, 1996.
 80. Allison, Jerry, and Terry Allison. "Partition Coefficients for Metals in Surface Water, Soil and Waste ." Office of Research and Development, US Environmental Protection Agency, Washington, DC, 2005.
 81. Andrews, E.D. "Entrainment of gravel from naturally sorted riverbed material." Geological Society of America Bulletin 94 (October 1983): 1225-1231.
 82. Ashwood, T.L., C.R. Olsen, I.L. Larsen, and P.D. Lowry. Sediment Contamination in Streams Surrounding the Oak Ridge Gaseous Diffusion Plant. Oak Ridge: Oak Ridge National Laboratory, 1986.
 83. Bao, Yixing. "Predicting sediment and Cesium-137 transported to offsite during extreme floods." Oak Ridge National Laboratory. Environmental Science Division Publication 4853, 1999.
 84. Bechtel Jacobs. "Determination of Site-Specific Aqueous Concentration Goals for Controlling Mercury Bioaccumulation in Fish in East Fork Poplar Creek: Result of Studies Undertaken by the Y-12 Biological Monitoring and Abatement Program (BMAP) at the Oak Ridge Y-12 Plant." Oak Ridge, TN, 1999.
 85. Beheshti, A.A., and B. Ataie-Ashtiani. "Analysis of threshold and incipient conditions for sediment movement." Coastal Engineering, 2008: 423-430.
 86. Brigham, Mark, Dennis Wentz, George Aiken, and David Krabbenhoft. "Mercury Cycling in Stream Ecosystems. 1. Water Column Chemistry and Transport." Environmental Science Technology 43 (2009): 2720-2725.
 87. Brooks, S.C., and G.R. Southworth. "History of Mercury use and Environmental Contamination at the Oak Ridge Y-12 Plant." Environmental Pollution, 2011: 219-228.
 88. Chapra, Steven. Surface Water-Quality Modeling . Long Grove, IL: Waveland Press, Inc, 1997.
 89. Cheng, Nian-Sheng. "Simplified Settling Velocity Formula for Sediment Particle," Journal of Hydraulic Engineering, 1997: 149-152.
 90. Choi, Sung-Uk, and Seungjo Kwak. "Theoretical and Probabilistic Analysis of incipient motion of sediment particles." KSCE Journal of Civil Engineering 5, no. 1 (March 2001): 59-65.
 91. DENR, NC. "North Carolina Department of Environment and Natural Resources. Total Maximum Daily Load for Mercury in the Cashie River, North Carolina. Public Review Draft 7/28/2004." NC DENR. 2004. North Carolina Department of Environment and Natural Resources. Total Maximum Daily Load for Mercury in the Cashie River, North Carolina. Public Review Draft 7/28/2004, North Carolina, 2004.
 92. DHI. Heavy Metal Template ECO Lab Scientific Description. Hørsholm, Denmark: Danish Hydraulic Institute, 2009.
 93. DHI. MIKE 11 A modelling system for rivers and channels, user guide. Hørsholm, Denmark: Danish Hydraulic Institute, 2009b.
 94. DHI. MIKE 11 Short Descriptions . Hørsholm, Denmark: Danish Hydraulic Institute, 2008.

95. DOE. "East Fork Poplar Creek – Sewer Line Beltway Remedial Investigation Report, Volume I, Science applications International Corporation, 1994," 1994.
96. DOE. Instream Contaminant Study Task 5, Summary Report. Oak ridge, Tennessee: Office of Natural Resources and Economic Development Tennessee Valley of Authority, 1986b, 223.
97. DOE. "Instream Contaminat Study Task 2, V2. Sediment Characterization." Office of Natural Resources and Economic Development Tennessee Valey of Authority, 1986.
98. DOE. "Proposed Plan for Interim Source Control Actions for Contaminated Soils, Sediments, and Groundwater (Outfall 51) which Contribute to Mercury and PCB Contamination to Surface Water in the Upper East Fork Poplar Creek Characterization Area." Oak Ridge, Tennessee: Department of Energy, 2001.
99. DOE. Recommendations to Address Technical Uncertainties in Mitigation and Remediation of Mercury at the Y-12 Plant, Oak Ridge. Office of Environmental Management, Department of Energy, Oak Ridge, Tennessee: Department of Energy, 2008.
100. DOE. Record of Decision for Phase II Interim Remedial Actions for Contaminated Soils and Scrapyard in Upper East Fork Poplar Creek. Oak Ridge, Tennessee: U.S. Department of Energy Office of Environmental Management, 2005.
101. DOE. Record of Decision for Soil, Buried Waste, and Subsurface Structure Actions in Zone 2, East Tennessee Technology Park. Oak Ridge, Tennessee: U.S. Department of Energy Office of Environmental Management, 2005b.
102. DOE. "Report on the Remedial Investigation of the Upper East Fork Poplar Creek Characterization Area at the Oak Ridge Y-12 Plant, Oak Ridge, Tennessee, Volume 1, DOE/OR/01-1641/V1&D2," 1998.
103. DOE. "Report on the Remedial Investigation of the Upper East Fork Poplar Creek Characterization Area at the Oak Ridge Y-12 Plant. Volume 1." Oak Ridge, Tennessee, 1998.
104. Ebinghaus, R., R.R. Turner, L.D. de Lacerda, O Vasiliev, and W Salomons. Mercury Contamnated Sites. New York: Springer, 1999.
105. Emmet et al., Owens. "Resuspension of Mercury-Contaminated Sediments from an In-Lake Industrial Waste Deposit." Journal of Environmental Engineering, July 2009: 526-534.
106. Gandhi et al., Nilima. "Development of a Mercury Speciation, Fate and Biotic Uptake (BIOTRANSPEC) Model; Application to Lahontan Reservoir (NEVADA, USA)." Environmental Toxicology and Chemistry 26, no. 11 (2007): 2260–2273.
107. Garde, R.J., and K.J. Tanga Raju. Mechanics of Sediment Transportation and Alluvial Stream Problems. Second Edition. John Wiley & Sons, 1985.
108. Gray, J. R., G.D Glysson, L.M Turcios, and G.E. Schwartz. Comparability of Suspended-Sediment Concentration and Total Suspended Solids Data, Water Resources Investigations Report 00-4191. Reston, Virginia.: U.S. Geological Survey, 2000.
109. Guo, Qizhong. "Correlation of Total Suspended Solids (TSS) and Suspended Sediment Concentration (SSC) Test Methods." Department of Civil and Environmental Engineering, The State University of New Jersey, Trenton, NJ, 2006.
110. Hallermeier, Robert. "Terminal Settling Velocity of Commonly Occurring Sand Grains." Sedimentology, 1981: 859-865.
111. Han, Fengxiang, et al. "extractability and Bioavailability of Mercury from a Mercury Sulfide Contaminated Soil in Oak Ridge. Tennessee, USA." Water Air Soil Pollution,

- 2008: 67-75.
112. Hill, Walter, Michael Ryon, John Smith, Marshall Adams, Harry Boston, and Arthur Stewart. "The Role of Periphyton in Mediating the Effects of Pollution in a Stream Ecosystem." *Environmental Management*, 2010: 563-576.
 113. Honeyman, Bruce D, and H Peter Santschi. "Metals in Aquatic Systems." *Environmental Science and Technology* 22, no. 8 (1988): 862-871.
 114. Kaleri, Cinthia. "Implementation Issues: Mercury Transport and Fate. combustion Risk Assessments in Region 6." EPA - Proceeding of the 12th International conference. Dallas - Texas, 2000.
 115. Kuwabara, James, and others. Flux of Dissolved Forms of Mercury Across the Sediment-water Interface in Lahontan Reservoir, Nevada. U.S. Geological Survey, Nevada: U.S. Geological Survey, 2002.
 116. LaGrega, Michael D, Philip L Buckingham, and Jeffrey C Evans. Hazardous Waste Management. Second. McGraw-Hill, 2001.
 117. Levine, Daniel, William Hargrove, and Hoffman Forrest. "Characterization of Sediments in the Clinch River, Tennessee, Using Remote Sensing and Multidimensional GIS Techniques." Vancouver, British Columbia, 1995. 548-551.
 118. Liao, Lixia, H.M. Selim, and R.D. DeLaune. "Mercury Adsorption-Desorption and Transport in Soils." *Journal of Environmental Quality* 38, no. July-August (2009): 1608-1616.
 119. Lyon, B.F. "Calculation of Soil-Water and Benthic Partition Coefficients for Mercury." *Chemosphere*, 1997: 791-808.
 120. Miller, Carrie L., George Southworth, Scott Brooks, and Baohua Gu. "Kinetic Controls in the Complexation between Mercury and Dissolved Organic Matter in a Contaminated Environment." *Environmental Science Technology* 43 (2009): 8548-8553.
 121. Moran, Barry. "Modeling of the Hydrologic Transport of mercury in the Upper East Fork Poplar Creek." Knoxville (Tennessee), December 1996.
 122. Morel, F. M., A.M. Kraepiel, and M Amyot. "The Chemical Cycle and Bioaccumulation of Mercury." *Annual Review of Ecology and Systematics* 29 (1998): 543-566.
 123. Nriagu, Ed. *The Biochemistry of Mercury in the Environment*. Amsterdam, The Netherlands, North Holland: Biomedical Press, 1979.
 124. Pant, P, and M Allen. "Interaction of Soil and Mercury as a Function of Soil Organic Carbon." *Bull Environmental Contaminant Toxicology*, 2007.
 125. Parkpoin, Preeda, Waewtaa Thongra-ar, Ronald DeLaune, and Aroon Jugsujinda. "Adsorption and Desorption of Mercury by Bangpakong River Sediments as Influenced by Salinities." *Journal of Environmental Science and Health*, 2001: 623-640.
 126. Pelcova, Pavlina, Jana Margetinova, Tomas Vaculovic, Josef Komarek, and Vlastimil Kuban. "Adsorption of Mercury Species on River Sediments - Effects of Selected Abiotic Parameters." *Central European Journal of Chemistry*, 2010: 116-125.
 127. Reimers, Robert, and Peter Krenkel. "Kinetics of Mercury Adsorption and Desorption in Sediments." *Water Pollution Control Federation* 46, no. 2 (1974): 352-365.
 128. Rothschild, E.R., et al. Investigation of Subsurface Mercury at the Oak Ridge Y-12 Plant, ORNL/TM-9092. Oak Ridge, TN: Oak Ridge National Laboratory, 1984.
 129. Schnoor, Jerald L. *Environmental Modeling. Fate and Transport of Pollutants in Water, Air, and Soil*. New York: John Wiley & sons, Inc., 1996.

130. Southworth, G.R., et al. Controlling Mercury Release from Source Zones to Surface Water: Initial Results of Pilot Tests at the Y-12 National Security Complex. Oak Ridge, TN: ORNL, 2009.
131. Southworth, George, Max Greeley, Mark Peterson, Kenneth Lowe, and Richard Kettelle. Sources of Mercury to East Fork Poplar Creek Downstream from the Y-12 National Security Complex: Inventories and Export Rates. Oak Ridge: Oak Ridge National Laboratory, 2010.
132. TDEC, Tennessee Department of Environment and Conservation, Division of Water Pollution Control. "Proposed Total Maximum Daily Load (TMDL) for Mercury in East Fork Poplar Creek, Lower Clinch River Watershed, Preliminary Second Draft. Anderson and Roane Counties." Oak Ridge, TN, 2008.
133. Turner, R.R., and G.R. Southworth. "Mercury-Contaminated Industrial and Mining Sites in North America: an Overview with Selected Case Studies in Mercury Contaminated Sites," R. Ebinghaus, R. R. Turner, L. D. de Lacerda, O. Vasiliev, and W. Salomons (Eds.). Berlin: Springer-Verlag, 1999.
134. USEPA. "Appendix A Chemical Specific Data Delisting Technical Support Document." October 2008. <http://www.epa.gov/reg5rcra/wptdiv/hazardous/delisting/appda1.pdf> (accessed September 08, 2010).
135. USEPA. Development of Duration-Curve Based Methods for Quantifying Variability and Change in Watershed Hydrology and Water Quality. Cincinnati, Ohio: United States Environmental Protection Agency, 2008.
136. USEPA. "Guidance on the Development, Evaluation, and Application of Environmental Models." Council for Regulatory Environmental Modeling, U.S. Environmental Protection Agency, Washington, DC, 2009.
137. USEPA. "Mercury Study Report to Congress. Volume III. Fate and Transport of Mercury in the Environment," 1997.
138. USEPA. "Standard Operating Procedure for the Analysis of Residue, non-filterable (Suspended Solids), Water, Method 160.2 NS (Gravimetric, 103-105oC)." Region 5 Central Regional Laboratory, 1999.
139. USGS. "Contaminant Sorption by Soil and Bed Sediment." 2000.
140. Van Rijn, L. "Sediment Transport, Part I, Bed Load Transport." *Journal of Hydraulic Engineering*, 1984: 1431-1456.
141. Van Rijn, Leo. "Sediment Transport, Part II: Suspended Load Transport." *Journal of Hydraulic Engineering* 110, no. 11 (November 1984b): 1613-1641.
142. Vermont Agency of Natural Resources. "Vermont Stream Geomorphic Assessment, Appendix O." 2009. <http://bit.ly/gY33oq> (accessed November 11, 2010).
143. Wehr, John, and Robert Sheath. *Fresh water algae of North America, Ecology and classification*. San Diego, CA: Academic Press, 2003.
144. Yin, Yujun, Herbert Allen, and C.P. Huang. "Kinetics of Mercury (II) Adsorption and Desorption in Soil." *Environmental Science and Technology* 31, no. 2 (1997): 496-502.

APPENDIX A RIVER NETWORK AND MIKE-SHE COUPLING

Table 57. River Network and MIKE-SHE Coupling Branches

Branch Name	US. Chaninage	DS. Chainage	Conductance	Leakage Coefficient
BC-A-N01	0	2627.009	Aquifer + Bed	1.00E-06
BC-A-S01	0	1679.789	Aquifer + Bed	1.00E-06
Bear Creek	0	12393.2	Aquifer + Bed	1.00E-06
Branch100	0	570.5153	Aquifer + Bed	1.00E-06
Branch101	0	645.5479	Aquifer + Bed	1.00E-06
Branch102	0	371.0575	Aquifer + Bed	1.00E-06
Branch103	0	367.1307	Aquifer + Bed	1.00E-06
Branch104	0	676.628	Aquifer + Bed	1.00E-06
Branch105	0	738.474	Aquifer + Bed	1.00E-06
Branch106	0	320.1355	Aquifer + Bed	1.00E-06
Branch107	0	494.1946	Aquifer + Bed	1.00E-06
Branch108	0	337.9415	Aquifer + Bed	1.00E-06
Branch109	0	272.4182	Aquifer + Bed	1.00E-06
Branch110	0	928.0936	Aquifer + Bed	1.00E-06
Branch111	0	512.9622	Aquifer + Bed	1.00E-06
Branch112	0	407.5125	Aquifer + Bed	1.00E-06
Branch113	0	885.2734	Aquifer + Bed	1.00E-06
Branch18	0	572.2349	Aquifer + Bed	1.00E-06
Branch19	0	767.0324	Aquifer + Bed	1.00E-06
Branch20	0	1508.714	Aquifer + Bed	1.00E-06
Branch21	0	714.3443	Aquifer + Bed	1.00E-06
Branch22	0	434.2925	Aquifer + Bed	1.00E-06
Branch23	0	733.9068	Aquifer + Bed	1.00E-06
Branch24	0	1010.745	Aquifer + Bed	1.00E-06
Branch25	0	574.901	Aquifer + Bed	1.00E-06
Branch26	0	1349.794	Aquifer + Bed	1.00E-06
Branch27	0	305.551	Aquifer + Bed	1.00E-06
Branch28	0	1385.653	Aquifer + Bed	1.00E-06
Branch29	0	321.9663	Aquifer + Bed	1.00E-06
Branch30	0	1220.469	Aquifer + Bed	1.00E-06
Branch31	0	1100.442	Aquifer + Bed	1.00E-06
Branch32	0	1119.248	Aquifer + Bed	1.00E-06
Branch33	0	640.3945	Aquifer + Bed	1.00E-06
Branch34	0	394.4704	Aquifer + Bed	1.00E-06
Branch35	0	1094.315	Aquifer + Bed	1.00E-06

Branch36	0	555.9898	Aquifer + Bed	1.00E-06
Branch37	0	1389.404	Aquifer + Bed	1.00E-06
Branch38	0	258.9063	Aquifer + Bed	1.00E-06
Branch39	0	763.9674	Aquifer + Bed	1.00E-06
Branch40	0	349.9719	Aquifer + Bed	1.00E-06
Branch41	0	306.8962	Aquifer + Bed	1.00E-06
Branch42	0	648.6201	Aquifer + Bed	1.00E-06
Branch43	0	410.2066	Aquifer + Bed	1.00E-06
Branch44	0	341.9655	Aquifer + Bed	1.00E-06
Branch45	0	345.3987	Aquifer + Bed	1.00E-06
Branch46	0	1343.248	Aquifer + Bed	1.00E-06
Branch47	0	491.9328	Aquifer + Bed	1.00E-06
Branch48	0	1123.569	Aquifer + Bed	1.00E-06
Branch49	0	613.0007	Aquifer + Bed	1.00E-06
Branch50	0	1074.729	Aquifer + Bed	1.00E-06
Branch51	0	1674.477	Aquifer + Bed	1.00E-06
Branch53	0	1168.691	Aquifer + Bed	1.00E-06
Branch54	0	614.2799	Aquifer + Bed	1.00E-06
Branch55	0	420.9591	Aquifer + Bed	1.00E-06
Branch56	0	1506.09	Aquifer + Bed	1.00E-06
Branch57	0	349.039	Aquifer + Bed	1.00E-06
Branch58	0	367.6437	Aquifer + Bed	1.00E-06
Branch59	0	1362.674	Aquifer + Bed	1.00E-06
Branch60	0	785.5916	Aquifer + Bed	1.00E-06
Branch61	0	455.3194	Aquifer + Bed	1.00E-06
Branch62	0	1090.513	Aquifer + Bed	1.00E-06
Branch63	0	1095.6	Aquifer + Bed	1.00E-06
Branch64	0	1783.792	Aquifer + Bed	1.00E-06
Branch65	0	365.3412	Aquifer + Bed	1.00E-06
Branch66	0	372.1474	Aquifer + Bed	1.00E-06
Branch67	0	565.5998	Aquifer + Bed	1.00E-06
Branch68	0	589.8957	Aquifer + Bed	1.00E-06
Branch69	0	710.8594	Aquifer + Bed	1.00E-06
Branch70	0	604.1159	Aquifer + Bed	1.00E-06
Branch71	0	603.7158	Aquifer + Bed	1.00E-06
Branch72	0	466.2401	Aquifer + Bed	1.00E-06
Branch73	0	1553.593	Aquifer + Bed	1.00E-06
Branch74	0	957.999	Aquifer + Bed	1.00E-06
Branch75	0	565.6058	Aquifer + Bed	1.00E-06
Branch76	0	386.094	Aquifer + Bed	1.00E-06
Branch77	0	757.1665	Aquifer + Bed	1.00E-06

Branch78	0	1180.437	Aquifer + Bed	1.00E-06
Branch79	0	747.8143	Aquifer + Bed	1.00E-06
Branch80	0	656.3352	Aquifer + Bed	1.00E-06
Branch81	0	1061.413	Aquifer + Bed	1.00E-06
Branch82	0	455.7928	Aquifer + Bed	1.00E-06
Branch83	0	459.7968	Aquifer + Bed	1.00E-06
Branch84	0	1335.563	Aquifer + Bed	1.00E-06
Branch85	0	253.1162	Aquifer + Bed	1.00E-06
Branch86	0	1598.993	Aquifer + Bed	1.00E-06
Branch87	0	1219.094	Aquifer + Bed	1.00E-06
Branch88	0	1504.984	Aquifer + Bed	1.00E-06
Branch89	0	602.005	Aquifer + Bed	1.00E-06
Branch90	0	776.6201	Aquifer + Bed	1.00E-06
Branch91	0	508.74	Aquifer + Bed	1.00E-06
Branch92	0	619.2092	Aquifer + Bed	1.00E-06
Branch93	0	696.9681	Aquifer + Bed	1.00E-06
Branch94	0	628.9183	Aquifer + Bed	1.00E-06
Branch95	0	643.7243	Aquifer + Bed	1.00E-06
Branch96	0	574.7264	Aquifer + Bed	1.00E-06
Branch97	0	643.2892	Aquifer + Bed	1.00E-06
Branch98	0	608.2769	Aquifer + Bed	1.00E-06
Branch99	0	568.2906	Aquifer + Bed	1.00E-06
EFPC	0	25485.2	Aquifer + Bed	1.00E-06
EFPC-A-N01	0	1820.508	Aquifer + Bed	1.00E-06
EFPC-A-N02	0	1546.164	Aquifer + Bed	1.00E-06
EFPC-A-N03	0	1616.786	Aquifer + Bed	1.00E-06
EFPC-A-N04	0	2934.288	Aquifer + Bed	1.00E-06
EFPC-A-N04-N01	0	1611.753	Aquifer + Bed	1.00E-06
EFPC-A-S01	0	2243.133	Aquifer + Bed	1.00E-06
EFPC-A-S02	0	1435.423	Aquifer + Bed	1.00E-06
EFPC-A-S03	0	1671.922	Aquifer + Bed	1.00E-06
EFPC-A-S04	0	2272.142	Aquifer + Bed	1.00E-06
GHB-A-S05	0	1829.85	Aquifer + Bed	1.00E-06
Gum Hollow Branch	0	4259.921	Aquifer + Bed	1.00E-06
Milton Branch	0	3414.32	Aquifer + Bed	1.00E-06
Pinhook Branch	0	2016.485	Aquifer + Bed	1.00E-06